The Thesis Committee for James William Patterson
Certifies that this is the approved version of the following thesis:

Placement and performance of pH-triggered polyacrylic acid in cement fractures

APPROVED BY
SUPERVISING COMMITTEE:

Supervisor:

Steven L. Bryant

Chun Huh

Placement and performance of pH-triggered polyacrylic acid in cement fractures

by

James William Patterson, B.S.P.E.

Thesis

Presented to the Faculty of the Graduate School of

The University of Texas at Austin

in Partial Fulfillment

of the Requirements

for the Degree of

Master of Science in Engineering

The University of Texas at Austin

May 2014

Dedication

To God, my family, and my friends.

Acknowledgements

I first want to thank Dr. Steven Bryant for all of the insight, guidance, and patience he has given me throughout my graduate studies. He has taught me to be quick on my toes in regards to back of the envelope calculations and to anticipate hard questions before they arise. His philosophy on research and life has made him a joy to work for and learn from.

I am indebted to Dr. Chun Huh for his timely humor and encouragement when I found myself burnt out on experimental research and for his vast knowledge of polymer behavior. Thanks must also be given to Dr. Paul Bommer for keeping me focused on the big picture when I started to lose sight of it and for his expertise in oilfield operations.

Special thanks go to Mohammad Reza Shafiei and Jostine Ho, who helped me with the rheology data used extensively in this thesis and with various side-experiments. I want to thank my labmates Scott T. Gabel, Doo Hyun Chung, Ricardo Salas Porras, Roy Wung, and Lina Lee for their company, conversation, and support over the last two years, which would have been too difficult and efficient without them.

Thanks also to Glen Baum and Gary Miscoe for helping me set up my experiments and for preparing the sawed cement cores. To Sophia Ortiz, for her help in procuring equipment and materials necessary for this research. To Nicholas Huerta, for his research that was essential to analyzing the acid pre-flush experiments.

This research was funded by the Department of Energy (grant DE-FE0009299 "AREA 2: Novel Materials for Robust Repair of Leaky Wellbores in CO2 Storage Formations").

Abstract

Placement and performance of pH-triggered polyacrylic acid in cement fractures

James William Patterson, M.S.E.

The University of Texas at Austin, 2014

Supervisor: Steven L. Bryant

A primary concern in the geologic storage of anthropogenic carbon dioxide is the leakage of buoyant CO_2 plumes into shallower formations, aquifers, or the surface. Man-made wells drilled through these formations present a potential leakage pathway for this CO_2 as the cement binding the well to the earth develops fractures or debonded microannuli form over time. Typically, wells with poor cementing or suspected leaks are subject to a cement-squeeze, in which new cement is injected to eliminate the leakage pathway. However, small fractures or leakage pathways are often difficult for oilfield cement to repair, as the cement dispersion is potentially screened out from dispersing fluid and cannot enter the fracture. Therefore a low-viscosity sealant is desired that can enter these leakage pathways easily and provide a robust seal.

A class of poly(acrylic acid) polymers known commercially as Carbopol® are pH-sensitive microgels and swell/thicken upon neutralization with alkali cement components. These polymer dispersions are tested for ease of placement into cement fractures and subsequent development of resistance to displacement. Laboratory

experiments involved injecting various unswollen polymer microgel dispersion into constructed cement fractures while measuring injection pressure and the pH of the polymer effluent to quantify the chemical reactions taking place and the induced viscosity changes. Fractures were constructed in order to allow for visual inspection of the polymer microgel swelling during and after injection, qualitatively useful in determining the polymer's efficiency at blocking cement fractures.

It was determined that polymer microgels undergo syneresis in the presence of calcium cations that are dissolved from minerals present in cement. The syneresis causes the polymer to collapse onto the cement fracture face and expelled water is left to fill the rest of the fracture, providing little to no resistance to subsequent flow. However, the syneresed polymer does show some potential in blocking or partially blocking small aperture fractures and is not entirely detrimental to fracture blockage in small amounts. An acid pre-flush prior to polymer injection has been seen to favorably reduce the amount of calcium and therefore extent of syneresis, allowing swollen polymer microgels to remain intact and block fluid flow.

Table of Contents

List of Tables

List of Figures

Chapter 1 Introduction

1.1 THESIS OUTLINE

The first chapter of this thesis will serve as an introduction to the problem studied and outline to the body of work presented in subsequent chapters, as well as research objectives. The second chapter is a literature review on topics related to the geologic storage of anthropogenic CO_2 and includes general well and cement information. This serves as a background for the reader to acquaint with the new investigation conducted here.

The third chapter described the experiments conducted with the polymer dispersions extensively used in chapters 4 and 5. The results of rheological tests and batch tests of polymer and cement, carried out to aid interpretation of the flow experiments, are also described throughout this thesis. The fourth chapter describes the results of polymer injection into cement fractures without acid pre-flush. Multiple core injection experiments are detailed along with the theoretical interpretations developed to explain the behavior observed, and conclusions are drawn from each. For each experiment, new observations led to improved theoretical interpretations on the mechanisms for the polymer flow and gelling behavior. The fifth chapter describes experiments in which cement fractures were pre-flushed with acid prior to polymer injection. The objective of this chapter was to find the optimal conditions for the polymer dispersion to be effective in plugging leakage pathways in cement fractures.

The sixth chapter draws overall conclusions from the work presented in this thesis and outlines future work that can be done in this field.

The Appendices contain information deemed necessary for more detailed understanding of experimental behavior.

1.2 RESEARCH OBJECTIVES

The primary objective of this research is to determine the viability of the use of polymer dispersions in sealing cement leakage pathways in wells drilled in geologic CO_2 storage formations. The optimal conditions for polymer blockage are sought, as well as situations in which the polymer gels are unfit for use. While multiple leakage pathways exist for buoyant CO_2 plumes, this research focuses on leaks found in and around wells previously drilled in these formations.

Chapter 2 Literature Review

2.1 GEOLOGIC CO_2 SEQUESTRATION

The increase in global demand for energy has led to the increase in anthropogenic carbon dioxide (CO_2) released into the atmosphere annually. Between 1990 to 2011, total CO_2 emissions in the United States have increased at an average annual rate of 0.5%, with 94% of this coming from fossil fuel sources. Approximately 35 gigatons of CO_2 from fossil fuels were expelled to the atmosphere globally in 2010 (EPA 2012). This massive release of CO_2 has pushed the atmospheric concentration up 31% since 1750, to levels likely exceeding those of the last 20 million years (IPCC 2001). Research has shown that increased atmospheric CO_2 levels has a profound negative effect on global climate, specifically rising sea levels and increasing extremes of precipitation patterns (IPCC 2013).

To offset the growing output of atmospheric CO_2, researchers around the world are investigating cleaner and more sustainable methods of energy production, but these technologies are decades away from being the workhorses of the global energy sector. Geologic carbon storage (GCS) shows potential to help bridge the transition to renewables by capturing anthropogenic CO_2 and injecting it into natural pore spaces in rocks deep below the surface of the earth (Kaldi et al., 2009). GCS involves the capture and compression of CO_2 from facilities with large scale emissions, such as power plants and refineries, which can then be injected into a variety of geologic formations (Orr, 2004). The most promising geologic storage targets are deep saline aquifers, as they typically have pressures high enough to keep CO_2 in a supercritical state, have little to no

economic or societal use for drinking or agriculture, and have the potential to hold thousands to tens of thousands of gigatons of CO_2 (Bruant et al. 2002).

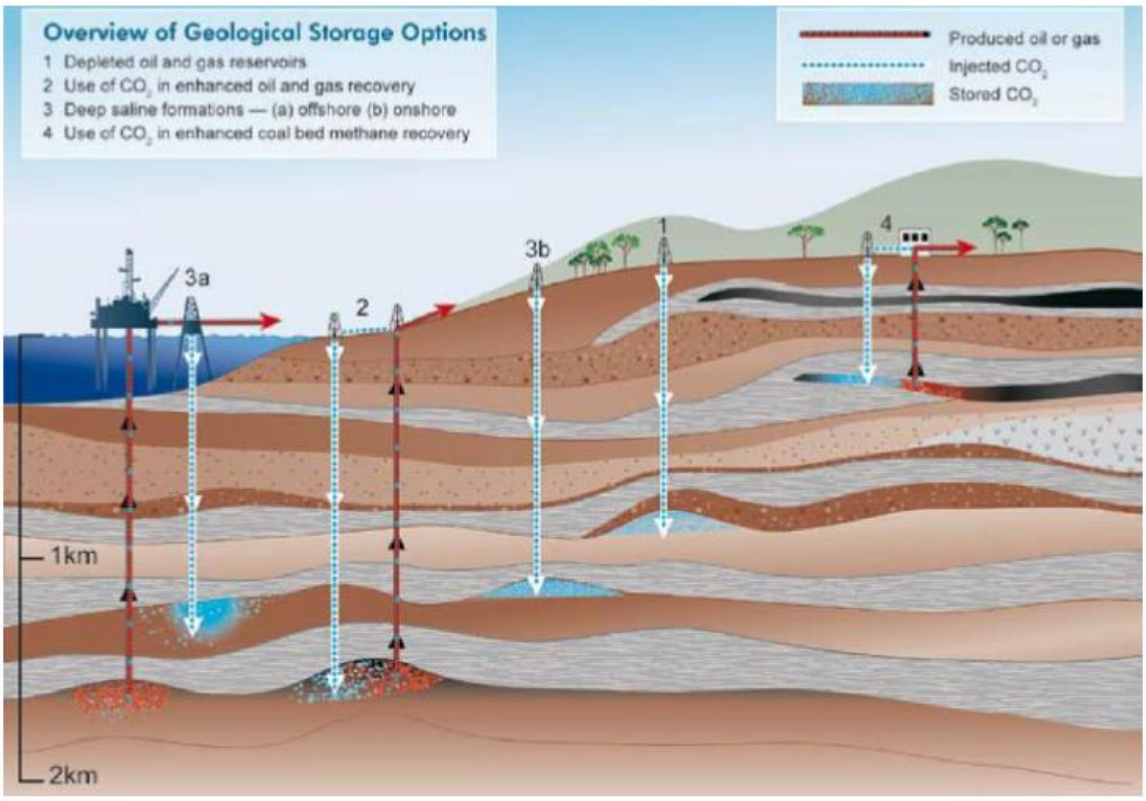

Figure 1: Schematic of possible storage locations for CO_2 in geologic formations (IPCC, 2005).

While GCS could be a valuable mechanism for reducing global CO_2 emissions, the capture, compression, and injection of CO_2 requires a large amount of power (Burton and Bryant, 2009). In the case of a power plant, this would require a significant fraction of the output power. There is also much concern over the long term safety and ability for the geologic formations to hold in the CO_2. CO_2 is buoyant in water in a supercritical phase and especially in a gaseous phase, causing it to rise to the top of a reservoir. As the buoyant CO_2 reaches the caprock, it begins to flow horizontally, spreading out across the top of the formation, and could come in contact with other wells

drilled or leaky faults running through the formation. These two features could provide a leakage pathway for CO_2 to escape the storage formation and enter fresh water aquifers or leak to the surface (Nordbotten, 2004). The increased pressure from the CO_2 injection could also fracture the sealing formations above or reactivate faults, causing seismic activity and subsequent CO_2 leakage (Bruant et al., 2002). Though these processes could require years of CO_2 injection or not appear for several decades, the long term risk must still be investigated. The IPCC (2005) suggests that a reservoir is unsuitable if it retains less than 99% of injected CO_2. Hepple and Benson (2002) state that reservoirs with leakage rates less than 0.01%/year, corresponding to 90% retention over 1000 years, would be effective formations for long term storage.

The possibility of these leakage pathways are an immediate problem from the perspective of industry and regulators, as the leakage and retention rates of geologic reservoirs is not well known or understood. There is also a need to show the public that GCS is a robust technology that can be utilized safely. These problems necessitate that the risk and extent of leakage be characterized and that solutions be developed (Oldenburg et al., 2009).

2.2 WELLBORE INTEGRITY

As buoyant CO_2 migrates upwards and horizontally in a reservoir, previously existing wells will be brought into contact with the corrosive CO_2-brine mixture. These wells are a key concern, as they are a potential weak point in the caprock that prevents CO_2 leakage. Many sedimentary basin reservoirs that are prime candidates for GCS happen to be in locations with closely spaced, preexisting wells that have been drilled

over the course of decades of petroleum exploration (Nicot, 2009). In many areas, hundreds of wells exist with no apparent owner or operator, so called "orphaned" wells, that were drilled with suspect methods and completions that would not withstand modern regulations (Hesson et al., 2013). Additionally, these old wells have been exposed to the elements longer than more recent wells, and therefore have had more time to develop leaks or other weaknesses (Watson and Bachu, 2008).

Wells are constructed such that the steel casing, which contains pipe or acts as the flow conduit, is cemented into the drilled hole in the formation rock. Ideally, the cement acts as a seal between the various formation layers that the well crosses through, and many modern regulations are in place to ensure that this cement is sealing. For example, a certain amount or height of cement may be required, or cement must be used to seal off specific formations, such as freshwater aquifers (TRRC 2013). The curing of cement can, however, be hampered by insufficient sweeping of the hole, leaving residual drilling mud behind, which prevents a proper seal between the steel and rock. During curing, any fluid inflow, such as a small influx of gas, could create small flow channels in the cement from one subsurface layer to another (Soter, 2003). Wellbore cement can also develop leaks over time, either by chemical attack from formation fluids or by mechanical stressing causing by pressure or thermal cycling resulting from the production of hot reservoir fluids or injection of relatively cold surface fluids (Milanovic and Smith, 2005). The cement itself can fracture under these stresses, creating rough, slot-like flow channels, or the cement can be debonded from the steel casing, also creating slot-like geometries for fluids to leak through.

2.3 Chemical Alteration of Cement

Cement is typically made by crushing calcium and silica rich minerals, such as calcium carbonates (limestone, coral), clays, and shales (Kutchko et al. 2007). These raw materials are crushed and heated to over 1400 °C, resulting in a material known as "clinker." The clinker is cooled, gypsum is added, and the mixture is ground into a fine powder.

The oil industry typically uses portland cement to provide the seal between the well casing and rock. Different types of oilfield cement are standardized by the American Petroleum Institute (API). Class H is a portland cement widely used in the oil industry in North America, of which the API sets minimum chemical (such as mineral composition) and physical (such as grain size and compressive strength) requirements (API 2011). Additives are typically included into portland cement before and during mixing in order to fit the needs of each individual well or field, but the four main components of the cement remain the same. These four minerals are found in the dry cement, before water is added to create the cement slurry, and are shown in Table 1.

Component	Shorthand	Chemical Formula
Dicalcium Silicate	C_2S	$2CaO•SiO_2$
Tricalcium Silicate	C_3S	$3CaO•SiO_2$
Tricalcium Aluminate	C_3A	$2CaO•Al_2O_3$
Tetracalcium Aluminoferrite	C_4AF	$4CaO•Al_2O_3•Fe_2O_3$

Table 1: List of primary mineral components in portland cement mix (Bourgoyne et al., 1986)

Of these four components, the silicates, dicalcium silicate and tricalcium silicate, comprise over 80 wt% of the cement, mostly in the form of C_3S (Kutchko et al. 2007). The cement mix is combined with water in a specific water to cement ratio to form

cement slurry, a pumpable liquid that can then be injected through the casing and into the annulus. The water also supplies the H_2O necessary to begin the exothermic hydration process in which the cement thickens and solidifies. The chemical hydration reactions are given below in Table 2.

Cement Slurry Component	Hydrated Cement Component
$2\ (2CaO{\bullet}SiO_2) + 4H_2O$	$3CaO{\bullet}2SiO_2{\bullet}3H_2O + Ca(OH)_2$
$2\ (3CaO{\bullet}SiO_2) + 6H_2O$	$3CaO{\bullet}2SiO_2{\bullet}3H_2O + 3Ca(OH)_2$
$4CaO{\bullet}Al_2O_3{\bullet}Fe_2O_3 + 2Ca(OH)_2 + 10H_2O$	$6CaO{\bullet}Al_2O_3{\bullet}Fe_2O_3{\bullet}12H_2O$
$3CaO{\bullet}Al_2O_3 + Ca(OH)_2 + 12H_2O$	$3CaO{\bullet}Al_2O_3{\bullet}Ca(OH)_2{\bullet}12H_2O$
$3CaO{\bullet}Al_2O_3 + CaSO_4{\bullet}2H_2O + 10H_2O$	$3CaO{\bullet}Al_2O_3{\bullet}CaSO_4{\bullet}12H_2O$

Table 2: List of primary mineral components in portland cement mix and their hydrated mineral forms (Bourgoyne et al., 1986).

Because most of the cement mix is silicates, it follows that almost 70 wt% of the hydrated cement is comprised of the silicate hydrated mineral, calcium silicate hydrate ($3CaO{\bullet}2SiO_2{\bullet}3H_2O$), known as C-S-H (Kutchko et al. 2007). This C-S-H acts as the primary binding material in the cement matrix. The other main hydration product is calcium hydroxide, $Ca(OH)_2$, known as portlandite, which grows rapidly to occupy pore spaces between other cement grains. There also exists a small amount of iron and aluminum hydrates.

The resulting hydrated cement is highly alkaline and will reach equilibrium with fluids at a pH of nearly 13. If the fluid pH drops below 13, cement minerals will dissolve to drive the system to equilibrium. The minerals that dissolve depend on the solution pH and the stability of the mineral (Beddoe and Dorner 2005). For example, calcium hydroxide is the most soluble of the cement constituents and will start to dissolve

at pH 12.4 and lower; calcium aluminates will dissolve below pH 10.5; aluminum hydroxides below pH 4.0; and iron-rich minerals below about pH 2.

2.4 Reactive Transport of Acid in Cement Fractures

As fluid moves through cement fractures, be they formed by cement-casing debonding or tensile failure, the fluid will react with the cement until the fluid-cement system is in equilibrium, hence the name reactive transport. If cement components are only dissolved by the moving fluid, flow channels will emerge in the matrix in a "worm hole" pattern (Szymczak et al., 2009). The formation of these worm holes depends on the acid injected (both type and pH), the minerals present, and the flow rate of the acid. In a fracture, the minerals at the fracture walls would be dissolved and the fracture would be widened.

However, Huerta (2013) shows that reactive transport of acid through cement fractures can include both dissolution and precipitation processes. These complex interactions can result in either the increase of flow area by cement wall dissolution or the constriction of flow area by secondary mineral precipitation. In the case of hydrochloric acid (HCl aq.) and CO_2 saturated brine injection into cement fractures, the calcium dissolved from portlandite present in cement is contributes to the precipitation of calcite in the fracture, downstream from the site of portlandite dissolution (Huerta, 2013). Overall, the leakage of these acidic fluids through cement fractures causes the cement to "self-heal" as the calcite precipitate constricts and ultimately restricts flow in the fracture.

2.5 Cement Squeeze Operations

Wells that are thought to have been poorly cemented or developed leaks in the cement are typically subject to a squeeze cementing operation. Squeeze cementing is defined by Goodwin (1984) as the forcing of cement slurry into a hole in well casing and

into cavities behind the casing for the purpose of ensuring cement integrity. However, squeeze cementing is often unsuccessful due to improper slurry placement or poorly designed cement slurries. Instead of sealing the void space behind casing, it is possible for new leakage pathways to be created by the fracturing of the near wellbore rock due to excessively high squeeze pressures (Goodwin 1984). It is also possible for the leakage pathways to be too small to allow the solid particles in cement slurry to pass through, causing the cement particles to filter out and only cement filtrate (essentially water) to penetrate the pathway (Toor 1983).

It is therefore desirable to develop a sealant that can enter the smallest of fractures and leakage pathways, yet still provide a strong seal against the buoyant leakage of $scCO_2$ plumes.

Chapter 3 Polymer Rheology and Batch Tests

The rheology of many polymer gels is generally non-Newtonian and can be characterized with Herschel-Bulkley rheological model (Choi, 2008). Due to the ionic state of the polymer chains, the polymer gel exhibits pH-sensitive behavior, altering the rheological parameters significantly as a function of pH. Due to the initial acidity of the polymer dispersion, alkaline minerals such as those found in Portland cement react quickly with the polymer molecules and increase the pH. The rheological behavior of the polymer gels and the effects of polymer-cement interaction are discussed below.

3.1 Polymer Rheology and Concentration

The primary polymer tested was Carbopol® 934, manufactured by Lubrizol Corporation, a cross linked polyacrylate in microgel form. The polymer is supplied as dry, tightly coiled polyacrylic acid chains that are then hydrated and partially uncoiled when dispersed in water. The dispersion of polymer into water results in an acidic solution, usually around pH 2.5-3, depending on the polymer concentration. At this point, the polymer dispersion is slightly more viscous than water. These can be significantly viscosified by the neutralization of the pH of the dispersion, as basic conditions increase the amount of dissociation of carboxyl groups, resulting in electrostatic repulsion between the polymer chains. By adding a basic solution, such as sodium hydroxide (NaOH), the polymer chains are further uncoiled and form highly swollen gel networks (Barry and Meyer, 1978).

In addition to the increased viscosity of the polymer dispersion, the swelling and entanglement of polymer chains at higher pH creates a yield stress in the fluid, causing the dispersion to behave as a solid under a small (less than a threshold) amount of shear stress. If the shear stress applied to the fluid exceeds the yield stress, the polymer

dispersion then flows and behaves as a liquid. Using a typical rheometer, this yield stress is obtained by measuring the shear stress of the fluid at lower and lower shear rates. From these data, the shear stress is extrapolated to a zero shear rate, giving the theoretical zero-rate shear stress, or yield stress. An example of such an extrapolation and behavior is given below in Figure 2. For microgel dispersions, as the shear rate approaches zero, the shear stress approaches the yield stress. This behavior contrasts with Newtonian fluids, which have zero shear stress at zero shear rate.

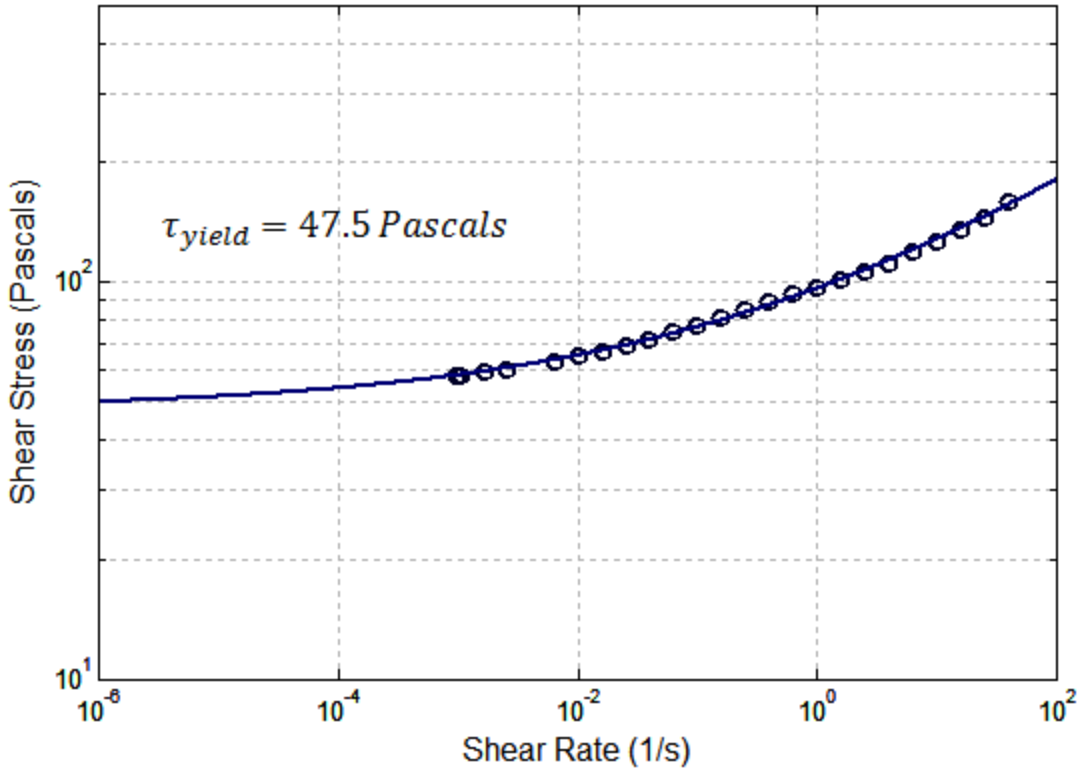

Figure 2: Example of yield stress extrapolation; circles are actual data gathered (AR-G2 Magnetic Bearing Rheometer), blue line is Herschel-Bulkley fit and extrapolation; yield stress = 47.5 Pascals. (Data provided by colleague Mohammadreza Shafiei, personal communication 2014)

The data were fit using a Herschel-Bulkley fluid model, in which the fluid rheology is defined by three parameters: yield stress, consistency index, and power law index:

$$\tau = \tau_{yield} + K\dot{\gamma}^{n}$$

The yield stress, τ_{yield}, determines the minimum shear rate at which the fluid will be moved; the consistency index, K, is similar to a Newtonian viscosity term; and the power law index, n, determines how the viscosity changes as a function of shear rate. These variables together determine the relationship bnetween the shear rate, $\dot{\gamma}$, and shear stress, τ.

By rearranging this equation, the apparent viscosity, $K_{apparent}$, can be calculated. The apparent viscosity is essentially what a Newtonian fluid's viscosity would have to be to create the same resistance to flow that the Herschel-Bulkley fluid exhibits at that specific flow rate. This allows for easy estimation of the relationship between shear rate and shear stress, or perhaps the relationship between pressure gradient and flow velocity in a conduit, for a given shear rate. The apparent viscosity will change as a function of shear rate.

$$\mu_{apparent} = \frac{\tau}{\dot{\gamma}} = \frac{\tau_{yield}}{\dot{\gamma}} + K\dot{\gamma}^{(n-1)}$$

For Carbopol 934 dispersion and gel, the power law index is always below unity, meaning that shearing the fluid at larger rates will result in a smaller apparent viscosity, known as shear thinning behavior. For example, a Newtonian fluid's shear rate will double as the shear stress is doubled, but a Herschel-Bulkley fluid's shear rate might double only if the shear stress is quadrupled.

When the acidic polymer dispersion is neutralized and the polymer chains fully uncoil, the dispersion gels and the yield stress and consistency index both increase.

Figure 3 below shows the effect of varying pH on the shear rate and shear stress relationship, while Table 3 shows the yield stress and consistency index for each sample.

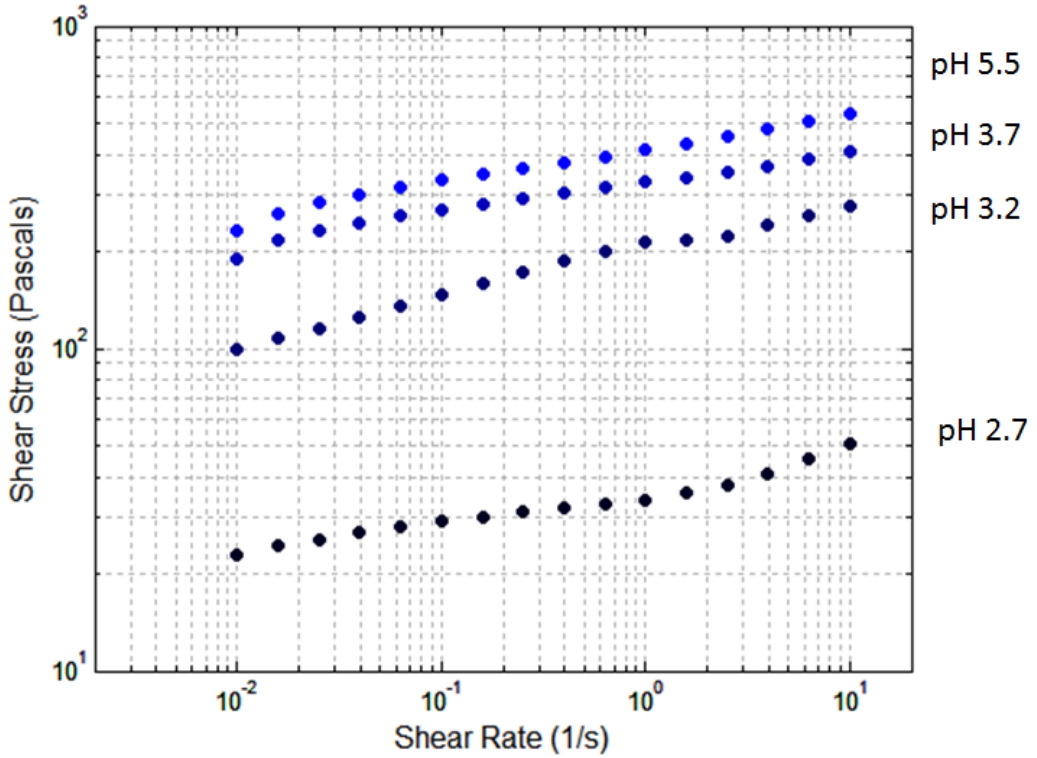

Figure 3: Shear stress vs shear rate for 3 wt% Carbopol 934 at various pH values, neutralized with sodium hydroxide, NaOH, solution (M. Shafiei, personal communication, April 2014).

Sample pH	Yield Stress (Pa)	Consistency Index (Pa-s)
2.7	22	12
3.2	32	123
3.7	172	155
5.5	223	188

Table 3: Increase of yield stress and consistency index of polymer gel with increasing pH, for 3 wt% Carbopol 934 and 0 wt% NaCl.

The shear stress increases with pH for any given shear rate, though the overall curve shapes are similar, indicating that the consistency index has increased while the power law index remained roughly constant. The extrapolated yield stress at zero shear

rate also increased with the pH, meaning that the minimum shear stress to move the gel as a fluid has increased. From pH 2.7 to 5.5, the yield stress increases by a factor of ten, from 22.4 Pa to 223.3 Pa. This increased yield stress with pH is the mechanism that will prove most valuable in sealing cement fractures, as it will theoretically stop the flow altogether as long as the pressure gradient remains below a threshold. For example, to displace a polymer gel with a 220 Pa yield stress from a 500 micron aperture fracture requires a pressure gradient of 39 psi per foot. For comparison, the pressure gradient associated with a buoyant plume of CO_2 is around 0.1 psi/ft. Figure 4 below shows the yield stress of the polymer gel as a function of pH. At pH values above 9, the gel's yield stress begins to decrease. Though the presence of hydroxide ions allows the polymer chains to fully uncoil and achieve maximum viscosity, an excess of hydroxide dampens the electrostatic repulsion of the carboxyl groups on the polymer chains (Noveon, 2002).

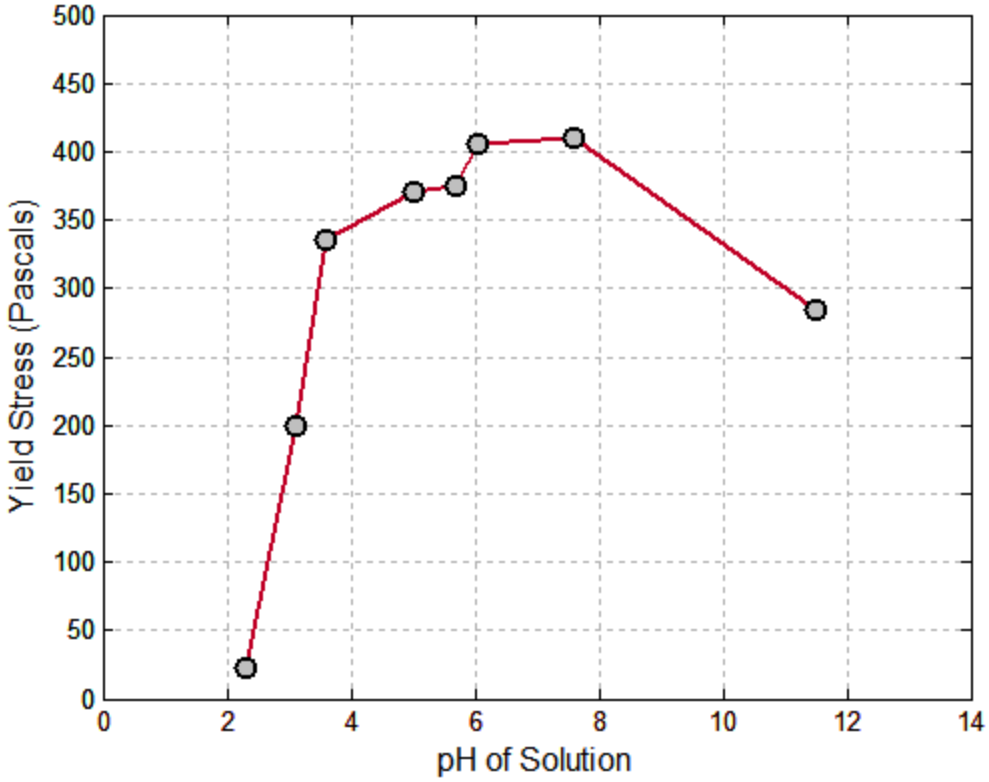

Figure 4: Yield stress vs pH of 3 wt% Carbopol 934 polymer dispersion and 0 wt% NaCl with plateau and drop off at high pH; measurements taken at room temperature and pressure (M. Shafiei, personal communication, April 2014).

Between pH 3 and 3.75 the yield stress of the polymer gel increases drastically. This is referred to as the critical gelation pH range. The consistency index of the polymer gel at this critical gelation pH range behaves similarly, increasing drastically then plateauing around pH 4 to 8.

The apparent viscosity of the polymer dispersion depends exponentially on the shear rate, as shown in Figure 5. As the shear rate increases, the shear-thinning fluid's apparent viscosity is reduced. The consistency index and yield stress are increased as the dispersion is neutralized, resulting in larger apparent viscosities as the pH increases.

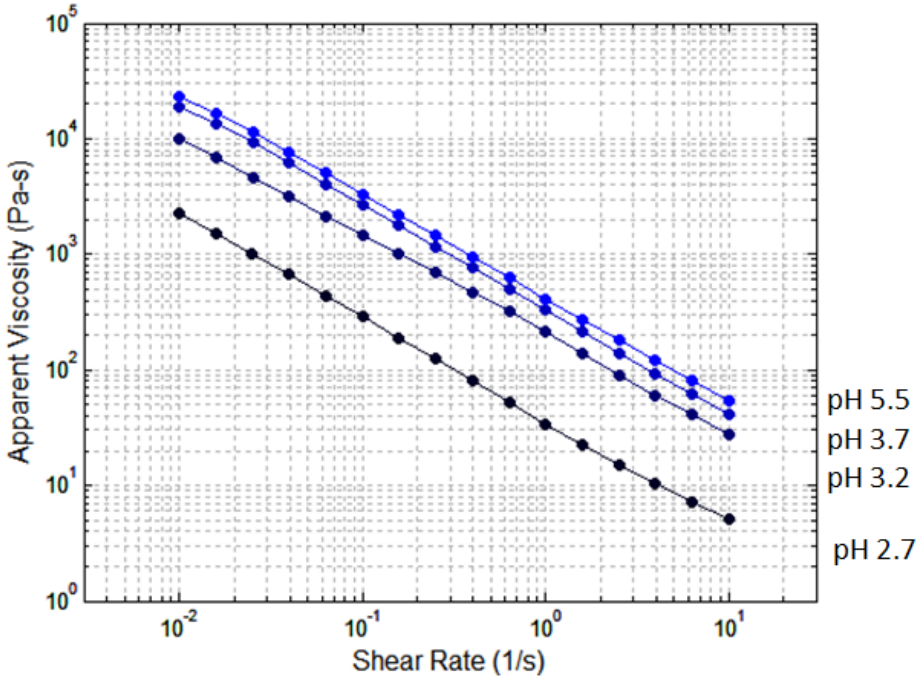

Figure 5: Apparent viscosity as a function of shear rate at 4 pH values for 3 wt% Carbopol 934 and 0 wt% NaCl.

3.2 Effect of Salts on Polymer Rheology

The pH of the gel is not the only factor that affects the gel's yield stress. The presence of cations has a strong effect on the yield stress, especially divalent cations such as calcium. Cations in the polymer dispersion will screen the carboxyl groups of the polymer chains, thereby reducing the electrostatic repulsion, making the chains less rigid and the dispersion less viscous (Barry and Meyer, 1978) and decreasing the gel yield stress. The effect on yield stress can be seen below in Figure 6, with rheological parameters shown in Table 4.

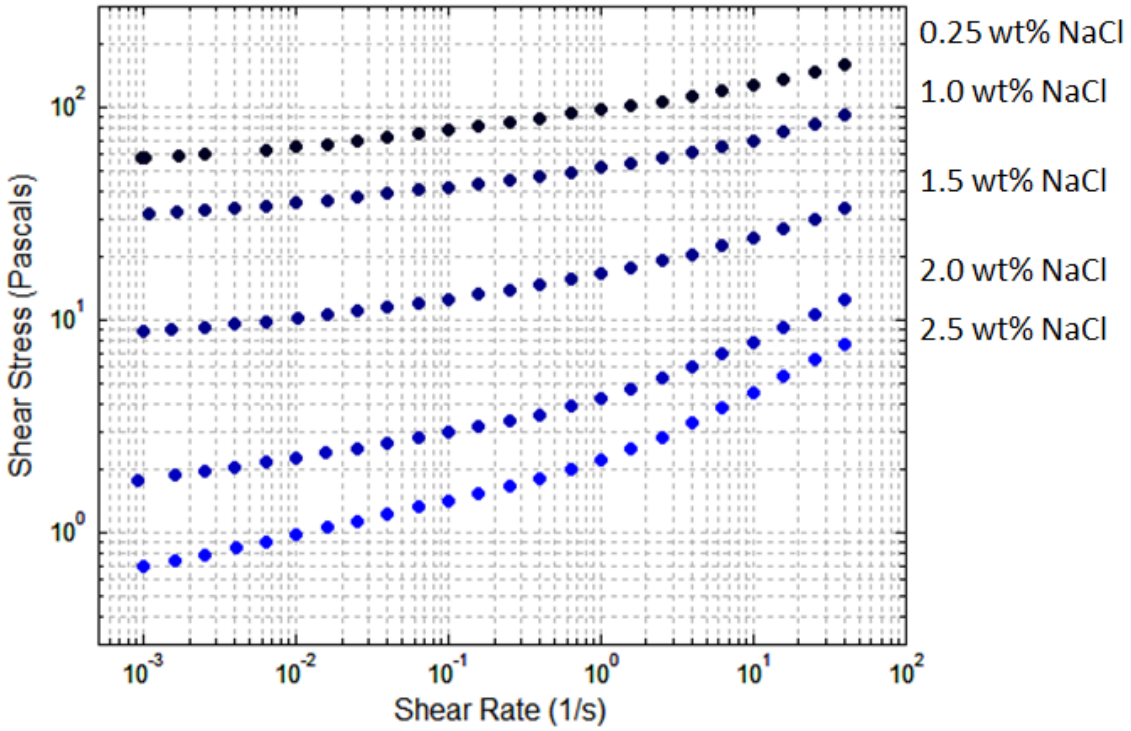

Figure 6: Shear stress vs shear rate for 3 wt% Carbopol 934 at various concentrations of NaCl salt and pH = 3.75 (Shafiei, personal communication, April 2014).

Sample NaCl Concentration (wt%)	Yield Stress (Pa)	Consistency Index (Pa-s)	Power Law Index
0.25	47	48.9	0.22
1.0	29	23.0	0.27
1.5	8.1	8.3	0.30
2.0	1.8	2.5	0.39
2.5	0.8	1.5	0.42

Table 4: Decrease of yield stress and consistency index of 3 wt% Carbopol 934 polymer gel with increasing salt concentration (cf. Figure 6).

The shear stress for a given shear rate is drastically decreased with an increasing concentration of sodium chloride salt. The extrapolated yield stress of the 0.25 wt% NaCl gel at a pH of 4.0 is 47.5 Pa, but drops by a factor of 60 down to 0.8 Pa with an increase in salt concentration to 2.5 wt% NaCl at the same pH. A trend can be seen in which the addition of salt causes the yield stress to decrease, the consistency index to decrease, and the power law index to increase. It is worth noting that water, a

Newtonian fluid, has a yield stress of 0 Pa, a consistency index of 0.001 Pa-s, and a power law index of 1. It can be concluded that the presence of salt causes the polymer dispersion to become more water-like in its rheology. Unfortunately, brines present in oil fields or saline aquifers can have brines with salt concentrations beyond 20 wt% and contain large amounts of divalent cations (Featherstone and Powell, 1981). This has several implications for the field application of this material:

1. Fresh water must be used to prepare polymer dispersions.
2. The procedure for injecting the prepared polymer dispersions must minimize mixing and/or contact with formation brines.
3. Long-term performance of material placed in a fracture in cement may depend on how fast cations can diffuse from the cement (due to reaction) or from brine in formations in contact with that part of the cement

The yield stress data for various pH values for a polymer dispersion of 3 wt% Carbopol 934 and 0.5 wt% NaCl is shown in Figure 7. It can be seen that the yield stress of this polymer dispersion is nearly zero at low pH values, but quickly increases with neutralization to aover 100 Pa yield stress. Although less data were collected for mid-range pH values, the build and subsequent decline at high pH is similar to the behavior seen in Figure 4.

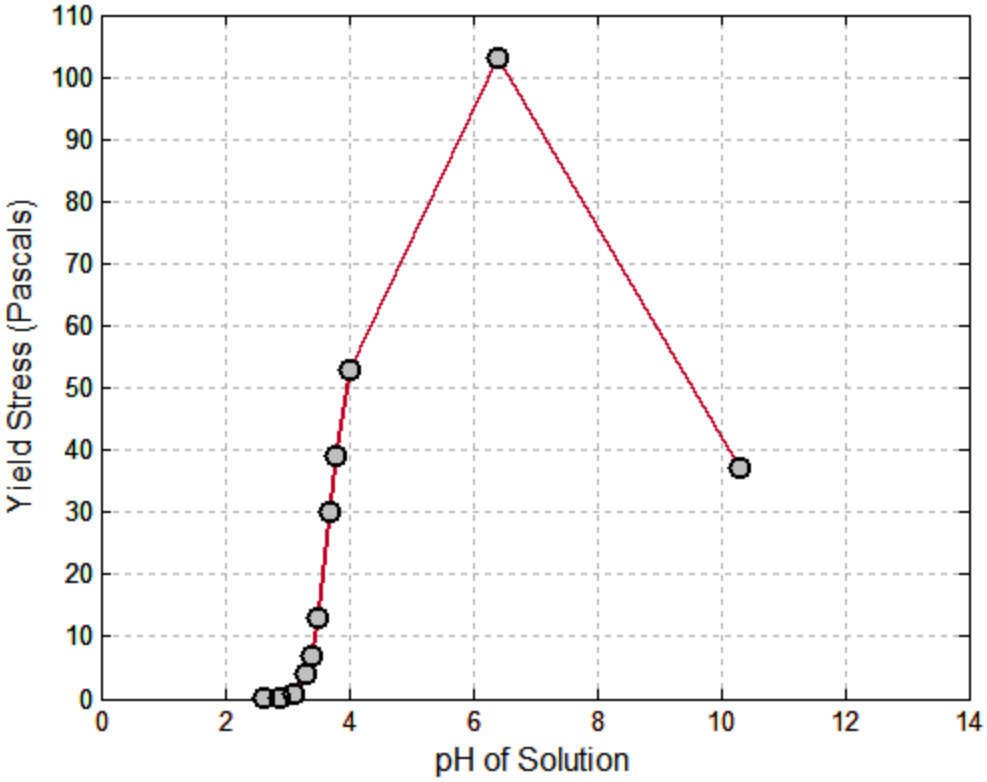

Figure 7: Yield stress vs pH of 3 wt% Carbopol 934 polymer dispersion and 0.5 wt% NaCl with peak and drop off at high pH; measurements taken at room temperature and pressure (Shafiei, personal communication, April 2014).

For a polymer dispersion of 3 wt% Carbopol 934 and 0 wt% NaCl at pH 3.5, rheology measurements were made at increasing temperature, from 30°C to 80°C. The shear stress as a function of shear rate behavior for this polymer is shown in Figure 8. It appears that temperature has very little effect on the polymer rheology, with the largest difference appearing at low shear rates, and the increased temperature increases the shear stress at these low shear rates.

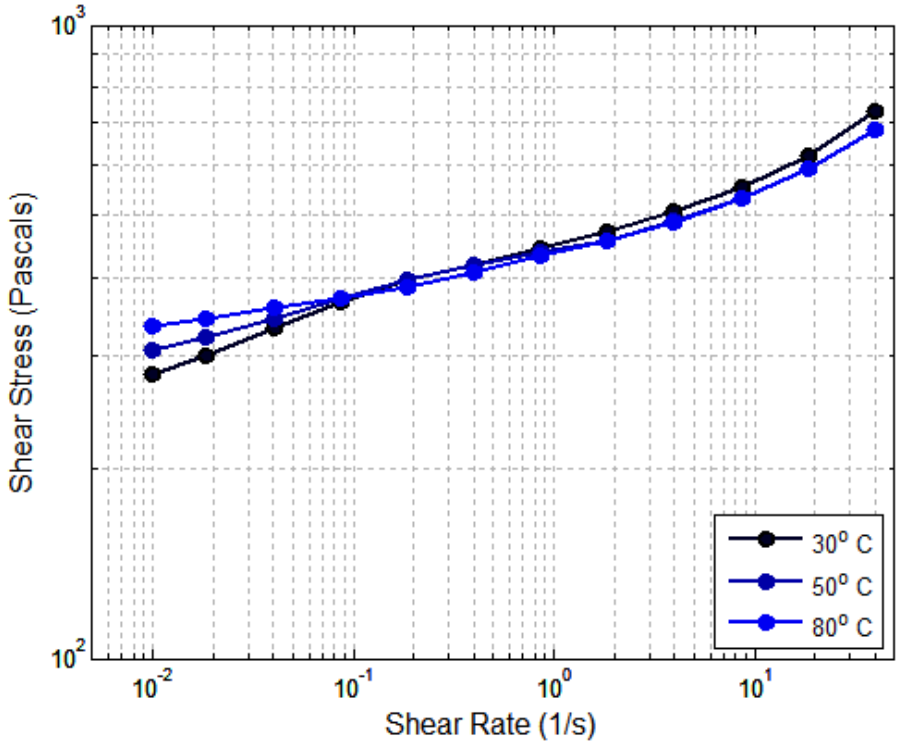

Figure 8: Shear stress vs shear rate for 3 wt% Carbopol 934 at pH 3.5 for increasing temperature (Shafiei, personal communication, April 2014).

3.3 Polymer Cement Reaction Batch Tests

3.3.1 Polymer and Cement

Cement is composed of a variety of minerals, but as long as the pH of the surrounding fluid is above 2 the soluble components are mostly limited to calcium silicate hydrate (C-S-H) and portlandite (calcium hydroxide). A polymer dispersion with 3 wt% Carbopol 934 has a pH of around 2.3, which is the lowest expected polymer pH, as concentrations of over 3 wt% it becomes increasingly difficult to mix and generate a homogeneous dispersion. Therefore, it is expected that the majority of the polymer-cement interaction will come from the C-S-H and portlandite dissolution. Batch tests were conducted by putting cured cement, either large pieces (~2") or smaller, crushed pieces (~0.1"), in contact with various different polymer dispersions and sealed from

atmosphere, then monitored intermittently up to weeks after initial mixing. The mixture was contained in plastic tubes, allowing for visual inspection.

Every polymer-cement batch test yielded an unexpected white, sponge-like semisolid that appeared on the cement surface. In most cases, a thin film of this semisolid appeared on the cement core surface within 1 hour after being submerged in polymer dispersion and grew in extent and thickness as time went on. Around or on top of this white semisolid a clear, water-like fluid is observed. However, parts of the polymer dispersion still swell and produce the clear gel that comes from polymer dispersion neutralization. The end result is that the cement causes the polymer dispersion to produce three distinct materials: polymer gel, semisolid, and water.

Fractured cement cores were submerged into polymer dispersion and the fracture was allowed to fill with polymer dispersion. Fracture gaps were made by placing a plastic spacer between the two cement halves. Figure 9 below shows a set of photographs of a batch test with a cement core with an axial fracture set in polymer dispersion for 24 hours, before and after. The fracture was held shut by a green rubber band, seen in the photograph.

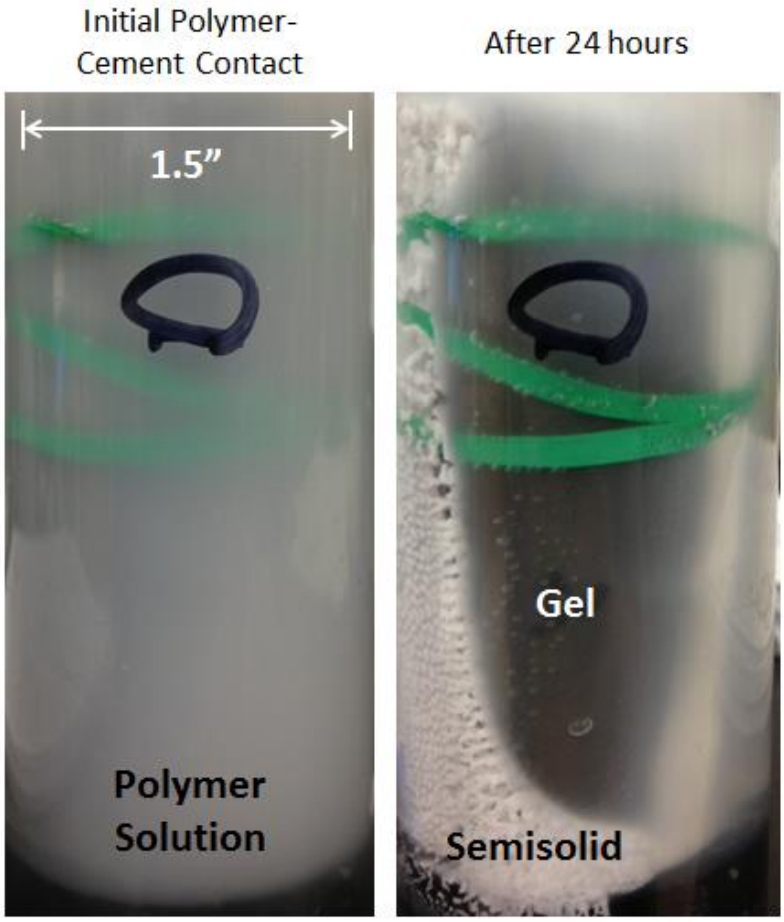

Figure 9: Batch test of 3 wt% Carbopol 934 polymer dispersion with a 2” by 1” fractured cement core in a 1.5” plastic tube, before and after a 24 hour shut in period. Green material is rubber band holding the fractured core halves together.

Within 24 hours of contact between the polymer dispersion and cement, the opaque polymer dispersion becomes either the clear gel or a white semisolid material. These three polymer phases are clearly separate from the others. Within just 24 hours, the polymer dispersion had almost totally converted to the gel or semisolid. It was also seen that more white semisolid would appear on the cement surface as time went on. In Figure 10 below, photographs were taken at 24 hour increments of a cement core with 3 wt% Carbopol 934 in a plastic tube.

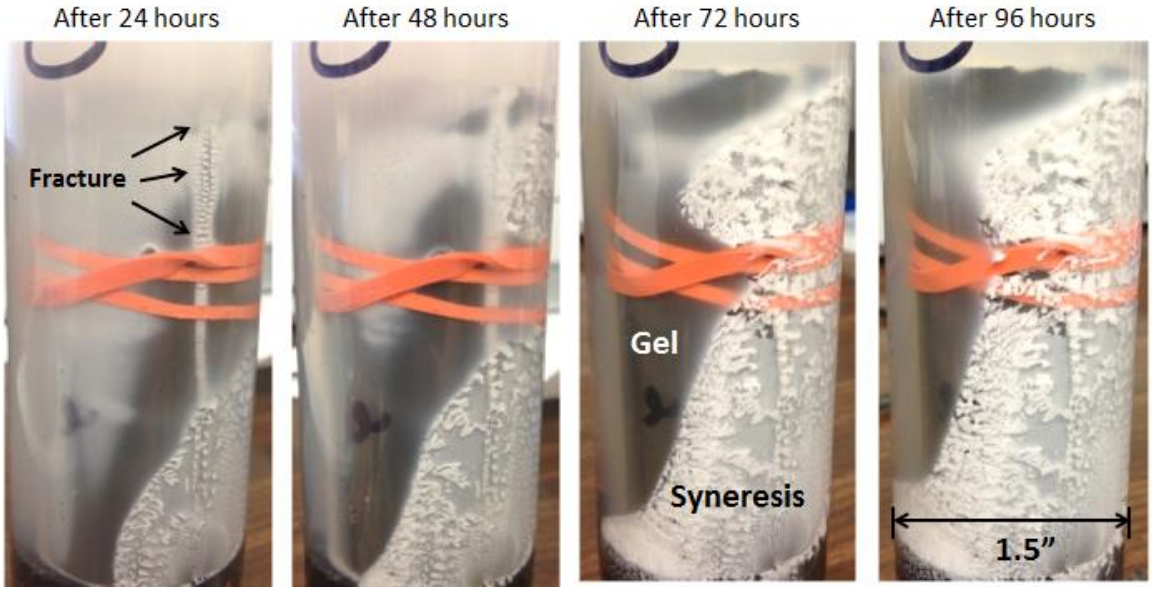

Figure 10: Advancement of white semisolid on cement surface with 3 wt% Carbopol 934 polymer dispersion.

The white semisolid on the right side of the core has a sponge-like texture and seems to grow from right to left as the cement sits in the polymer dispersion. The left-most picture, after 24 hours of exposure, the polymer dispersion appears unreacted on the left side of the core, the bottom right of the core is covered in the semisolid, while the strip between the two phases is clear polymer gel. In each photograph, the clear gel and white semisolid regions move leftwards. This heterogeneity is commonly observed in these experiments, and indicates that the polymer-cement reaction has several phases: polymer dispersion, polymer gel, then white semisolid. The white semisolid is consistently seen along with a free water phase, generally on the side or top of the cement core. Figure 11 shows the free water phase between cracks in the white semisolid.

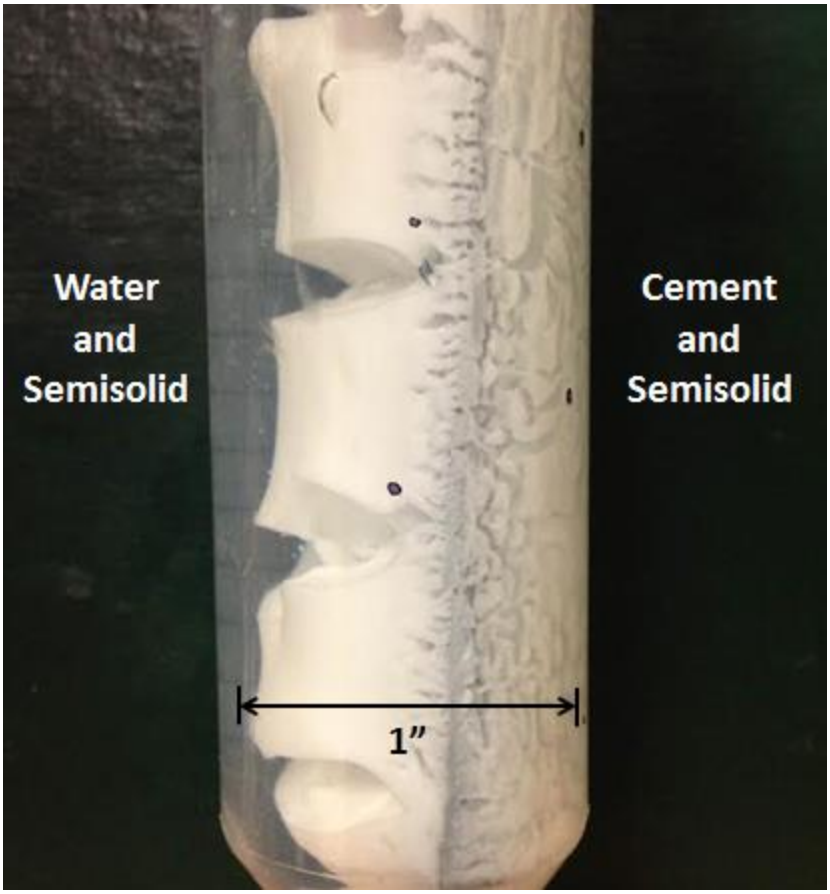

Figure 11: Photograph of white semisolid cracks forming in the presence of 3 wt% Carbopol 934 with half of a cement core; free water is seen between cracks. The cement core half occupies the right side of the image.

The right side of Figure 11 contains the cement half-core, while the left side originally contained a volume of polymer dispersion. Over time, the large volume of polymer dispersion slowly contracted and formed a few large cracks. Water is seen to move freely through these cracks. The water between the cracks is free-moving and a sample collected showed a pH of over 12, indicating that the polymer had fully reacted with the cement, followed by additional cement mineral dissolution to drive up the pH.

Table 5 below summarizes the observed polymer phases and their descriptions.

	Color	Viscosity	Location
Polymer Dispersion	White/Opaque	Thin gel	n/a (consumed)
Polymer Gel	Clear	Thick gel	Various
Semisolid	White	Sponge-like solid	On cement surfaces
Water	Clear	Newtonian	Next to semisolid

Table 5: Polymer phases that appear when polymer dispersion contacts cement for extended periods.

As mentioned above, the white semisolid appears to grow with time, and in some cases forms a "mudcrack" pattern over the cement that propagates into longer cracks with time. However, clear water fills and surrounds these cracks, eliminating a dehydration or drying effect as the cause. A polymer effect known as "syneresis" is thought to cause these cracks and the white semisolid in general. Syneresis is a process by which polymer gels expel pore water from the polymer network and begin to contract (Grachev et al., 2008). This implies that the white, sponge-like semisolid is a tangled polymer network that has collapsed on itself, essentially becoming precipitated onto the cement surface. Figure 12 below shows more detailed photographs of the mud crack pattern, with arrows corresponding to the same location on each photo.

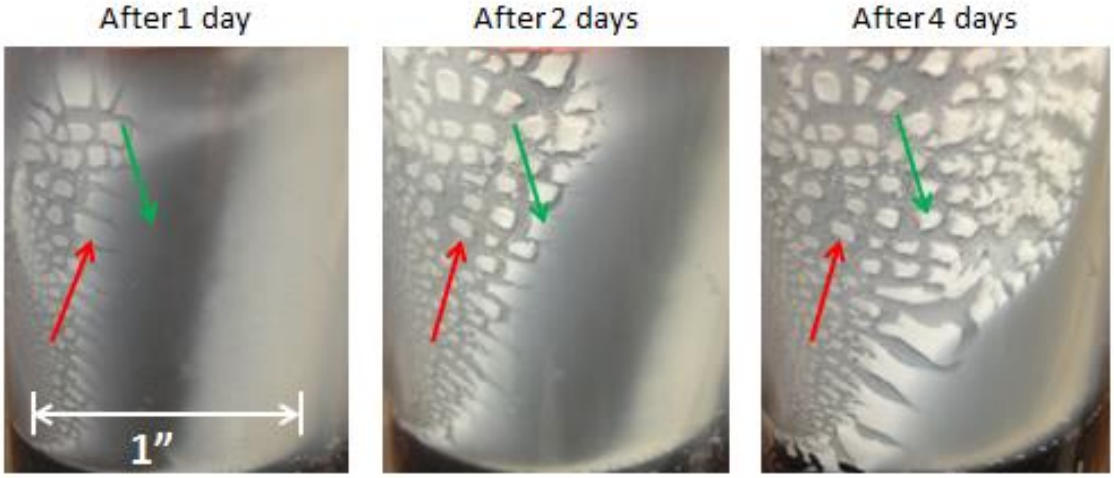

Figure 12: Detailed photographs of syneresis cracks forming on cement surface with 3 wt% Carbopol 934 polymer dispersion; red and green arrows correspond to identical spatial locations in each photograph.

The boundary between clear gel and syneresed polymer moves from left to right in the photographs, as the syneresis cracks propagate to the right as well. The squares of syneresed polymer further contract and dissociate as the syneresis front moves past them. These "mud cracks" were also observed more frequently when the polymer dispersions were contained in a narrow gap between the cement and plastic container.

When the fractured cement cores were taken out of the polymer-filled plastic tube, the two halves were separated. Figure 13 below shows a photograph of the inside of a cement fracture after the batch test was performed.

Figure 13: Interior of a cement fracture filled with 3 wt% Carbopol 934 polymer dispersion and allowed to sit for 4 days.

The syneresis cracks have formed on the inside of the fracture as well, but appear smaller than the outer cracks. This shows that syneresis will most likely be present in

the case of polymer injection into cement fractures, but the effect on the polymer's sealing capabilities is yet to be determined.

To test the effect of salts on the syneresis, three cement cores were prepared with different saturating fluids: deionized water (the control), 5 wt% NaCl brine, and 5 wt% $CaCl_2$ brine. The cores were then submerged in 3 wt% Carbopol 934 and 0 wt% NaCl polymer dispersion. After 24 hours, the DI and NaCl brine saturated cores had similar degrees of syneresed polymer adhered to the cement surface. The $CaCl_2$ brine saturated core, however, had completely syneresed all of the polymer dispersion very wuickly, leaving only a thick layer of syneresed polymer on the cement surface and free water at the top of the core. These cores are shown below in Figure 14.

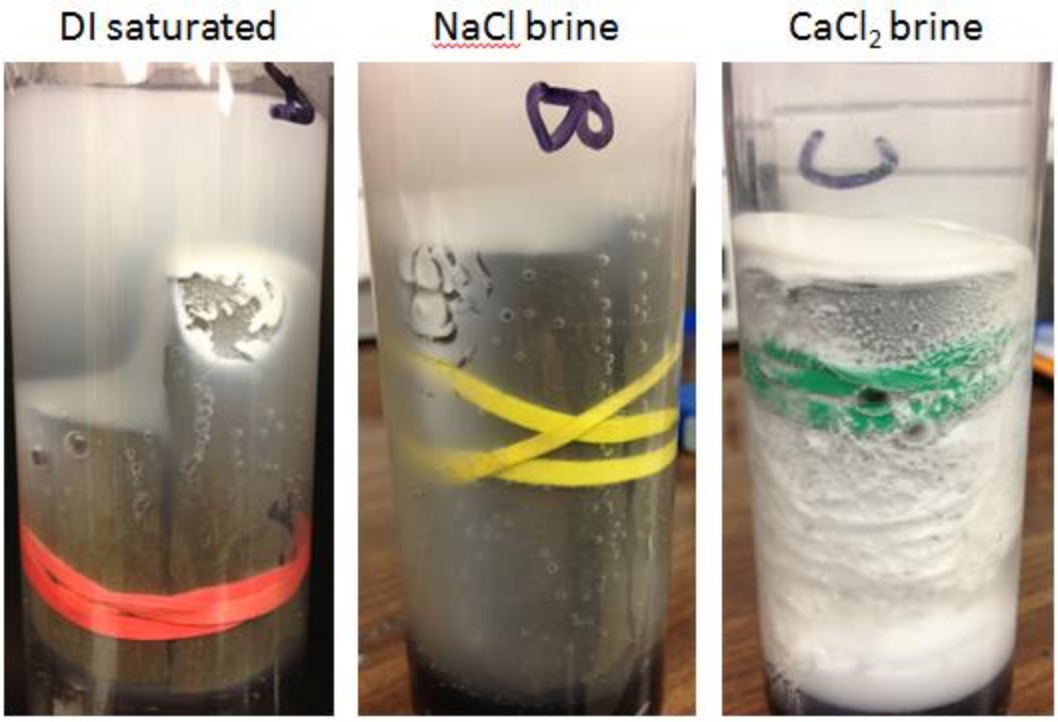

Figure 14: Cement cores with different saturating fluids (from left to right: DI water, NaCl brine, $CaCl_2$ brine) in contact with 3 wt% Carbopol 934 and 0 wt% NaCl polymer dispersion.

3.3.2 Polymer and Berea Sandstone

A batch test was conducted with a fractured Berea sandstone core submerged in polymer dispersion in order to better understand what minerals directly cause the syneresis effect. Berea sandstone contains much less calcium and alkali components than cement, and in general reacts slower with acid than Portland cement (Choi, 2008). When exposed to the Berea sandstone, the polymer slowly gelated over the course of several days, much slower than the gelation observed with cement samples. In the first week, no syneresis was observed, but after three weeks it was obvious that the polymer had separated into a free water phase and syneresed gel phase. The color of the syneresed phase, however, was a red-pink color instead of white, likely due to the clay minerals present.

3.4 NON-REACTIVE POLYMER FLOW

While the rheology of the polymer dispersion and polymer gel were characterized in depth using high-precision rheometers and various interpretation techniques, it was important to establish a reliable connection between rheometer data and actual injection data. Rheology data and analytical solutions for Herschel-Bulkley flow in a tube and slot allow for prediction of injection pressure through these geometries. Therefore, predicted injection pressures and observed experimental injection pressures were compared to verify the reliability of these predictions.

3.4.1 Herschel-Bulkley flow equations

Herschel-Bulkley fluids are characterized by having both a yield stress (as in Bingham plastic fluids) and a power law exponent, known as the flow behavior index, in addition to the consistency index, similar to viscosity. The fluid will not flow until the shear stress exceeds the yield stress, but when the yield stress is exceeded, the fluid

moves in a "core" or "plug" of unmoving fluid where the yield stress is still greater than shear stress. Figure 15 shows this behavior for flow in a circular pipe or tube of radius *R*.

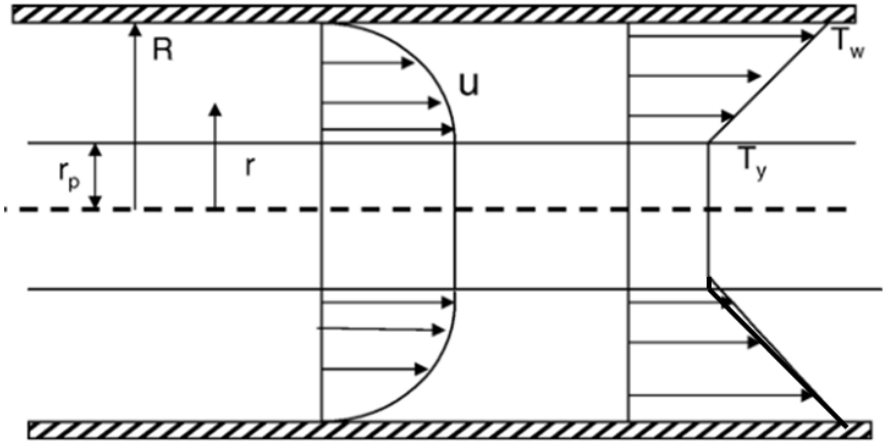

Figure 15: Flow diagram of Herschel-Bulkley flow in a pipe; where *R* is pipe radius, r_p is plug radius, T_w is shear stress at the pipe wall, T_y is the yield stress of the plug, and *u* is fluid velocity. Fluid is moving from left to right (Kelessidis et al., 2006)

The shear stress at the conduit wall controls flow initiation. The shear stress can be calculated for all points in the conduit, but at the wall the shear stress is given as:

$$\tau_w = \frac{R}{2}\frac{\Delta P}{\Delta L}$$

where ΔP is the pressure drop across the conduit and ΔL is the length of the conduit, given it is filled with the Herschel-Bulkley fluid. Flow is initiated when the wall shear stress reaches the yield stress ($\tau_w = \tau_y$), and we rearrange to find the flow initiation pressure drop:

$$\Delta P = 2\frac{\tau_w \Delta L}{R}$$

Herschel-Bulkley fluids flow similarly in a narrow slot geometry, where the slot aperture is much smaller than the slot width. Figure 16 shows the fluid behavior for flow in a slot.

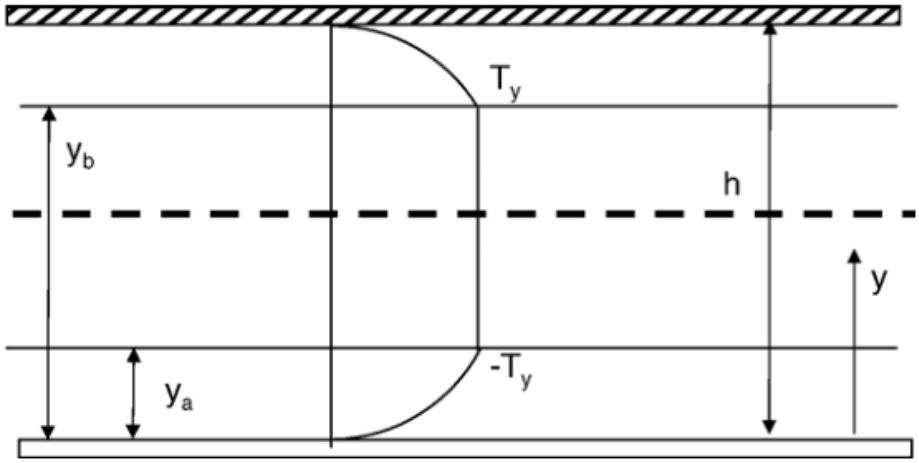

Figure 16: Flow diagram of Herschel-Bulkley flow in a slot; where *h* is the full slot aperture, y_a and y_b describe the plug's thickness, T_y is the yield stress of the plug, and *u* is fluid velocity. Fluid is moving from left to right. (Kelessidis et al., 2006)

Similarly, the shear stress at the slot wall can be rearranged to find the flow initiation pressure drop:

$$\tau_w = \frac{h}{2}\frac{\Delta \mathrm{P}}{\Delta \mathrm{L}} \quad \rightarrow \quad \Delta \mathrm{P} = 2\frac{\tau_w \Delta \mathrm{L}}{h}$$

Analytical solutions have been developed by Kelessidis et al. (2006) and allow for the prediction of flow rate in a tube and slot with Herschel-Bulkley fluids.

Tube: $$q = \frac{\pi\, n}{K^{1/n}} * \frac{\left(\frac{\Delta PR}{\Delta L 2} - \tau_y\right)^{1/n+1}}{1+2n} * \left[\frac{\left(\frac{\Delta PR}{\Delta L 2} - \tau_y\right)^2}{1+3n} + \frac{2\tau_y\left(\frac{\Delta PR}{\Delta L 2} - \tau_y\right)}{1+2n} + \frac{\tau_y^2}{1+n}\right] \qquad (1)$$

Slot: $$q = \left[\frac{wh^{2+\frac{1}{n}}\left(\frac{1\Delta P}{K\Delta L}\right)^{1/n}}{2^{1/n}\left(\frac{1}{n}+1\right)\left(\frac{2}{n}+4\right)}\right] * \left(1 - \frac{\tau_y}{\left[\frac{h}{2}\right]\left(\frac{\Delta P}{\Delta L}\right)}\right)^{1+1/n} * \left[\frac{\frac{\tau_y}{h\left(\frac{\Delta P}{\Delta L}\right)} + \frac{1}{n} + 1}{2^{1/n}\left(\frac{1}{n}+1\right)\left(\frac{2}{n}+4\right)}\right] \qquad (2)$$

where K is the consistency index, n is the flow behavior index (power law index), τ_y is the yield stress, ΔP is the pressure drop, ΔL is the length of the conduit, w is the width of the slot, and h is the aperture of the slot.

3.4.2 Experimental procedures

To inject the polymer dispersion or gel into the tube geometry, a steel accumulator containing polymer dispersion was used. A schematic of the experimental setup can be seen below in Figure 17. Using an ISCO 500D Syringe Pump, (a), deionized water is injected from the pump into one end of the accumulator, (b), moving the piston, and slowly displacing the polymer dispersion on the other end. Water is colored blue while polymer dispersion is colored red. The polymer dispersion travels into the flow conduit, (c), and then exits the core at atmospheric conditions. There is no reaction between the polymer dispersion and steel inside of the accumulator. To measure the polymer dispersion's injection pressure, a Rosemount 3051C Pressure Transducer, (d), was used.

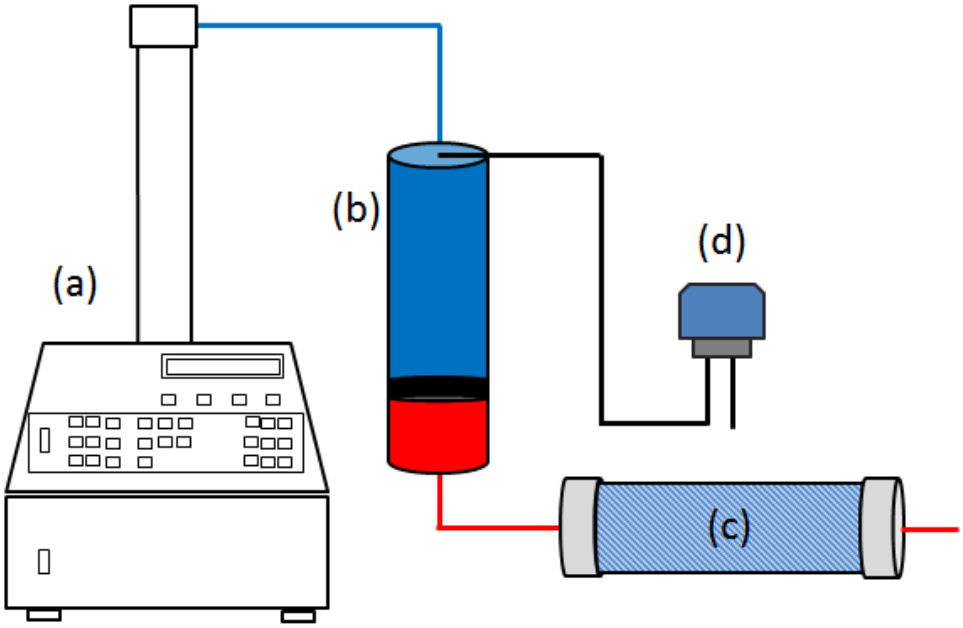

Figure 17: Schematic of setup for injection of polymer dispersion into fractured cement core and effluent collection. Water pump (a), fluid accumulator (b), flow conduit (c), and pressure transducer (d).

The pressure transducer measures the pressure difference of two points. In this case, the flow channels were open to atmosphere at the downstream exit, so the low pressure line of the transducer was also left open to atmospheric conditions during the experiments, allowing the transducer to easily measure the pressure drop across the core. The high pressure end was originally connected to the beginning of the flow tube, but this caused polymer dispersion to enter the narrow pressure lines and, in some cases, the gel's yield stress prevented the injection pressure from being properly transmitted. The high pressure end was then moved to the inlet of the water chamber of the accumulator. Tests showed the pressure required to move the accumulator's piston was negligible.

The slot geometry between the two plastic plates, however, is preceded and followed by plastic core end caps, which hydraulically connect the plastic slot to injection and outlet flow lines. These lines are typically 1/8" plastic or steel tubing. Therefore, significant pressure losses were incurred between the accumulator and slot inlet, as well

as the slot outlet and atmosphere. Holes were drilled to the immediate inlet and outlet of the fracture, tube fittings were installed, and the pressure transducer was connected to these pressure taps. A schematic of the slot geometry and the pressure tap location can be seen below in Figure 18. The pressure drop across the slot is then able to be measured accurately, regardless of the pressure losses before or after the slot.

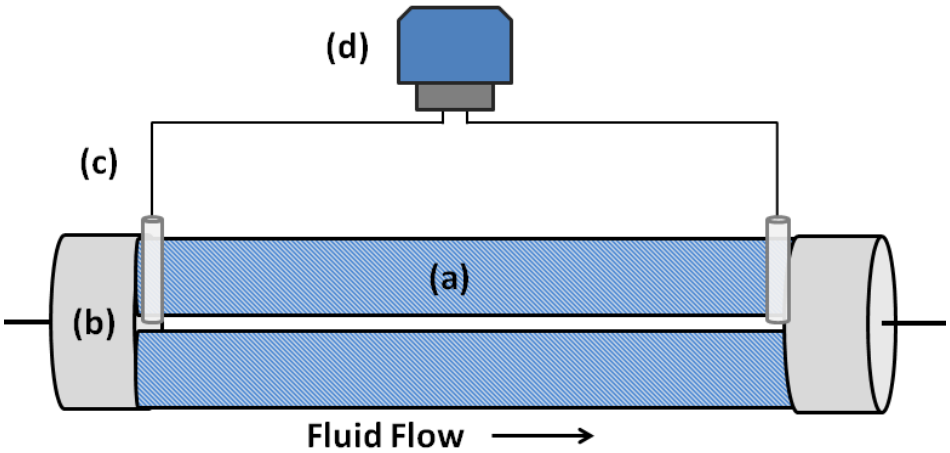

Figure 18: Schematic of plastic-plastic slot geometry with pressure taps at both inlet and outlet endcaps. Plastic plates (a), core endcaps (b), drilled pressure taps (c), and pressure transducer (d).

No chemical or rheological reaction occurred between the polymer dispersion and plastic flow channels. Polymer dispersion was injected through these channels at a known flow rate and the injection pressure was allowed to equilibrate over time so that each flow rate corresponded to a specific injection pressure. The Herschel-Bulkley parameters of the polymer dispersion were measured using an AR-G2 Magnetic Bearing Rheometer. The flow rates in the conduit were monotonically increased in a stepwise fashion after each steady state was reached until the accumulator was emptied of polymer dispersion. The pressure drop at each flow rate was recorded. Using equations (1) and (2) from Kelessidis et al. (2006) and the measured Herschel-Bulkley rheological parameters, an expected flow rate was calculated for each of these pressure drops. The expected flow rate and actual flow rate for each step were compared. The Herschel-

Bulkley flow parameters were then varied to obtain a least squared fit between the actual flow rate into the conduit and the calculated flow rate from equations (1) and (2).

The polymer dispersions that were injected were collected at the exit of the apparatus and the very same polymer was used to determine the rheological properties, ensuring consistent sampling. Care was also taken to insure that air bubbles were not allowed into the polymer end of the accumulator, as bubbles traveling through the flow channels drastically reduced the injection pressure and increased the equilibration time. At high injection pressures and low flow rates (i.e. very viscous gels) the air bubble problem is exacerbated by the volumetric expansion of the bubble, clearing the flow channel.

3.4.2 Comparison of Results

Polymer dispersion (3 wt% Carbopol 934, 0 wt% NaCl) was injected into a 12" long, 1/8" OD metal tube with an inner diameter of 1.8 mm. The Herschel-Bulkley parameters (yield stress, τ_{yield}; consistency index, K; and power law index, n) of the polymer dispersion given by the AR-G2 Magnetic Bearing Rheometer and the experimental best fit for flow in a tube are shown in Table 6. The rheometer values for consistency index and yield stress are slightly higher, while the power law index is slightly lower.

	Rheometer Values	Best Fit – Tube Flow
Yield Stress (τ_{yield})	17.8	14.4
Consistency (K)	5.8	5.5
Power Law Index (n)	0.40	0.45

Table 6: Herschel-Bulkley parameters for polymer dispersion from rheometer (AR-G2 Magnetic Bearing Rheometer) and the best fit values for flow in a metal tube.

Each actual flow rate and calculated flow rate data point correspond to a single pressure drop. These rates can thus be plotted together to show the quality of the fit between the two. This comparison is shown in Figure 19. The "Calculated Flow Rate" data on the y-axis of the graphs are calculated using the Herschel-Bulkley parameters from either the rheometer values (left panel) or the best fit parameters (right panel).

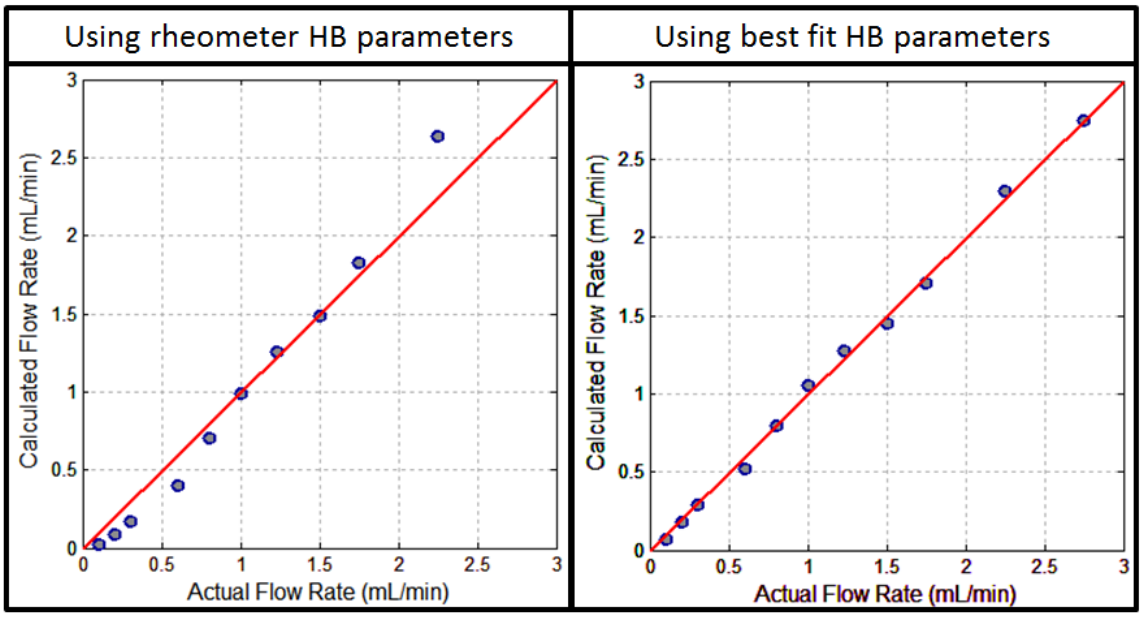

Figure 19: Calculated flow rate vs actual flow rate for polymer dispersion in a tube. Left: calculated flow rate using rheometer Herschel-Bulkley parameters from Table 6. Right: calculated flow rate using best fit H-B parameters from Table 6. Pressure drop data acquired during polymer injection used in calculated flow rates.

Ideally, the data would fall on a 1:1 line, as shown in red in Figure 19. It can be seen that the fit is improved by using the best fit Herschel-Bulkley parameters, though the parameter values are quite similar between the two graphs.

The best fit Herschel-Bulkley parameters from the polymer injection into a slot are shown with the rheometer values in Table 7. The same polymer dispersion (3 wt% Carbopol 934 and 0 wt% NaCl) from injection into a tube was used for injection in the

slot. The power law and consistency indices in the two cases are similar, but the best fit yield stress is 50% lower in the best fit case.

	Rheometer Values	Best Fit – Slot Flow
Yield Stress (τ_{yield})	17.8	8.9
Consistency (K)	5.8	5.9
Power Law Index (n)	0.40	0.38

Table 7: Herschel-Bulkley parameters for polymer dispersion from rheometer (AR-G2 Magnetic Bearing Rheometer) and the best fit values for flow in a plastic rectangular slot.

The implications of the yield stress differences are shown in Figure 20. Using the rheometer HB parameters, the calculated flow rate is greater underestimated, causing the data points to fall below the 1:1 red line. This indicates that the polymer dispersion is behaving less viscous (i.e. a higher flow rate for the same pressure drop) during flow in a plastic slot than the rheometer data indicate. The data fit is greatly improved by using the best-fit parameters given in Table 7, indicating that the best-fit parameters are an accurate representation of the rheology behavior of flow in the slot.

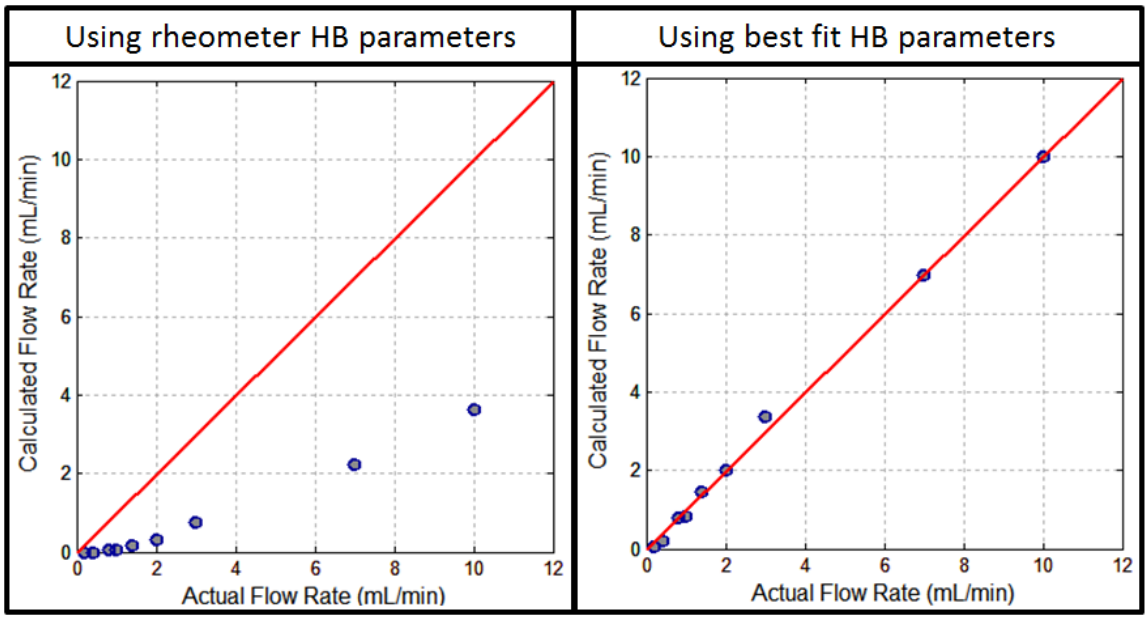

Figure 20: Calculated flow rate vs actual flow rate for polymer dispersion in a slot. Left: calculated flow rate using rheometer Herschel-Bulkley parameters from Table 7. Right: calculated flow rate using best fit H-B parameters from Table 7. Pressure drop data acquired during polymer injection used in calculated flow rates.

	Rheometer Values	Best Fit Tube Flow	Best Fit Slot Flow
Yield Stress (τ_{yield})	17.8	14.4	8.9
Consistency (K)	5.8	5.5	5.9
Power Law Index (n)	0.40	0.45	0.38

Table 8: Experimental rheological parameters taken as best fit from flow in pipes and slots

The power law and consistency indices are fairly consistent between the three cases, but the rheometer values for yield stress are 25% higher than the pipe flow best fit yield stress and 100% higher than the slot flow best fit yield stress. One possible explanation for the discrepancy in actual vs. predicted flow rate is the incorrect assumption of a no-slip boundary at the pipe/slot walls. The channels through which polymer flowed were smooth faces in which slip could occur, allowing the polymer to move with less drag (i.e. less pressure loss) and also would cause the polymer to move at pressure gradients below the flow initiation pressure gradient. The pipe flow yield stress

is only slightly reduced because the tube was made of steel, whereas the slot flow yield stress is greatly reduced because the slot surfaces were made of plastic.

Another possibility is that any air bubbles in the container could go into solution during high pressure conditions. In some cases, moving polymer in the channels was seen to have no bubbles present, but when the accumulator's back pressure was removed, reducing the injection pressure, small air bubbles appeared in the tube/slot, despite no polymer or air going into the channel. The rheometer measurements are taken at standard pressure, 14.7 psia. The presence of air in solution would decrease the observed viscosity, reducing the polymer's consistency and yield stress.

Another factor that likely contributes to the lack of correlation in the slot geometry data is defects in the construction of the flow channel. Irregularities in the aperture, such as one side being narrower/wider than the other or an increase/decrease in aperture with length, could have a strong impact on the polymer's behavior. These construction errors would not be present in the tube geometry, as the tube was pre-constructed and is almost perfectly uniform, explaining the better fit in the tube conduit. Similarly, the radius of the tube is known (given by the manufacturer), whereas the aperture of the slot is back-calculated from the flow rate and pressure drop data during water injection experiments, introducing error and lumping geometric irregularities into the term "effective hydraulic aperture." The Herschel-Bulkley flow equations in a slot are very sensitive to slot aperture and the flow initiation pressure is linearly dependent on the slot aperture, where a wider aperture results in a lower FIP. Therefore, any irregularities in aperture will significantly impact the pressure drop, which in turn results in inaccurate calculated flow rates.

3.4.3 Bubble Flow in Slot Phenomena

While trying to determine the actual flow channel during polymer injection into cement-plastic plate cores, both small particles (mainly glitter) and small bubbles were used, either one at a time or together. When bubbles and glitter were both present in the polymer flow through the fracture, the bubble's velocity in the channel was clearly and consistently higher than the glitter particle's. Additionally, larger bubbles clearly moved quicker than small bubbles. Initially, this was thought to be due to gravitational effects, as the polymer flow was upwards and the bubble density is much less than the polymer or glitter particle's density. However, the same phenomenon was observed when polymer flow was reverse, injecting from the top to the bottom, so that gravity effects would result in bubbles moving slower than the polymer dispersion and glitter particles, as well as injecting horizontally such that gravity effects were eliminated.

Bubbles were added to the injection inlet by briefly stopping flow, opening a valve to the inlet, injecting air using a hypodermic needle, then closing and resuming flow as quickly as possible, disrupting the flow as little as possible. Small particles of glitter were added to the polymer dispersion in order to determine its actual velocity in the fracture and to provide a reference for which to compare the bubble velocities. A white background was placed behind the clear plastic-plastic slot to increase the visibility of both particles and bubbles. The slot was then filmed with a high definition camera on a tripod.

Still images were captured from these videos and Figure 21 shows a time lapse of a small and large air bubble in the slot during polymer injection. The core was held horizontal to eliminate gravity effects in the direction of injection (hence why the bubbles both appear at the top part of the slot) and polymer dispersion was injected at a constant rate. The small bubble highlighted in red is moving at the same speed as the glitter

particles suspended in the polymer dispersion, and indicating that the small bubble does not move faster than the fluid. The large bubble highlighted in yellow, however, moves faster than the small bubble and suspended particles, and can be seen overtaking the smaller bubble between 5 and 12 seconds.

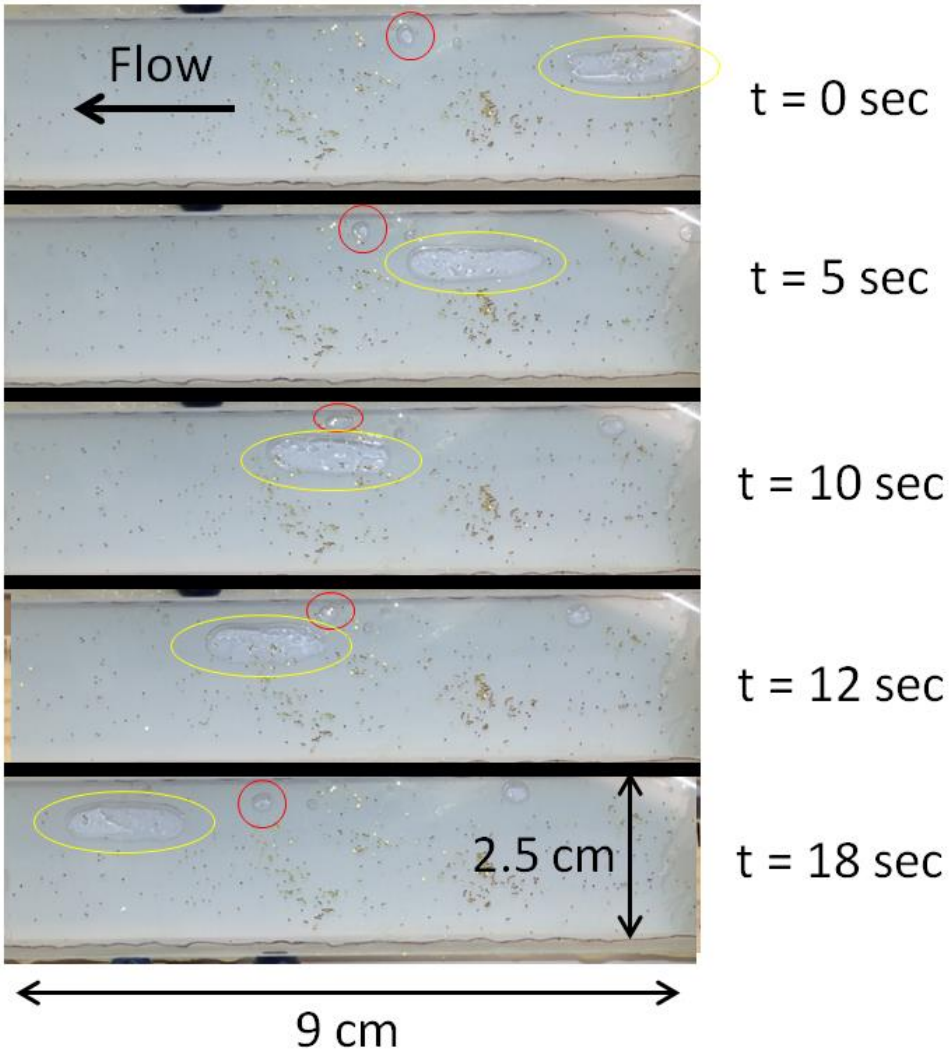

Figure 21: Time lapse of bubble and glitter movement during polymer flow in a clear plastic-plastic slot. Small red circle highlights the small air bubble that is moving at the same speed as polymer flow, while the large yellow circle highlights the large air bubbles, which moves faster than the polymer flow and overtakes the small air bubble.

This experiment was repeated was many different bubble sizes, flow rates, and injection directions. In every case, small bubbles with diameters on the order of millimeters traveled through the slot at the same velocity as the surrounding polymer dispersion and suspended particles. Large bubbles with diameters above some threshold of around 1 cm had increased velocities, regardless of flow rate or injection direction, and were elongated in the direction of flow. This elongation can be seen in the large bubble highlighted in yellow on Figure 21. Above the size threshold necessary for increased velocity it was also observed that the largest bubbles had the largest velocity increase, while medium bubbles has a moderate velocity increase. A possible mechanism for this behavior is discussed in Appendix C.

Chapter 4 Polymer Injection and Displacement Experiments

This chapter introduces the apparatus and methods for injecting polymer dispersion into cement fractures and describes the results of these experiments. The main objective of these experiments is to determine the ability of polymer dispersions to gelate in cement fractures and prevent subsequent fluid flow. The pressure drop across the fracture and pH of the polymer effluent are measured and are used to develop hypotheses on the complex flow of the Herschel-Bulkley, pH triggered polymer dispersion and its reactive transport through conduits with cement walls. Results from these experiments indicate that the polymer dispersion, without additives or the use of a pre-flush, cannot consistently block leaks or fluid flow through cement fractures.

Section 4.2 consists of the data collected from polymer injection experiments into cement-cement fractured cores and discussion of the results. Because the data were inconclusive, a new core apparatus was implemented to allow for visual inspection of the fracture during and after polymer injection. These experiments are shown and discussed in section 4.3.

4.1 Experimental Methods and Setup

4.1.1 Polymer Injection

A schematic of the experimental setup for polymer injection into fractured cement cores is shown below in Figure 22. Similar to polymer dispersion injection into the plastic plate slot, injection into a cement core required the use of the ISCO Syringe Pump (a), a steel accumulator (b), a cement fracture core (c), and a pressure transducer (d). Additionally, a pH probe (e) samples the pH of the polymer effluent as it comes out from the cement fracture and is collected with an effluent collector (f). The pressure transducer lines leading to the fractured cement core are both elevated to the same height

in order to negate any possible hydrostatic pressure effects in the pressure lines. Together with the initial polymer dispersion, the effluent pH can be used to calculate the total reaction occurring inside the fracture. This pH can also be used to estimate the polymer's rheological properties, given the polymer has been characterized at several pH values.

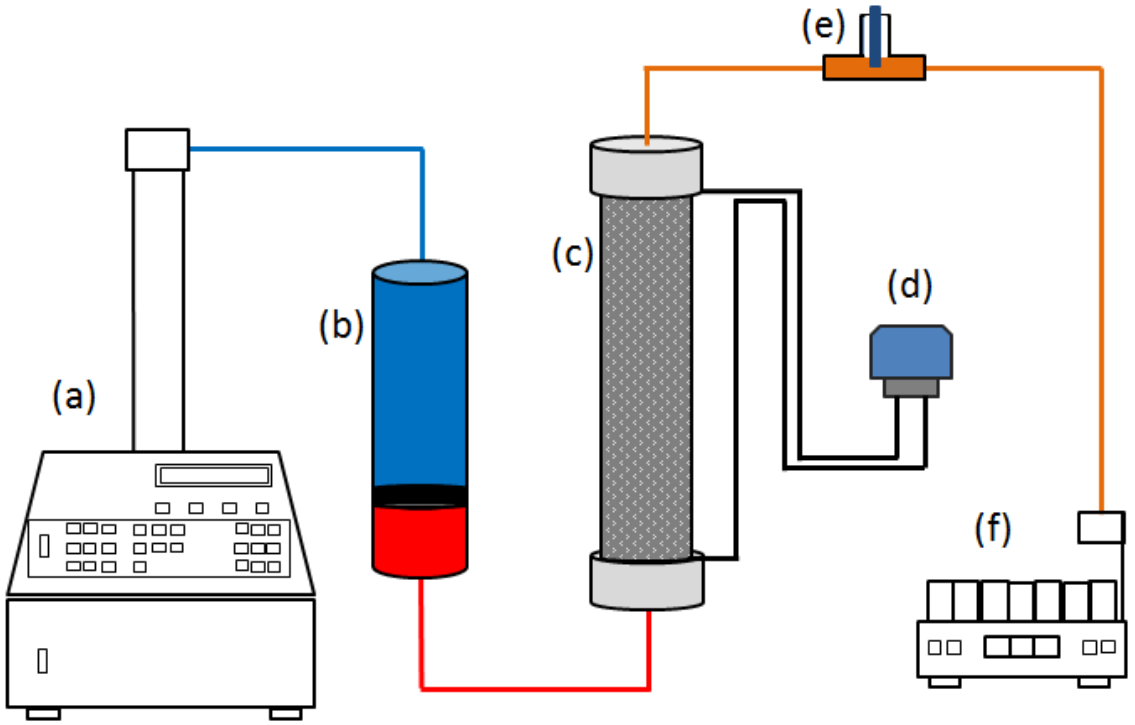

Figure 22: Schematic of setup for injection of polymer dispersion into fractured cement core and effluent collection. Water pump (a), fluid accumulator with polymer dispersion (b), cement fracture core (c), pressure transducer (d), pH probe (e), and effluent collector (f).

There exists a "dead volume" of tubing and valves between the cement core outlet and the pH probe, meaning that the pH of any given polymer gel sample is measured some set time after the polymer sample traveled through the cement fracture and registering the pressure drop across it. Dead volume was minimized and quantified, and all experiments were operated at a fixed injection rate in order to keep this time difference constant. The time difference was measured by recording the time between

when the polymer dispersion exited the fracture and when it first contacted the pH probe. This time difference was then used to time-shift the pH data, such that any one time corresponds to the same fluid sample, both in pressure drop and pH data.

The flow rates of each polymer injection experiment are expressed in a nondimensional "fracture volumes" of injection. A fracture volume is defined below

$$FV = hwL$$

where h is the fracture aperture, w is the fracture width, and L is the fracture length. This allows for simple comparison between polymer injection experiments in cement fractures with different fracture apertures and volumes. The flow rates in experiments are varied between 0.016 FV/min and 1 FV/min. These values correspond to a 64 minute and 1 minute residence time, the amount of time a sample of polymer dispersion remains in the cement fracture, respectively.

4.1.2 Gel Strength Experiments

After polymer injection, all cores are undisturbed for a given period of time, usually between 24 and 96 hours (1 to 4 days) to ensure that the majority of the polymer-cement reaction has gone forward, so that pH has increased to neutral or even basic conditions and the polymer is therefore fully gelled. After this shut-in period, brine or deionized water was used to displace the gel inside the fracture. Brine or DI water was put into contact with the inlet of the fracture and pressure was slowly increased while the outlet of the fracture was open to atmospheric pressure. The injection pressure was recorded by a pressure transducer with the high-pressure line connected to the displacing fluid and the low-pressure line open to atmosphere. Inlet and outlet endcaps are cleaned of any remaining polymer gel in order to ensure that the pressure required to displace gel from the fracture is recorded, as opposed to the pressure required to displace gel through

the inlet/outlet. As previously discussed, the poly(acrylic acid) polymer gel displays Herschel-Bulkley flow properties. Therefore, the gel will remain stationary in the fracture until the applied shear stress exceeds the gel's yield stress. For rectangular slot geometry (where slot width >> slot aperture), the shear stress is greatest at the walls of the slot and is analytically known (Kelessidis et al.2006):

$$\tau_{wall} = \frac{h}{2}\frac{\Delta P}{\Delta L}$$

where h is the aperture of the slot, ΔP is the pressure drop across the slot, and ΔL is the length of the gel filled slot. Therefore, the gel will flow and be displaced under the following conditions:

$$\frac{\Delta P}{\Delta L} > 2\frac{\tau_{yield}}{h}$$

where τ_{yield} is the gel's yield stress. Essentially, the pressure drop required to displace the gel is directly proportional to the yield stress of the gel and inversely proportional to the aperture of the fracture. It should be noted that this pressure gradient is independent of slot width, and therefore is valid regardless of the width of gel displaced. In a circular conduit or pipe, the polymer gel will be displaced under the following conditions (Kelessidis et al., 2006):

$$\frac{\Delta P}{\Delta L} > 2\frac{\tau_{yield}}{r_{conduit}}$$

It is necessary to investigate the displacement behavior of the polymer gel in a rectangular slot. Based on experiments reported below, two possibilities are of interest: either the polymer gel will be displaced from the slot uniformly (i.e. across the entire width of the slot), or a small circular flow channel will form in the gel. These possibilities are shown below in Figure 23.

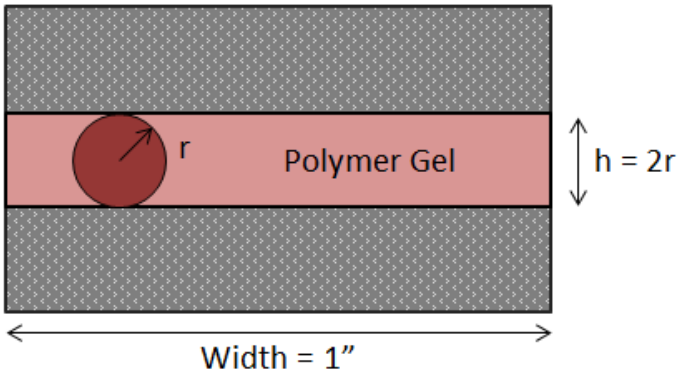

Figure 23: Diagram of possible geometry of gel displacement by injected water. Flow is normal to the page. Light red indicates polymer gel filling a rectangular slot in a cement-cement fracture, while the dark red circle indicates a possible displacement conduit within the gel.

Comparing the displacement conditions of the two geometries, it is apparent that the pressure gradient required to displace the polymer gel in the entire slot uniformly is half the gradient required to displace gel in a circular conduit, assuming that the boundary between the moving cylinder gel and stationary gel surrounding the cylinder is a no-slip boundary. This is shown in the following equation:

$$2\frac{\tau_{yield}}{h} = \left[2\frac{\tau_{yield}}{(2r_{conduit})}\right]_{rectangular} < \left[2\frac{\tau_{yield}}{r_{conduit}}\right]_{circular}$$

This comes from the fact that the radius of the largest circular conduit that can be inscribed in the slot is half the slot's aperture. Therefore, given that the gel's strength is homogeneous throughout the slot, polymer gel will be displaced from the entire slot. On the other hand if the slot has variable aperture, then the widest part of the slot would have the smallest pressure gradient for gel displacement, and non-uniform displacement could more easily arise. Moreover the displacement process is self-reinforcing: partial displacement reduces the length ΔL across which the pressure drop is applied, increasing the gradient locally and thus localizing the displacement.

With the aperture of the slot known and polymer rheology characterized, the minimum placement and displacement pressure gradient can be predicted and later compared to experimental data. During the displacement experiments, the recorded pressure data generally increase as pressure is slowly applied, then drop sharply as the displacing fluid breaks through or displaces the polymer gel.

4.1.3 Gel Longevity Experiments

The polymer gel's longevity in the cement fractures is tested in a similar fashion to the gel strength experiments, discussed in Chapter 4.1.2, except the pressure gradients are held constant and held consistently for long periods of time (days, weeks, months) to discover how long the gel effectively seals these cement fractures. The long term effects of cement, brine, and applied pressure – conditions likely encountered in real world wells – are investigated. All experiments, however, were conducted at room temperature.

After polymer is injected into a cement fracture, the polymer is undisturbed for 24 to 96 hours, the endcaps are cleaned of residual polymer, and the core is connected to a pressure manifold. The pressure manifold consists of an elevated container of displacing fluid (brine, DI water, etc.) that is hydraulically connected to a series of valves leading to cement cores. A schematic of this pressure manifold is shown below in Figure 24, shown with a container of brine (a), four cement fracture cores (b), and the outlet of the cores in a U-tube setup. This pressure difference is supplied by the hydraulic potential difference of the container and core and is applied simultaneously to multiple cement cores, allowing for multiple experiments to be run simultaneously and continuously.

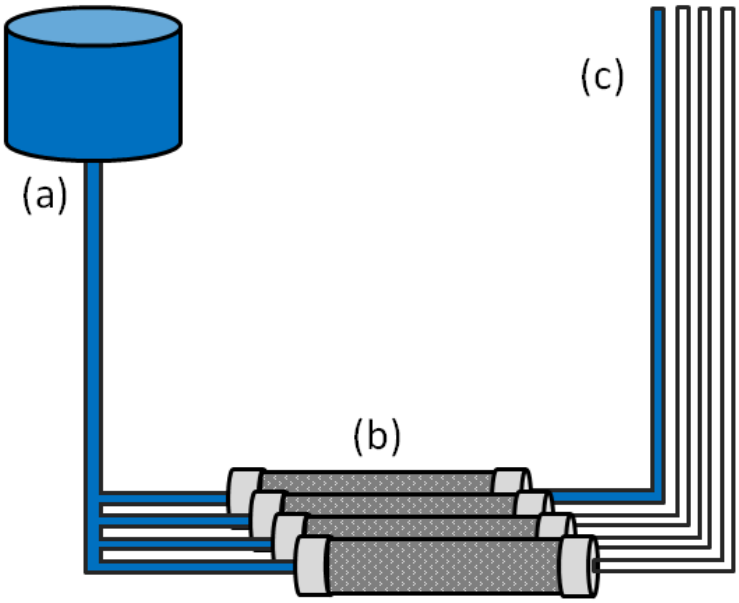

Figure 24: Schematic of pressure manifold for long term pressure testing of multiple cement fracture cores. Brine container (a), four cement fracture cores (b), and outlet U-tube (c) with one core broken through (blue fluid in downstream tube).

When the polymer gel within a fractured core is no longer able to hold back pressure from the brine, then brine is able to leak through to the core outlet (cf. Figure 24). The outlet of each core is connected to tubing that rises to the height of the brine container, thereby making a U-tube setup. This allows for visual confirmation that a core has failed, identification of which core has failed, and also does not disrupt the pressure being applied to the other cement fracture cores.

4.2 Cement-Cement Fractures

4.2.1 Cement Core Construction and Preparation

The first step in preparing the fractured cement cores is the casting of the cement core. Cement slurry was prepared by mixing deionized water with Class H cement in a 0.38:1 water to cement weight ratio with no additives. Slurry was poured into 6” long by 1” diameter plastic cylinders. Samples were allowed to cure for at least 30 days, insuring adequate cement hydration.

After curing, some cement cores were laid down into the load frame one at a time while still inside the plastic sheath. A schematic of the Brazilian test can be seen in Figure 25. Application of the load constitutes the Brazilian test: at sufficient load, the core fails in tension, creating axial tensile fractures along the length of the core. The fracture often has deviated fracture paths at either end. This typically fractures the core into two pieces, though the fracture between the two pieces is rough and irregular. The plastic sheath serves to apply enough confining stress to prevent excessive secondary fracturing, shattering, and more divergent fracture propagation. These tensile fractures tend to have some tortuosity, and fluid flow distribution in the fracture will be heterogeneous and rather unpredictable, though the overall flow rate can be characterized reasonably well in terms of an equivalent uniform slot aperture. Cement fracture cores made in this way will be referred to as "cement-cement Brazilian" cores.

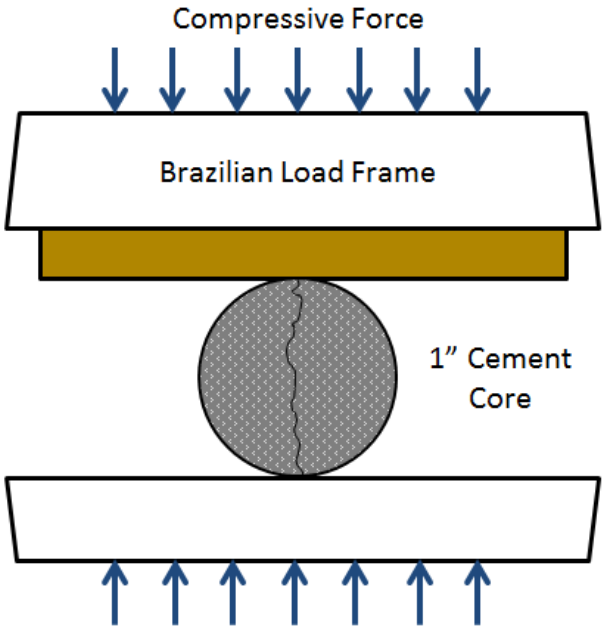

Figure 25: Diagram of Brazilian load test on cement cylinders. Compressive force is applied to create axial tensile fractures along the length of the core.

To make a cement-cement fractured core, the cores with tensile fractures had both halves put back together with some offset in the direction of the length of the core. This was done in order to prevent the core halves from mating and thus closing the fracture and preventing subsequent fluid flow. The offset halves were then epoxied together along the edges of the length of the fracture and epoxied to core endcaps at both ends. The endcaps are then taped and sealed, then the whole core is put into a plastic tube into which a less viscous epoxy is poured until the entire core is submerged. The epoxy is allowed to cure for at least 24 hours. At this point the core will finally be totally sealed from atmosphere, except for the two endcaps. The tape covering the endcaps is removed and Swagelok tubing adapters are screwed into the endcaps, connecting the core to the pump system.

To make fractures that were more homogeneous and had flatter surfaces, cement cores were sawed in half using a rock saw. The rock saw used water, instead of mud or oil to prevent inhalation of dust, which does not affect the cement. The two core halves were cleaned and sealed together using the same epoxy method as described above for tensile fractured cores. These cores will be referred to as "cement-cement sawed" cores.

4.2.1.1 Determination of Effective Hydraulic Aperture

Once the cement core has been constructed, it is necessary to determine the dimensions of the fracture. In tensile fractured cores, the fractures will be heterogeneous and the true aperture will vary with length and width throughout the core, but the fracture can be approximated as a slot with a single aperture. By flowing fluid through the core at various flow rates, the pressure drop across the fracture can be measured and together the "hydraulic aperture" can be calculated. This aperture, B, is calculated using the following equation:

$$B = \left[\frac{12\mu QL}{W\Delta P}\right]^{\frac{1}{3}}$$

where μ is the fluid viscosity, Q is the volumetric flow rate, L is the length of the fracture, W is the width of the fracture, and ΔP is the pressure drop across the fracture. By measuring the dimensions of the core beforehand and by injecting water (with a known viscosity of 1 centipoise), the aperture is found. During water injection into the cement fractures, the flow rate is known and determined set by the pump, while the inlet and outlet pressures are measured by pressure transducer. For each flow rate, the water is injected for at least 30 seconds, then the pressure drop for the flow rate is averaged. Afterwards, the pump is turned off and the zero flow rate pressure drop is recorded for several minutes and averaged. A small, nonzero pressure drop is recorded even when no flow occurs due to static experimental pressures and the resolution of the pressure transducer. The average static pressure drop is then subtracted from the entire pressure drop data, effectively removing these static effects. An example of the pressure response during a permeability test is shown below in Figure 26.

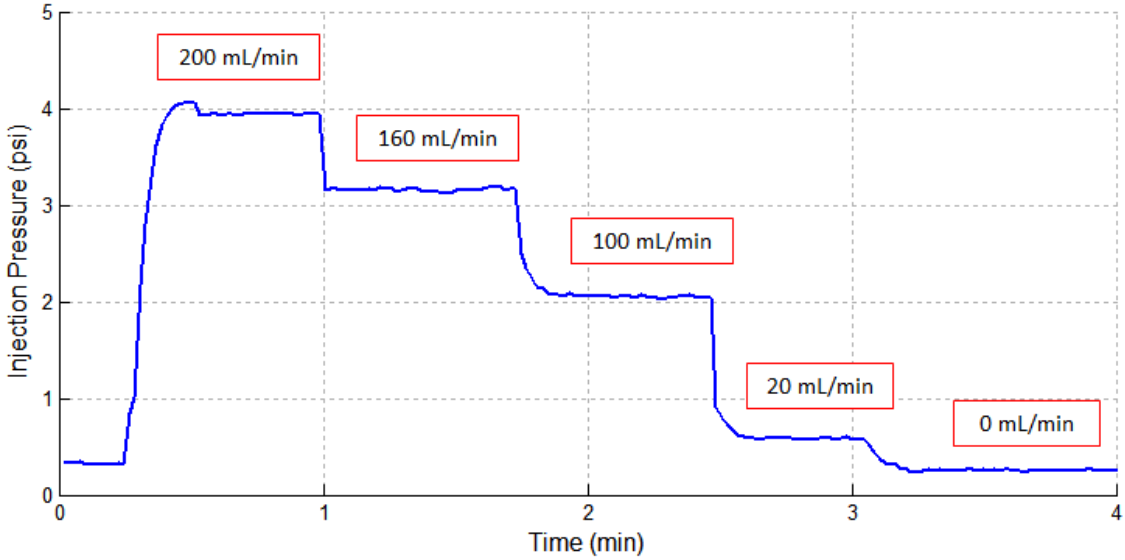

Figure 26: Example of pressure drop during permeability test at various flow rates. The nonzero pressure at a flow rate of 0 mL/min (late time) is an offset which is subtracted from all measurements of pressure during an experiment.

The flow rates are always varied from high to low, as the highest flow rate has the highest pressure, which has the tendency to compress and liberate any bubbles that have accumulated in the fracture. This can be seen during the first part of the 200 mL/min flow period, where the pressure spikes, then decreased by about 0.1 psi. The pressure is lowered when all the bubbles in the fracture or at the inlet are forced out of the system. This manifests itself in a slight pressure decrease from the initial zero flow period to the zero flow period after the other rates.

It is possible for two different cores to have the same effective hydraulic aperture, yet different fracture volumes. This arises due to the volume of a fracture being linearly related to the fracture aperture, while the pressure drop through a fracture during water injection is related to the cube of the fracture aperture. The effect is especially seen in cement-cement Brazilian fractured cores, where the flow channel significantly narrows and widens as a function of length through the core. Cement-plastic plate Brazilian fracture cores have similar apertures, as the flat plastic plate removes much of the

fracture aperture variations. Cement-plastic plate sawed cores have nearly identical volumetric and hydraulic apertures.

4.2.1.2 Necessity of Vacuum Saturating Cement Cores

Although cement is generally thought of as impermeable, it is in fact permeable to air and water and can have porosities up to 22% (Huerta 2013). During core preparation, air easily fills the cement pore space and replaces small amounts of evaporated water, which is actually desirable due to the adverse effects of water on epoxy. Because cement is preferentially wetting to water over air, water will spontaneously imbibe into the cement matrix, displacing the air until the air pressure is high enough to hold back the water's capillary pressure. When water imbibes from the cement's fracture face, air becomes trapped in the matrix away from the fracture. The compressibility of the air pocket can interfere with accurate pressure measurements during water or polymer injection.

To verify this compressibility effect, Core 6F-5 was prepared and saturated with deionized water without the use of a vacuum pump. The high pressure line of the pressure transducer was connected to the core while the low pressure line was open to atmosphere, giving the pressure inside the fracture. Water was slowly injected into the core to build up pressure, then stopped when 40 psi was reached. The pressure of the fracture is given in Figure 27 below.

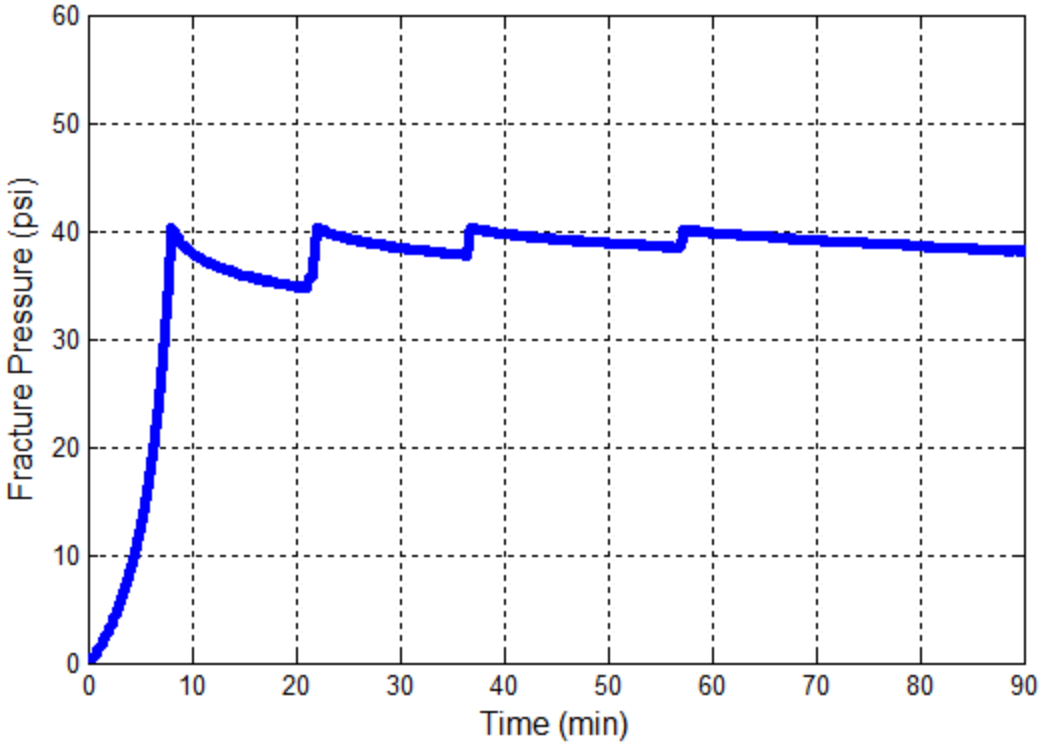

Figure 27: Pressure buildup/falloff tests of Core 6F-5 show repeated declines due to compressibility of air in cement matrix. Local maxima correspond to the moment of shut in, while local minima correspond to the moment injection was restarted.

Though the inlet and outlet were closed after 40 psi was reached, the pressure slowly declines and reaches an asymptote. The cement matrix air compresses and relieves some pressure from the fracture, but does so slowly due to the low cement permeability. Additional water was injected at 20 minutes until the pressure reached 40 psi, then was shut in again. This process was repeated several times, as indicated by the abrupt increases in pressure to 40 psi. After each step, the pressure decline became slower, indicating that the air pressure was reaching equilibrium with the fracture pressure. To verify the hypothesis, the pressure was then decreased and the response is shown in Figure 28.

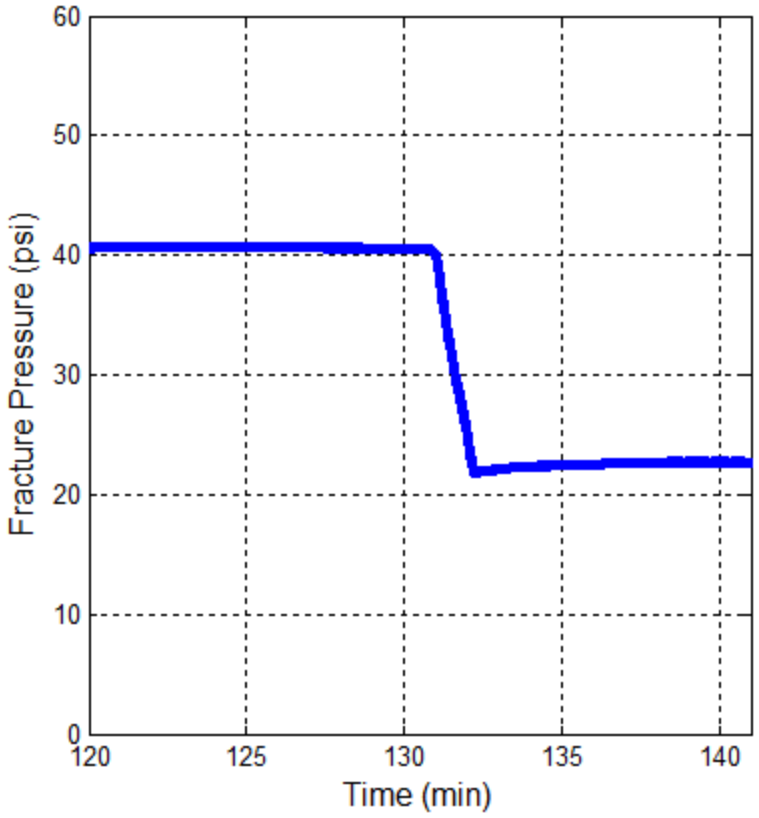

Figure 28: Pressure falloff test of Core 6F-5, conducted after series of buildups in Figure 27, shows slow buildup due to compressibility of air in cement matrix

The pressure had reached equilibrium at 40 psi and pressure was bled off down to 22 psi. The core inlet and outlet were closed, yet the pressure in the fracture slowly increases to 23 psi. The air pressure from inside the cement matrix, which had reached equilibrium at 40 psi, forced water back into the fracture, increasing the fracture pressure slightly. To prevent this pressure adjustment, later cores were vacuum saturated.

After the core was built and the epoxy allowed to harden, the fracture was evacuated of air using a vacuum pump for 24 hours. After vacuum, deionized water was introduced without any air entering the system. Without vacuum, air would remain in the cement matrix and would compress when the fracture water pressure increased,

skewing future data. The permeability of cement matrix is very low, so the question arises of whether 24 hours is adequate vacuum time, but it was concluded that there is almost no difference between 24 and 48 hours of vacuum. A similar pressure test was run on Core 6F-9 and is shown in Figure 29.

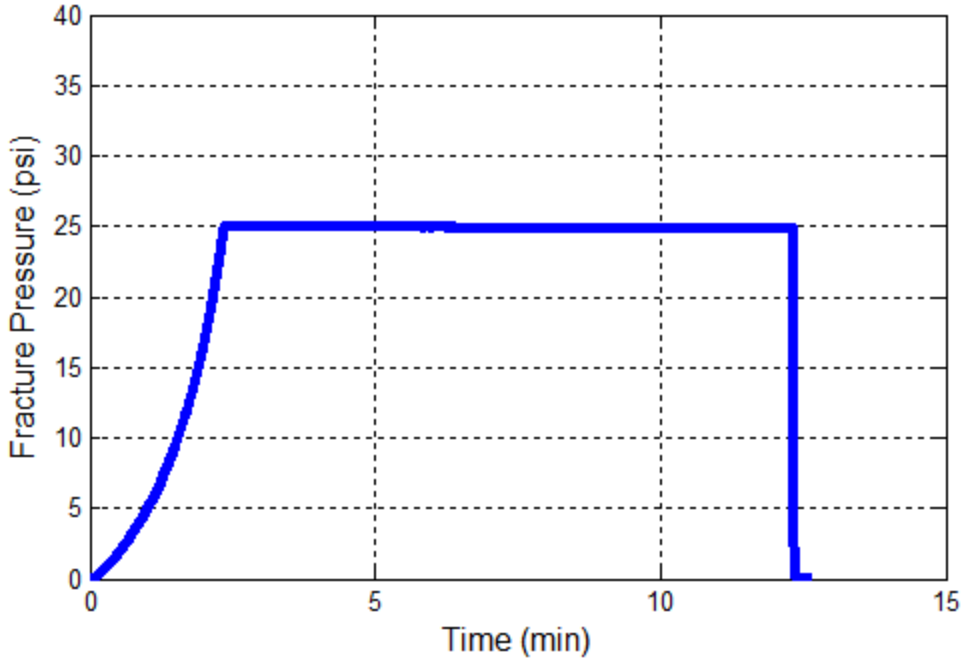

Figure 29: Pressure buildup/falloff test of Core 6F-9; pressure stays constant due to vacuum saturation of the core, which removed air from cement matrix.

Again, water was injected slowly until 25 psi was reached, then shut in. The pressure response is clearly more constant than Core 6F-5. There was some minor decrease in pressure, but it was determined to be an acceptable loss and at a rate orders of magnitude less than the pressure losses observed in cores that were not saturated under vacuum.

4.2.2 Apparent Viscosity of Reactive Polymer in Fractures

As discussed in Chapter 3.1, Carbopol polymer dispersions are rheologically described as Herschel-Bulkley fluids, a non-Newtonian fluid with a yield stress (τ_{yield}), consistency index (K), and power law index (n). This causes the shear stress of the fluid to be a nonlinear function of shear rate, shown in Figure 2. To put this terms of fluid flow in a pipe/tube or slot, the pressure drop across the conduit will vary nonlinearly with the flow rate, resulting in an apparent viscosity that also varies with flow rate. The apparent viscosity will also change as a function of the Herschel-Bulkley parameters, τ_{yield}, K, n, which vary as a function of pH. The pH of the polymer dispersion changes as it flows through the cement fracture. Though the apparent viscosity is a function of many variables that change continuously inside the fracture, it is simply calculated from measurements during an experiment with only the known slot dimensions (width (W), length (L), aperture (B)), pressure drop (ΔP), and flow rate (Q). The following equation, previously used to measure the slot's aperture when injected with water, is rearranged to solve for apparent viscosity

$$B = \left[\frac{12\mu_{apparent}QL}{W\Delta P}\right]^{\frac{1}{3}} \qquad \rightarrow \qquad \mu_{apparent} = \frac{B^3 W\Delta P}{12QL}$$

The polymer rheology is always changing as a function of time and length along the core. The slot aperture changes with length, due to irregularities created during slot construction, as well as time, due to buildup of polymer gel and/or syneresed polymer on the slot walls. The apparent viscosity lumps these factors together and gives a single, average value that describes the viscous forces present in the fracture that allows easy comparison of the intrinsic polymer properties between experiments with different aperture, flow rate and/or pressure gradient. Figure 30 shows calculated values of flow rate and apparent viscosity as a function of pressure drop in a polymer injection

experiment in a slot. The lowest pressure shown is the flow initiation pressure – any pressure drop below this value corresponds to immobile polymer. The rheological properties of the polymer are constant, i.e. no reaction with cement occurs.

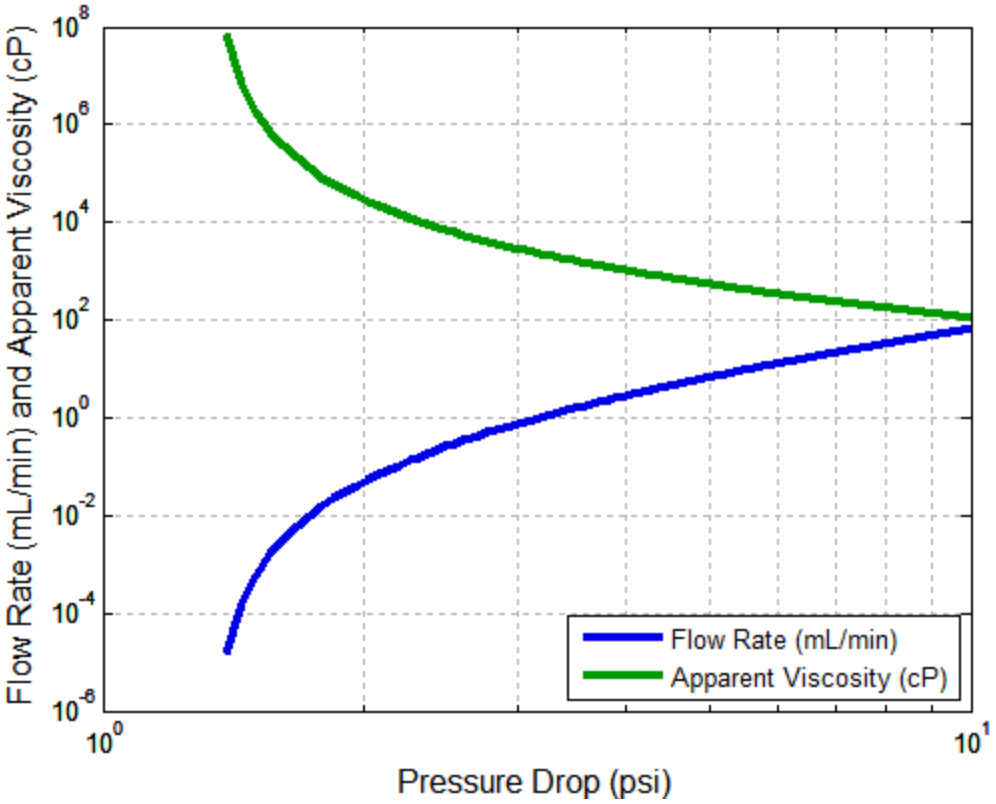

Figure 30: Simulated flow rate (blue curve) and apparent viscosity (green curve) as a function of pressure drop on a log-log plot. The core dimensions were a 500 micron aperture, 6" by 1" rectangular slot. Polymer rheology parameters were typical of 3 wt% Carbopol 934 with 0 wt% NaCl at pH 2.5 (τ_{yield} = 15 Pa, K = 5 Pa-s, n = 0.4). Flow initiation pressure is 1.33 psi, below which the apparent viscosity is infinite and the flow rate is zero.

At pressures near the flow initiation pressure, the apparent viscosity is very large, resulting in a very small flow rate. However, a 50% increase in pressure drop to 2 psi decreases the apparent viscosity by a factor of nearly 100. The polymer "thins" out with the increased pressure drop, resulting in a lower apparent viscosity, which in turn causes

the flow rate to increase inversely. This behavior is due to the power law index being less than unity, meaning that the polymer dispersion is a shear thinning fluid.

The pressure data gathered during polymer injection into fractured cement cores can be used to calculate the apparent viscosity. In Figure 30, the flow rate was not constant, but was directly calculated from pressure drop. The flow rate increases much faster than the pressure gradient, thereby reducing the apparent viscosity as pressure drop increased. But if flow rate is held constant, as is the case in most polymer injection experiments, an increasing pressure drop corresponds to an increasing apparent viscosity in a linear relationship. This behavior is shown in Figure 31 for several flow rates, where the apparent viscosity decreases as flow rate increase for a given pressure drop.

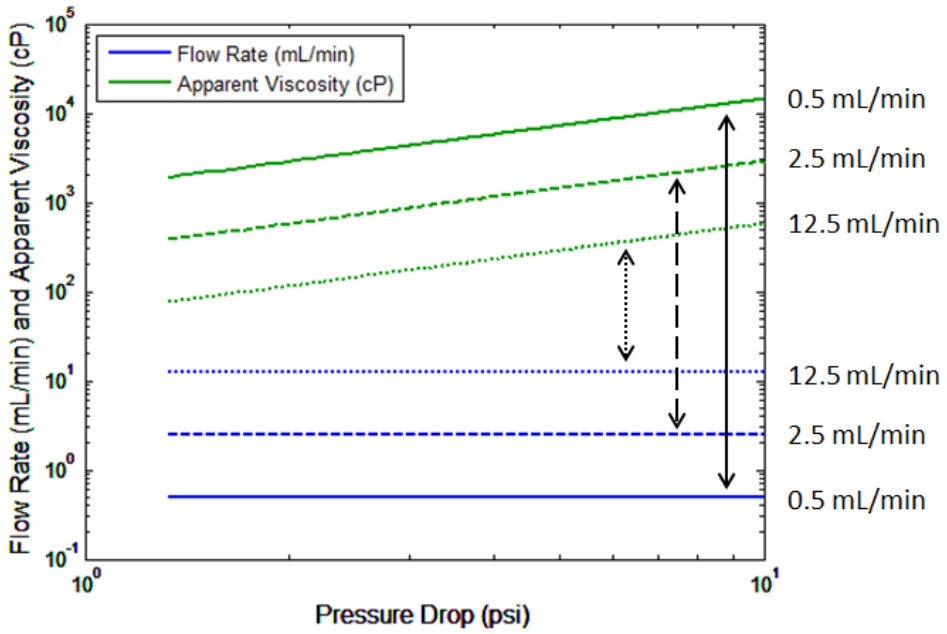

Figure 31: Calculated apparent viscosity (green) as a function of pressure drop on a log-log plot. Flow rate (blue) is held constant at 0.5, 2.5, and 12.5 mL/min. The core dimensions were a 500 micron aperture, 6" by 1" rectangular slot. Polymer rheology parameters were typical of 3 wt% Carbopol 934 with 0 wt% NaCl at pH 2.5 (τ_{yield} = 15 Pa, K = 5 Pa-s, n = 0.4). Flow initiation pressure is 1.33 psi, below which the apparent viscosity is infinite and the flow rate is zero.

In actual polymer injection experiments, the pressure drop data can be converted to equivalent apparent viscosities. For example, the pressure data from Core 6FP-3 is converted into equivalent apparent viscosity and shown in Figure 32.

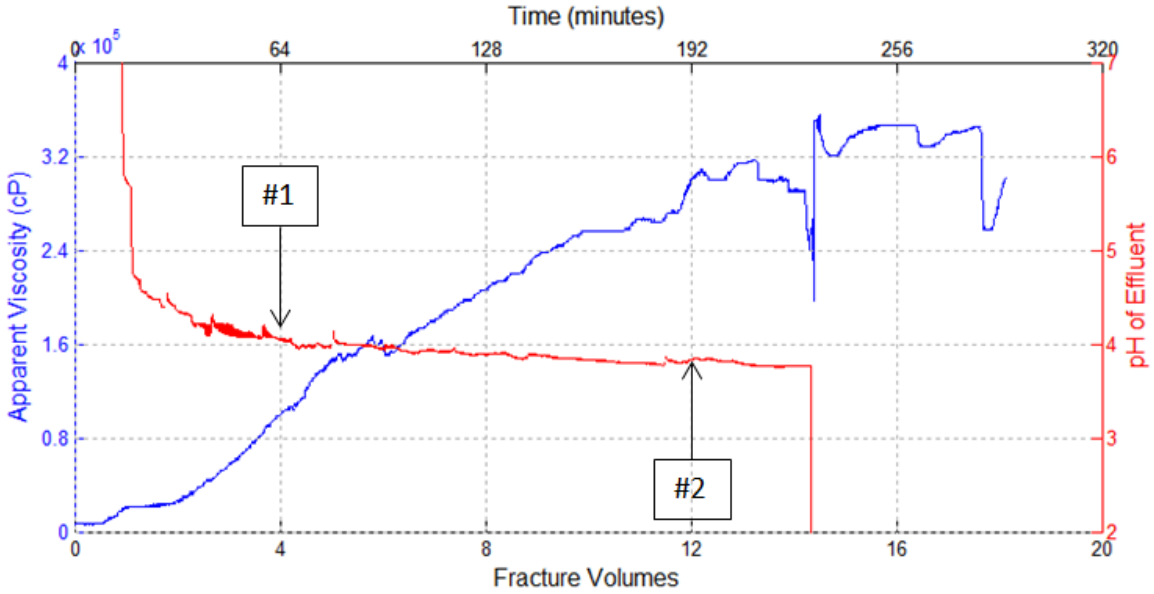

Figure 32: Plot of apparent viscosity (calculated from pressure data, shown in blue) and effluent viscosity history during polymer injection into Core 6FP-3. Apparent viscosity is linearly related to pressure drop when flow rate is constant. Apparent viscosity at points #1 and #2 is calculated from Herschel-Bulkley parameters from rheology measurements on polymer dispersion of same salinity and pH and are shown in Table 3.

At two representative times (4 fracture volumes and 12 fracture volumes injected), the apparent viscosity was calculated from the pressure measurement. Then the effluent pH at each point was used to interpolate within the rheology data for this polymer dispersion (3 wt% Carbopol 934 and 0 wt% NaCl) and obtain the Herschel-Bulkley (HB) parameters at these points. The flow rate and HB parameter values were then used to calculate the apparent viscosity and are shown along with the pressure-measurement-derived apparent viscosity in Table 9.

Point	Pressure Drop	Apparent Viscosity from Pressure Drop	Effluent pH	Apparent Viscosity from pH and rheology
#1	3 psi	10,000 cP	4	107,000 cP
#2	10 psi	30,000 cP	3.8	104,000 cP

Table 9: Apparent viscosity from pressure drop and pH data at two points during polymer injection (3 wt% Carbopol 934 and 0 wt% NaCl) in Core 6FP-3 (cf. Figure 32).

At point #1, it is clear that the rheology model predicts a much larger apparent viscosity than the effective value during the flow experiment. The difference is substantial and requires discussion. As mentioned in Chapter 3.4.2, the rheological behavior in unreactive flow in slots differed noticeably from predictions based on rheometer data. This was attributed to possible slippage along the plastic plate that comprises half of the fracture. A no-slip boundary assumption is inherent in the HB flow equations – therefore, the addition of slippage in experimental data would result in higher than predicted flow rates for a given pressure drop, reducing the effective permeability.

This same behavior is thought to cause the discrepancies here, in combination with other factors. For example at point #1, when the pressure drop is slowly building, this indicates that the pressure gauge has not reached pressure equilibrium with the slot. This behavior is described in Figure 104 given in Appendix B. Essentially, the high viscosity of the polymer gel causes the gel to enter the pressure lines slowly, causing the pressure drop data to be delayed as the gel enters the line. This results in a temporary underestimation of pressure gradient and therefore an underestimated apparent viscosity. However, from Figure 32 the apparent viscosity appears to plateau near point #2 at around 34,000 cP, indicating that the pressure transducer has reached pressure equilibrium with the slot. This viscosity is still significantly lower than the pH/rheology calculated apparent viscosity of 100,000+ cP. Similar to the data shown in Table 8 and Figure 20, in which the rheology data gave elevated yield stress values that lead to

reduced pressure drop in the slot conduit, the experimental pressure drop data is lower than the rheology data predicts. This again may be due to the erroneous no-slip boundary assumption used to calculate the viscosity from the rheology model, as Core 6FP-3 uses a plastic plate as one of the fracture halves.

It should also be noted that the rheometer measurements on this polymer (3 wt% Carbopol 934, 0 wt% NaCl) was neutralized using sodium hydroxide, NaOH, and therefore does not take into account the presence of calcium cations, which reduce the yield stress, consistency index, and therefore the apparent viscosity, more than sodium cations. This could cause the pH/rheology calculated apparent viscosity to be artificially increased compared to the actual polymer rheology.

Finally it is important to recall that the effluent pH is an upper bound for the pH of the polymer dispersion within the fracture. The polymer's pH in the fracture will be a gradient from the initial pH and the effluent pH, and therefore the average pH in the fracture will be lower than the effluent pH. Using the effluent pH will therefore overestimate the apparent viscosity. The polymer dispersion at the fracture inlet has a yield stress of 17.8 Pa, a consistency index of 5.8 Pa-s, and a power law index of 0.4. Using these inlet parmeters, the apparent viscosity of the polymer during injection is calculated to be 6200 cP. Using the inlet and outlet HB parameters to calculate an apparent viscosity yields a lower and upper bound, while the apparent viscosity calculated from the pressure drop should fall within these bounds. This is consistent with the calculated viscosities in Core 6FP-3, as shown in Table 10.

Calculation Method	Inlet Polymer (Lower Bound)	From Pressure Drop (point #2)	Effluent Polymer (Upper Bound)
Apparent Viscosity	6,200 cP	34,000 cP	107,000 cP

Table 10: Apparent viscosities calculated from the inlet rheology, effluent rheology, and pressure drop.

4.2.3 Initial Polymer Injection Tests

4.2.3.1 Core 6F-9

Batch tests and rheological measurements had previously shown that a polymer dispersion of 3 wt% Carbopol 934 and 0.5 wt% NaCl would be a good candidate, as it has low viscosity at initial conditions, allowing for good injectivity, but can still gelate inside the fracture. This is shown in the yield stress vs pH plot in Figure 4 in Chapter 3.2. The initial yield stress upon mixing, around pH 2.5, is nearly zero, but yield stresses over 100 Pa can be developed as the polymer dispersion is neutralized and gels. Core 6F-9 (also shown in the pressure test in Figure 29 above) was injected with this polymer dispersion at a rate of 0.5 mL/min, resulting in a fracture residence time of around 4 minutes. The fracture length is about 6 in (15 cm). The experiment is summarized below in Figure 33. For this experiment, the pH of the effluent was not continuously measured, but is instead shown as discrete steps. Samples were collected and pH of each sample was measured.

Core	Aperture	Polymer Injected	Residence Time	Volume Injected	Fracture Type	SS App. Viscosity
6F-9	0.336 mm	3 wt% Carbopol 934 0.5 wt% NaCl	4 min	18 FVs	Cement-Cement Brazilian	137 cP

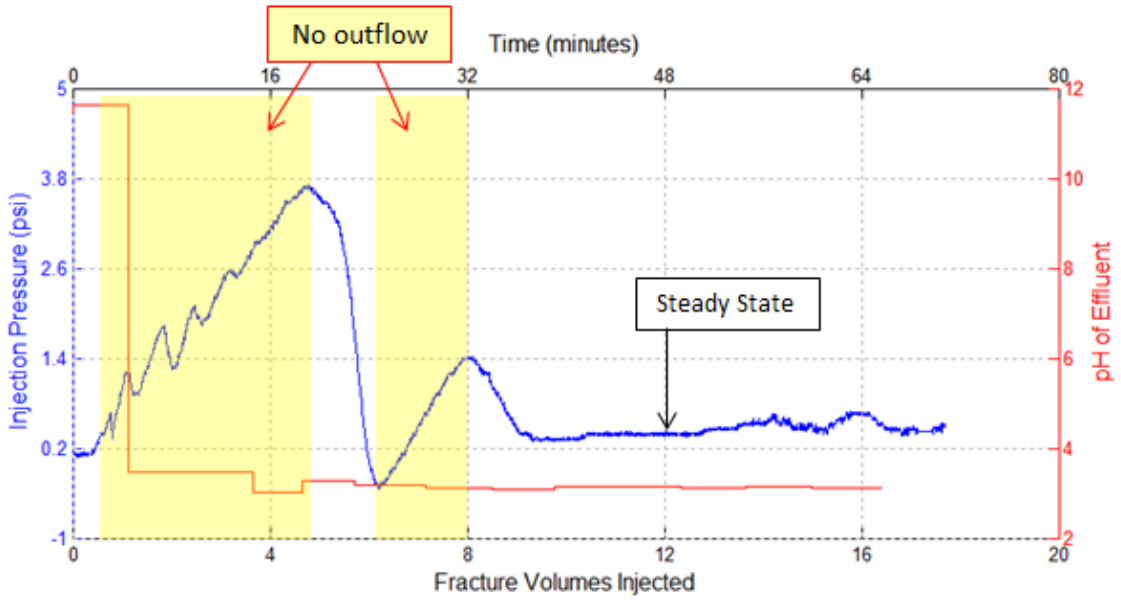

Figure 33: Data recorded during steady polymer injection (3 wt% Carbopol 934, 0.5 wt% NaCl, and DI water) into Core 6F-9. Despite steady injection, no fluid exited the core during periods of pressure buildups (from 1 FV to 6 FV and from 7 FV to 9 FV). Point #1 indicates steady state pressure drop.

Because samples were collected after the effluent went through the cement fracture and some dead volume at the outlet, it was necessary to assign time values to each sample in order to align the pressure drop and effluent pH of a given volume of polymer dispersion. For example, the first sample collected traveled through the cement fracture between 0 and 1 FVs and was collected between 3 and 4 FVs. It is necessary to subtract 3 FVs from the effluent times in order to show the two curves in sync. Although no effluent exited the core during the highlighted regions on Figure 33, the pH of the effluent collected subsequently was measured and is shown at the time it would have eluted, hence the reason pH readings exist in periods of no outflow.

The first effluent sample (shown from 0 to 1 FVs) had a pH value of 11.62, and appeared to be entirely water, free of any injection polymer. It was determined that this

sample was simply the deionized water that initially filled the cement fracture. Because this water was allowed to remain inside the cement fracture before polymer injection, a small amount of portlandite was dissolved from the cement and elevated the sample's pH. As the polymer is injected into the fracture, this water is displaced and reaches the pH probe ahead of the polymer dispersion, temporarily driving up the recorded pH, as seen in Figure 33. This behavior was seen in every subsequent polymer injection experiment. Because the high pH region is seen for only a fraction of the injection period, the pH axis is expanded and shown in Figure 34 to better show polymer dispersion effluent pH history.

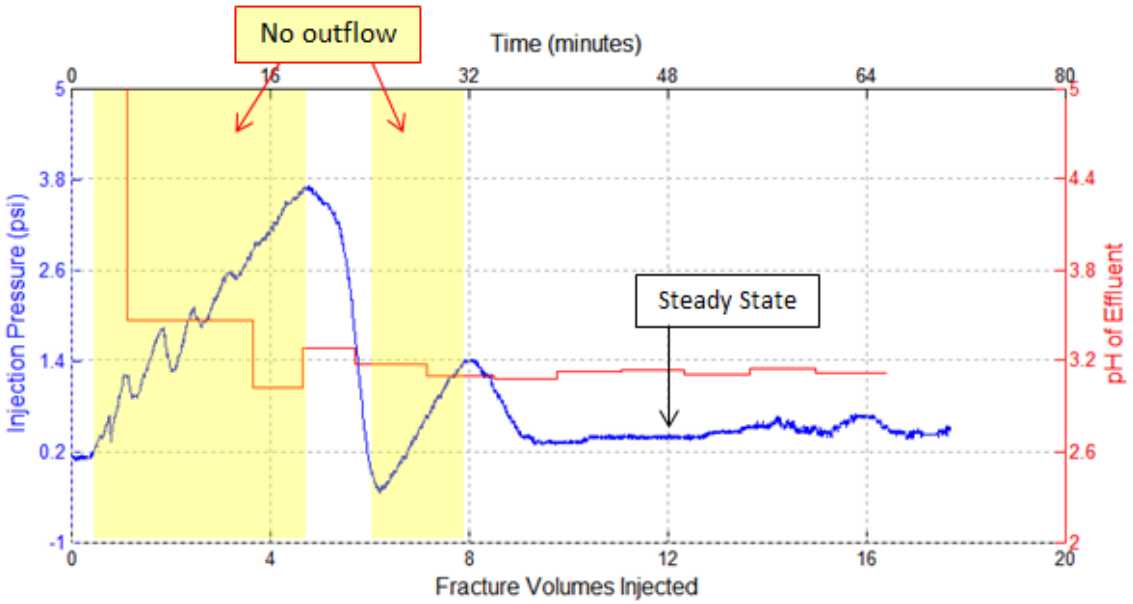

Figure 34: Same as Figure 32 with pH axis expanded.

The pressure behavior during polymer injection is notably non-monotonic. Two sustained pressure build ups occur before 8 fracture volumes have been injected. During both of these pressure building periods, no fluid exited the core, despite the constant injection rate into the core. This indicates the injected fluid encountered some blockage, which began to increase the pressure instead. After these build ups, the fluid flow out of

the core was much higher than the injection rate of 0.5 mL/min while the pressure was decreasing, indicating that the pressure blockage was cleared and the fluid was able to flow again. This pressure and flow start/stop behavior also affected the pH of the effluent: during the pressure build up periods, the polymer dispersion had a residence time larger than 4 minutes and therefore had an elevated pH. Similarly, when the pressure was relieved, fluid flowed quickly through the core and the polymer dispersion had a smaller residence time and therefore exited the core with a lower pH. Steady state is thought to occur between 9 and 16 fracture volumes, though some pressure drop variations are seen between 14 and 16 FVs. This steady state pressure drop corresponds to an apparent polymer viscosity of 172 cP if the entire fracture width is assumed to be open to flow. If the flow channel is constricted, the apparent viscosity will be reduced proportional to the decrease in width and the cube of the reduction in aperture.

The pH at steady state is around 3.1, which for this polymer formulation (3 wt% Carbopol 934 and 0.5 wt% NaCl) corresponds to a yield stress of 1.1 Pa, consistency index of 2 Pa-s, and a power law index of 0.36. With these HB parameters known, the rheology predicted apparent viscosity is 450 cP, nearly 3 times higher than the apparent viscosity according to the pressure drop data. As discussed earlier, this discrepancy could be due to the fact that the effluent pH is the maximum pH observed in the fracture. Therefore, the effluent's HB parameters are higher than the average parameters seen inside the fracture, and will therefore overpredict the apparent viscosity. The polymer's HB parameters at the inlet (at pH 2.3) give a yield stress of 0.13 Pa, a consistency index of 0.35 Pa-s, and a power law index of 0.46. The apparent viscosity of the polymer with these HB parameters is 95 cP. The inlet and outlet HB parameters give a lower and upper bound on apparent viscosity of 95 cP and 450 cP, with the apparent viscosity from pressure drop falling between these at 172 cP.

It must be kept in mind that the pressure transducer measures the pressure at two points: the inlet and outlet of the fracture. When the pressure drop across the core decreases suddenly, as it did around 6 fracture volumes in Figure 33, it means that either the inlet pressure decreased or the outlet pressure increased. The pressure drop goes below zero mid-way through polymer injection, indicating that there is some issue with the pressure measurements. During this period, fluid was seen continually exiting the outlet of the core, and because fluid always moves from high to low pressure it is concluded that the measurements are suspect. In this case, the negative pressure drop is thought to be due to the effect of having yield stress fluid in the pressure lines. This effect is discussed in length in Appendix B. In essence, the polymer dispersion and gel have difficulty entering into the pressure lines so that the pressure data is inaccurately represented.

This could occur if the yield stress of the polymer dispersion at the inlet of the core is greater than the polymer at the outlet, causing the high pressure line to transmit a pressure that is smaller than the actual pressure, while the low pressure line transmits a more accurate pressure. However, polymer dispersion moving through the cement fracture should exhibit a larger yield stress as it moves, due to increased pH and consequent gelation. But as the batch tests between polymer dispersion and cement have shown, this is not always the case, as the polymer can undergo syneresis and lose its strength.

The temporary negative pressure drop is seemingly corrected when the flow through the slot is blocked for a second time, between 6 and 8 fracture volumes.

A possible explanation for the blockage is that the incoming polymer reacted rapidly with the cement and formed a gel, whose yield stress was larger than the pressure gradient across the core. The gradient at the maximum injection pressure (around 6 FV

injected) is about 7 psi/ft, at which point flow is observed through the core. This would correspond to the fracture being filled with a fluid of yield stress 27 Pa, while the pH of the effluent at this time is 3.6. Figure 7 shows that this polymer formulation (3 wt% Carbopol 934 and 0.5 wt% NaCl) is capable of developing a yield stress of around 21 Pa at pH 3.6, too low to hold back this pressure gradient alone. There are two probable explanations that account for the additional yield stress seen in Figure 34.

1. The effluent was collected in 2-3 mL sample collection vials and the pH of 3.6 is an average pH of the sample, not the instantaneous pH. Therefore, the polymer dispersion during this pressure build up could have been higher than 3.6, but was subsequently mixed with lower pH effluent when fluid began to flow from the outlet. This is more likely for the first few fracture volumes of polymer injection, when the pH changes significantly from sample to sample. From Figure 7, at pH 3.6 small changes in pH can greatly change the gel's yield stress, e.g. at pH 3.8 the yield stress is 39 Pa. It is therefore reasonable that the fluid blockage was caused entirely by the yield stress of the polymer gel.
2. The flow channel was slightly constricted by syneresed polymer, reducing the aperture of the cement fracture. This would allow a polymer gel with a yield stress lower than 27 Pa to block fluid flow. For example, a 50% reduction in fracture aperture would cause the 3.5 psi pressure drop to correspond with a 13.5 Pa yield stress fluid, well within the range for a pH 3.6 polymer gel of 3 wt% Carbopol 934 and 0.5 wt% NaCl to block fluid flow. A ~15% reduction in aperture would cause a 21 Pa fluid to be displaced at 3.5 psi, as we have in Figure 34.

The strength of the polymer gel inside the fracture was tested after being shut in to equilibrate for four days. Water was injected slowly, at 0.5 mL/min (0.25 fracture volumes per minute) into the inlet of the fracture and the injection pressure was measured, as shown in Figure 35. This is referred to as a polymer strength test. The injection pressure builds over several minutes while flow is held back until the injection fluid broke through the core and quickly flowed out of the core, indicated by the pressure drop around 6 minutes elapsed time. Water injection was continued after breakthrough to determine the new effective aperture of the slot. Prior to polymer injection, the aperture of the slot was such that injecting 0.5 mL/min of water into the fracture would yield a negligible pressure drop. It can be seen here that the pressure drop declines from 1.5 psi to about 0.5 psi over the course of the next 10 minutes. This indicates that the polymer gel was not completely removed, but that some gel remains and decreases the effective permeability of the fracture. The maximum pressure drop withheld, just before water breakthrough, was around 6 psi, or 12 psi/ft. The injection pressure at the inlet increases until the flow initiation pressure (FIP) of the polymer in the fracture is exceeded. This FIP corresponds to a fluid filling the fracture with yield stress of 46 Pa. A sample of the gel could not be collected for a pH measurement, but cement can drive the pH of fluids up to around 13 and had likely done so to the polymer in the fracture over the course of 4 days. The maximum pH of the polymer gel tested in Figure 7 was 10.3, with a yield stress of 37 Pa and increasing the pH would further decrease the yield stress. It is therefore unlikely that the polymer gel was solely responsible for the fluid blockage. After four days, as can be seen in the batch test of polymer and cement in Figure 10, the polymer could have undergone considerable syneresis which could have completely blocked the fluid flow itself or reduced the aperture and worked in conjunction with the polymer gel present.

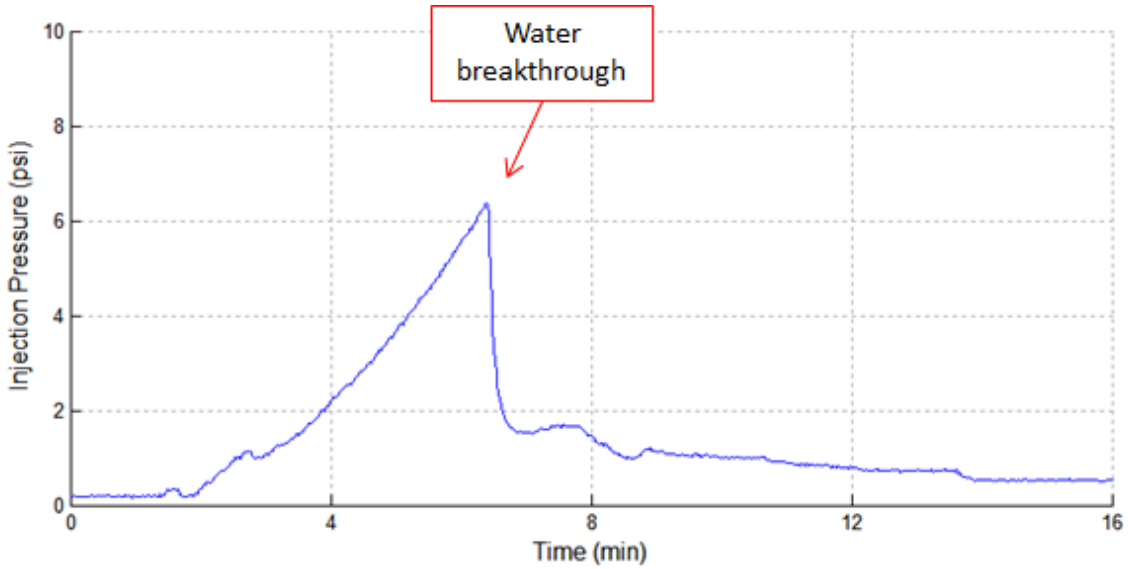

Figure 35: Polymer strength test in Core 6F-9 after 4 days of shut in time. No flow occurs during the pressure buildup period from 0 to 6 minutes, until the polymer is displaced at 6 minutes and water begins to flow through the core until the build up pressure is relieved.

The effluent consisted of mostly the displacement water and thus did not confirm if the blockage was due to polymer gel or syneresed polymer. The slow decline of the pressure drop afterwards, during water injection, indicates some widening of the flow channel over time. This was confirmed by increasing the rate of injection of water into the core. Pressure data for this test are shown in Figure 36. For each step, the injection was completely stopped, then the flow rates shown were applied. The pressure drop across the core spikes upwards for each flow rate, then slowly declines as injection continues, again indicating a widening of the flow channel. Also note that the pressure data were shifted down 0.7 psi in order to set the static (no injection) pressure to zero.

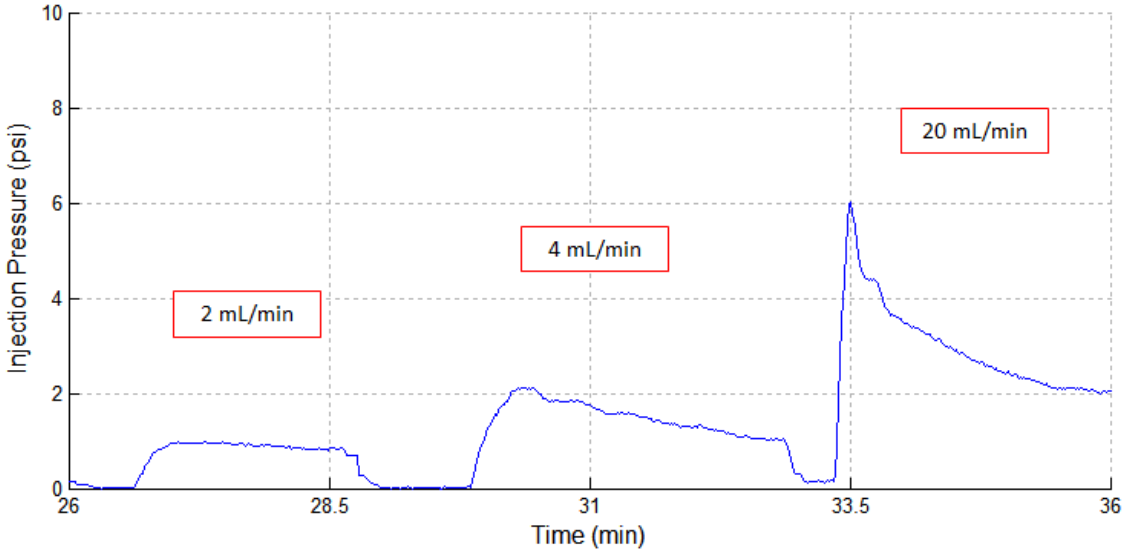

Figure 36: Following breakthrough in polymer strength test in core 6F-9, a series of increasing DI water flow rates yielded gradual decline in injection pressure, consistent with widening the flow channel through the gel at increasing flow rates due to incremental displacement of polymer gel or syneresed polymer from fracture.

From these flow rates and pressure drops, the flow area reduction can be estimated. There are two ways in which the flow area can be reduced: a decrease in aperture, B, due to a layer of syneresed polymer over the fracture faces, or a decrease in fracture width, W, as no flow regions are created and flow is constricted to the center of the fracture. The aperture and width can be estimated using the following equations while holding the other variable constant:

$$B_{reduced} = \left[\frac{12\mu QL}{W_{original}\Delta P}\right]^{\frac{1}{3}} \qquad W_{reduced} = \frac{12\mu QL}{B_{\text{original}}^{3}\Delta P}$$

where μ is the viscosity of water, Q is the flow rate, L is the length of the fracture, and ΔP is the pressure drop across the fracture. The magnitude of both aperture or width reduction for each of the flow rates in Figure 36 are estimated and shown in Table 11. The apertures and widths calculated are then compared to the initial dimensions and given as "% open." If there were no aperture or width reduction, they would be considered "100% open."

Flow Rate (mL/min)	SS Pressure Drop (psi)	Effective Hydraulic **Aperture** (mm)	% Open **Aperture**	Effective Hydraulic **Width** (mm)	% Open **Width**
2	0.8	0.076	23%	0.29	1.1%
4	1.1	0.086	26%	0.42	1.7%
20	2.0	0.120	36%	1.17	4.6%

Table 11: Effective hydraulic apertures calculated from Figure 36 and compared to the initial effective hydraulic aperture for Core 6F-9 of 0.206 mm.

It should be noted that the width is related linearly to the flow rate to pressure drop ratio, while the aperture is related to the cube root of this ratio, resulting in different "% open" values for aperture and width. But the effects from both are similar (for example, $(0.36)^3 \approx 0.046$). Both aperture reduction and width reduction due to syneresis are observed, as is discussed in Chapter 4.3.2.4 and shown in Figure 59.

4.2.3.2 Core 6F-12

Similar to Core 6F-9, polymer dispersion consisting of 3 wt% Carbopol 934 and 0.5 wt% NaCl was injected into Core 6F-12, which also had a similar aperture to Core 6F-9. The geometry and polymer type is therefore constant between the two experiments, but the injection rate in Core 6F-12 was half the rate of Core 6F-9 in order to determine the effect of residence time on the injection pressure. The pressure data are shown below in Figure 37. Again, the pH data are discrete, average measurements and are shown in stair-step increments.

Core	Aperture	Polymer Injected	Residence Time	Volume Injected	Fracture Type	SS App. Viscosity
6F-12	0.271 mm	3 wt% Carbopol 934 0.5 wt% NaCl	8 min	20 FVs	Cement-Cement Brazilian	451 cP

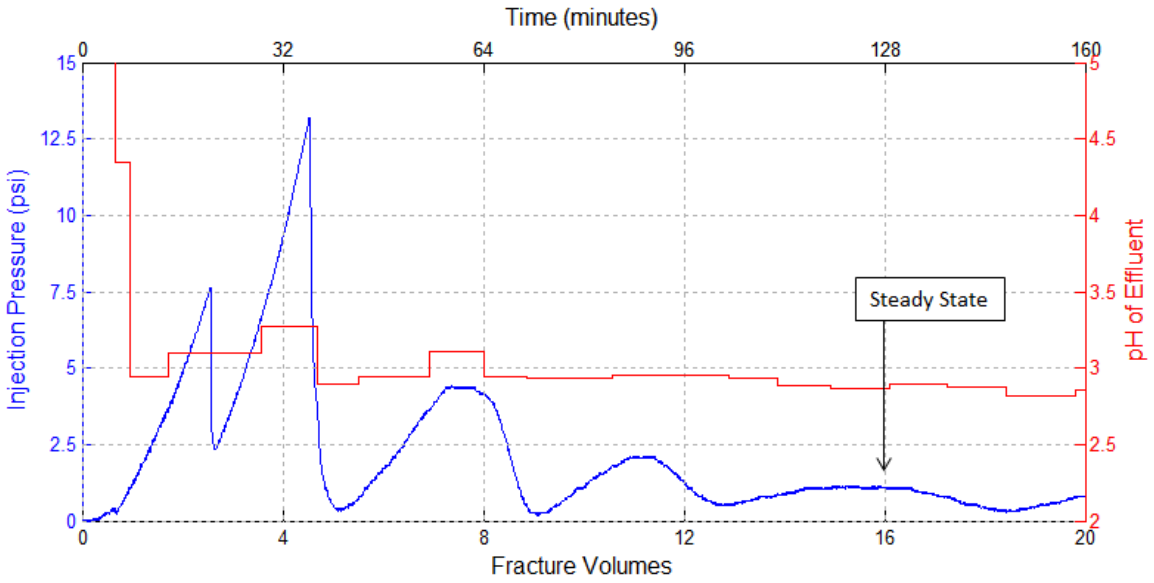

Figure 37: Data recorded during polymer injection (3 wt% Carbopol 934, 0.5 wt% NaCl, and DI water) into Core 6F-12. No fluid exited the core until 2.5 FV had been injected. Subsequent pressure buildups and peaks at 5 FV, 7 FV and 11 FV were also associated with reduced effluent rate; see Figure 38.

The pressure drop trend is similar to that of Core 6F-9, but with higher pressure spikes and more irregular, non-monotonic behavior. Again, some of the pressure build up periods coincided with reduced flow rates out of the core. The outflow rate was measured by collecting the effluent (pH measurements are shown above) while noting the duration of collection, then the volume of each sample was measured. From the total volume and collection time, an average flow rate is calculated and shown with the pressure data in Figure 38. The actual flow rate into the core, 0.25 mL/min, is shown as a black, dashed line.

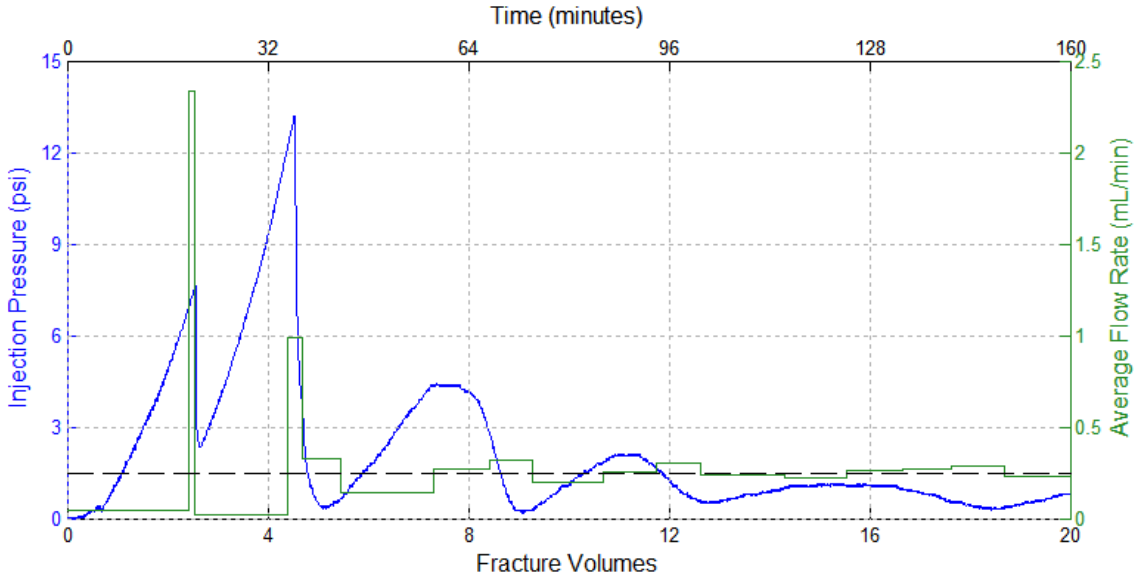

Figure 38: Pressure and flow rate data recorded during polymer injection (3 wt% Carbopol 934, 0 wt% NaCl, and DI water) into Core 6F-12; black, dashed line indicates the actual flow rate into the core

During the first two pressure build up periods, the outflow rate is significantly lower than the injection rate, but the outflow spikes as the pressure declines rapidly. The first and second pressure buildups correspond to a fracture being filled with a fluid of yield stress of 47 Pa and 84 Pa, respectively, and the effluent pH at these peaks were around 3.1 and 3.3, respectively. From Figure 7 it is clear that these yield stresses cannot be reached by a polymer gel with these pH values. The yield stresses for pH 3.1 and 3.3 are 0.7 Pa and 4 Pa, respectively. The averaging effect of the sample collection is unlikely to account for this discrepancy, as the pH of the gel would need to reach 4.0 for the first peak and nearly 5.0 for the second, and therefore polymer yield strength cannot solely account for the fluid blockage in Figure 37. The increased fluid blockage is therefore attributed to either syneresed polymer fully blocking the fracture or a combination of syneresed polymer and the pH averaging effect also seen in Core 6F-9.

The transition between the first and second buildup, around 3 FVs, could be due to pieces of syneresis polymer or polymer gel being displaced from one local

constriction, temporarily allowing flow until the gel/syneresed polymer plugged a second local constriction in the fracture slot.

Based on the shape of the pressure data and the outflow rate data, it is clear that the first two pressure build up periods are distinctly different than the third and fourth: the rate of pressure increase is larger, the pressure decline is faster, and they correspond with little to no flow through the core. The subsequent pressure build ups coincide with reduced, but not negligible, outflow rates and eventually level out around the actual injection rate. This is likely due to the fact that, after the second breakthrough, around 5 FVs, the surface of the cement was unable to neutralize the polymer dispersion quickly enough to form enough gel or syneresed polymer to fully block flow, but was able to significantly viscosify the fluid.

The third and fourth pressure buildup periods had pressure drops of 4.4 and 2 psi, respectively. Because exit flow occurred during these periods, it is incorrect to associate the peaks with the yield stress of the fluid. However, the yield stress at these pressure peaks must be exceeded for flow to occur, so the maximum pressure drop of each peak gives an upper limit for the polymer dispersion's actual yield stress. The third and fourth peak correspond to a yield stress upper limit of 27 Pa and 12 Pa, respectively. From the effluent pH at these peaks, 3.1 and 2.95, Figure 7 shows that it is impossible for the polymer dispersion to have yield stresses of this magnitude at these pH values for 3 wt% Carbopol 934 and 0.5 wt% NaCl. The yield stress of the polymer gel for these pH values are below 1 Pa. Therefore, some mechanism other than the polymer's yield stress must be at work. The subsequent, slow pressure oscillations are thought to be due to cycles of partial flow channel blockages from syneresed polymer and the displacement of the semisolid. Steady state is reached around 16 FVs of polymer injection and

corresponds to an apparent viscosity of 4501 cP, calculated from the pressure drop through the fracture, assuming the fracture is fully open.

However, the apparent viscosity calculated from the initial polymer dispersion and pH of the effluent at steady state set upper and lower bounds of 110 cP and 200 cP, both of which are below the 450 cP apparent viscosity calculated from the pressure drop. Therefore, the assumption that the fracture is fully open and unconstructed is invalid, in which case the apparent viscosity from the pressure drop will be overestimated. If the width of the flow channel is constricted 67%, then the actual apparent viscosity would be 150 cP, midway between the lower and upper bounds and consistent with the rheology data. Similarly, the apparent viscosity will be reduced to 150 cP if the fracture aperture is reduced by 12%, due to the cubic relationship between aperture and apparent viscosity. This served to strengthen the hypothesis that the flow channel is constricted by polymer gel or syneresed polymer.

As before, Core 6F-12 was shut in for four days, after which pressure was applied with deionized water to the core inlet to displace the polymer gel or syneresed polymer. The injection pressure is shown below in Figure 39. The injection rate for the pressure test was 0.125 mL/min, four times slower than for the polymer strength test of Core 6F-9.

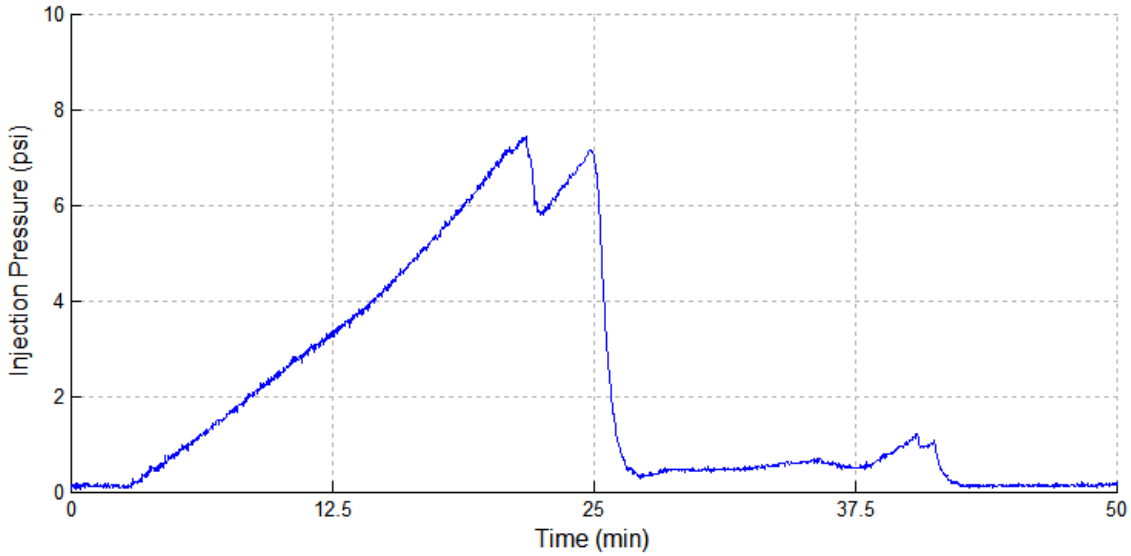

Figure 39: Polymer strength test in Core 6F-12 after 4 days of shut in time. A small amount of fluid exited the outlet between the first and second spike, around 20 min,

Instead of the single pressure buildup period that was seen in Figure 35 for Core 6F-9, core 6F-12 exhibited a long building period (about 20 minutes, Fig 33) followed by a small decrease and another short building period. The maximum value during the pressure buildup corresponds to a 46 Pa yield stress fluid filling the fracture. The pH of the gel present in the fracture was again unable to be obtained, but is likely over pH 12, as the fluid had 4 days to equilibrate with the cement surface. Referring back to Figure 7, the highest pH value tested was 10.3 and the polymer gel had a yield stress of 37 Pa. It is likely that increasing the pH over 10.3 will result in a lower yield stress, therefore the polymer gel most likely could not have solely held back the 7.5 psi pressure drop seen in Figure 39. It is again likely that the fracture slot was partially constricted by syneresed polymer and filled with polymer gel or completely filled with syneresed polymer.

The displacement of polymer gel should only have one pressure building period until the flow initiation pressure is reached (as was the case in Figure 35 for Core 6F-9), followed by a sharp pressure decrease until steady state is reached between the flow rate

and polymer gel around the flow channel. This expected behavior is not seen here; instead, the pressure drop decreases slightly, then begins to increase again. This second, short pressure buildup is attributed to syneresed polymer or polymer gel being transported to a local constriction and there blocking flow.

4.2.3.3 Core 6F-14

Experiment 6F-14 used a core similar to Cores 6F-9 and 6F-12, but the injected polymer concentration was increased to 4.5 wt% Carbopol 934, while keeping the salt concentration constant at 0.5 wt% NaCl. The rheology of this polymer formulation was not extensively tested, as this is the only experiment in which it was used, but the increased concentration of polymer counterbalanced the negative effects of the salt concentration. Compared to 3 wt% Carbopol 934 and 0.5 wt% NaCl, this polymer formulation will have increase yield stress and consistency index values.

Core	Aperture	Polymer Injected	Residence Time	Volume Injected	Fracture Type	SS App. Viscosity
6F-14	0.359 mm	4.5 wt% Carbopol 934 0.5 wt% NaCl	8.2 min	14 FVs	Cement-Cement Brazilian	6295 cP

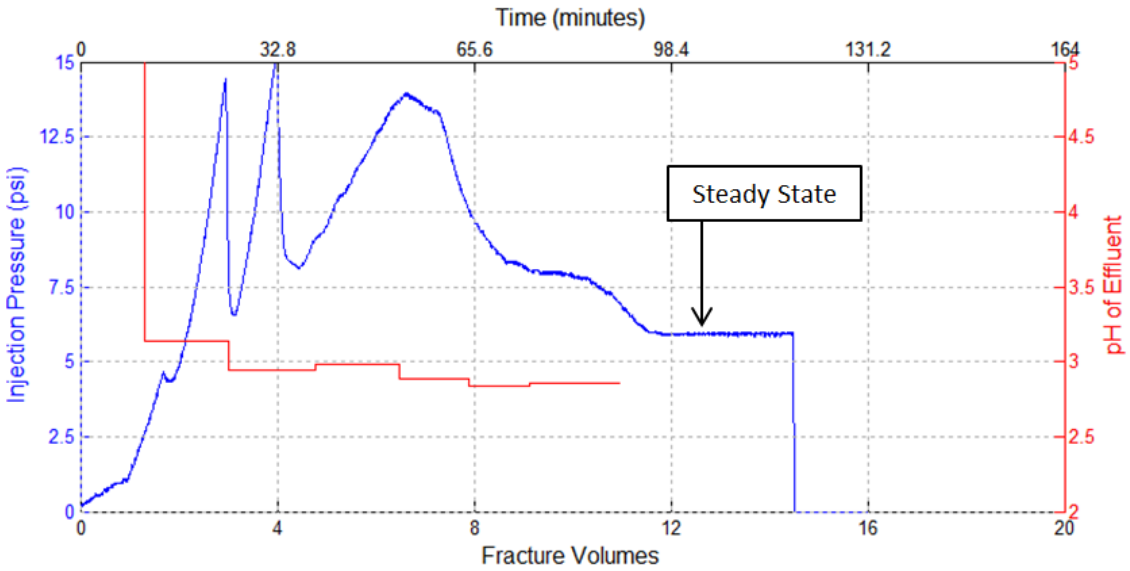

Figure 40: Data recorded during polymer injection (4.5 wt% Carbopol 934, 0.5 wt% NaCl, and DI water) into Core 6F-14. No effluent from the core was observed until 4 FV had been pumped; effluent pH history is corrected to what would have eluted at the time indicated.

Much like Core 6F-12, the pressure data from Core 6F-14 has two pressure building periods that have similar rates of pressure increase, followed by another period with a slower build up rate. The first two peaks (at 3 FV and 4 FV) both correspond to a fluid in the fracture with yield stress of 124 Pa, while the third peak around 7 FVs corresponds to a fluid of 113 Pa. These yield stress magnitudes are nearly attainable with the 3 wt% Carbopol 934 and 0.5 wt% NaCl polymer dispersion shown in Figure 7, and are therefore quite likely to be obtainable with the 4.5 wt% Carbopol 934 and 0.5 wt% NaCl (which has increased values of yield stress and consistency index). The steady state period between 12 and 15 FVs corresponds to an effective polymer viscosity

of 6293 cP, higher than Cores 6F-9 and 6F-12. This is due to the increased polymer concentration of the injection polymer dispersion.

The non-monotonic pressure drop behavior is similar to the polymer injection data collected from Core 6F-13, seen in Figure 37. Again, this is attributed to polymer gel and/or syneresed polymer being displaced from one part of the cement-cement fracture and becoming stuck in second location in the fracture. Cores 6F-9, 6F-12, and 6F-14 all exhibit this behavior that could be attributed to either syneresed polymer blockages or a reduction in flow area due to syneresed polymer.

Core 6F-14 was shut in for four days to allow the polymer to fully react with the cement, then a polymer strength test was performed. Pressure was slowly increased by injecting deionized water into the inlet of the core until the displacing water broke through the fracture. The pressure data for this test is shown below in Figure 41.

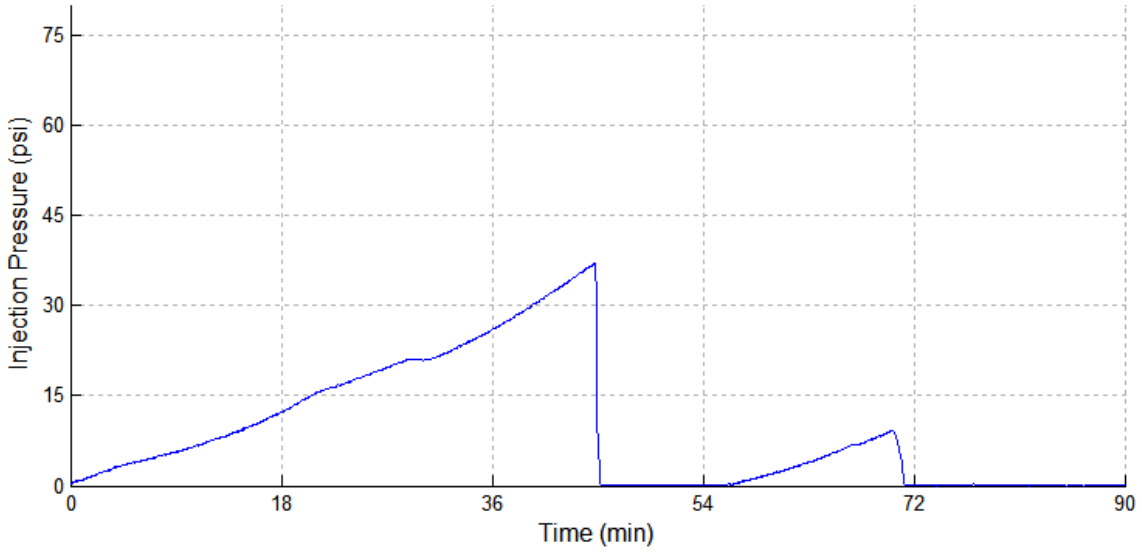

Figure 41: Polymer strength test in Core 6F-14 after 4 days of shut in time

The flow rate into the core was decreased periodically during the first pressure build up in order to reduce the rate of pressure increase. The displacement water finally

broke through at around 37 psi, corresponding to a pressure gradient of 74 psi/ft and a 306 Pa yield stress fluid, larger than any previous breakthrough experiment and over twice as large as the polymer injection pressure. The yield stress of 4.5 wt% Carbopol 934 and 0.5 wt% NaCl polymer dispersion at high pH was not measured, but the tests at other pH values show that it behaves similarly to 3 wt% Carbopol 934 and 0 wt% NaCl, as shown in Figure 4. Using this rough estimation, a 306 Pa yield stress at high pH is conceivable. After the water breaks through there is another, smaller pressure build up and decline. This was unexpected, as the pressure drop between these two build up periods is negligible and constant for about 10 minutes, which would indicate a clear channel for water flow has been created within and through the polymer gel. This behavior is similar to the breakthrough pressures from Core 6F-9 and Core 6F-12.

The core was then continuously injected with deionized water after the breakthrough occurred, with several rate changes along during this time. The pressure data is shown below in Figure 42. The data shown in Figure 41 is still included in the figure as the first 90 minutes, but is followed by further water injection.

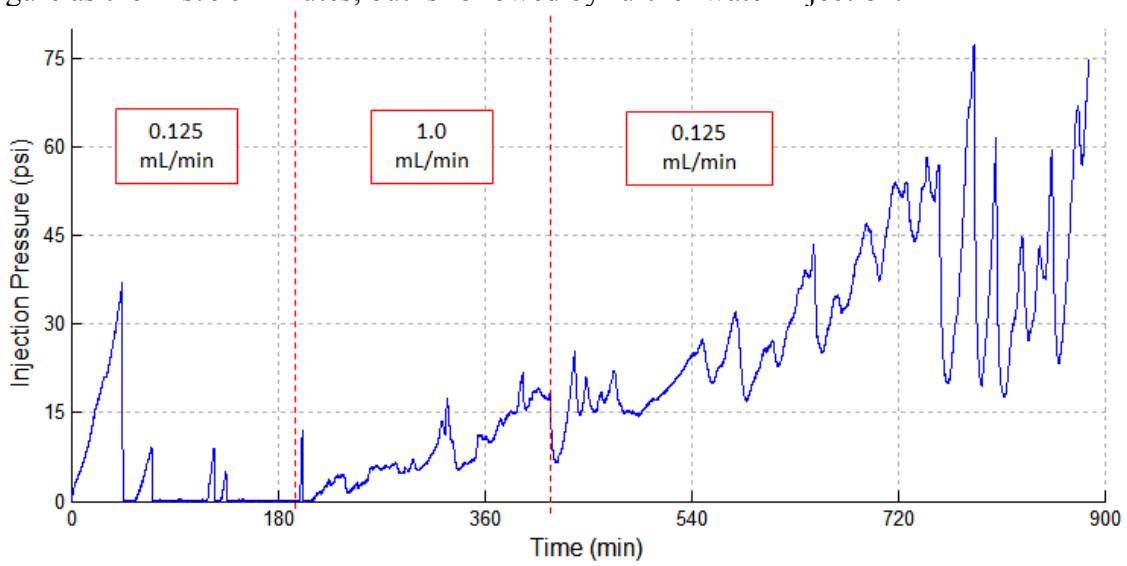

Figure 42: Pressure data during (0 to 90 min) and after (90 to 900 min) polymer strength test of Core 6F-14; flow rates given on graph

The injection pressure varies more and more erratically after 100 min when the flow rate was increased from 0.125 to 1.0 mL/min. The flow rate was slowed again to 0.125 mL/min, but the pressure variation continued and became even more erratic. Unfortunately, this behavior does not answer the questions put forth by previous experiments, but instead raises more questions of its own. At first, the behavior was thought to be instrumentation error, as neither behavior of this sort nor such high injection pressures had yet been seen. Water injection was stopped and the core was shut in for 12 hours, then deionized water was again injected into the core inlet at a rate of 0.125 mL/min. This second polymer strength test is shown in Figure 43 below. The injection pressure increased very quickly to 80 psi, at which time injection was stopped in order to prevent damage to the epoxy core holder, e.g. causing leaks. The pressure slowly decreased over time and droplets of water were seen to come out of the core outlet.

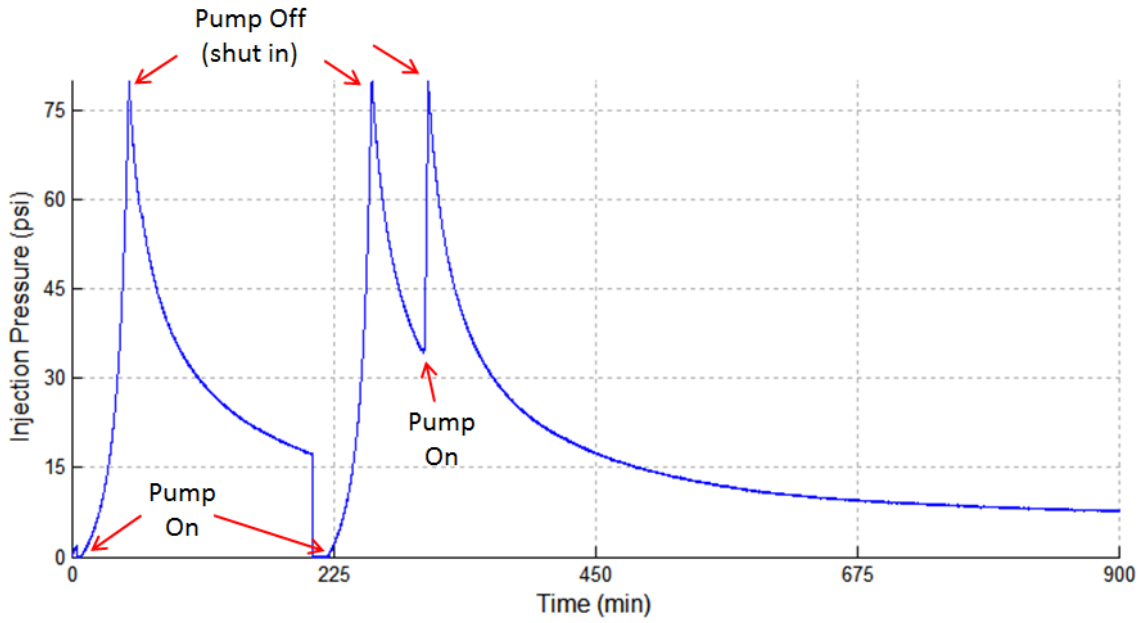

Figure 43: Second polymer strength test in Core 6F-14 after 12 hour of shut in time, following the water injection reported in Figure 42. Peaks correspond to halting injection (rate = 0.125 mL/min) to avoid over-pressuring the coreholder.

After a few hours of pressure decline via the effluent water droplets, the inlet pressure was relieved and the system was checked for leaks external to the core itself. After the system was double checked, water was injected again at the same rate and again stopped at 80 psi. The decline and water outflow were observed again. The pressure was increased to 80 psi a third time. This is a similar method as was used in the pressure buildup/falloff tests in a closed core, shown earlier in Figure 27, in which water was injected then the pressure decline was measured after injection was stopped. Unlike the results in Figure 27, the pressure decline was identical for each of the buildup/falloff steps. To show the similarity, the three pressure declines are plotted as a function of time since shut-in (the moment the pump was turned off), laying them on top of each other, in Figure 44. The declines are labeled in terms of which decline they refer to in Figure 43: first, second, and third. Because the pump was turned off at 80 psi for each decline, the y-intercept is 80 psi for all three declines. It can be seen that the three curves are nearly perfectly on top of each other, with the red line being the second pressure decline as seen on Figure 43, and therefore the shortest curve on the graph, terminated after 45 minutes.

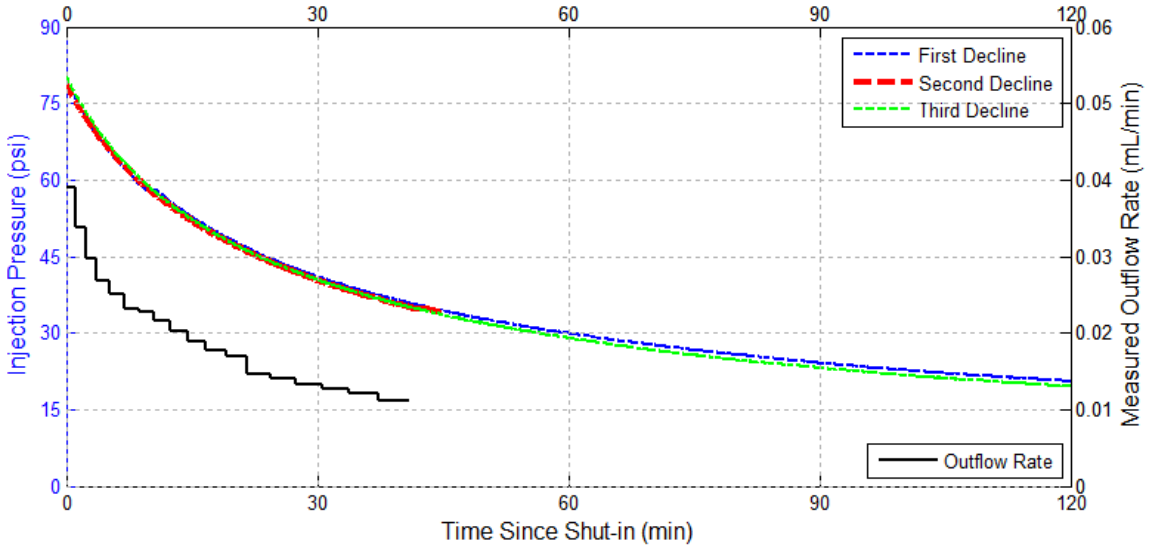

Figure 44: Pressure falloff curves (dashed) from Core 6F-14 (as shown in Figure 43) plotted as a function of time since shut-in and outflow rate (solid) during second decline. All three pressure declines are nearly identical, overlapping each other in much of the graph.

This behavior of the pressure decline shows that the cement of the core is not taking in the water by compression of air in the matrix, but instead some other mechanism is allowing small rates of water to pass through. During these pressure decline periods, the injected water was slowly exiting the core's outlet. The effluent was collected over the course of several hours, allowing for the calculation of flow rate through the core. The pressure drop across the core during the collection of each sample was also recorded. With the measured flow rate (Q), measured pressure drop (ΔP), and known fluid viscosity of water (μ) of one centipoise, an apparent permeability can be calculated using Darcy's law:

$$k_{effective} = \frac{Q\mu L}{A * \Delta P}$$

where A is the flow area, taken here to be the area of the one inch diameter cement core, and L is the length of the core. The effective permeability of the core is measured for each sample in order to determine whether flow is occurring in the cement matrix or

through some fracture blockage. The permeability is calculated for each flow rate and pressure pair and is plotted as a function of pressure in Figure 45.

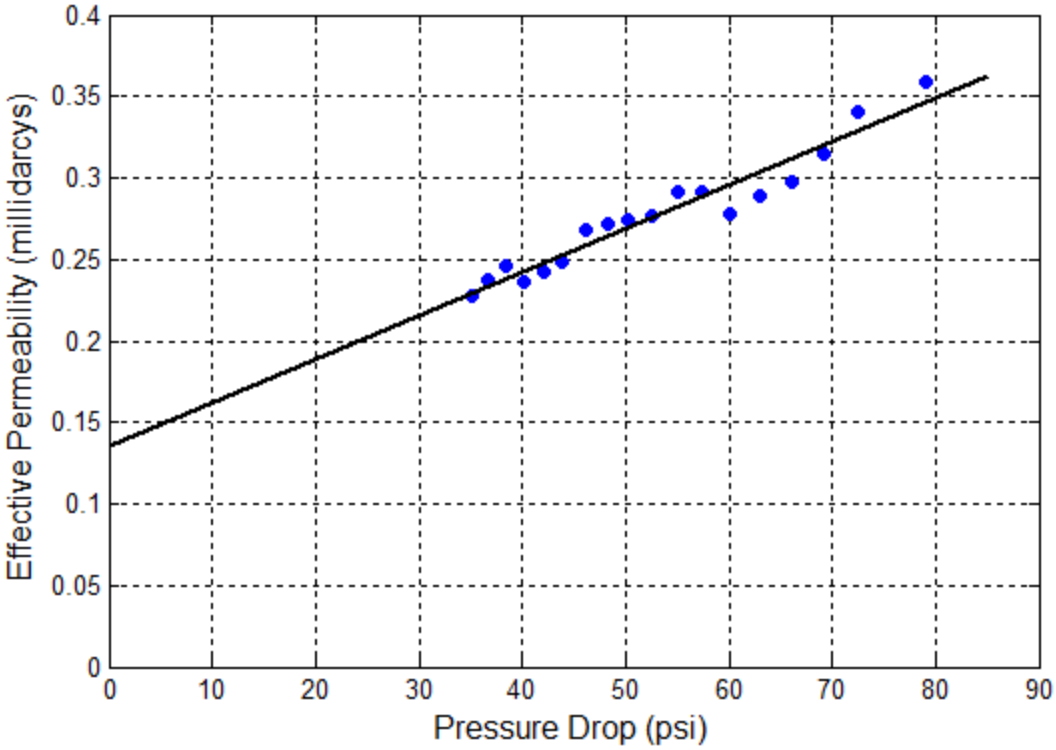

Figure 45: Effective permeabilities to water as a function of pressure in Core 6F-14 with best fit extrapolation to zero pressure drop. Flow rates and pressures taken during pressure buildup/falloff tests shown in Figure 43, then used to calculate effective permeabilities.

Class H cement permeabilities are generally below 200 microdarcys (Kutchko et al., 2009), while the effective permeabilities through Core 6F-14 are between 200 and 400 microdarcys. This indicates that it is possible that the cement matrix is contributing to the fluid flow, though it cannot account for all of it. Additionally, flow in the cement matrix would give a constant permeability independent of pressure, but Figure 45 shows an increasing permeability with increasing pressure drop. It can be seen that the extrapolation of the calculated permeabilities in Figure 46 does not intersect the y-axis at zero effective permeability, but rather at around 135 microdarcys, which is a plausible

permeability for class H cement (Kutchko et al., 2009). This indicates that fluid is flowing in the cement matrix and through the blockage that exists in the fracture.

The proposed hypothesis for this changing permeability is that, although the epoxy core holders can hold pressures over 80 psi in traditional cores, the pressure in the fracture pushes apart the two cement faces and temporarily increases the aperture of the slot. The polymer blockage inside the fracture remains and prevents fluid from quickly leaving the core, but the additional flow space allows some flow out of the core. As the pressure decreases, the additional aperture is reduced, allowing less flow. For example, just after shut in, at 80 psi, the effective permeability is 360 microdarcys which would correspond to a 1" wide fracture with a 0.0044 mm (4.4 micron) aperture. Comparatively, the effective permeability at 40 psi is 230 microdarcys, corresponding to a 0.0038 mm (3.9 micron) aperture slot. Since the nominal aperture of the fracture is 359 microns at the beginning of the experiment (Figure 40), this very small effective aperture is consistent with a blockage of the fracture by not-quite-impermeable material such as syneresed polymer.

This odd behavior of the fluid breakthrough prompted the use of a new type of core in which visual inspection of the fracture is possible. The ability to see the fracture blockages in real time would allow for more accurate description of blockage mechanisms and will show the location of the blockage.

4.3 Cement-Plastic Plate Fractures

The results of the cement-cement fracture cores 6F-6, 6F-12 and 6F-14 made it imperative to be able to visually inspect the fractures before, during, and after injection. The epoxy core holder used in cement-cement fractures allowed only for post-injection inspection, and even this was difficult and rendered the core unusable afterwards. A

method was therefore developed to inspect the fracture in real time by using epoxy to seal half a cement core to a thick clear plastic plate.

4.3.1 Cement-Plastic Core Construction

Cement-plastic cores are built by taking one half of the sawed or fractured cement cylinder and using epoxy to attach it to a plastic plate. For a single cement cylinder that is fractured during the Brazilian test, the core fractures in such a way that slightly concave and convex halves are created. A diagram of this concave/convex fracture behavior and how it fits with a plastic plate is shown below in

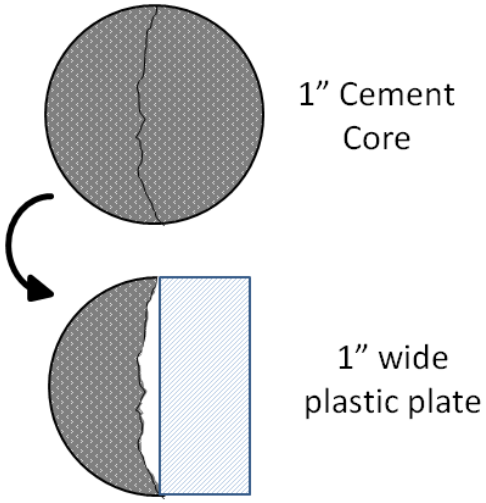

Figure 46: Diagram of tensile fracture in a cement core, made during Brazilian test. The core half with the concave side is chosen to be attached to the clear plastic plate.

Core endcaps are epoxied onto both ends of the core. The plastic plate is built with holes at both ends into which 1/4 inch Swagelok fittings can be epoxied, which served as pressure taps into the fracture and ensures that the pressure losses through inlet and outlet fittings are excluded from estimates of apparent viscosity. Unlike regular epoxy core holders, these cores are not submerged in epoxy, but the secondary epoxy is used to coat the cement side of the core to prevent any evaporation after water saturation. The cement and fracture are totally sealed from atmosphere, but with an inlet and outlet.

The cement-plastic cores showed a tendency to have small leaks, but the core setup was simple and discovery of leaks was instantaneous, as well as the leak location, which proved useful to enable small repairs. These cores can hold pressures up to 40 psi, but a general 20 psi pressure limit was used to prevent excessive wear on the sealing epoxy.

The traditional epoxy core holders were also prone to leaks, but they were much more difficult to identify and fix.

4.3.2 Polymer Injection and Results

Polymer injection experiments were carried out in multiple cores with varying injection, polymer, and fracture parameters. Many of these cores encountered experimental difficulties, especially in the form of leaks through the epoxy connecting the fracture to the plastic endcaps. Experiments which did not encounter these difficulties, or which were sufficiently repaired, are listed in Table 12 with relevant injection polymer and core parameters. These experiments are described in detail in the following section.

Core	Aperture[a] (mm)	Carbopol 934 wt%	NaCl wt%	Residence Time (min)
6FP-1	0.744	3	0.5	32
6FP-2	0.388	3	0	32
6FP-3	0.613	3	0	16
6FP-4	0.511	3	0	16
6FP-5	0.712	3	0	16
6FP-6	0.542	3	0	16
6FP-11	0.399	3	0	**1**
6FP-13	0.399	3	0	1
6FP-15	0.358	0.5	0	1

Table 12: Polymer injection experiments in cement-plastic plate fracture cores, with injected polymer properties and core apertures.

To recognize and describe the pressure drop and effluent pH data that are observed in these experiments, a list of six typical results and their interpretation are shown below in Figure 47.

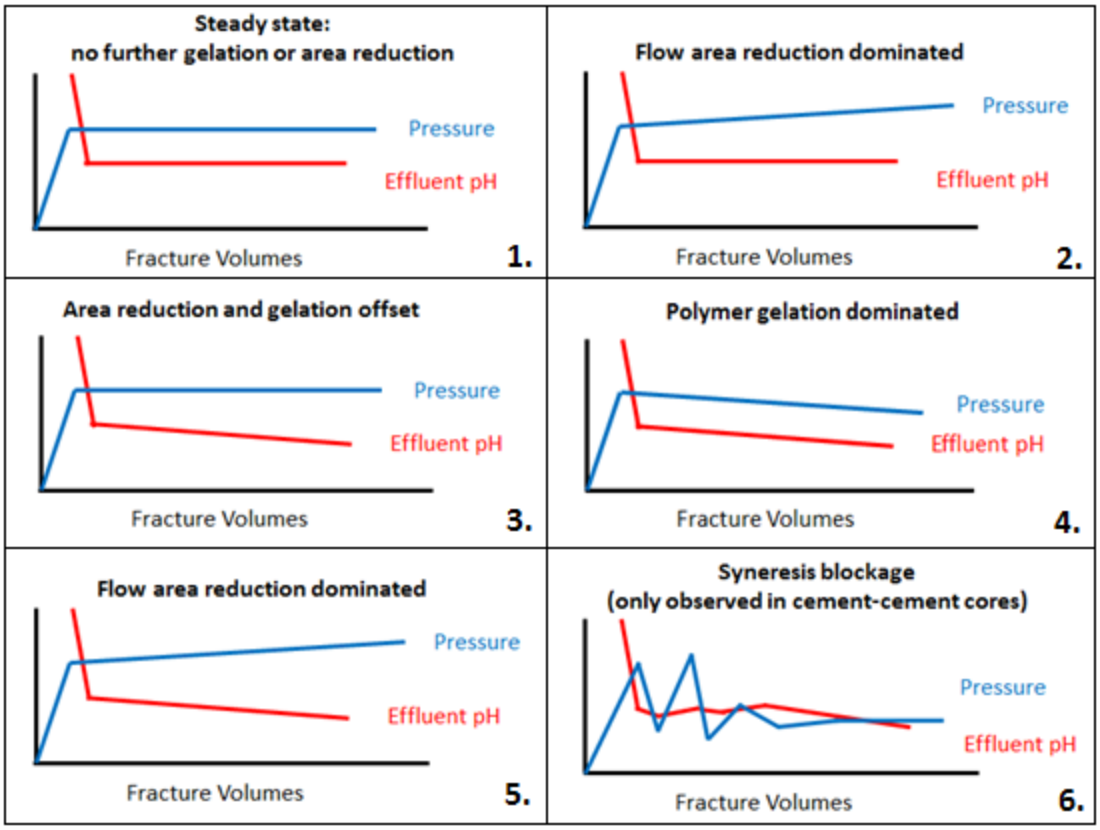

Figure 47: List of typical pressure drop and effluent pH responses during polymer injection into cement-cement or cement-plastic plate fractures. Panel 1: steady state; polymer neutralization increases its viscosity until fracture exit is reached. Panels 2-5: Unsteady responses. Two main mechanisms control the pressure drop response: gelation of the polymer dispersion in the fracture and flow area reduction due to syneresis effects. Panel 6 shows a third mechanism, syneresis blockage and displacement.

In general, two mechanisms control the pressure drop response: gelation of the polymer dispersion in the fracture and flow area reduction due to syneresis effects. The explanations and inferences for the six general trends, shown in Figure 47 are as follows:

1. The pH initially decreases as the polymer effluent reaches the pH probe and the pressure drop initially increases as polymer fills the fracture and pressure lines,

but both then remain constant. Depending on the pH value, this indicates either that no reaction is occurring at all (effluent pH = injected pH) or that the cumulative extent of reaction is constant. It also indicates that syneresis effects are not constricting the flow any further than it already has, if at all.

2. The pH remains constant after polymer effluent initially reaches the pH probe. Depending on the pH value, this indicates either that no reaction is occurring at all or that the total reaction is constant. The pressure drop, however, increases over time, indicating that syneresis effects are constricting the flow channel.
3. The effluent pH steadily decreases, which generally decreases the consistency index and yield stress of the polymer dispersion. Despite this decreased viscosity, the pressure drop remains constant. This likely indicates that polymer gelation effects and syneresis flow channel reduction effects are balancing each other out.
4. The effluent pH steadily decreases, decreasing the consistency index and yield stress of the polymer dispersion. The pressure drop is also decreasing. This generally indicates that the decreasing viscosity of the polymer dispersion is reducing the pressure drop more than flow channel constriction, if any exists, can increase it.
5. The effluent pH steadily decreases, which decreasing the consistency index and yield stress of the polymer dispersion. Despite the decreased effluent viscosity, the pressure drop steadily increases. This generally indicates that syneresis effects are constricting the flow channel in the fracture and increasing the pressure drop more than the decreasing viscosity can reduce it.
6. This type of result is only seen in Core 6F-9, 6F-12, and 6F-14 – all cement-cement fractured cores in which both pressure drop and effluent pH alternatingly

increase and decrease. This behavior is thought to be due to syneresed polymer blocking flow at localized regions inside the fracture, which are subsequently broken through by the pressurized polymer dispersion.

4.3.2.1 Core 6FP-1

The effects of syneresis had been seen in all batch tests, as shown in Chapter 3.3, but the extent of the effect had not yet been visually confirmed in a polymer injection experiment. Experiment 6FP-1 (the added "P" to denote plastic plate), seen below in Figure 48, was injected with polymer dispersion with the typical 3 wt% Carbopol 934, but also has 0.5 wt% NaCl salt, reducing the consistency index and yield stress. The cement was naturally and irregularly fractured via the Brazilian test. The polymer dispersion injection rate into the core began at 0.194 mL/min, resulting in a 16 minute residence time in the fracture, but the rate was decreased to give a 32 minute residence time, then decreased again to give a 64 minute residence time. These flow rate changes are shown on Figure 48. It can be seen that the effluent pH begins to increase as soon as the flow rate is reduced, both at 1 and 5 FVs of polymer injection. This is because slow flow rates allow for more reaction between the polymer and cement, increasing the pH.

Core	Aperture	Polymer Injected	Residence Time	Volume Injected	Fracture Type
6FP-1	0.744mm	3 wt% Carbopol 934 0.5 wt% NaCl	32, 64 min	25 FVs	Cement-Plastic Brazilian

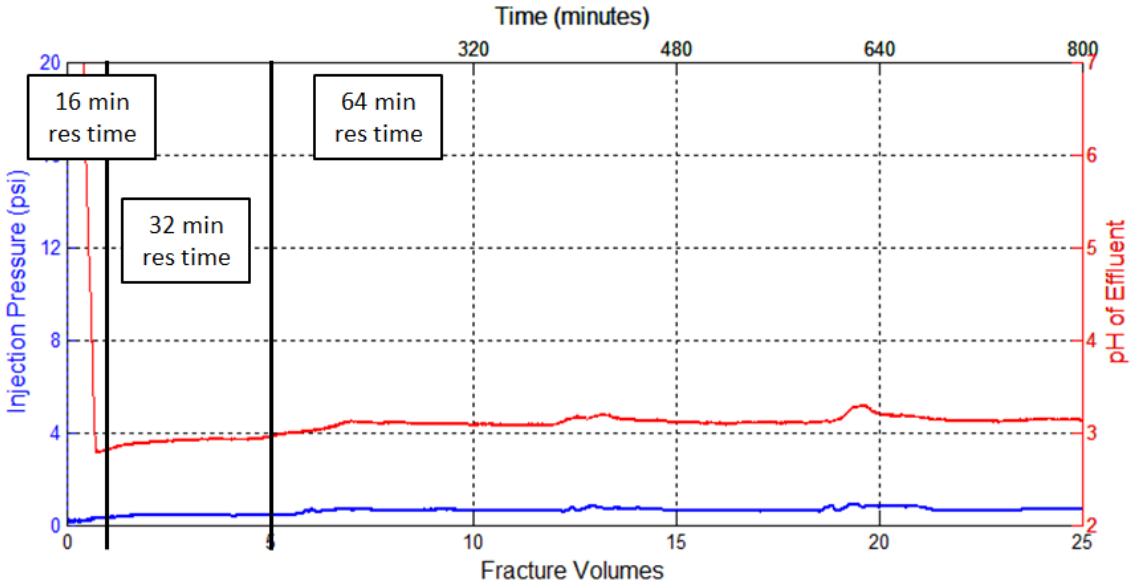

Figure 48: Data recorded during polymer injection (3 wt% Carbopol 934, 0.5 wt% NaCl, and DI water) into Core 6FP-1.

The pressure drop history in Core 6FP-1 is drastically different than Cores 6F-9 and 6F-12, despite each core being injected with the same polymer formulation (3 wt% Carbopol 934 and 0.5 wt% NaCl). The magnitude of pressure drop in Core 6FP-1 is very low and is relatively unchanged throughout the 25 fracture volumes injected over the course of 800 minutes, whereas 6F-9 and 6F-12 have pressure histories with many peaks and troughs with magnitudes 4 and 15 times larger, respectively.

The effective hydraulic aperture of 6FP-1 is larger (~100%) than 6F-9 and 6F-12 and therefore will impact the pressure drop significantly. With an aperture twice as large, the pressure drop through a core will be $1/8^{th}$ as large. While this is significant, it doesn't entirely explain the difference in behavior between these experiments. In Core 6FP-1 the non-monotonic behavior is completely absent.

This replacement of half the cement fracture with a plastic plate is thought to have a stronger effect on the flow channel than the polymer/cement reaction rate. Cores 6F-9 and 6F-12 were created by fracturing a cement core using the Brazilian test, then offsetting the two halves and putting them back together, as described in Chapter 4.2.1. This creates an irregular flow channel through the fracture that widens and narrows with width and length along the core, creating pinch points at some points and large openings at others. The reported hydraulic aperture is the average aperture throughout the entire core, as described in Chapter 4.2.1.1. The flow channels in cement-plastic plate fractures, however, are more uniform, as one face of the fracture is flat and does not follow the contours of the opposite face. Therefore, two cores with the same effective hydraulic aperture, one a cement-cement fracture and the other a cement-plastic plate fracture, could have drastically different local apertures along the length of the flow channel. A diagram of these fracture geometries is shown in Figure 49.

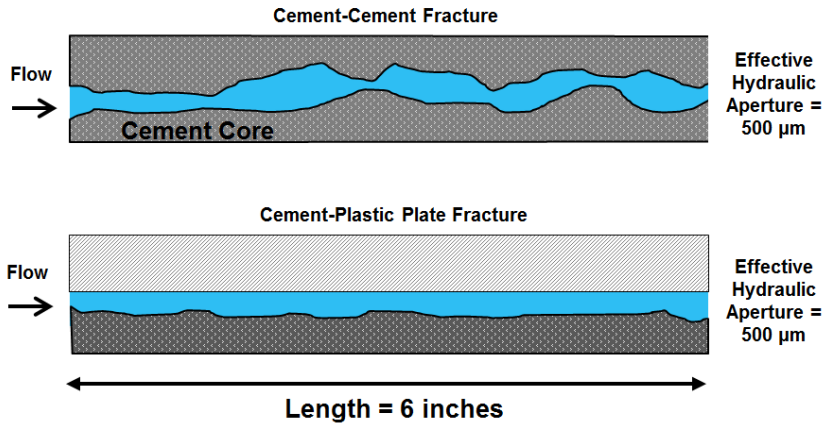

Figure 49: Diagram of differences in actual aperture between cement-cement fracture and cement-plastic plate fracture, note especially the pinch points in the cement-cement fracture, despite similar effective hydraulic apertures (note: figure not drawn to scale).

It is observed that the 50% decrease in flow rate at 5 FVs of polymer injection (i.e. doubling of residence time) results in a slightly larger pressure drop through the core.

At 4 FVs, the apparent viscosity is calculated to be around 6,400 cP while the apparent viscosity at 12 FVs is calculated to be around 22,000 cP. The pressure drop is very small in Core 6FP-1, near the resolution of the pressure transducer, so these apparent viscosities are approximations. At 12 FVs, the apparent viscosities calculated from the initial polymer and effluent HB parameters give a lower and upper bound of 1300 cP and 9200 cP. Similar to 6F-12, the apparent viscosity calculated from pressure drop exceeds the upper limit from the effluent rheology, which is thought to be due to flow channel constriction. The presence of this flow channel is confirmed in the photographs taken during polymer injection, show in Figure 50.

As described in Chapter 4.3.1, cement-plastic plate fractures using Brazilian fractured cement were made using the concave half of the cement core, thus creating the flow channel shown in the bottom panel of Figure 49. For a given effective hydraulic aperture, a cement-cement fracture will be more likely to have local, discrete blockages of syneresis polymer. This behavior is further discussed in Chapter 4.3.4.

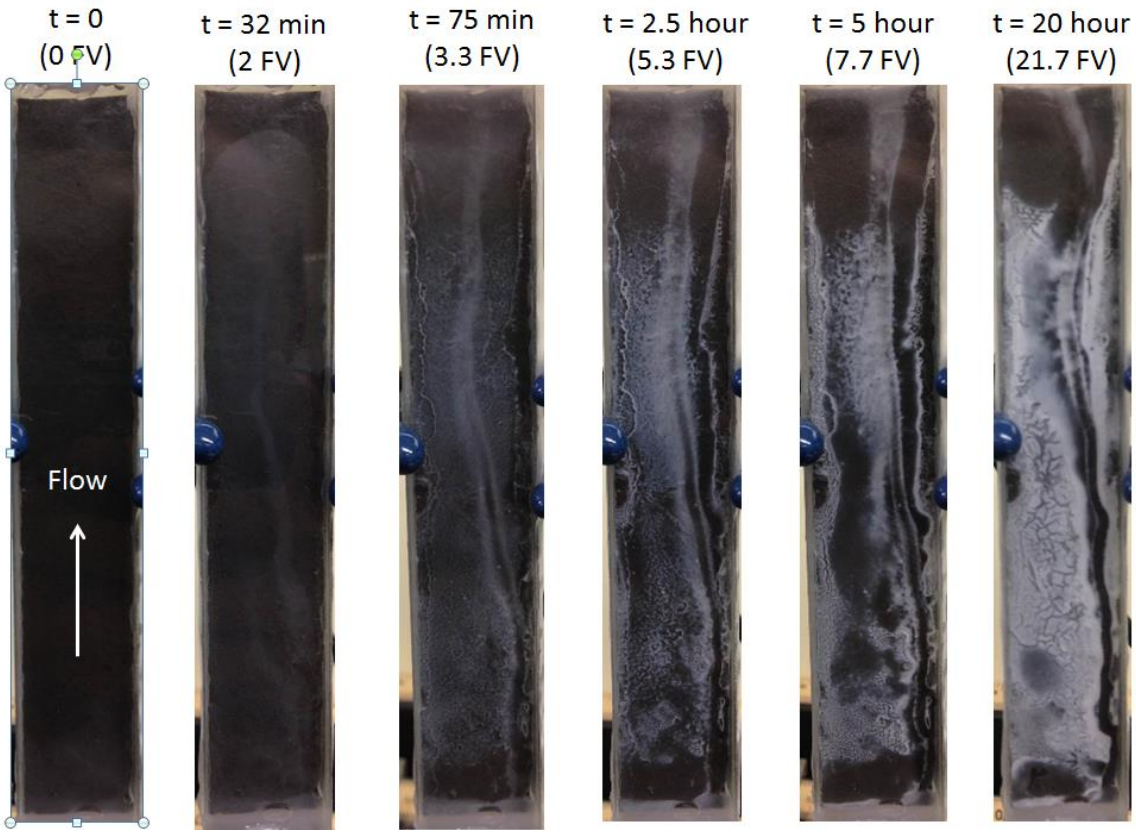

Figure 50: Photographs of Core 6FP-1 during polymer injection (3 wt% Carbopol 934, 0.5 wt% NaCl) at various times. Leftmost image is before polymer injection, rightmost is near end of injection. View is through the clear plastic plate that makes up one face of the fracture.

Figure 48 shows that the pressure drop and effluent pH history are more or less constant at mid to late time, indicating that steady state has been reached. The effluent pH is above the injected polymer pH, confirming that a reaction has occurred. It is clear from Figure 50 that syneresed polymer is present in the fracture and that a flow channel does exist, but it can be inferred in conjunction with the pressure drop and effluent pH data that the majority of the flow channel constriction had occurred early on, between 0 to 6 fracture volumes.

However, the photographs show a narrow flow channel being surrounded by syneresed polymer, and the pressure data show a slight increase in pressure drop as more fracture volumes are injected. From these, it is clear that the flow channel is slowly

constricting as polymer undergoes syneresis onto the cement face, reducing the available flow area and therefore proportionally increasing the pressure drop. The pressure drop across the core only slightly increases over time, so it can be inferred that the flow constriction is minor as well. Interestingly, the pH quickly dives below 3, then slowly increases, indicating that the acid is more readily consumed as time goes on. This could be attributed to the longer residence times when the flow rate is decreased and the presence of salt, which both serve to increase the amount of polymer that is lost due to syneresis.

The severity of the syneresis effect on the polymer in fractures was unknown until Core 6FP-1 was shut in after polymer injection. Figure 51 shows several photographs taken days after polymer injection. The mud crack pattern observed in the batch tests (cf. Figure 10, Figure 11, Figure 12) is seen covering all but the very top of the cement-plastic fracture. Most of the syneresis has occurred within 48 hours, and would likely occur faster in narrower slots with less polymer volume. The core was then subjected to a polymer strength test in which deionized water with red dye was slowly injected into the core inlet (at the bottom, see Figure 52), building pressure until breakthrough. As discussed for the polymer strength tests for cement-cement fractures in Chapter 4.2.3, the polymer gel's yield stress will not permit flow until the flow initiation pressure is reached, at which point gel is displaced and water has a pathway for flow through the fracture. The maximum pressure at the core inlet during this experiment, just before water breakthrough, corresponds to the flow initiation pressure of the polymer gel.

The polymer gel in Core 6FP-1 held back a negligible pressure gradient before the red water displaced it. Figure 52 shows this red water infiltration. At the bottom, near the core inlet, the red water goes through a narrow channel in what looks to be polymer gel, whereas the gel in the middle of the core is affected by syneresis and the red water

quickly disperses to fill the whole fracture. Syneresis is the contraction of polymer gel that expels water in the process. This mechanism will cause the polymer gel that originally fully filled the fracture to contract and expel water, creating regions in the fracture that are filled with water, a Newtonian fluid. Because the water has no yield stress, it is unable to hold pressure, and the red displacing fluid flows easily through the core.

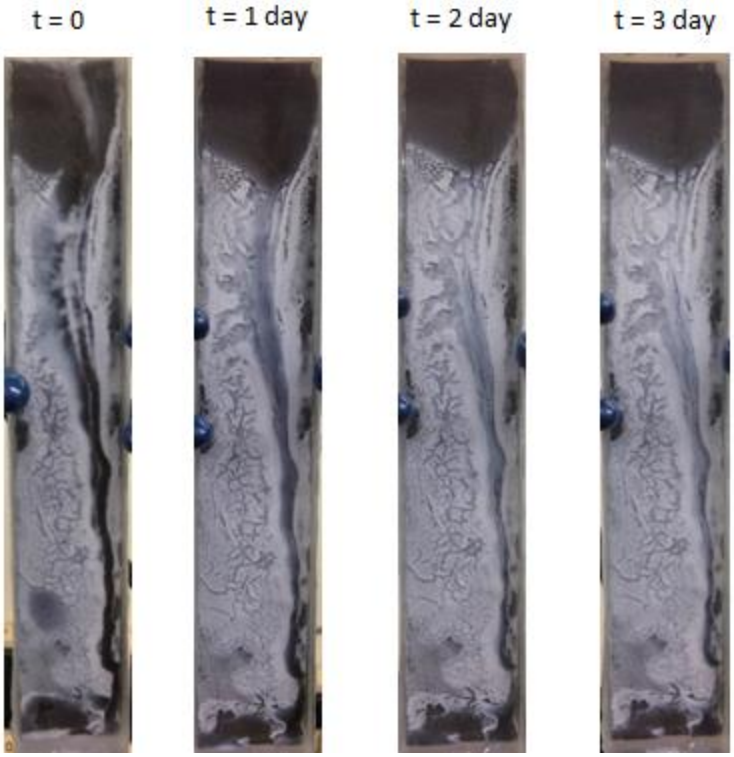

Figure 51: Photograph of Core 6FP-1 held at static conditions following polymer injection (3 wt% Carbopol 934 and 0.5 wt% NaCl) at various times (elapsed since shut-in after polymer injection). Leftmost image is immediately after polymer injection.

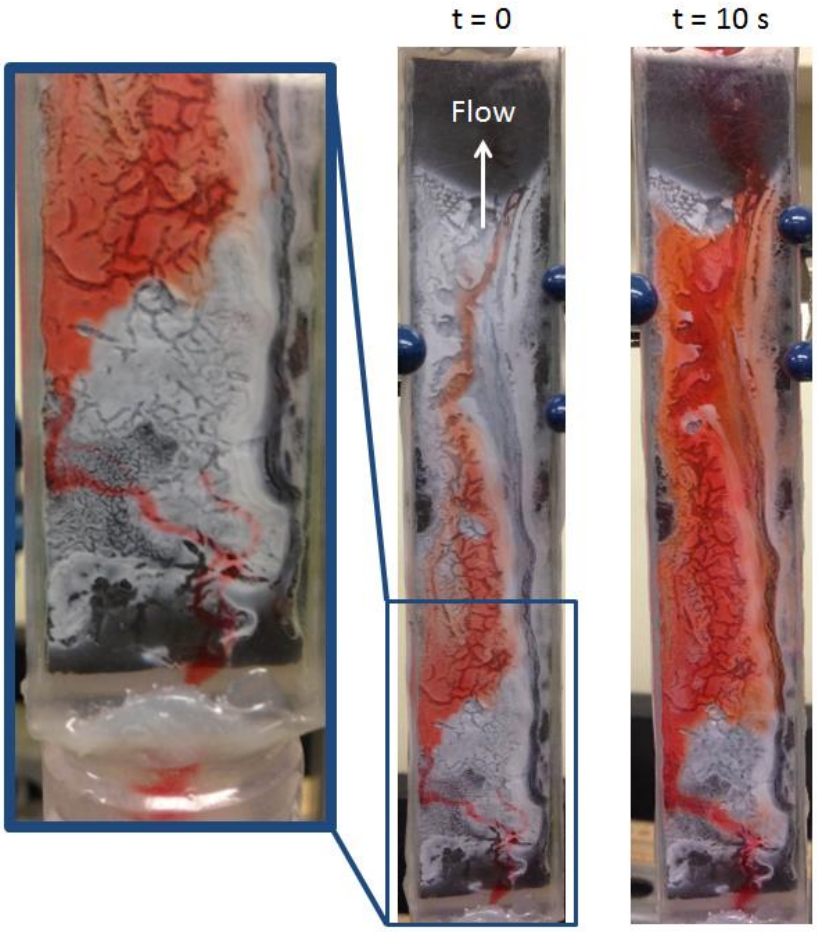

Figure 52: Photograph of breakthrough during pressure strength test in Core 6FP-1. Red DI water was used to displace contents of the fracture, which included syneresed polymer (white), polymer gel (clear) and water (alsp clear) expelled from the syneresed polymer.

4.3.2.2 Core 6FP-2

Core 6FP-2 was injected with 3 wt% Carbopol 934 polymer dispersion without salt. The cement fracture face was formed by causing the cement core to fail in tension via the Brazilian test. The flow rate was initially set at 0.44 mL/min for a polymer residence time of 32 minutes. Figure 53 shows the data collected during polymer injection. The injection pressure is much higher than the injection pressure from Core 6FP-1 and continually rises, even after the fracture is completely filled with polymer.

During the experiment, the pH probe did not reliably record real-time effluent pH, but the data collected provides an average pH.

When the flow rate was doubled after 7 fracture volumes, the slope of the plot of pressure vs time also increases. At 6 FVs of polymer injection, the apparent viscosity is around 60,000 cP, but when the flow rate is doubled the apparent viscosity increases to 70,000 cP. As a shear thinning fluid without pH-sensitive effects, the apparent viscosity should decrease as flow rate is increased, but here it increases by ~17%. The doubled flow rate would also reduce the polymer-cement reaction rate, which in turn would decrease the polymer's yield stress and consistency index.

Core	Aperture	Polymer Injected	Residence Time	Volume Injected	Fracture Type
6FP-2	0.388 mm	3 wt% Carbopol 934 0 wt% NaCl	32 min	10 FVs	Cement-Plastic Brazilian

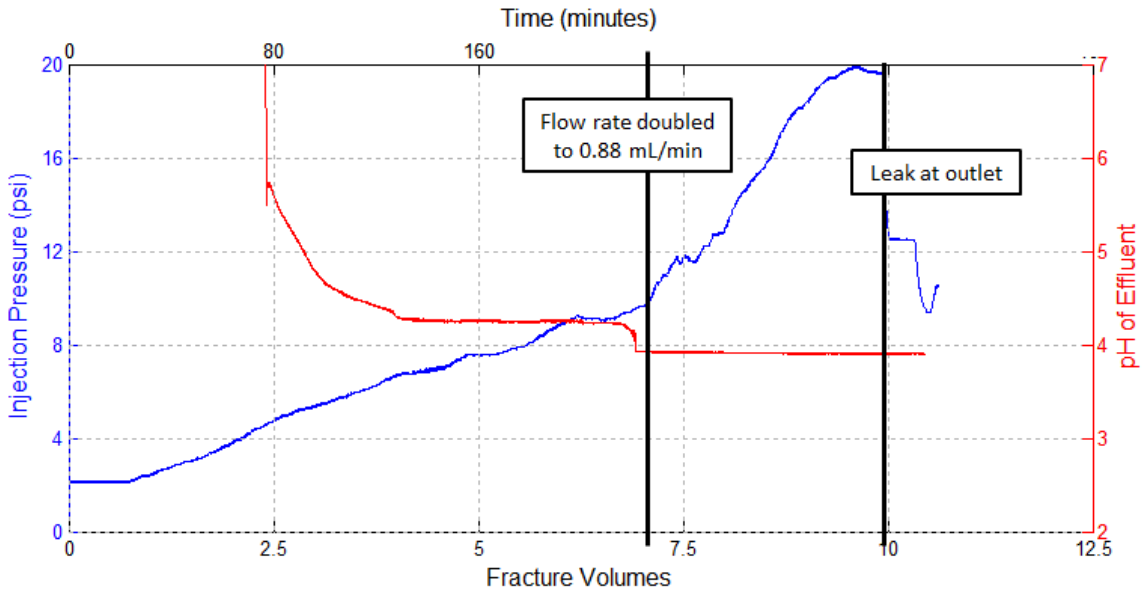

Figure 53: Data recorded during polymer injection (3 wt% Carbopol 934, 0 wt% NaCl, and DI water) into Core 6FP-2.

This pressure drop behavior was unlike previous experiments (6F series and 6FP-1) in that the pressure continuously and monotonically builds during the entire experiment. This was also the first polymer injection experiment in which this polymer formulation, 3 wt% Carbopol 934 and 0 wt% NaCl, was used. Without the addition of any NaCl into the polymer dispersion, the yield stress and consistency index of the polymer were significantly higher, as previously shown in Figure 6 and Table 4.

Because the apparent viscosity of the polymer increases from 6 FV and 9 FV, despite the increase in shear rate and reduction in pH, there must be another mechanism at work. There are two possibilities that could account for this behavior.

1. Core 6FP-2 was constructed with 1/8" OD plastic pressure lines, which are sufficiently large to allow accurate pressure transmission when the 3 wt% Carbopol 934 and 0.5 wt% NaCl polymer dispersion is used. With the more viscous dispersion used in Core 6FP-2, the inlet and outlet pressures will not be as accurately or quickly transmitted to the pressure transducer. This behavior is discussed in Appendix B. It is possible that the pressures in the inlet and outlet pressure lines had not yet equilibrated with the pressure in the actual core and were not correctly measuring the actual pressure drop in the core.
2. The flow channel of the polymer dispersion was constricted by syneresed polymer over time, reducing the width and/or aperture of the cement-plastic plate fracture.

Figure 54 shows the photographs taken during polymer injection, as well as 12 hours after shut in. While the syneresis mud crack pattern is absent, the white calcified gel is still present and a flow channel (dark narrow pathway on left side of fracture) is

evident. After shut in, the entire fracture, even the flow channel, is covered in calcified gel.

Core 6FP-2 was plagued with leaks during the end of displacement experiments, but repairs were made and the core was connected to the long term, low pressure gradient manifold. These leaks did not affect the polymer injection experiment. The polymer was able to hold back the 2.5 psi/ft gradient from brine for 2 weeks, but it was determined that the brine was being blocked by a thick region of syneresis polymer instead of the polymer gel. This is discussed further in 4.3.3 Conclusions and Discussion below.

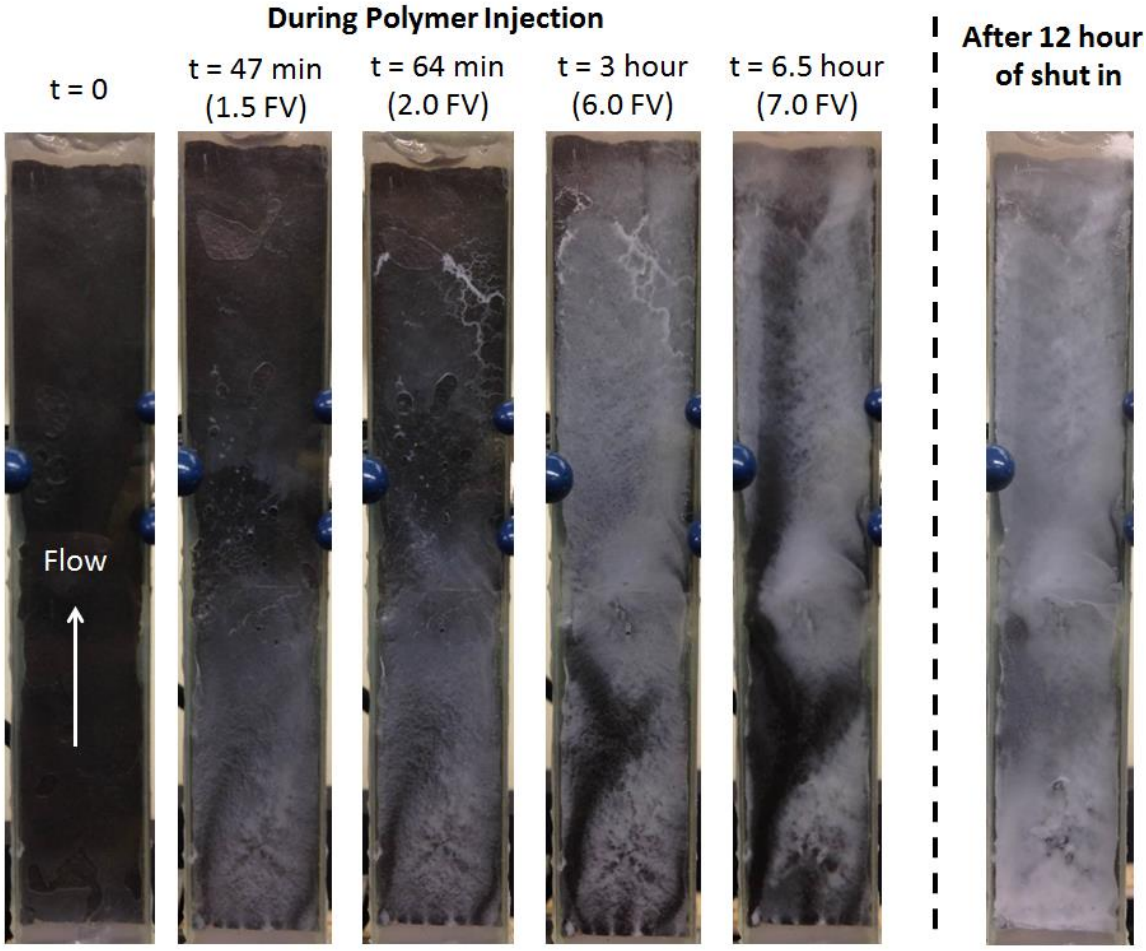

Figure 54: Photograph of Core 6FP-2 during polymer injection (3 wt% Carbopol 934). White material is presumed to be syneresed polymer deposited onto the cement fracture face.

4.3.2.3 Core 6FP-3

Experiment 6FP-3 used the same injection parameters and polymer dispersion as 6FP-2, but with refined methods and a single, constant injection rate for a polymer residence time of 16 minutes. The cement was fractured in tension. The pressure and pH data are shown in Figure 55 below. The various spikes in both data curves are due to movement of the pH probe to ensure that the pH data accurately represents the effluent pH. Similar to Core 6FP-2, the pressure slowly builds up as fracture volumes are injected, but seems to reach a plateau between 14 and 18 FVs. Similar to 6FP-2, Core 6FP-3 used 1/8" OD pressure lines and therefore the slow pressure drop build between 0 to 14 FVs could be an artifact of the slow gel movement into the pressure lines.

Core	Aperture	Polymer Injected	Residence Time	Volume Injected	Fracture Type
6FP-3	0.613 mm	3 wt% Carbopol 934 0 wt% NaCl	16 min	18 FVs	Cement-Plastic Brazilian

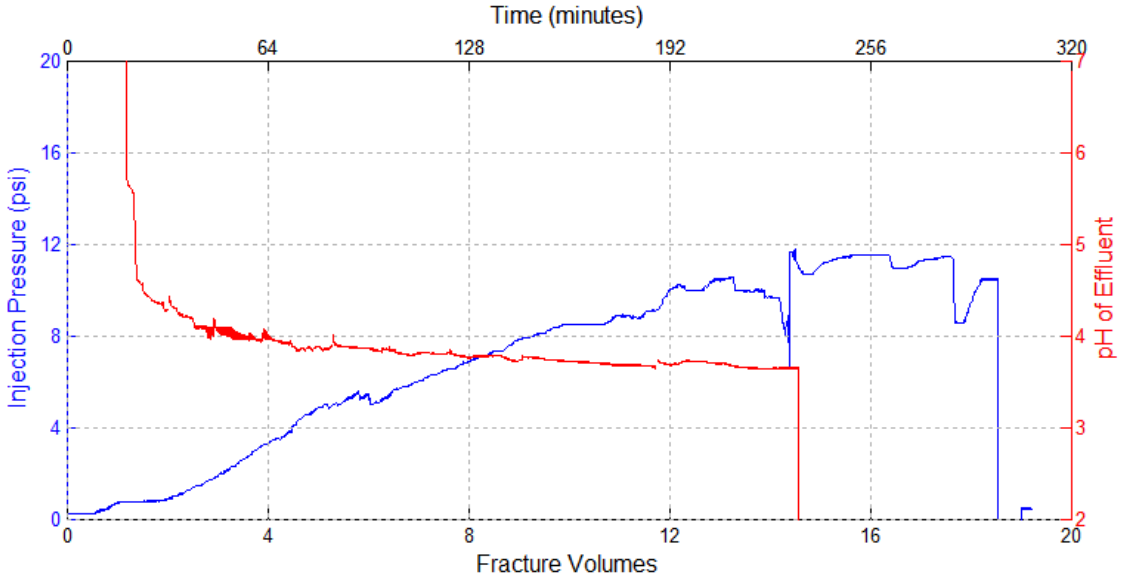

Figure 55: Data recorded during polymer injection (3 wt% Carbopol 934, 0 wt% NaCl, and DI water) into Core 6FP-3.

Figure 56 shows the photographs taken during polymer injection and afterwards of Core 6FP-3. Between 12 and 18 fracture volumes injected, during which the pressure drop has nearly plateaued, there is little visual change occurring. The apparent viscosity of the polymer dispersion at 4 FVs is 10,000 cP and at 13 FVs, near steady state, the apparent viscosity is 31,000 cP, calculated from the pressure drop data. It was shown in Table 10 that these apparent viscosities were between the lower and upper bounds set by the polymer rheology at the inlet and outlet. Core 6FP-3 was constructed with the 1/8" OD plastic pressure lines, indicating that the long pressure build up over time may be due to inaccurate pressure drop readings while the pressure lines equilibrate. The effect may also be due, at least partially, to syneresis polymer constricting flow. These are the same effects that were seen in Core 6FP-2.

Initially, it was thought that syneresis was the main factor responsible for these observations. As syneresis deposits polymer onto the cement surface, the pressure drop and fluid velocity increase. Deposition of syneresis polymer is slowed when the fluid velocity becomes large enough to strip and remove the topmost polymer from the deposited layer, and eventually steady state is reached in this way, i.e. the rate of deposition of syneresed polymer is balanced by the rate of detachment of polymer. This is an important point that will significantly increase the injection pressure and must be accounted for. Core 6FP-3 was also connected to the long term pressure manifold and maintained pressure for 13 days, but like 6FP-2 the brine was held back by the syneresed polymer, not the polymer gel.

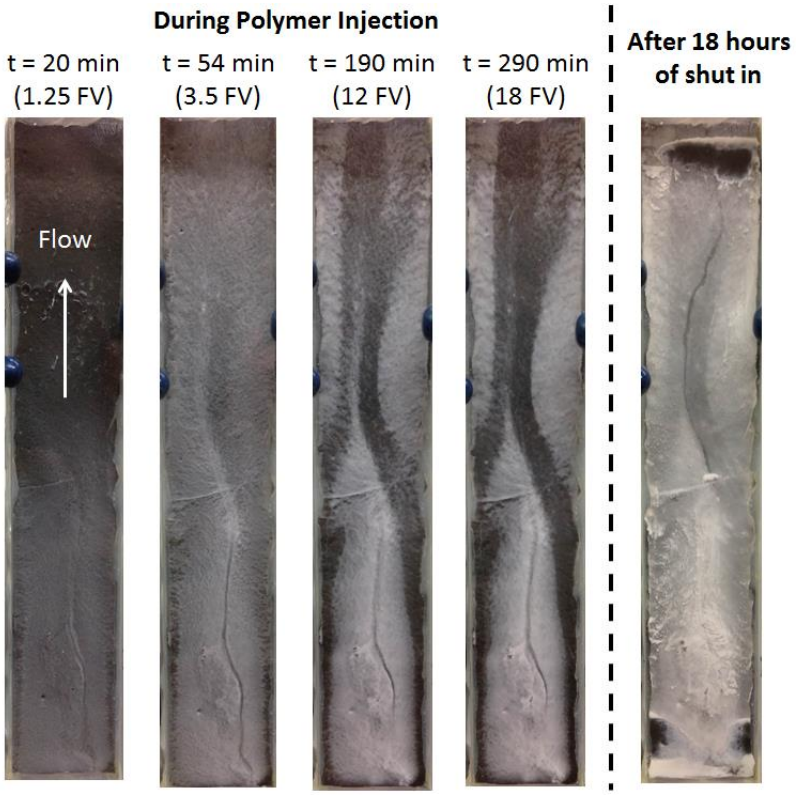

Figure 56: Photograph of Core 6FP-3 during polymer injection (3 wt% Carbopol 934, 0.5 wt% NaCl). White material is presumed to be syneresed polymer; the dark channel evident at 190 min and 290 min allows steady state flow and reaction (see late time behavior in Figure 55) and becomes less perceptible after shut in due to syneresis with Ca^{++} dissolved from cement.

Cores 6FP-1, 6FP-2, and 6FP-3 were irregularly fractured cores, and the flow channels absent of syneresed polymer flow channels followed the large aperture regions in the slot. As seen in Figure 56 above, there exist two flow channels at the bottom half of the fracture, which converge into one channel at the top half. The nonuniformity in the initial fracture geometry complicates the interpretation, and it would be desirable to have a uniform slot aperture, both in the length and width dimensions.

4.3.2.4 Core 6FP-4

In Core 6FP-4, the slot was constructed using a cement core that was sawed in half, providing a fat fracture face. Again, 3 wt% Carbopol 934 polymer dispersion was injected into the fracture, and the results are shown below in Figure 57. The injection

pressure and pH profile are nearly identical with Figure 55: the pressure plateau reaches about 11 psi at the 16 fracture volumes injected mark and the end pH is around 3.75 for both. Again, Core 6FP-4 used the 1/8" OD pressure lines, which may have induced artifacts in the form of the continuous pressure build over time.

Core	Aperture	Polymer Injected	Residence Time	Volume Injected	Fracture Type
6FP-4	0.511 mm	3 wt% Carbopol 934 0 wt% NaCl	16 min	16 FVs	Cement-Plastic Sawed

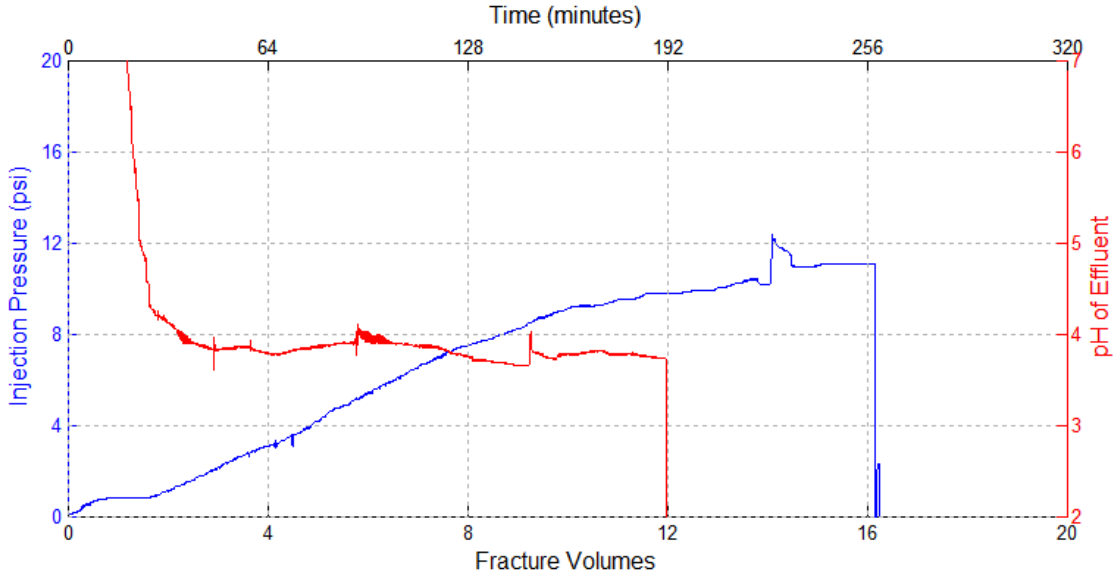

Figure 57: Data recorded during polymer injection (3 wt% Carbopol 934, 0 wt% NaCl, and DI water) into Core 6FP-4.

At 6 FVs of polymer injection, the apparent viscosity is calculated from the pressure drop data to be 35,000 cP, while at 12 FVs the apparent viscosity is around 64,000 cP. At 12 FVs, the pH of the effluent indicates that the effluent has a yield stress of 175 Pa. If the fracture was entirely filled with this 175 Pa yield stress fluid, no flow would occur until a pressure drop of 15 psi was reached. However, the effluent pH of 3.8 at 12 FVs is the maximum polymer pH, where the polymer inside the fracture

exhibits a gradient from the inlet minimum to outlet maximum. Therefore, flow can and does exist at 12 FVs when the pressure drop is 10 psi.

The photographs taken during polymer injection can be seen in Figure 58 below. Again a narrow polymer flow channel is created as more fracture volumes are injected, but the texture of the syneresis is much smoother in Core 6FP-4 compared to 6FP-3, due to the fracture being sawn in half instead of fractured by the Brazilian test. This experiment also shows more clearly a process by which syneresed polymer is deposited over the whole fracture face, then is stripped away as the flow converges. Figure 59 zooms in on a section of cement before polymer injection and after 6 and 13 fracture volumes of polymer injection. It's clear that the white syneresis polymer has covered the cement after 6 fracture volumes, but is then removed after 13 fracture volumes. Yet it is also clear that, after 18 hours of shut in, the syneresed polymer has reformed on this dark flow path. Because the fluid movement prevented the deposition of syneresed polymer, the lack of fluid movement during shut in causes any syneresed polymer deposited to remain in place in the former flow channel.

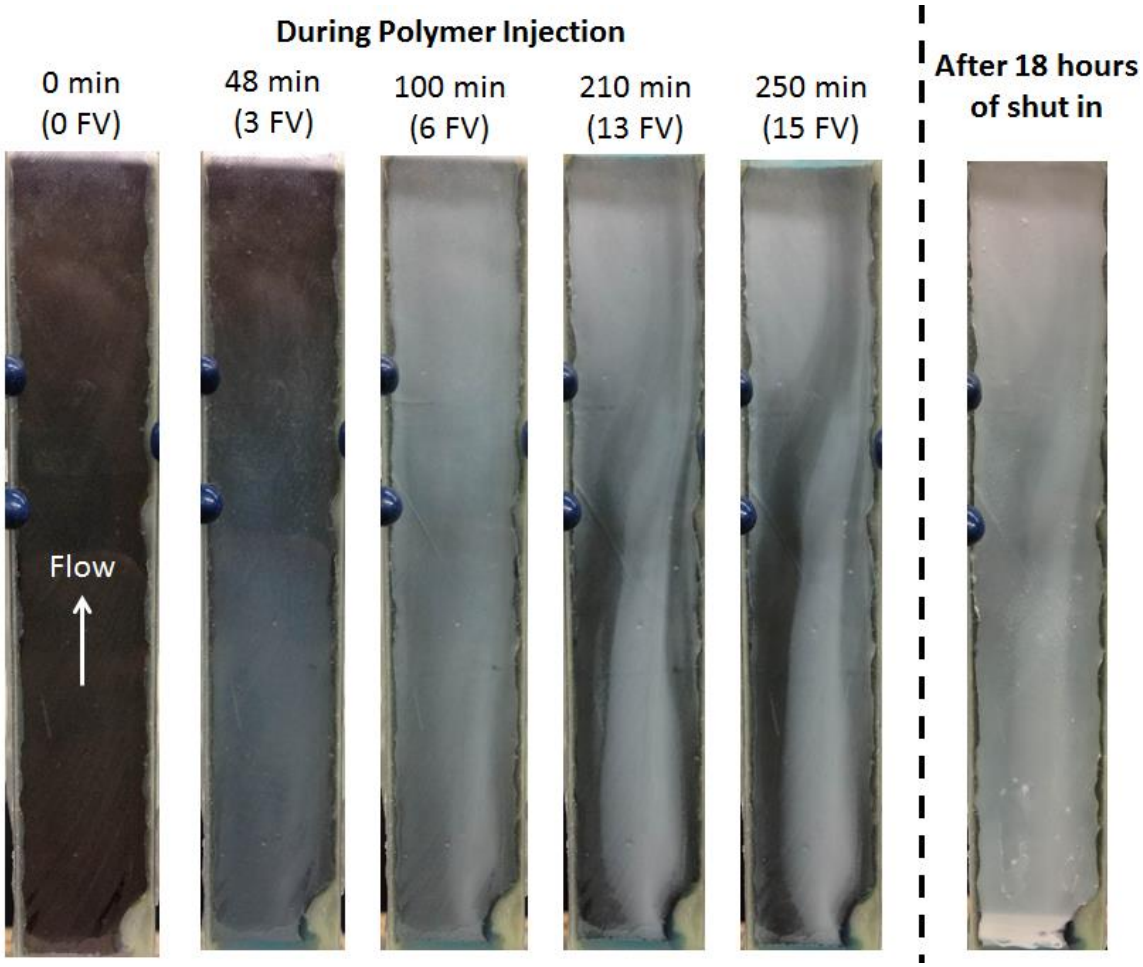

Figure 58: Photographs of Core 6FP-4 during polymer injection (3 wt% Carbopol 934, 0.5 wt% NaCl).

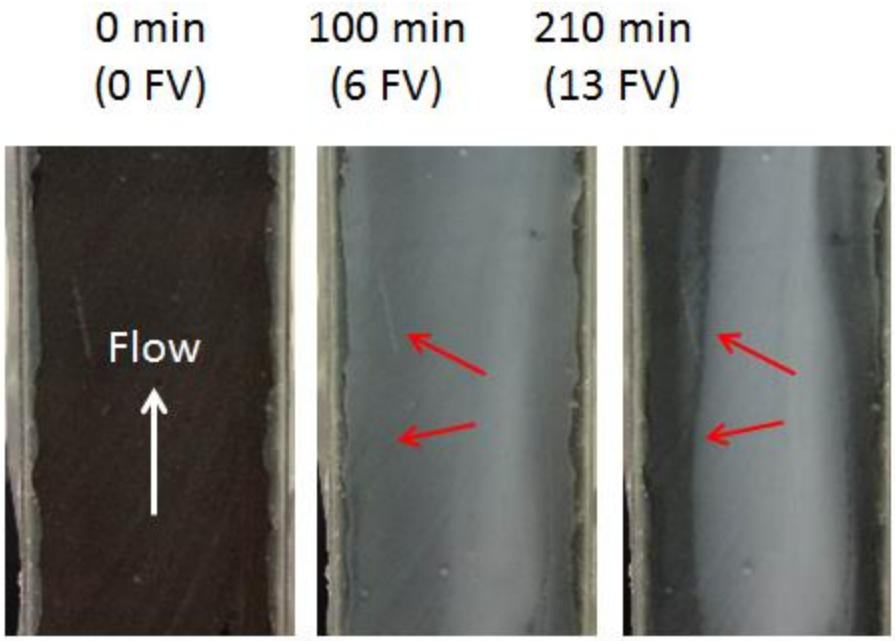

Figure 59: Photographs of Core 6FP-4 during polymer injection; red arrows indicate the removal of syneresis polymer from the cement face.

Figure 59 shows that even in a slot that has relatively uniform aperture, complex flow patterns emerge. These patterns are difficult to quantify, but Figure 60 below gives a qualitative overview of the mechanism. The flow area decreases and eventually shifts towards a more circular channel, the ideal flow channel as wall friction is minimized. It should be noted that thepolymer's yield stress also influences this pattern. Regions with the smallest aperture have the smallest shear stress and are therefore more likely to be blocked by polymer gel, becoming essentially no flow regions as well.

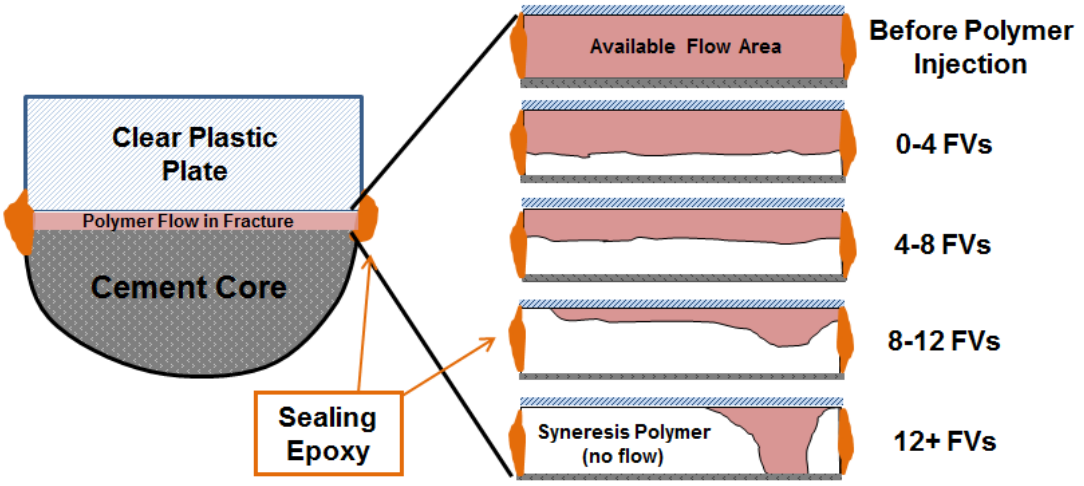

Figure 60: Diagram of mechanism for flow area reduction due to syneresis polymer (fracture slots not to scale); available flow area (normal to page) in red and syneresis polymer in white, with approximate fracture volume values. The competition between deposition of polymer due to reaction with calcium cations and stripping of deposited polymer by viscous flow leads to a steady state flow pattern at 12+ fracture volumes injected.

Core 6FP-4 was connected to the long term pressure manifold at a pressure gradient of 2.5 psi/ft. Although the only change between 6FP-3 and 6FP-4 was the roughness of the cement fracture face, Core 6FP-4 was unable to hold back the 2.5 psi and brine breakthrough occurred instantaneously. This difference in fracture blocking capability is discussed in more detail in 4.3.3 Conclusions and Discussion.

4.3.2.5 Core 6FP-5

Core 6FP-5 featured a large aperture fracture (700+ microns) and was injected with 3 wt% Carbopol 934 and 0 wt% NaCl polymer dispersion. The pressure and pH response can be seen below in Figure 61.

Core	Aperture	Polymer Injected	Residence Time	Volume Injected	Fracture Type
6FP-5	0.712 mm	3 wt% Carbopol 934 0 wt% NaCl	16 min	20 FVs	Cement-Plastic Brazilian

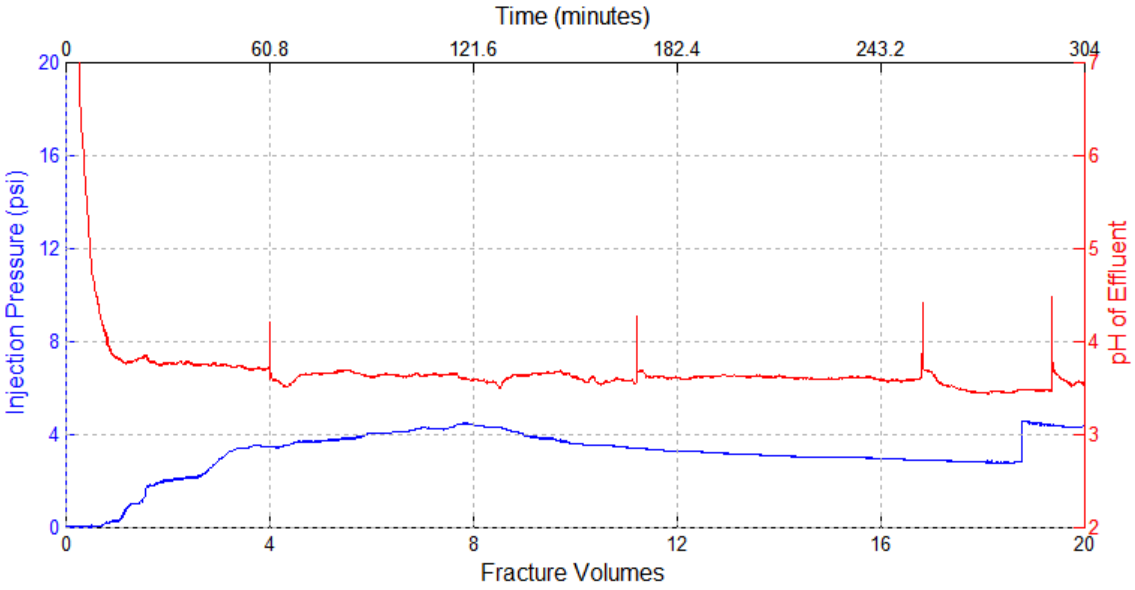

Figure 61: Data recorded during polymer injection (3 wt% Carbopol 934, 0 wt% NaCl, and DI water) into Core 6FP-5.

Interestingly, the pressure builds up as expected, but then starts to slowly decline after 8 fracture volumes. At the peak pressure drop at 8 FVs, the apparent viscosity is calculated to be around 53,000 cP, while at 16 FVs the apparent viscosity is 36,000 cP. Similar to Core 6FP-4, the effluent pH for this polymer formulation (3 wt% Carbopol 934 and 0 wt% NaCl) gives a yield stress of 144 Pa, which would require a 8.5 psi pressure drop to displace if it filled the entire fracture. The fracture is not entirely filled with this polymer however, but is filled with polymer with less yield stress. Polymer is flowing at 12 FVs with a pressure drop of only ~3 psi. The 53,000 cP apparent viscosity from the pressure drop data is therefore plausible, as the upper bound is infinite (no flow).

Similar to Core 6FP-2, 6FP-3, and 6FP-4, this core used 1/8" OD pressure lines to measure pressure drop, which could have caused the pressure drop to appear to

steadily increase, when in reality it may be steady (the behavior of Core 6FP-6, discussed in the next section, provides quantitative support for this possibility). Therefore, two mechanism hypotheses are put forth to explain the nonmonotonic pressure drop behavior in core 6FP-5:

1. The polymer flow behavior is gelation dominated (as shown in panel 4 of Figure 47) which causes the pressure drop to slowly decrease as the yield stress and consistency index of the polymer dispersion decreases with decreasing pH. However, the early portion of this behavior is masked by the slow pressure drop increase caused by the 1/8" OD pressure lines. This behavior is described in Appendix B and shown in Figure 104. At around 8FVs, as shown in Figure 61, the measured pressure drop and the actual pressure drop are equivalent, ending the artificial pressure drop build caused by the pressure lines. After 8 FVs of injected polymer, the measured pressure drop slowly decreases along with the actual pressure drop.
2. If the measured pressure drop error described in 1. does not occur or is not significant, then the nonmonotonic behavior could be due to the effluent pH dropping below the critical gelation pH of the polymer. The effluent pH history of cores 6FP-2, 6FP-3, and 6FP-4 (which were injected with the same polymer dispersion as 6FP-5) never went below pH 3.7, but the effluent pH in Core 6FP-5 dips below 3.5 at nearly the same time as the pressure drop begins to decline. Figure 4 in Chapter 3.1 shows how the yield stress of 3 wt% Carbopol 934 and 0 wt% NaCl decreases suddenly as the pH of the polymer is reduced below around 3.5, going from 340 Pa at pH 3.5 to 200 Pa at pH 3.75. The consistency index of the polymer dispersion behaves in a similar way. Therefore, it is possible that as the effluent's pH drops below this critical pH,

the viscosity of the polymer dispersion, and therefore the injection pressure drop, both begin to decline.

The effluent pH could be decreasing due to the decreasing amount of mineral reactants at the cement surface or a reduction in total reaction due to a narrowing flow channel caused by syneresed polymer. It is likely that both of these factors contribute to the overall effluent pH decrease.

After polymer injection, core 6FP-5 experienced multiple leaks in the epoxy holding the endcaps to the cement-plastic plate core that were detrimental to long term pressure testing and the short term maximum polymer strength test. Therefore, no tests were able to be performed to determine the polymer's strength in the fracture after a period of shut in. These leaks had no effect on the polymer injection data shown above in Figure 61.

4.3.2.6 Core 6FP-6

With more understanding of the syneresis mechanism and flow paths, concern was raised as to whether the polymer fluid flow is definitively occurring in the proposed flow channels (the dark narrow pathways evident in photographs late in polymer injection, before shut in; see Figure 56 and Figure 58 for examples), or if flow is occurring in other areas as well. Core 6FP-6 was injected with 3 wt% Carbopol 934 and 0 wt% NaCl polymer dispersion (similar to Cores 6FP-2 to 6FP-5) with blue food coloring dye added and bubbles periodically added to the inlet and injected into a naturally fractured cement core. The dye and bubbles are intended to give a visual indication of the actual flow path of the bulk of the polymer dispersion through the core. Pressure and pH responses are shown in Figure 62

Core 6FP-6 featured a new design for pressure measurement, using 1/4" OD plastic tubes to transmit pressure to the pressure transducer. The advantages of this setup are outlined in Appendix B and can be seen in the fact that the pressure drop history in Figure 62 increases and plateaus quickly, indicating that the pressure drop increase artifact (as seen in Core 6FP-2 between 1 and 10 FV, in Core 6FP-3 between 2 and 12 FV, in Core 6FP-4 between 2 and 12 FV, and possibly in Core 6FP-5 between 4 and 8 FV) has been significantly reduced.

Core	Aperture	Polymer Injected	Residence Time	Volume Injected	Fracture Type
6FP-6	0.542 mm	3 wt% Carbopol 934 0 wt% NaCl	16 min	20 FVs	Cement-Plastic Brazilian

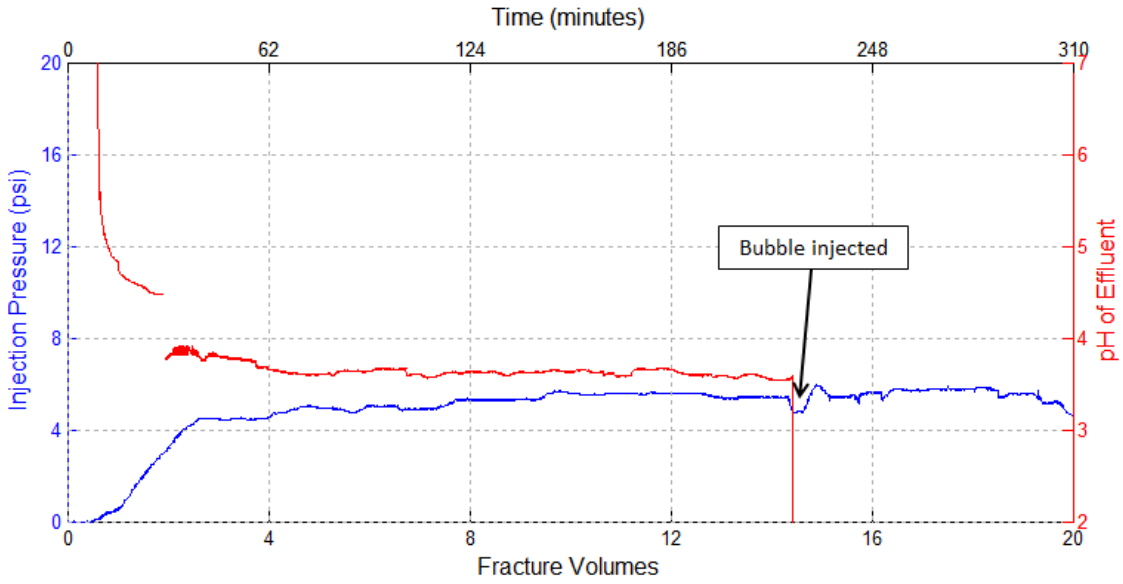

Figure 62: Data recorded during polymer injection (3 wt% Carbopol 934, 0 wt% NaCl, and DI water) into Core 6FP-6.

The effluent pH can be seen to decrease very slowly between 4 and 14 fracture volumes of polymer injection. The pressure drop, however, increases slightly during this period, similar to the behavior described in either panel 2 or panel 5 in Figure 47 in which

the pressure drop increases due to constriction of the flow channel via syneresis. At 12 FVs of polymer injection, approximately steady state, the apparent viscosity is calculated to be around 39,000 cP. The effluent pH again corresponds to a large yield stress fluid that give an infinite apparent viscosity upper bound (no flow).

The extent of syneresis in the cement-plastic plate fracture can be seen in Figure 63 below. The flow pattern is complex, due to a pinch point in the middle/left of the fracture that diverts flow, caused by the irregular topography of the tension fractured cement core.

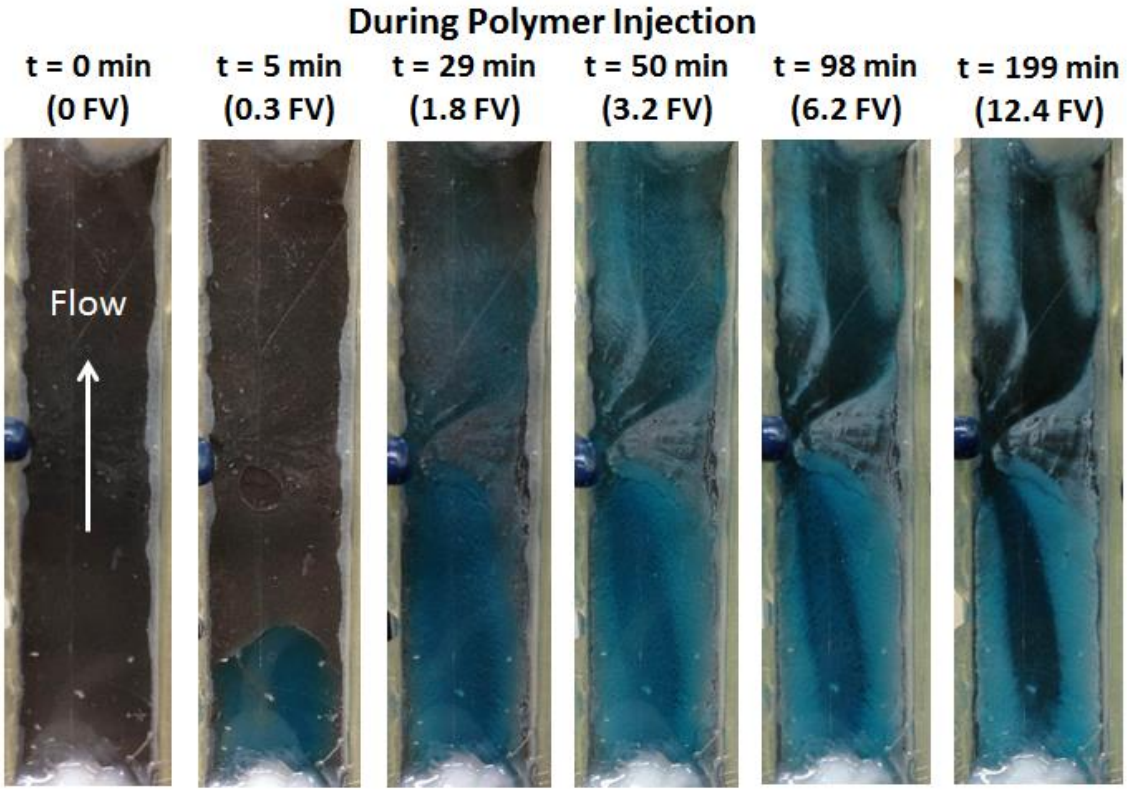

Figure 63: Photographs of Core 6FP-6 during polymer injection (3 wt% Carbopol 934 and 0 wt% NaCl, dyed blue in this experiment for the sake of visibility)

After 14 fracture volumes were injected, a small bubble of air was introduced into the inlet of the system and allowed to move upwards through the core to verify the location of the primary flow conduit. Photographs taken during the bubble's injection

can be seen in Figure 64, with the bubble encircled in white. The bubble stayed within the dark boundaries that had been hypothesized as the main flow channel. The velocity of the bubble was much higher than the polymer dispersion velocity in the slot, a phenomenon previously observed in the plastic-plastic plate polymer injection experiments and discussed in Chapter 3.4.3.

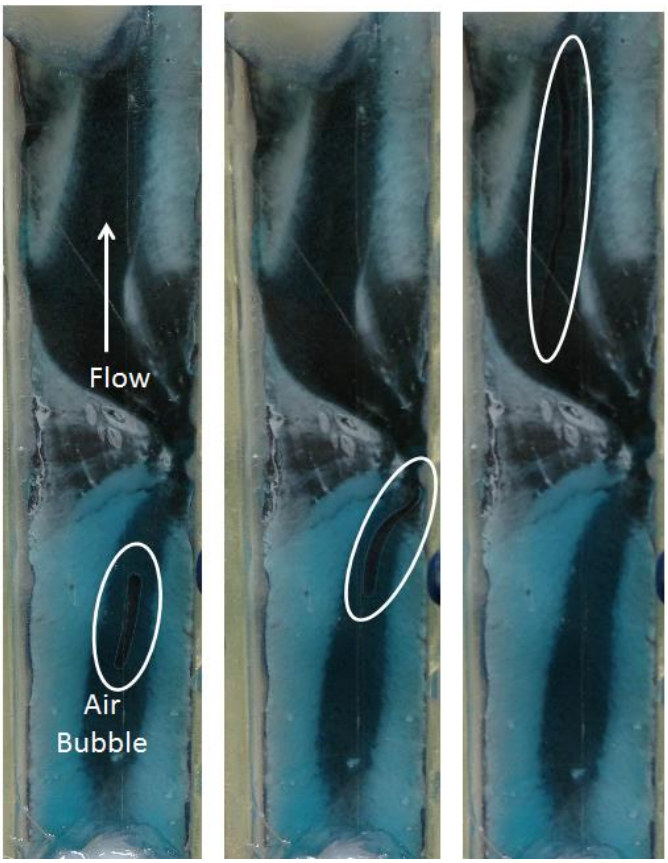

Figure 64: Photographs of Core 6FP-6 during polymer injection (3 wt% Carbopol 934 and 0 wt% NaCl) with air bubble (darker region within white oval) traveling upwards after being entrained with the polymer at t = 14 FV, photographs seconds apart. This fracture is 6 inches long in the direction of flow.

This confirmed the visual interpretation of white areas as regions of restricted flow, while dark channels indicate primary conduits for flow of polymer. This restriction of the area open to flow within the fracture has important implications for conceptual and

mathematical modeling of the placement of this type of polymer into fractured cement. One implication is that the residence time of the injected polymer decreases during injection, so that the extent of reaction decreases. It appears that this feedback drives the system to a steady state. Another implication is that the apparent viscosity calculated from the pressure drop by assuming the entire fracture is open to flow is not the actual viscosity. One reason is that the effective permeability of the fracture is smaller when flow is restricted to a channel, increasing the pressure drop (all else being equal) which appears as an increase in apparent viscosity. The other reason is that the shear rate is larger in the actual channel than it would be in the fracture and moreover is variable in the direction of flow. Since the polymer exhibits shear thinning behavior, this causes the calculated value to be smaller than it would be at the presumed shear rate. This obviously complicates the comparison of polymer rheology measured in batch and the polymer viscosity while flowing through the fracture.

4.3.2.7 Core 6FP-11

Core 6FP-11 was injected with 3 wt% Carbopol 934 and 0 wt% NaCl, but with a 1 minute residence time, such that the time and fracture volume axes are equivalent. Pressure drop and pH data are shown in Figure 65 below. Like Core 6FP-6, Core 6FP-11 was built with the wider 1/4" OD pressure lines, resulting in a pressure drop that increases quickly at early time (0 to 5 FVs) and plateaus quickly (after 5 FVs). The pressure drop plateaus at around 7.5 psi and remains fairly constant, despite the continuously decreasing effluent pH. This is similar to the behavior detailed in panel 3 of Figure 47 shown earlier in Chapter 4.3.2. and could indicate that the syneresis flow channel constriction and decreasing polymer gelation offset each other, keeping the pressure drop constant.

The flow rate was set such that the residence time of polymer in the fracture was 1 minute, the lowest residence time of any polymer injection experiment up to this point. Syneresis occurs despite the much shorter residence time, indicating that it may be the result of reactions within the boundary layer of fluid at the cement surface. The effluent pH is also significantly lower than was seen during polymer injection into Cores 6FP-2 through 6FP-6 and generally stays below the critical gelation pH range of 3 to 3.75 during injection. This is expected, as less residence time gives the hydroxide from cement less time to diffuse into the polymer, and as the readily available cement minerals are dissolved, the rate of reaction decreases, resulting in a lower effluent pH.

Core	Aperture	Polymer Injected	Residence Time	Volume Injected	Fracture Type
6FP-11	0.399 mm	3 wt% Carbopol 934 0 wt% NaCl	1 min	50 FVs	Cement-Plastic Sawed

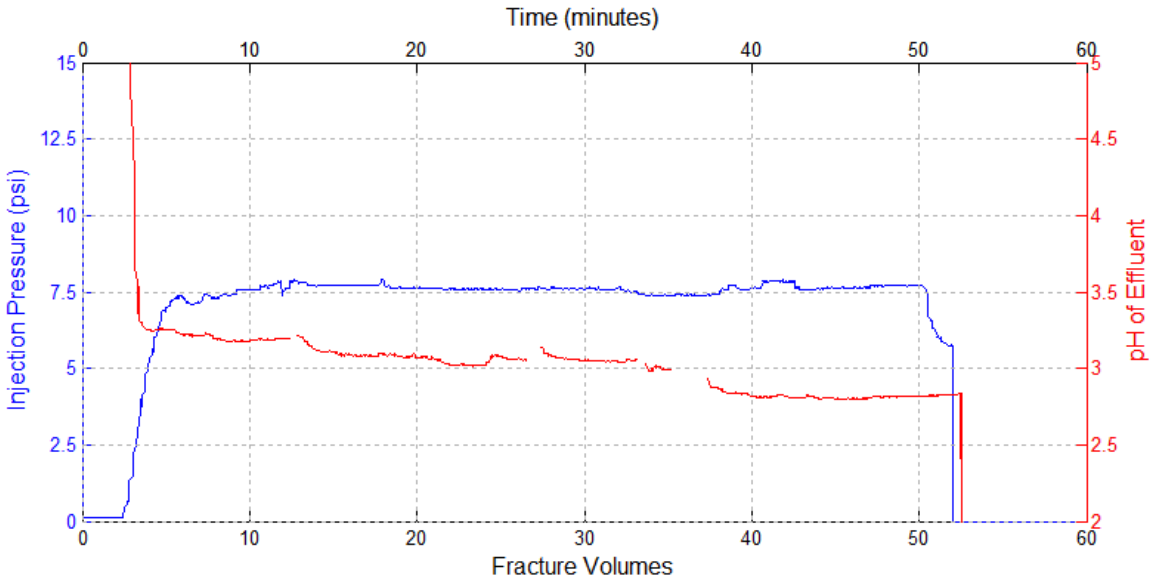

Figure 65: Data recorded during polymer injection (3 wt% Carbopol 934, 0 wt% NaCl, and DI water) into Core 6FP-11.

The apparent viscosity between 10 FVs and 50 FVs is nearly constant at around 1,900 cP, which is much lower than the apparent viscosities seen in Cores 6FP-2, 6FP-3,

6FP-4, 6FP-5, and 6FP-6 (all cores injected with 3 wt% Carbopol 934 and 0 wt% NaCl, same as Core 6FP-11). This is because the flow rate into Core 6FP-11 is significantly higher than these, resulting in a higher shear rate. As discussed previously, the polymer dispersion exhibits shear thinning flow behavior, thus the increase shear rate results in a lower apparent viscosity. The effluent pH at 10 FVs gives an apparent viscosity upper bound of 17,700 cP, while the effluent pH at 50 FVs gives 4,600 cP. The initial polymer dispersion rheology gives a lower bound on apparent viscosity of 1,400 cP. Therefore the apparent viscosity from pressure data is consistent with these bounds.

In another attempt to determine the polymer flow channel, small reflective particles were added to the polymer dispersion. The concentration of the particles was low and therefore had no effect on the polymer rheology, but they did occasionally stick to the plastic plate or cement surface and aggregate as fracture volumes were injected. Photographs taken during polymer injection are given in Figure 66. A flow channel can be seen to form as early as 18 fracture volumes, or 18 minutes, of polymer injection and remains until the end of injection at 50 FVs. This agrees with the hypothesis made from the pressure drop data that a channel must form and constrict flow in order to offset the reduced gelation of the polymer dispersion. The fact that the channel becomes white after shut-in supports the idea that the injection evolves toward a nearly steady state, in which the residence time for reaction becomes shorter until there is no longer enough reaction occurring to further restrict the flow area. When the residence time becomes large (after shut-in) the reaction between polymer and cement minerals proceeds toward completion.

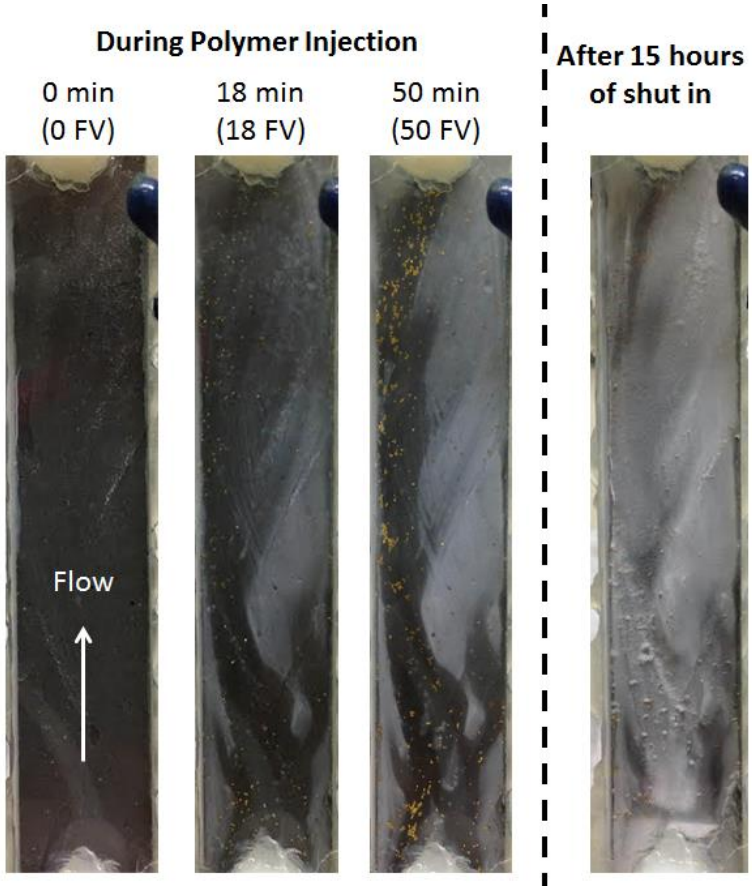

Figure 66: Photographs of Core 6FP-11 during polymer injection (3 wt% Carbopol 934, 0.5 wt% NaCl); gold particles can be seen in primary flow channel at 18 min and 50 min.

Core 6FP-11 was connected to the long term, small pressure gradient manifold. The polymer held back a 2.5 psi/ft gradient for over 28 days before an irreparable leak in the coreholder (not the polymer) occurred and forced an end to the experiment. However, it was determined afterwards that there was no polymer gel remaining in the fracture, but rather the syneresis polymer was blocking the flow.

4.3.2.8 Core 6FP-13

Experiment 6FP-13 was run with nearly the same parameters as 6FP-11. Core 6FP-13 had a nearly identical hydraulic aperture and was injected with the same type of polymer at the same flow rate, but for only 10 fracture volumes instead of 50. This was

done in order to determine the effect that total fracture volumes of polymer injected has on the pressure holdback performance. Because of the small volumes involved and short duration, effluent pH data were unable to be recorded accurately, but comparison of pressure drops between Core 6FP-11 and Core 6FP-13 is shown in Figure 67 as blue and red pressure data curves, respectively.

Core	Aperture	Polymer Injected	Residence Time	Volume Injected	Fracture Type
6FP-13	0.399 mm	3 wt% Carbopol 934 0 wt% NaCl	1 min	10 FVs	Cement-Plastic Sawed

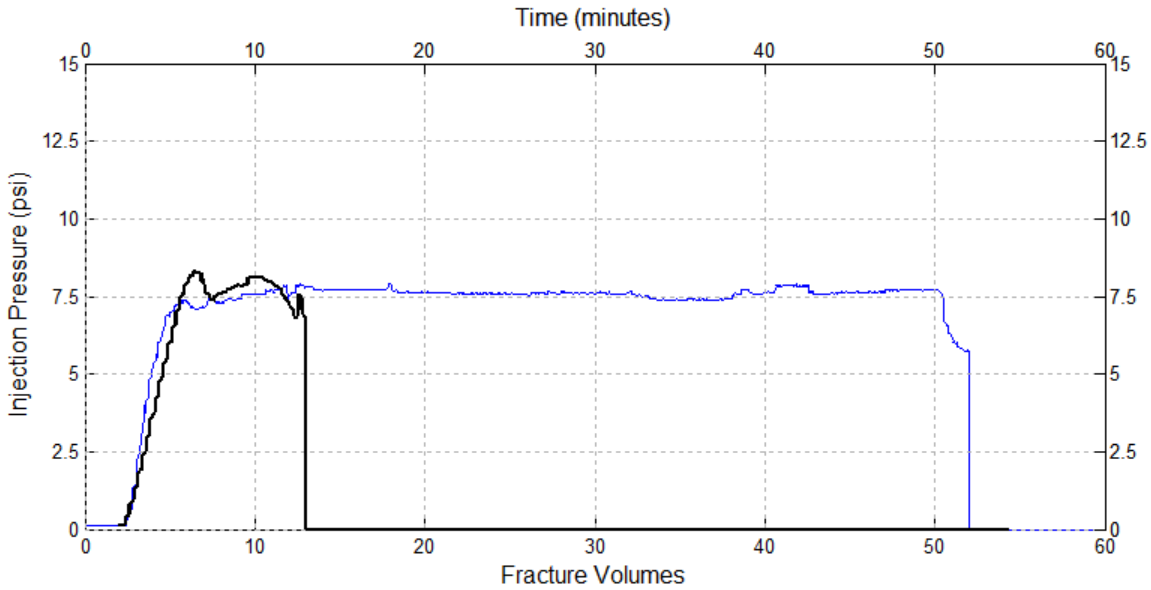

Figure 67: Data recorded during polymer injection (3 wt% Carbopol 934, 0 wt% NaCl, and DI water) into Core 6FP-11 (blue) and 6FP-13 (black).

The pressure response for 6FP-11 and 6FP-13 are very similar during the first 8 fracture volumes injected, before 6FP-13 was terminated. Unlike 6FP-11, Core 6FP-13 was unable to hold back the 2.5 psi/ft pressure gradient of the long term pressure test and allowed brine breakthrough immediately. These experiments suggest that the total polymer injected and/or the total injection time could have a significant impact on

polymer strength test performance. Two possible explanations for why 6FP-11 performed better than 6FP-13 are as follows:

1. Fluid blockage in 6FP-11 was found to be caused by syneresed polymer, and not gelated polymer with a yield stress, whereas 6FP-13 is thought to have been unable to block fluid flow because syneresis reduced the polymer volume without creating aperture-blocking syneresed polymer. In other words, it is possible that syneresed polymer blocks fluid flow randomly, and the difference in the two expeirments is merely statistical. This would imply that the increased amount of polymer injection did not play a significant role in core 6FP-11's blockage.
2. Increasing the amount of polymer injected into Core 6FP-11 caused more calcium cations to be dissolved and removed from the fracture face than 6FP-13. With less calcium, the polymer inside the fracture of 6FP-11 retained some yield strength and/or the syneresis effects did not contract the polymer chains as severely. This would cause the fracture to be less filled with water expelled during syneresis, allowing for fluid blockage.

4.3.2.9 Core 6FP-15

6FP-15 was injected with 300 fracture volumes of 0.5 wt% Carbopol 934 at 1 fracture volume per minute. Compared to Core 6FP-11, the polymer concentration is reduced by a factor of 6, but the total injected volume in increased by a factor of 6, resulting in an identical total polymer mass injected, but increasing the total injection time by 6 fold. The pressure and pH data are shown in Figure 68. It should be noted that the unreacted pH of the 0.5 wt% Carbopol 934 polymer is around 3.15, slightly higher than the 3 wt% polymer due to smaller polymer concentration.

Core	Aperture	Polymer Injected	Residence Time	Volume Injected	Fracture Type
6FP-15	0.358 mm	0.5 wt% Carbopol 934 0 wt% NaCl	1 min	300 FVs	Cement-Plastic Sawed

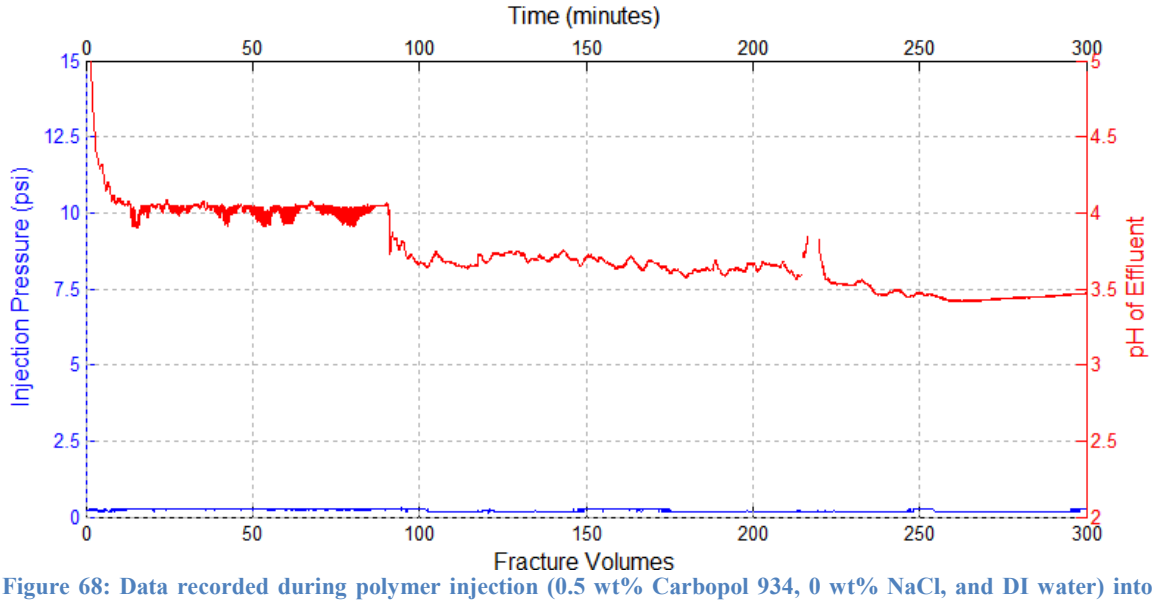

Figure 68: Data recorded during polymer injection (0.5 wt% Carbopol 934, 0 wt% NaCl, and DI water) into Core 6FP-15.

The injection pressure into the fracture is almost negligible, as 0.5 wt% polymer has a near-zero yield stress and nearly water-like viscosity. The pH probe encountered measurement errors during the first 90 fracture volumes, but resumed accurate measurement thereafter. Taking three points from Figure 68 at 50 FVs, 150 FVs, and 250 FVs, it's clear that the pH between the points changes (from 4.0, to 3.7, to 3.5, respectively), but the pressure drop remains negligible for all three. The apparent viscosity at these points is around 15 cP, which is the minimum resolution for the pressure transducer.

After polymer injection, core 6FP-15 was connected to the long term pressure manifold, but was unable to hold back the 2.5 psi/ft gradient and brine broke through immediately.

4.3.3 Conclusions and Discussion

There were a total of 10 polymer injection experiments into cement-plastic plate cores. Of these, 7 cores were unable to hold back the 2.5 psi/ft gradient of the long term pressure experiment, despite the fact that many of these fractures had polymer injection pressure gradients well over 2.5 psi/ft. This resulted in displacement fluid breakthrough immediately after the pressure was applied. Table 8 below shows the various cores with injection parameters and the number of days each was able to hold back the 2.5 psi/ft gradient. Blank spaces in the hold back column indicate that brine broke through the slot immediately.

Core	Aperture (mm)	Carbopol 934 wt%	NaCl wt%	Residence Time (min)	Volume Injected (FVs)	Max Pressure grad during inj. (psi/ft)	Hold Back 2.5 psi/ft
6FP-1	0.744	3	0.5	32	25	0.8	-
6FP-2	0.388	3	0	32	10	40	14 days
6FP-3	0.613	3	0	16	18	23	13 days
6FP-4	0.511	3	0	16	16	22	-
6FP-5	0.712	3	0	16	20	9	-
6FP-6	0.542	3	0	16	20	12	-
6FP-11	0.399	3	0	**1**	50	15	28 days
6FP-13	0.399	3	0	1	16	15	-
6FP-15	0.358	0.5	0	1	300	0.1	-

Table 13: List of core and injection properties with polymer strength test performance.

There is little consistency in the core and injection parameters that leads to successful blockage of the cement-plastic plate fractures. For example, core 6FP-2 and Core 6FP-13 are nearly identical in aperture, polymer injected, residence time, etc., yet Core 6FP-2 held back the displacing fluid for nearly two weeks while Core 6FP-13 didn't hold it at all. The performance appears to be bimodal: the cores either held back pressure for weeks or not at all. A new hypothesis had to be developed to account for

these irregularities in criteria for failure or success. The mechanism for failure appears to be: the polymer is degraded by the process of syneresis which expels water from the polymer matrix, creating a thin conduit above the syneresed polymer that contains Newtonian fluid (water). The water-filled conduit, though possibly quite small, nevertheless allows fluid flow immediately when a pressure gradient is applied. A diagram of this behavior is shown in Figure 69 below.

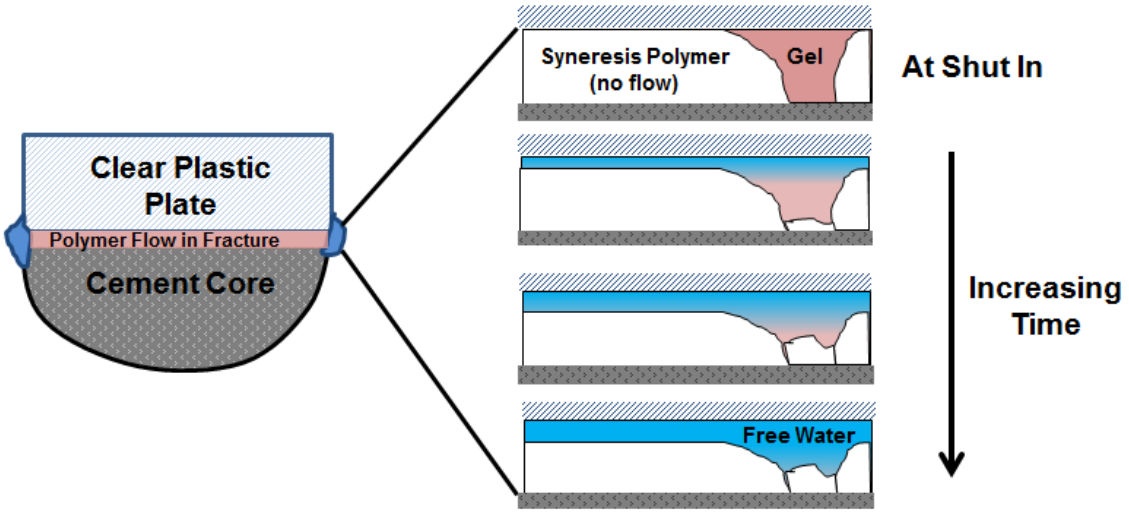

Figure 69: Diagram of syneresis of polymer gel across width of cement-plastic plate core during shut in (figure not to scale). Pressure gradient is normal to the page. Continued reaction with the cement and consequent syneresis causes the polymer gel to shrink with time, leaving part of the cross section filled with only water expelled from the gel.

Initially, just after polymer injection, the flow channel in the syneresed polymer is filled with gelated polymer. Over time, the channel gel begins to undergo syneresis, depositing polymer on the cement surface and leaving free water above. When a pressure gradient is applied to the slot after some shut in time, the free water offers no resistance to the displacing fluid, as it has no yield stress, and is immediately displaced.

However, there were three cores that were not only to hold back the 2.5 psi/ft pressure gradient, but were able to hold it for several days or weeks. After this period,

the polymer had fully undergone syneresis, and the blockage was unaffected by the displacing fluid's salt (NaCl) content. Polymer gel is very sensitive to salt and will lose yield stress and viscosity when in contact with brine. Therefore, it appears the blockage could be provided by something other than the polymer gel itself. Visual inspection of the cores indicated the possibility that the displacing fluid was held back at a particular point in the fracture. To determine the nature of this blockage, the cores were taken off the long term pressure test and the outlets (the side of the core not in contact with displacing fluid) were turned upside down. When pointed downwards, water from inside the fractures poured down and out of the cores. Not all the fracture volume was emptied, however; a pockets of air remained behind the blockages, confirming the suspicion that the pressure was being held back by a discrete blockage and not a slot full of gel. In these cases, the mechanism for success is thus: the polymer gel was degraded by syneresis, but the syneresis polymer happened to bridge the space between the plastic plate and the cement face. A diagram of this behavior is shown in Figure 70.

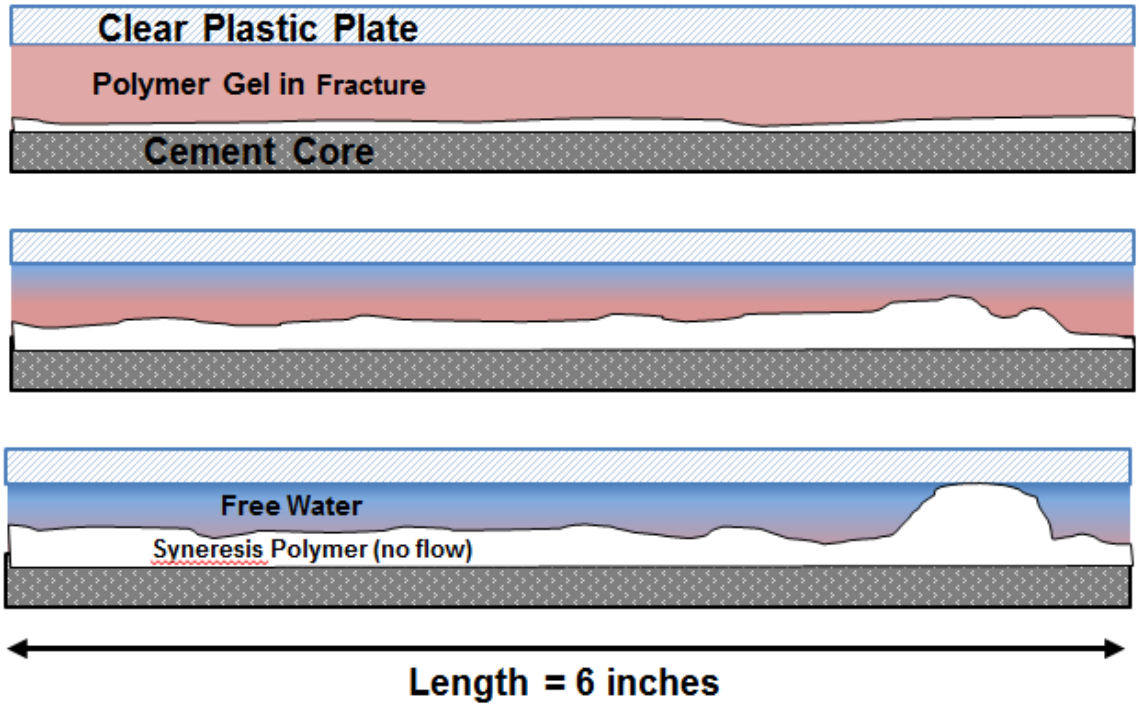

Figure 70: Diagram of syneresis of polymer along length of cement-plastic plate core during shut in (figure not to scale). Pressure gradient is left to right. The coincidental remnant of polymer gel spanning the entire aperture of the fracture (far right of bottom panel) blocks flow, even though much of the gel has undergone syneresis. If no such remnant happens to remain, the polymer does not block flow at all. This would explain the "hit or miss" results in Table 13 for experiments conducted under similar conditions.

Syneresis generally pulls the polymer towards the source of the calcium cations (in this case, the cement surface) which is driving the syneresis. The polymer nearest the cement will have the largest calcium concentration and will therefore synerese and pull the above polymer downwards. However, as the mud-crack pattern seen in Figure 12 shows, the syneresis polymer is also pulled laterally into clumps. It is therefore possible that a section of syneresis polymer remains in contact with both the cement surface and the plastic plate (or opposite cement face, in the case of cement-cement fractures), then contracts laterally until the entire width of the fracture is blocked. This also explains why the salt concentration from the displacement experiments seemed to have no effect on the performance of the blockage. The presence of NaCl has little effect on the white syneresed material, as shown in Figure 14.

While this mechanism has shown that it could be able to hold back pressure for long periods of time, only injecting polymer dispersion into the cement/plastic plate fracture yields inconsistent results.

4.3.4 Comparison to cement-cement fractures

Although the mechanism of fluid flow blockage for the cement-plastic plate fractures is fairly well understood, thanks to the added data from visual inspection during/after polymer injection, the pressure data results from the cement-cement fractures are drastically different, making it difficult to apply the mechanisms that are judged to apply for the cement-plastic plate fractures. Representative pressure data from polymer injection into both of these core types, 6F-12 and 6FP-1, is shown below in Figure 71. For the same injection polymer formulation (3 wt% Carbopol 934 and 0.5 wt% NaCl) and similar apparent viscosities, the cement-plastic plate core hardly saw any pressure drop, while the cement-cement core had a pressure drop of nearly 15 psi.

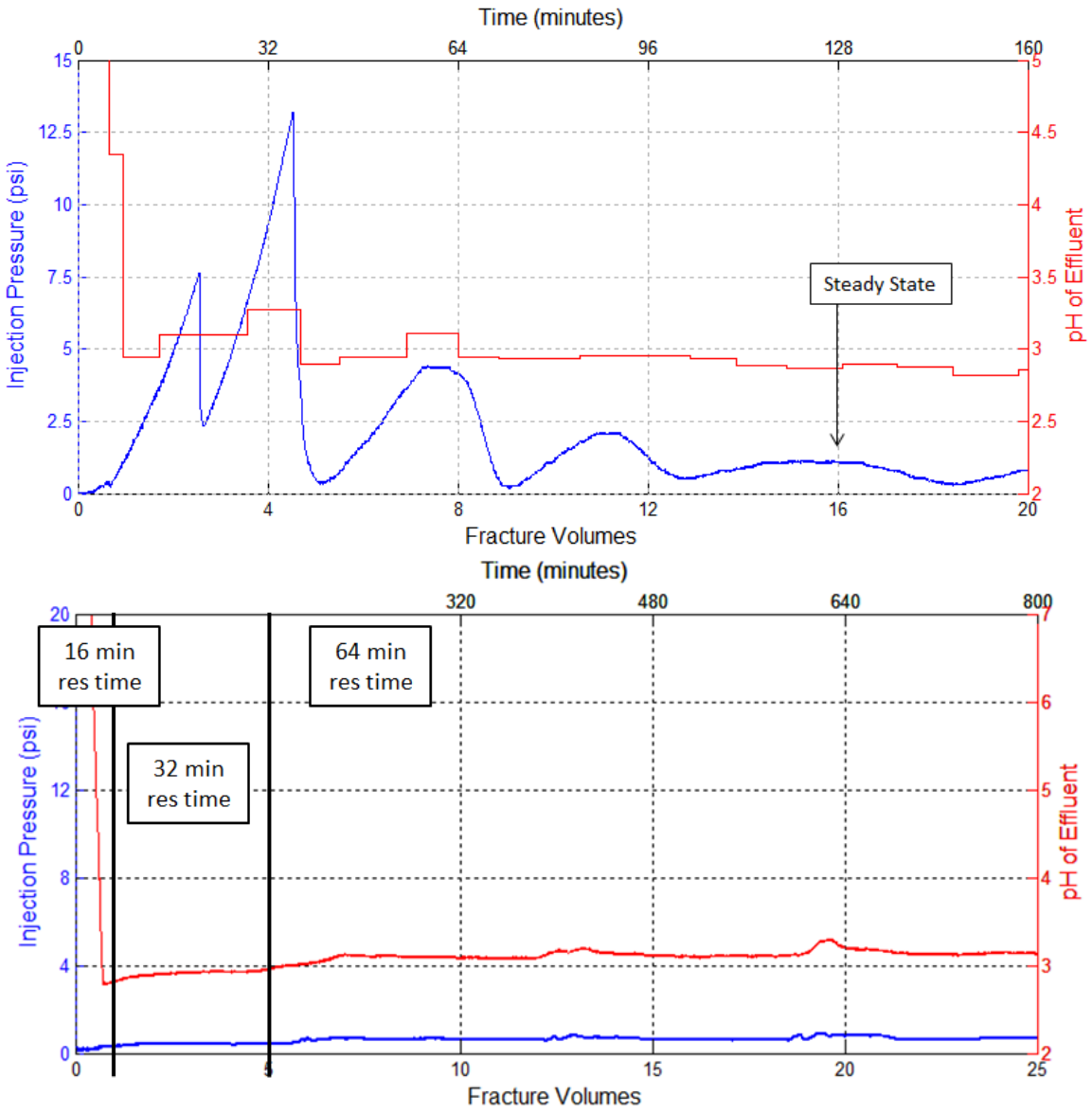

Figure 71: Comparison of cement-cement (top graph, Core 6F-12) and cement-plastic plate (bottom graph, Core 6FP-1) fractures during polymer injection

Core 6FP-1 had an apparent viscosity of 6,400 cP at 4 FVs of polymer injection, during which time the injection residence time was 32 minutes. The injection rate was decreased by a factor of 2, which resulted in an apparent viscosity of around 22,000 cP at 12 FVs. This doubling of the residence time resulted in a roughly 4-fold increase in apparent viscosity. Therefore, if the residence time had been reduced by a factor of 4,

from 32 minutes to 8 minutes, the apparent viscosity is predicted to decrease by a factor of 16 from 5,600 cP to approximately 400 cP. This is consistent with the apparent viscosity observed in Core 6F-12 (shown at top of Figure 71), which was calculated to be 450 cP when injected with polymer with an 8 minute residence time.

It was also seen that Core 6FP-1 was the only core in which the apparent viscosity calculated from the pressure drop exceeded the upper bound calculated from the effluent pH and rheology. This is likely due to the presence of significant channeling during polymer injection, as seen in Figure 50. The pressure drop in Core 6FP-1 was very low, such that pressure changes were hard to resolve by the pressure transducer, which could therefore artificially elevate the pressure drop, and therefore apparent viscosity calculations.

While the steady state apparent viscosities of the two experiments are consistent, the large peaks and troughs seen in Core 6F-12 are absent in Core 6FP-1. Between these two cores, the injection polymer (3 wt% Carbopol 934 and 0.5 wt% NaCl) was similar, but the fracture aperture of Core 6FP-1 was nearly twice as large as Core 6F-12. Perhaps more importlantly, Core 6FP-1 was constructed with one cement half replaced by a flat plastic plate. In a cement-cement fracture that is created by putting the cement core in tensile failure, the fracture is irregular and the path is tortuous, but both halves of the core are equally irregular and tortuous. When these two halves are put together, some regions have very narrow apertures while others have very wide apertures. It is possible that the syneresed polymer is attaching to the cement walls at the narrow aperture spots and quickly bridging the gap to the other cement wall, blocking flow. With the slow flow rates, the pressure builds up very slowly, but during this time more syneresed polymer is being deposited, thickening the flow obstruction. Eventually, the rate of pressure increase overcomes the syneresed polymer deposition and water is able to

break through. Subsequent blockages are formed as the syneresed polymer is stripped from the walls and plugs the small aperture region again. A schematic of this behavior is shown in Figure 72.

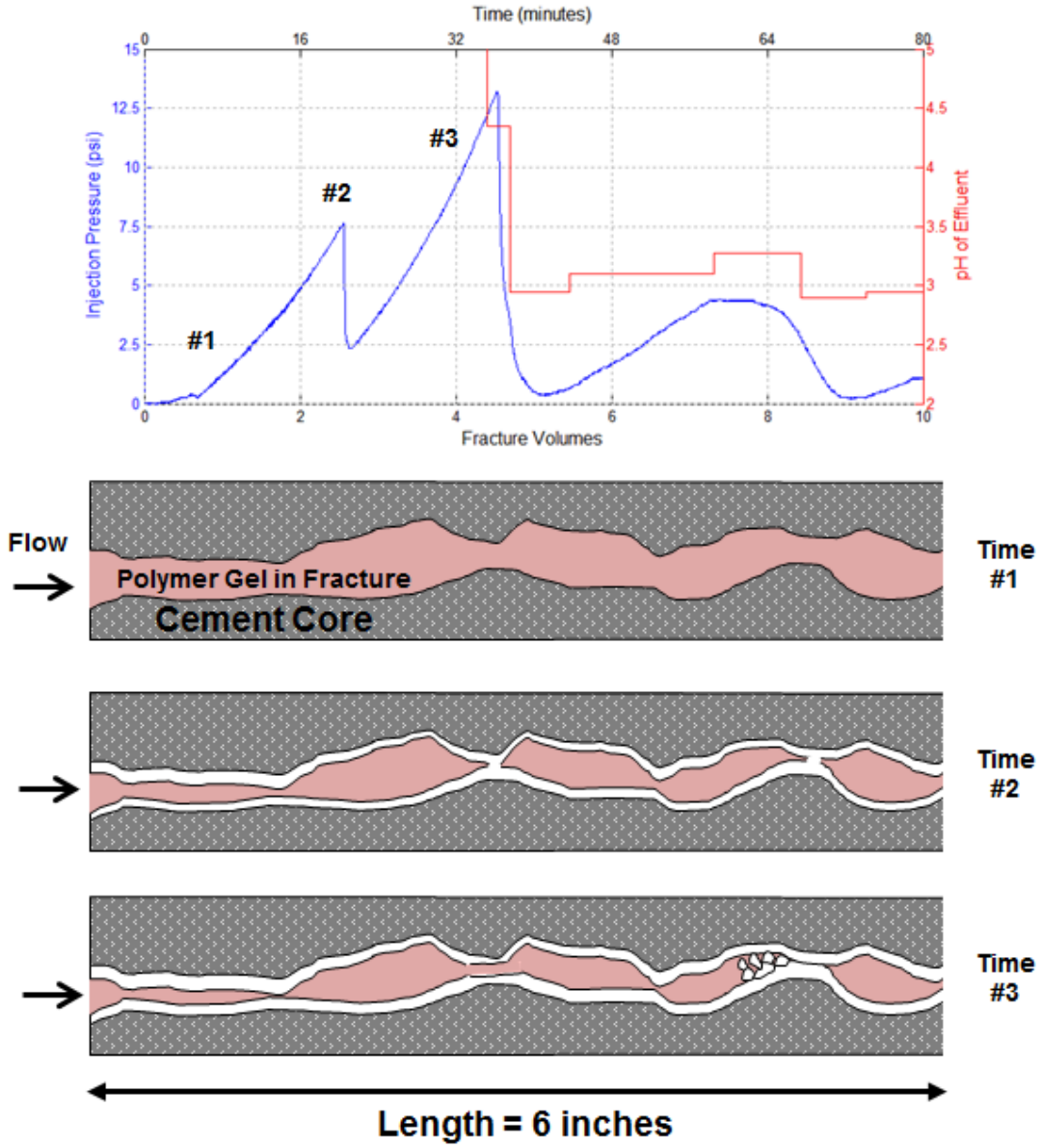

Figure 72: Diagram of polymer injection into cement-cement tension fractured cores; view is from the side of the fracture (aperture in vertical direction, length in horizontal); fracture width is normal to page. Data from polymer injection into Core 6F-12 is used as an example with three points selected and theorized syneresed polymer blockage behavior at each time. Time #2 and #3 both represent fractures that fully block fluid flow.

At time #2, the syneresed polymer has coated the fracture and bridged the aperture, blocking fluid flow. The pressure builds up until the blockage is broken through, but the syneresed polymer from the initial blockage travels down the flow path and aggregates at another blockage downstream at Time #3.

With cement-plastic plate cores, however, the flat plastic plate does not conform to the cement's fracture surface, creating a more constant flow channel with more consistent apertures throughout. The behavior seen in Figure 72 is similar to the behavior of the cement-plastic plate cores during shut in after polymer injection, as seen in Figure 70. This behavior has never been observed in cement-plastic plate cores, as confirmed by visual inspection of the cores.

Chapter 5 Pre-flushing Fractures with Acid

5.1 MOTIVATION

The frequent failure of the polymer gel to adequately block flow and hold back pressure in model fractures described in the previous chapter was attributed to the high concentration of divalent calcium cations. The source of the cations is the dissolution of the calcium-rich components in cement fracture wall. These cations react with the carboxylate groups on the polymer, binding the polymer chains together to form a relatively rigid and dense solid and promoting syneresis. The water expelled during syneresis occupies volume previously filled with gel, and thus readily allows other fluids to flow through the fracture. Efforts were made to obtain a cation-compatible polymer, but no polymer formulation proved successful.

Investigation was switched to determine the viability of flushing the cement fractures with a strong acid to dissolve and displace the calcium-rich portlandite prior to polymer injection. It has been shown that hydrochloric acid (HCl) will reduce calcium content in cement fractures in areas that are contacted directly by the acid (Huerta, 2013). As acid flows through the fracture, the pH is increased and the portlandite available at the cement surface is reduced. Along with the reduction of available portlandite at the cement surface, the acid flows along the cement fracture and increases in pH. When the calcium-rich fluid reaches a sufficiently high pH, the presence of atmospheric CO_2 dissolved in the fluid will cause the calcium and CO_2 to precipitate calcium carbonate ($CaCO_3$) out of solution and onto the cement surface. This calcium carbonate precipitate will limit the diffusion of calcium from dissolved portlandite by created a low-permeability layer on the cement. This layer may also penetrate into the cement itself, further decreasing the diffusion rates (Huerta, 2013). With the decreased presence of calcium ions and the reduced diffusion rates, the polymer dispersion may be sufficiently

protected to gelate and form a flow barrier in the fracture that is not subsequently degraded by the cations.

Pre-flushing cement fractures with acid could also recreate conditions that could be present in GCS wells. If a well in a CO_2 injection field has leaky cement fractures, the fracture could have been flushed with many fracture volumes of CO_2 saturated brine, which is moderately acidic. Replicating this chemical environment requires high pressure and elevated temperature. HCl is a useful analog acid, allowing for the appropriate values of pH to be used while continuing to operate at low pressure injection and simple preparation.

5.2 Experimental Methods

Because hydrochloric acid readily attacks many metal surfaces, the steel accumulator could not be used as a reservoir. Instead, two glass columns were used with mineral oil acting as the "piston" that drove the acid solution and prevent mixing with the pump's deionized water. Figure 73 shows how this was accomplished. Column (b) was initially filled with mineral oil and Column (c) was filled with HCl acid solution. As DI water was injected into the bottom of Column (b), the oil was displaced into Column (c) and the acid displaced into the cement fracture core.

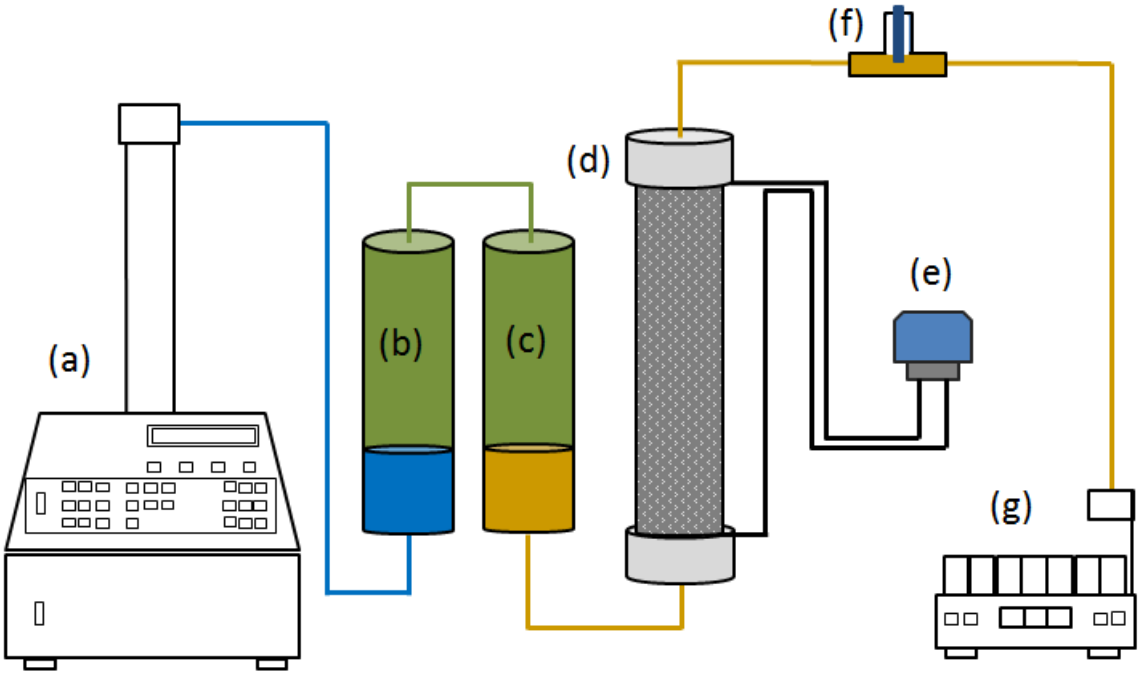

Figure 73: Schematic of experimental setup for acid injection. Water pump (a), glass column of oil (green) above DI (blue) water (b), glass column of oil above acid solution (orange) (c), fractured cement core (d), pressure transducer (e), pH probe (f), and effluent collector (g).

The total volume of each column was around 200 mL, which was the limiting factor for the volume of acid that could be injected at one time. If more than 200 mL of acid was to be injected, the system was simply run for 200 mL until the oil filled Column (c), then temporarily stopped in order to reset the setup by recycling the oil back to Column (b) and cleaning any residual oil in Column (c). Acid was then placed into Column B again and injected was resumed. This downtime was minimized, but still allowed the fluid in the fracture to reach high pH values and can be seen periodically on acid injection experiment results as a spike in the pH.

5.3 Acid Alteration of Cement

5.3.1 Dissolution of Portlandite

Knowing the pH of the acid injected and the pH of the effluent, the cumulative amount of alkali mineral dissolved can be approximated, assuming that the HCl solution reacts

primarily with portlandite ($Ca(OH)_2$). For acid solutions below pH 6, this is a fair assumption, as the portlandite is easily and quickly dissolved (Beddoe and Dorner, 2005). This then allows for the estimation of total calcium cations transported out of the cement fracture, which will aid in determining how much calcium must be removed before the subsequently injected polymer dispersion is able to avoid syneresis. The reaction between hydrochloric acid and portlandite is given as

$$2H^+(aq) + 2Cl^-(aq) + Ca(OH)_2\,(s) \rightarrow 2H_2O\,(l) + Ca^{2+}(aq) + 2Cl^-(aq)$$

If these are the only reactants, then it is clear that for every two protons reacted with the portlandite, one divalent calcium cation is released. Using the pH of the acid and effluent as a proxy, the concentration of calcium in the effluent can be estimated by

$$[Ca^{2+}] = \frac{\Delta[H^+] - \Delta[OH^-]}{2}$$

$$= \frac{(10^{-pH_{acid}} - 10^{-pH_{effluent}}) - (10^{-pOH_{acid}} - 10^{-pOH_{effluent}})}{2}$$

For example, one of the cement cores was injected with pH 2.28 HCl solution and the effluent at one point was measured to be pH 6.2. Using the equation above, then the effluent's calcium concentration would be roughly 0.0026 Molar, or 105 ppm. If the calcium originated solely from portlandite, the total amount of dissolved portlandite can be calculated using with the following equations:

$$\text{g Ca(OH)}_2 = [\text{Ca}^{2+}] * \frac{74}{40} * Q * \Delta t$$

where Q is the volumetric flow rate of acid out of the core, Δt is the time interval associate with the outlet pH from the previous equation, and $\frac{74}{40}$ converts the units from

grams of calcium ions to grams of portlandite (molecular weight of calcium is 40, while portlandite is 74).

To verify this result, the calcium cation concentration of this same effluent sample was measured using a Dionex ICS-1100 ion chomatograph. The sample had to be diluted with 5 parts deionized water in order to fall between 0.3 and 30 ppm of calcium. The calcium concentration of this diluted solution was 20.8 ppm, giving a concentration of 125.0 ppm in the effluent, within 20% of the estimation made from the pH. Doubtless there are other reactions occurring between the acid and the cement, but this assumption allows for a good estimate of calcium content in the effluent and total portlandite dissolved.

5.3.2 Iron/Aluminum Precipitate During Acid Injection

Batch tests were conducted to determine the effect of different pH acid solutions in contact with a small flake of cement. In each case, 0.06 grams of cement were put in contact with 9 mL of acid solution of various concentrations, i.e. various pH values. Photographs of the results of the batch tests are shown below in Figure 74. The color of the cement appears unaltered between pH 1.8 to 2.25, but pH 1.0 and 1.2 acid changes the color of the cement to an orange, rust color. Therefore, somewhere between pH 1.2 and 1.8 is the point at which the acid will begin to discolor the cement in this way.

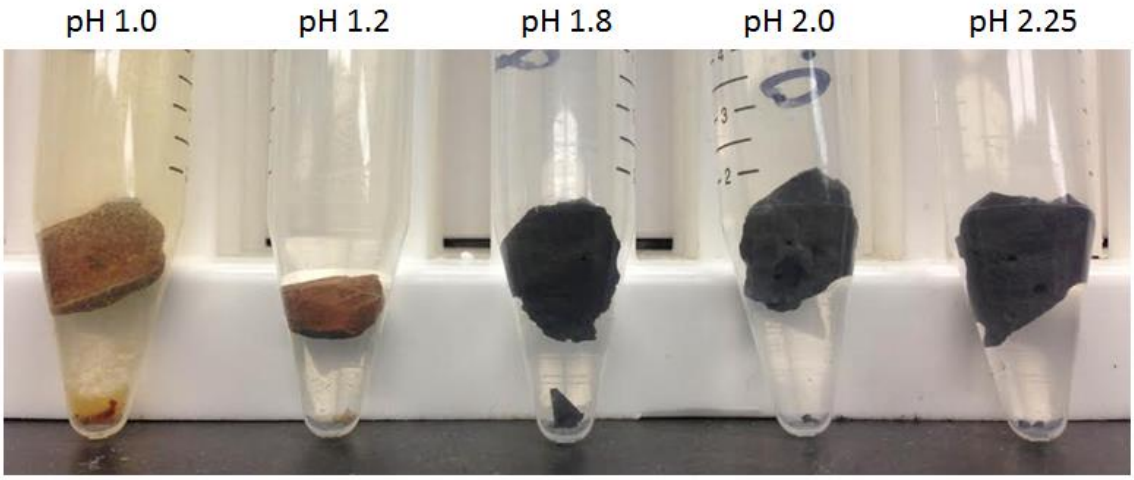

Figure 74: Photographs of batch tests with cement in contact with hydrochloric acid solution of varying pH

HCl acid was typically injected at the same pH as the freshly mixed polymer dispersion, near pH 2.3, in order to keep the pH conditions similar between the two injections. Over the course of hundreds of fracture volumes, the cement contacted by the acid would become discolored, changing from dark gray to a dark brown. When the pH of the injecting acid was set below pH 2, the cement was discolored to a strong orange color, similar to rust. This same discoloration has been seen previously and is due to an iron/aluminum insoluble precipitate forming on the cement surface (Huerta 2013). Similar to the mechanism by which calcite could potentially block the flow of calcium ions, these insoluble precipitates could limit the diffusion of calcium into the fracture.

5.3.3 Permeability changes

Prior to acid injection, the effective permeability of the cement fractures was measured before and after acid injection to determine whether the acid pre-flush affected the permeability of the fractures. In most cases, the acid pre-flush increased the effective aperture of the cement fractures, while in other cases the aperture was decreased. This behavior has been seen in previous acid injection experiments into

cement fractures and is attributed to the precipitation of calcite in the slot (Huerta et al, 2013), with the carbon dioxide coming from interactions between the acid solution and atmospheric air prior to injection. Huerta et al observed this calcite precipitation while injecting hydrochloric acid, and saw a more exaggerated case of it while injecting CO_2 saturated brine. Huerta gives a diagram explaining the mechanism of calcite precipitation in the presence of CO_2 saturated brine, given below in Figure 75.

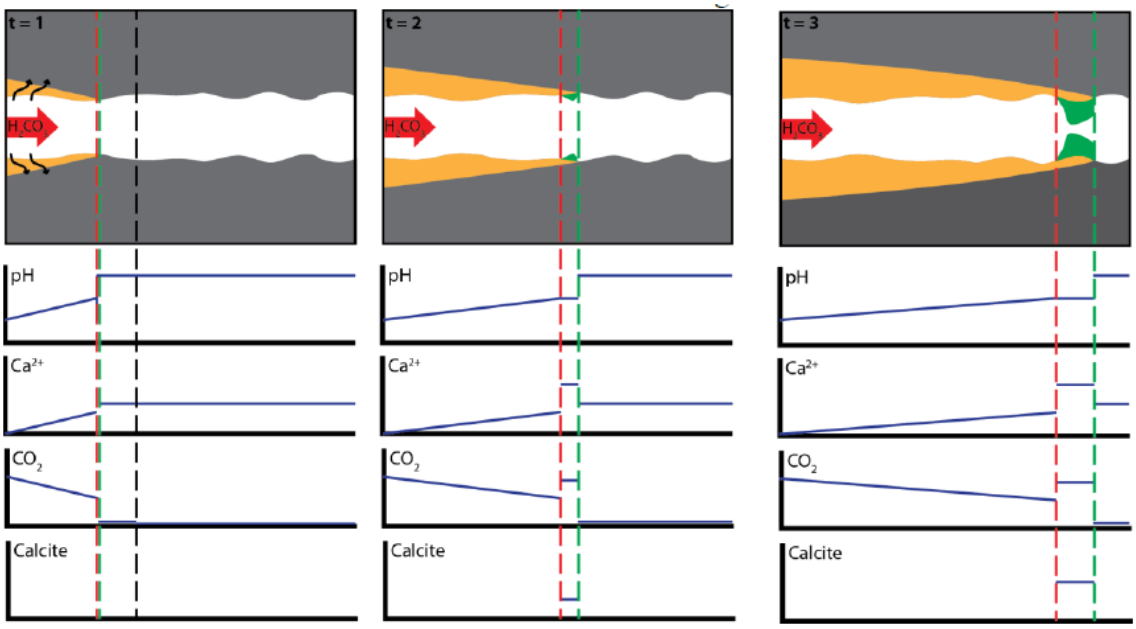

Figure 75: Schematic of hydraulic aperture reduction via calcite precipitation (green region) in acid injection into cement (gray) fractures; the calcium is supplied by acid dissolution of portlandite from the cement matrix (orange) (from Huerta et al 2013).

As the acid enters the fracture, portlandite is dissolved, driving up the pH and calcium content in the fracture. After some distance of propagation along the fracture, the calcium concentration, along with CO_2, and pH are such that the fluid is saturated with respect to calcium carbonate. Calcium hydroxide, however, continues to be dissolved and drive up pH and calcium levels, causing excess calcite to precipitate onto the cement surface.

5.4 Pressure drop and pH response of cement fracture

Table 14 summarizes the cores in which HCl was injected prior to polymer injection, along with the aperture in the slot before and after the acid pre-flush.

Core	Aperture Before Acid (mm)	Aperture After Acid (mm)	pH of Acid Injected	Portlandite Consumed (g)
6FP-24	0.157	0.168	1.18	0.229
6FP-26	0.270	0.314	2.21	0.004
6FP-27	0.288	0.229	2.28	0.254
6FP-28	0.211	0.246	1.00	0.411

Table 14: Polymer injection experiments in which an HCl acid pre-flush was utilized.

5.4.1 Core 6FP-24

Core 6FP-24 was the first core into which hydrochloric acid was injected prior to polymer injection. The batch tests had shown that HCl acid and cement will form an orange, rust-colored precipitate at pH values below roughly 2. To determine the effect of this iron-rich precipitate on the polymer dispersion and polymer gel, the first acid solution to be injected was at pH 1.16. The pressure and pH response in the fracture during part of the acid injection is shown below in Figure 76. The stair-step nature of the pressure drop is due to the resolution of the pressure transducer, which is around 0.07 psi.

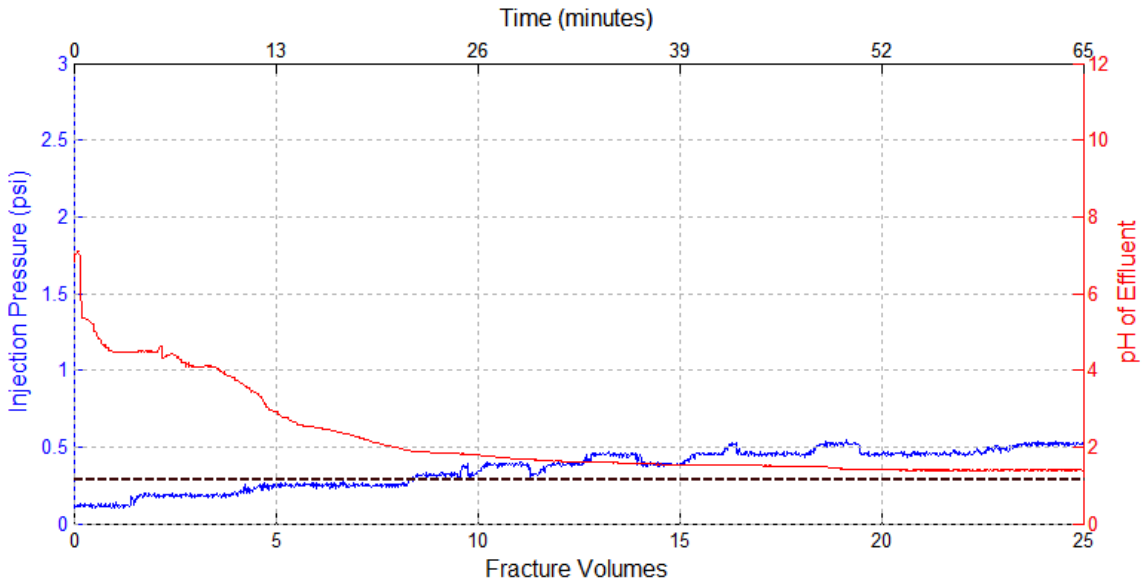

Figure 76: Data recorded during first stage of acid injection (pH 1.16 HCl solution) into Core 6FP-24; black dashed line indicates pH of injected acid

The pH of the effluent is initially close to 7, indicating that the fluid initially present in the fracture (typically pH 12) and the injected acid (pH 1.2) had mixed to some extent before reaching the pH probe. The injection pressure during the acid injection slowly increases, but the magnitude of the pressure drop is insignificant compared to typical polymer injection experiments described in Chapter 4. After about 40 minutes, the effluent pH approaches the pH of the injected acid. The flow rate was set for roughly one fracture volume injected every 150 seconds, allowing the acid only 2.5 minutes to react with the cement's surface before exiting the core. As the acid consumes the portlandite at the cement surface, hydroxide ions become less readily available and must diffuse from the cement matrix underneath the reacted surface. This slows acid consumption, and consequently the effluent pH approaches the injected pH after the readily available alkali has been consumed.

After 4 days of shut in, a second stage of acid was injected into Core 6FP-24, using pH 1.87 HCl solution. This was done in order to determine the effect of shut in time on the pH of the effluent and the cement fracture's ability to neutralize the acid. This injection period is shown below in Figure 77. The initial effluent pH was over 10, then decreased as acid was injected down to around 3.75. This indicates that minerals exist in the cement that will drive the pH above 10, but that rate of dissolution and/or diffusion is too slow to neutralize the pH 1.16 acid injected in Figure 76.

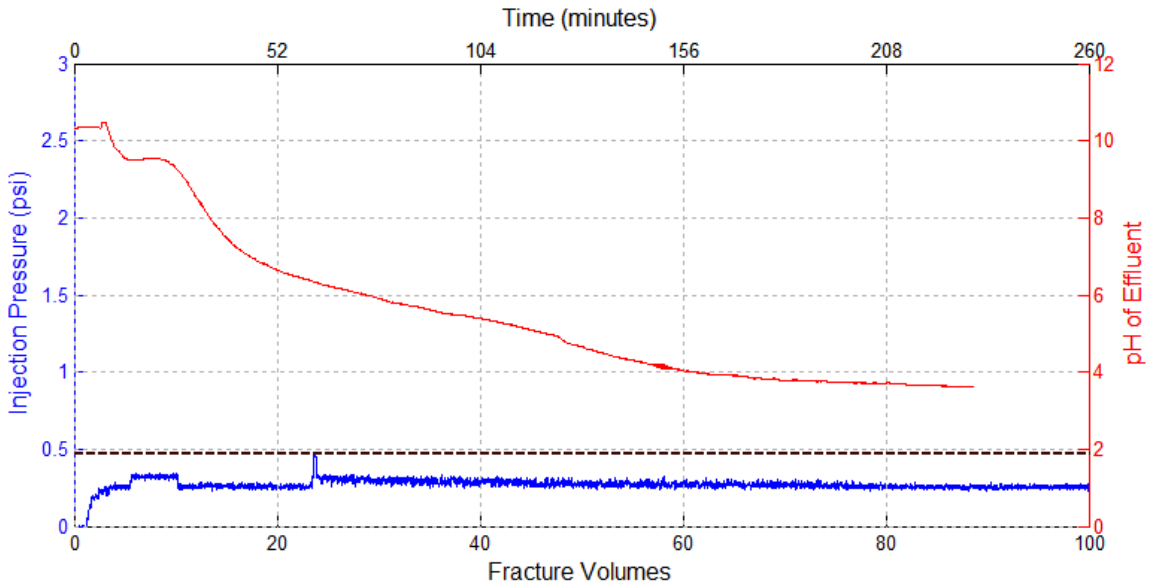

Figure 77: Data recorded during second stage of acid injection (pH 1.87 HCl solution) into Core 6FP-24; black dashed line indicates pH of injected acid. Initial pH is above 10, despite previous acid injection test (shown in Figure 76).

By using the effluent pH and initial pH, the concentration of calcium ions in acid effluent can be estimated. With the concentration and the known injection rate, the total calcium transported out of the cement fracture can be calculated. It is estimated that the acid injection into Core 6FP-24 dissolved and transported 0.229 grams of portlandite ($Ca(OH)_2$) out of the fracture. From a practical point of view, this is 0.12 g of calcium cations no longer available to react with polymer subsequently injected into this fracture.

From a stoichiometric point of view, this is 0.006 g of calcium removed per cm^2 of fracture surface. 62% of this removal occurred during the first 20 FV of pH 1.16 acid injection and 38% occurred during 80 FV of pH 1.87 acid injection. At the residence time of this experiment, this corresponds to 6.2E-3 gmol of HCl supplied to the fracture, or 1.6E-4 gmol per cm^2 of fracture surface. Because this estimation takes into account initial pH, effluent pH, and flow rate, it is a useful metric for comparing the overall effect of acid injection experiments and for evaluating the amount and concentration of acid that might be used in the field and the rate at which to inject it.

The hydraulic aperture of the fracture was measured before and after acid injection, to determine the effect of the acid solution on fracture permeability. The pressure drop through the slot for various flow rates is shown below in Table 15 along with the average hydraulic aperture inferred from the slope of the pressure drop vs flow rate data.

Flow Rate (mL/min)	Pressure Drop Before Acid Injection	Pressure Drop After Acid Injection
200	8.68	6.93
160	7.05	5.74
100	4.74	3.62
20	1.11	0.86
0	0	0
Hydraulic Aperture (mm)	0.157	0.168

Table 15: Injection pressures at various rates and hydraulic aperture of Core 6FP-24 before and after two stages of HCl acid injection

The pressure drop for each flow rate has decreased after acid injection, indicating the acid has effectively widened the flow channel.

After HCl injection and the second permeability test, Core 6FP-24 was injected with roughly 50 fracture volumes of 3 wt% Carbopol 934 and 0 wt% NaCl dispersion. The pressure drop and pH data are shown below in Figure 78.

Core	Aperture	Polymer Injected	Residence Time	Volume Injected	Fracture Type
6FP-24	0.168 mm	3 wt% Carbopol 934 0 wt% NaCl	1 min	52 FVs	Cement-Plastic Sawed

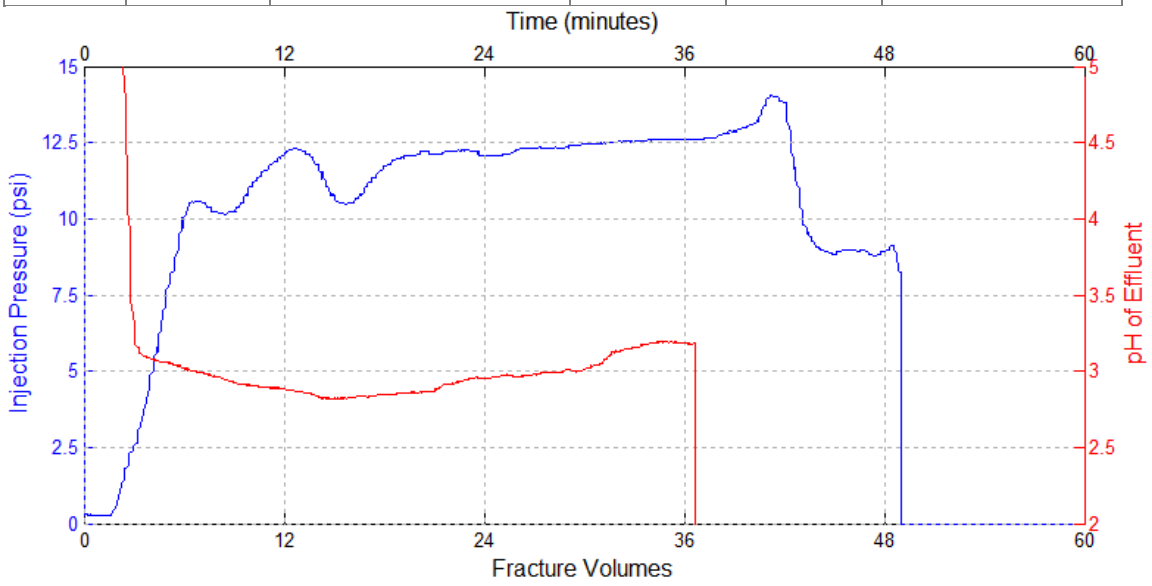

Figure 78: Data recorded during polymer injection (3 wt% Carbopol 934, 0 wt% NaCl, and DI water) into Core 6FP-24 after the acid injection into this core shown in Figure 77.

The pressure drop's build and plateau with time are somewhat irregular, but overall are similar to previous injection experiments of this polymer dispersion. The apparent viscosity at 30 FVs of polymer injection is calculated to be around 323 cP. This apparent viscosity is relatively low compared to previous experiments with this polymer solution (3 wt% Carbopol 934 and 0 wt% NaCl), but is consistent with the relatively small aperture, and therefore increased shear rate inside the core. The effluent at 30 FVs gives an upper bound on the apparent viscosity of 4800 cP. The effluent pH

history differs qualitatively from previous experiments, however: the pH decreases initially, then after 15 fracture volumes increases from pH 2.8 to 3.2. This pH trend reversal has not been seen in any polymer injection experiments. The mechanism for this pH behavior is proposed below in Chapter 5.5.2.

Core 6FP-24 was shut in for 48 hours, then connected to the long term pressure test manifold at a pressure gradient of around 5 psi/ft with 3 wt% NaCl brine applied to the inlet. The core was able to hold back pressure and has held back the brine for 20 weeks, and is still holding the pressure. Photographs of Core 6FP-24 are shown below in Figure 79 (note: the lighting in the two images is different). The left image was immediately after the 52 FVs of polymer injection, while the right image was taken 4 weeks after polymer injection. Syneresed polymer is absent in the left image and is hardly seen in the right image, despite being shut in for four weeks.

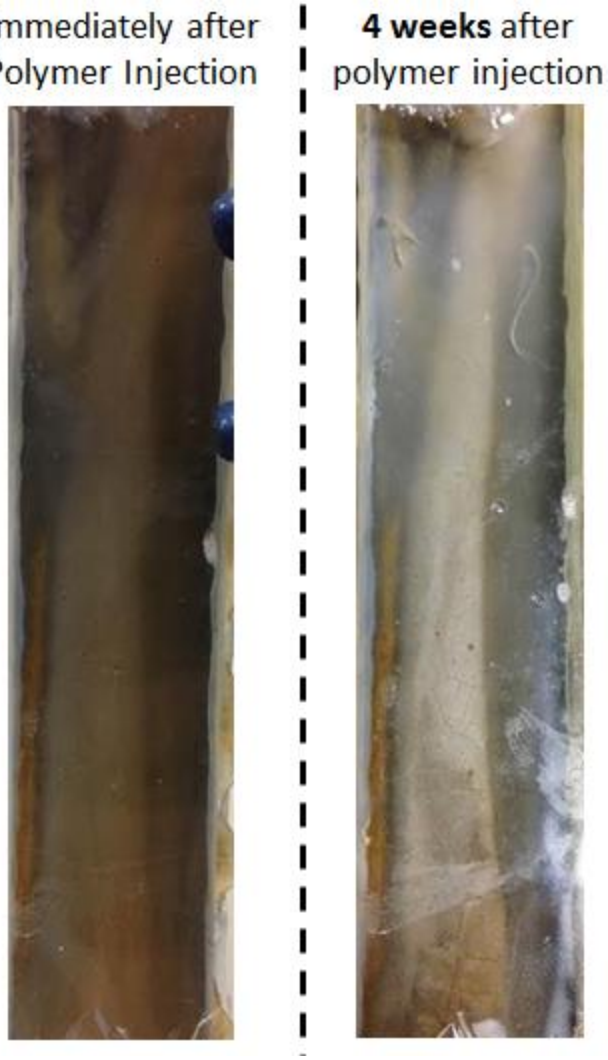

Figure 79: Photographs of Core 6FP-24 during and after polymer injection (3 wt% Carbopol 934 and 0 wt% NaCl). Core was pre-flushed with HCl acid.

5.4.2 Core 6FP-26

Acid injection experiment 6FP-26 used hydrochloric acid with a higher pH and less HCl was injected overall. The objective was to determine the effect of total HCl injected and pH of the injection acid. Core 6FP-26 was injected with several hundred fracture volumes of pH 2.21 HCl solution over the course of several days. This pH is

similar to the pH of the polymer dispersion (3 wt% Carbopol 934 with 0 wt% NaCl) injected and is high enough to prevent the iron-rich precipitate discussed in section 5.3.2 from forming. The pressure drop and effluent pH of the core during acid injection are shown below in Figure 80.

Core	Aperture	pH of Acid Injected	Residence Time	Volume Injected	Fracture Type
6FP-26	0.270 mm	2.21	8 min	38 FVs	Cement-Plastic Sawed

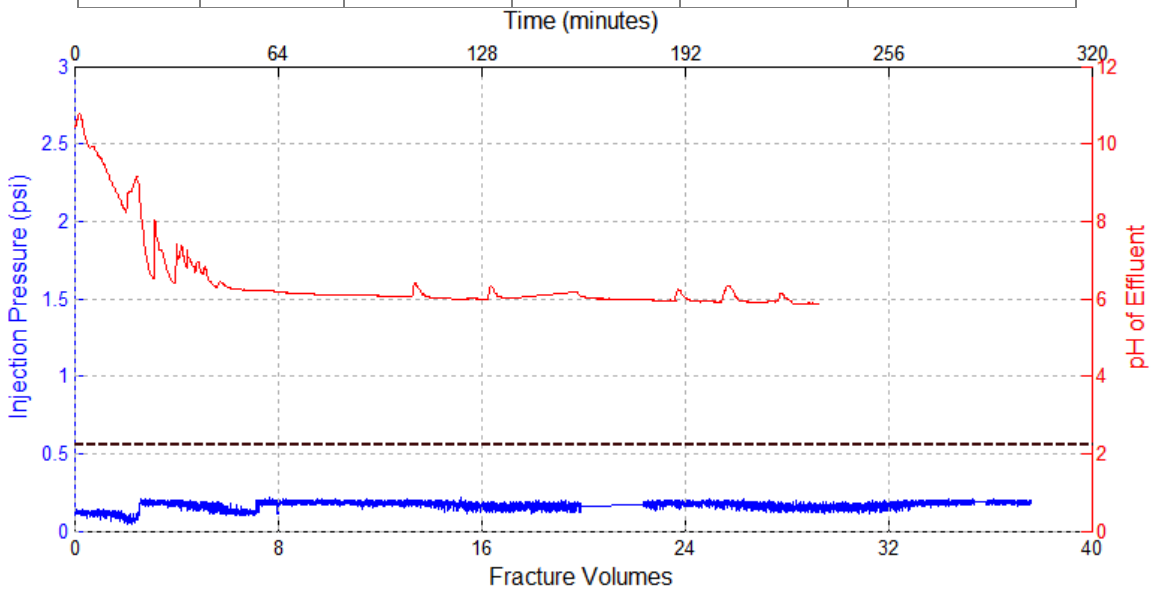

Figure 80: Data recorded during first stage of acid injection (pH 2.29 HCl solution) into Core 6FP-26; black dashed line indicates pH of injected acid.

The pH probe was cleaned occasionally to determine the accuracy of the measurements, similar to the cleaning done during polymer injection experiments. After cleaning, the pH probe's response generally went back to the pH values before cleaning, indicating that the pH probe doesn't require periodic cleaning, and that future experiments need not undergo the process.

The pressure drop of the acid injection is negligible, as the viscosity of the HCl solution, a Newtonian fluid with zero yield stress, is one centipoise and the solution is

injected very slowly into the fracture. The pH data provide more insight into the behavior of the acid in the fracture. The effluent pH at early time is near 11 as the cement surface's alkali minerals are quickly dissolved, but in this case the pH plateaus around 6, well above the pH of the injection acid of 2.21. At this point the hydroxide ions are diffusion limited: the rate of diffusion of hydroxide ions is high enough to neutralize the acid, but not enough to then increase the pH past 6. The pH stays at this plateau for several hours, indicating that steady state has been reached between the injected hydrogen ions and diffused hydroxide ions.

The pressure drops at various flow rates and the hydraulic aperture of Core 6FP-26 are given below in Table 16. Values for the 20 mL/min flow rate are not given, as the pressure drop was very low, nearing the resolution of the pressure transducer. The hydraulic aperture of the slot is increased slightly, leading to lower pressure drops for the given flow rates. This is consistent with the results from Core 6FP-24, shown in Table 15 above.

Flow Rate (mL/min)	Pressure Drop Before Acid Injection	Pressure Drop After Acid Injection
200	1.77	1.09
160	1.41	0.88
100	0.82	0.54
20	-	-
0	0	0
Hydraulic Aperture (mm)	0.270	0.314

Table 16: Injection pressures at various rates and hydraulic aperture of Core 6FP-26 before and after HCl acid injection

The total portlandite dissolved and transported out of the fracture by the acid was approximately 0.004 grams, roughly 2% of the total portlandite dissolved in the acid injection into Core 6FP-24. This is due to the reduced amount of total HCl injected in

Core 6FP-26. Though this is a small amount of alkali mineral dissolved, injecting polymer dispersion into this core helped to determine how much acid must be injected for the acid pre-flush to be effective in preventing syneresis. The large mass of acid delivered at a low pH was seen to be effective in Core 6FP-24, but Core 6FP-26 will determine the effectiveness of small mass of acid delivered at a higher pH. The pressure drop and effluent pH histories of the experiment are shown in Figure 81.

Core	Aperture	Polymer Injected	Residence Time	Volume Injected	Fracture Type
6FP-26	0.314 mm	3 wt% Carbopol 934 0 wt% NaCl	1 min	52 FVs	Cement-Plastic Sawed

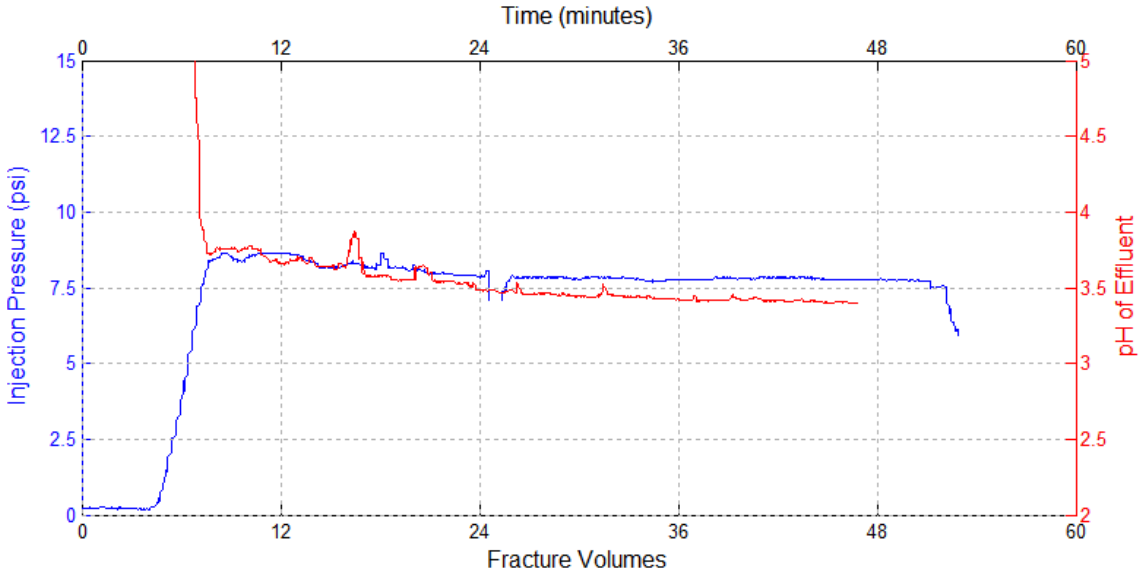

Figure 81: Data recorded during polymer injection (3 wt% Carbopol 934, 0 wt% NaCl, and DI water) into Core 6FP-26 following acid injection (cf. Figure 80)

The pressure drop through the fracture quickly increases, plateaus, then begins to decrease slowly over the next 50 minutes, during which the pH slowly declines from 3.7 to 3.4. This behavior is described in panel 4 in Figure 47 and indicates that the pressure drop decline is primarily due to the reduction in yield stress and consistency index of the polymer dispersion. At these pH values in the critical gelation pH range, the viscosity of

the polymer dispersion decreases rapidly with pH decrease, and as such the pressure drop decrease can be attributed to a drop in the polymer viscosity. The apparent viscosity at 12 FVs of polymer injection is calculated to be around 1,220 cP, while at 48 FVs the apparent viscosity is around 1,140 cP. The upper bound of the apparent viscosity calculated from the HB parameters of the effluent at 12 FVs is around 22,100 cP. Again, the pressure drop data give lower apparent viscosities due to the fact that the effluent's rheology is not observed throughout the fracture, but only at the outlet.

The effluent pH history is monotonically decreasing, unlike the response seen during polymer injection into Core 6FP-24, as shown in Figure 78. However, the pH values are similar to those seen in polymer injection experiments with cores that were not treated with an acid pre-flush, i.e. the effluent pH during polymer injection shows no observable effect of the acid pre-flush. Photographs of Core 6FP-26 during polymer injection are shown in Figure 82. The acid flush before polymer injection resulted in no observable discoloration in the cement, nor did it prevent the white syneresis polymer from appearing in the fracture during polymer injection.

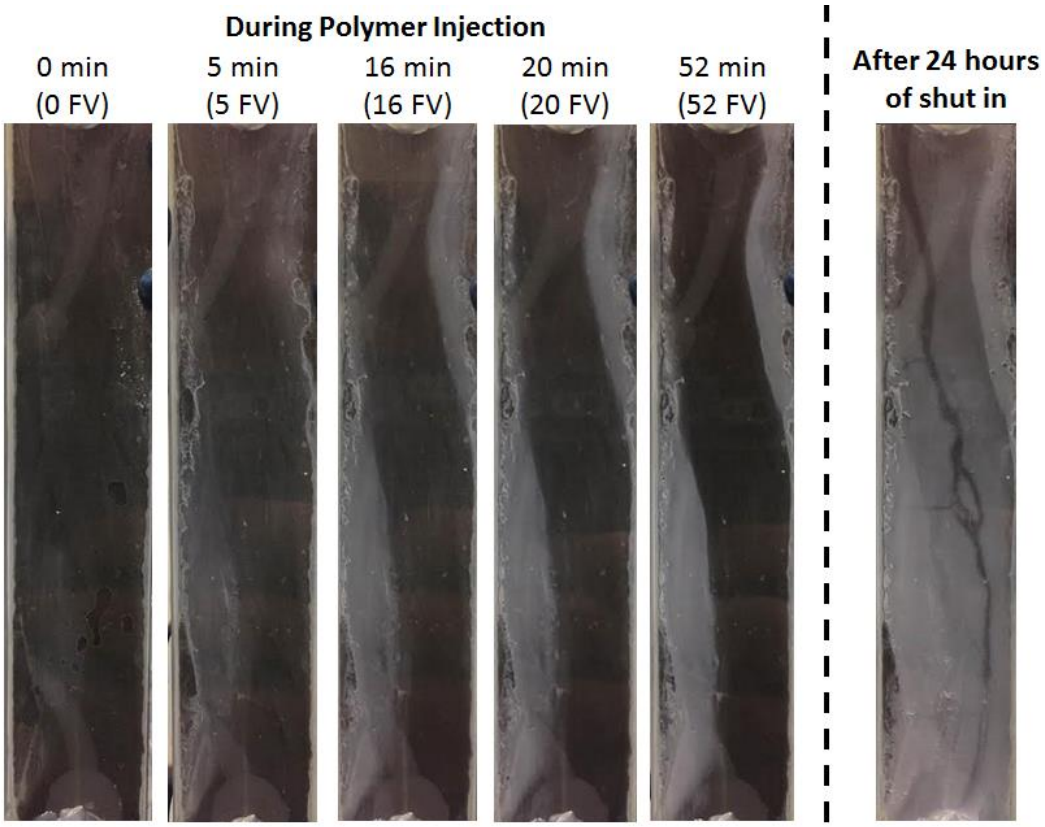

Figure 82: Photographs of Core 6FP-26 during polymer injection (3 wt% Carbopol 934, 0 wt% NaCl, deionized water) following HCl pre-flush; note that some reflections from the plastic plate's surface are visible, but are not indicative of events inside the fracture.

After the 24 hour shut in period, deionized water was injected into the core's inlet slowly (0.1 mL/min). Pressure built up in the inlet as the polymer gel prevented flow, until the pressure exceeded the flow initiation pressure and the water broke through the fracture. The inlet water pressure is shown below in Figure 89. Breakthrough occurred around 12 minutes of injection time, and water injection was continued until the 24 minute mark.

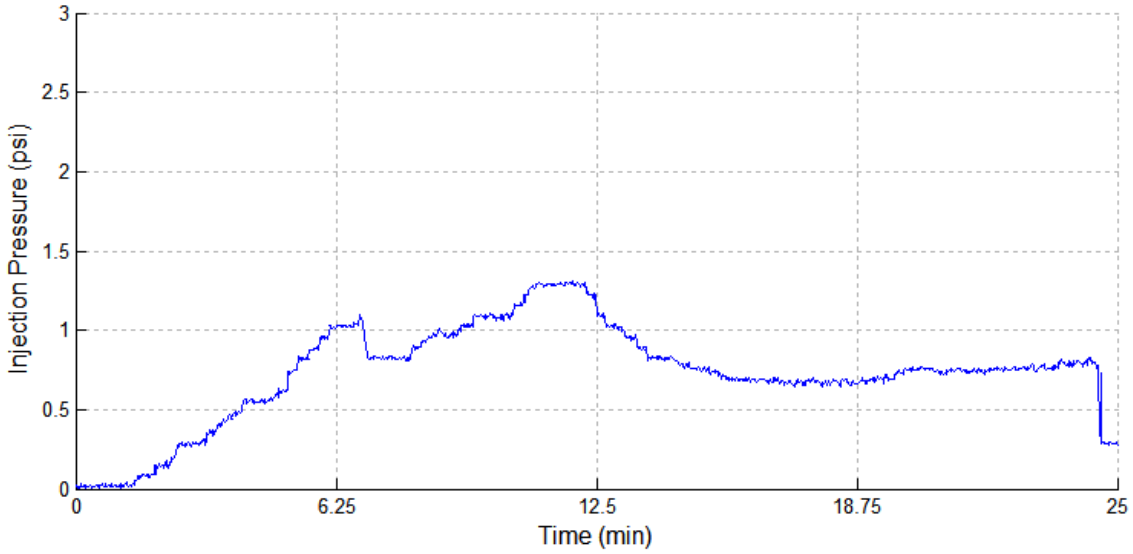

Figure 83: Polymer strength test in Core 6FP-26 after 24 hours of shut in time; constant injection of 0.1 mL/min of water led to displacement of the gel when the injection pressure reached 1.3 psi.

The polymer gel in the fracture was able to hold back about 1.3 psi, corresponding to a gradient of 2.6 psi/ft. The effective yield stress of the polymer gel is calculated to be around 10 Pascals, calculated using the flow initiation pressure equations and the core's aperture. The yield stress of the injected polymer dispersion is close to 15 Pascals, indicating that the polymer present in the fracture was weaker than even the injected fluid, despite the neutralization due to alkaline cement components. This suggests that the polymer dispersion has undergone significant syneresis, reducing its ability to hold back pressure. Photographs taken during water breakthrough support this and are shown in Figure 84. The displacement water was dyed red and can be seen filling a significant portion of the flow channel that had been created during polymer injection. This indicates that syneresis has occurred in this channel and part of the channel is filled with expelled water due to syneresis.

After water breakthrough, the water injection pressure is consistent with a fracture aperture of 35 microns (0.035 mm), a decrease of nearly 90% from the original fracture aperture. This indicates significant flow channel constriction.

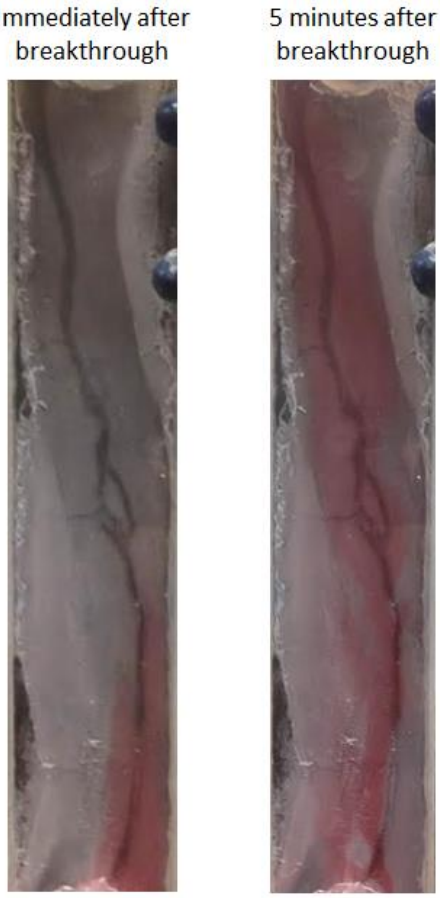

Figure 84: Photographs taken during water breakthrough of Core 6FP-26. Water is dyed red for easy identification. The water spreads to occupy a large part of the former flow channel formed during polymer injection, indicating that syneresis has left this space partially filled with syneresed water.

5.4.3 Core 6FP-27

In experiment 6FP-26, both injection acid pH and total HCl injected were varied. Core 6FP-27 was injected with pH 2.28 hydrochloric acid, similar to the pH of the acid injected into Core 6FP-26, but with more fracture volumes injected, increasing the total HCl injected. The acid was injected over the course of several days. Due to

experimental setup restrictions, the acid was injected in 140 mL increments, roughly 125 fracture volumes, for each acid injection experiment. The first of these injection periods is shown below in Figure 85 below.

Core	Aperture	pH of Acid Injected	Residence Time	Volume Injected	Fracture Type
6FP-27	0.288 mm	2.21	8 min	130 FVs	Cement-Plastic Sawed

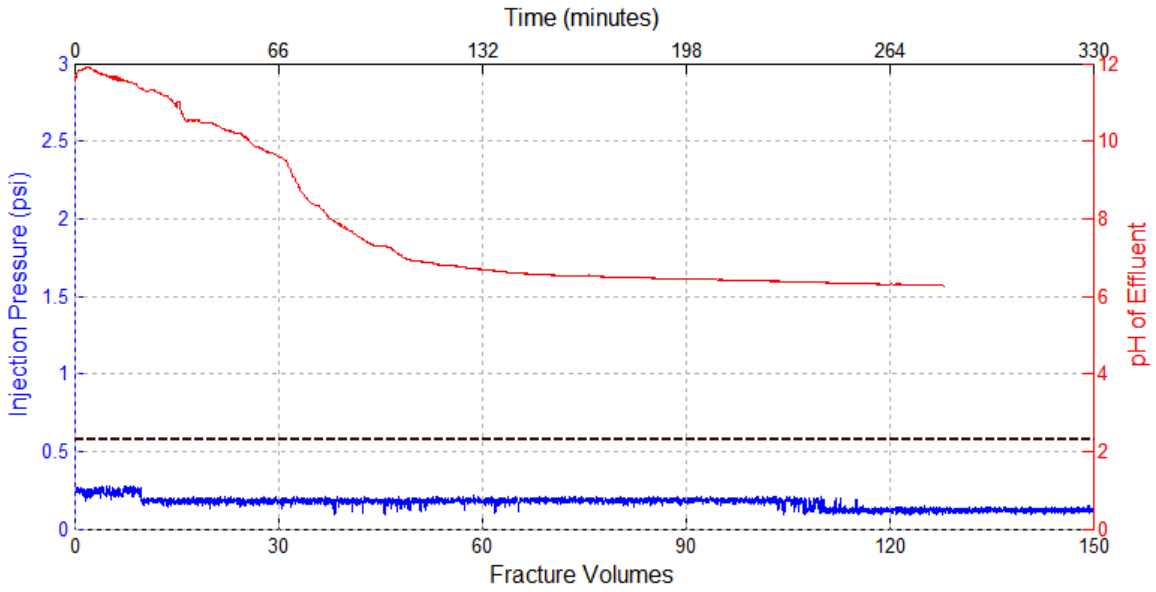

Figure 85: Data recorded during first stage of acid injection (pH 2.29 HCl solution) into Core 6FP-27; black dashed line indicates pH of injected acid

The effluent that initially reaches the pH probe is the water initially present in the fracture, with a pH close to 12. As injected fluid begins to reach the probe, the pH still remains relatively high, indicating that the hydrogen ions are entirely consumed by the cement's portlandite, or some other hydroxide bearing mineral, and extra hydroxide ions are leached into the effluent. After nearly 60 fracture volumes, the pH drops below 7 when the hydroxide ions are no longer entering the fracture quickly enough to consume all of the acid's hydrogen ions.

As the acid injection continues and consumes the alkali minerals just under the cement surface, the hydroxide ions must diffuse to the fracture from deeper in the cement matrix. Additional stages of acid were injected into Core 6FP-27 with the same pH 2.3 HCl solution, as well as one acid stage in which the injected pH was 1.8. One of these later injection stages, the 7th stage, is shown in Figure 86 below. Again, the unreacted pH of the injected acid is shown as a black, dashed line.

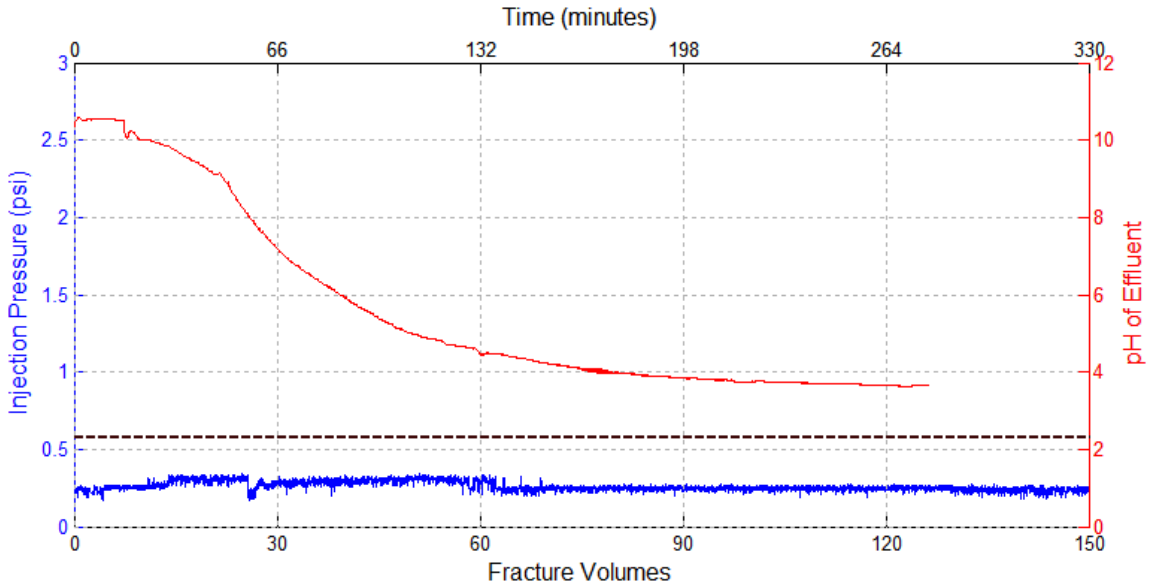

Figure 86: Data recorded during seventh stage of acid injection (pH 2.29 HCl solution) into Core 6FP-27; black dashed line indicates pH of injected acid

While the shape of the pH decline is similar to the first acid injection experiment in Figure 85, the effluent pH goes well below 4 after 120 fracture volumes have been injected. This means the acid exits the cement fracture with near 1000 times more hydrogen ions than it did during the first round of injection. It is also seen that the initial pH of the fluid in the core when injection resumes is above 10, indicating the cement still contains alkali minerals to drive up the pH, but requires several hours for the diffusion and reaction to occur. The shut-in period while the acid vessel is re-filled between acid

injection stages provides enough time for this reaction to occur. This supports the proposed mechanism of a diffusion-limited reaction inside the fracture.

The cement core underwent some discoloration during acid injection when the hydrochloric acid solution was 2.29, turning the gray cement face into a dark brown color. This discoloration was increased as more acid was injected. During the acid injection in which the solution was pH 1.8, the cement surface took on a strong orange color, similar to rust. This particular discoloration has been seen to occur when acid is used below pH 2 and is thought to be due to an iron/aluminum insoluble precipitate forming on the cement surface (Huerta, 2013), with iron coming from the upstream dissolution of other cement minerals.

Cumulatively over the several acid injection periods into Core 6FP-27, an estimated 0.254 grams of portlandite were dissolved and transported out of the core. This is about 10% more than the portlandite dissolved in Core 6FP-24, but took much more time due to the higher pH of hydrochloric acid. 32% of the dissolution occurred during the injection of pH 1.8 acid.

As with every core, the effective permeability was measured before any polymer or acid injection and a "hydraulic aperture" was calculated. After acid injection, these are measured again using the same methods and flow rates. The injection pressures and hydraulic apertures of these measurements are given below in Table 17. The aperture of Core 6FP-27 was reduced during acid injection, causing the pressure drops for the various flow rates to nearly double.

Flow Rate (mL/min)	Pressure Drop Before Acid Injection	Pressure Drop After Acid Injection
200	1.40	3.07
160	1.08	2.23
100	0.73	1.27
20	0.13	0.27
0	0	0
Hydraulic Aperture (mm)	0.288	0.229

Table 17: Injection pressures at various rates and hydraulic aperture of Core 6FP-27 before and after roughly 900 fracture volumes of pH 2.28 HCl injection.

This effect on the cement's hydraulic aperture is attributed to the precipitation of calcite ($CaCO_3$) towards the outlet of the fracture (Huerta, 2013). This comes from the calcium concentration increasing with distance along the fracture in the presence of the acid's dissolved carbon dioxide (CO_2), which comes from contact with air during handling before injection, and the increasing pH of the liquid as it moves through the fracture. In terms of mineral reactions, portlandite is dissolved by the acid, increasing the calcium concentration and the pH until both are sufficiently high to precipitate calcite onto the cement's surface. This added material reduces the aperture of the slot locally, reducing the overall hydraulic aperture of the slot. This behavior is described by Huerta (2013) and a diagram of the behavior is shown in Figure 75. It is unclear, however, what factors determine whether a cement fracture's aperture will increase or decrease after acid injection.

Polymer dispersion was injected into Core 6FP-27 with 3 wt% Carbopol 934 and 0 wt% NaCl while recording pressure drop and effluent pH. The data are shown below in Figure 87. The effluent pH initially is around 11, as the core was shut in for 24 hours

after acid injection, allowing hydroxide to diffuse from the core to the water, increasing the pH.

Core	Aperture	Polymer Injected	Residence Time	Volume Injected	Fracture Type
6FP-27	0.229 mm	3 wt% Carbopol 934 0 wt% NaCl	1 min	52 FVs	Cement-Plastic Sawed

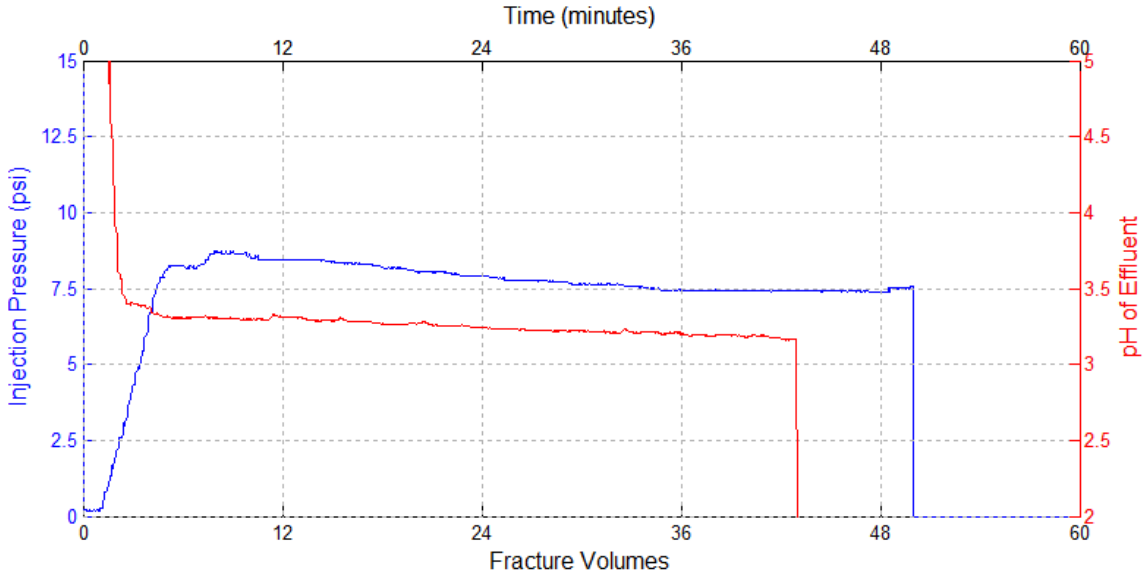

Figure 87: Data recorded during polymer injection (3 wt% Carbopol 934, 0 wt% NaCl, and DI water) into Core 6FP-27 following a HCl pre-flush.

Despite the addition of an acid pre-flush, the effluent pH for Core 6FP-27 decreases to around 3.2, which is similar to the effluent pH of polymer injection into cores without an acid pre-flush. The injection pressure increases quickly, plateaus, then slowly declines, which could coincide with a reduction in polymer gel viscosity as the pH of the effluent decreases. The apparent viscosity at 10 FVs is approximately 580 cP, then decreases to around 500 cP at 48 FVs, within the bounds of the apparent viscosity given by the rheology data and effluent pH.

Photographs taken during polymer injection are shown in Figure 88.

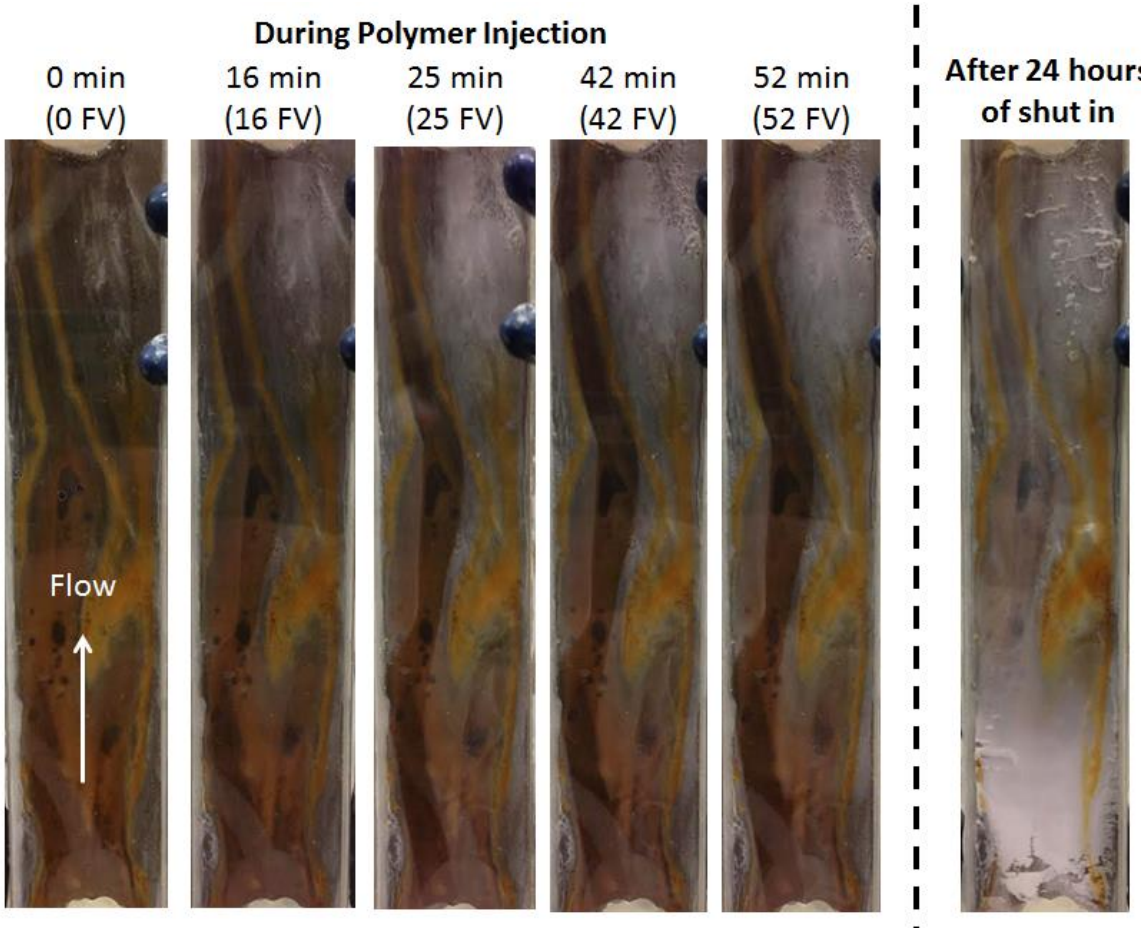

Figure 88: Photographs of Core 6FP-27 during polymer injection (3 wt% Carbopol 934, 0 wt% NaCl, deionized water) following HCl pre-flush; note that some reflections from the plastic plate's surface are visible, but are not indicative of events inside the fracture

The photographs show that very little syneresis polymer appeared during polymer injection. This is a promising step, as the presence of syneresis polymer is thought to degrade the polymer gel's ability to hold back fluids. However, after 24 hours of shut in (the far right photograph) syneresis polymer (white) can be seen covering nearly the entire cement surface at the bottom one or two inches of the fracture.

After the 24 hour shut in period, deionized water was injected into the core's inlet slowly (0.1 mL/min). Injection pressure built up as the polymer gel prevented flow, until the pressure gradient exceeded the yield stress and the water broke through the

fracture. The inlet water pressure is shown below in Figure 89. Breakthrough occurred around 15 minutes of injection time, and water injection was continued until the 43 minute mark.

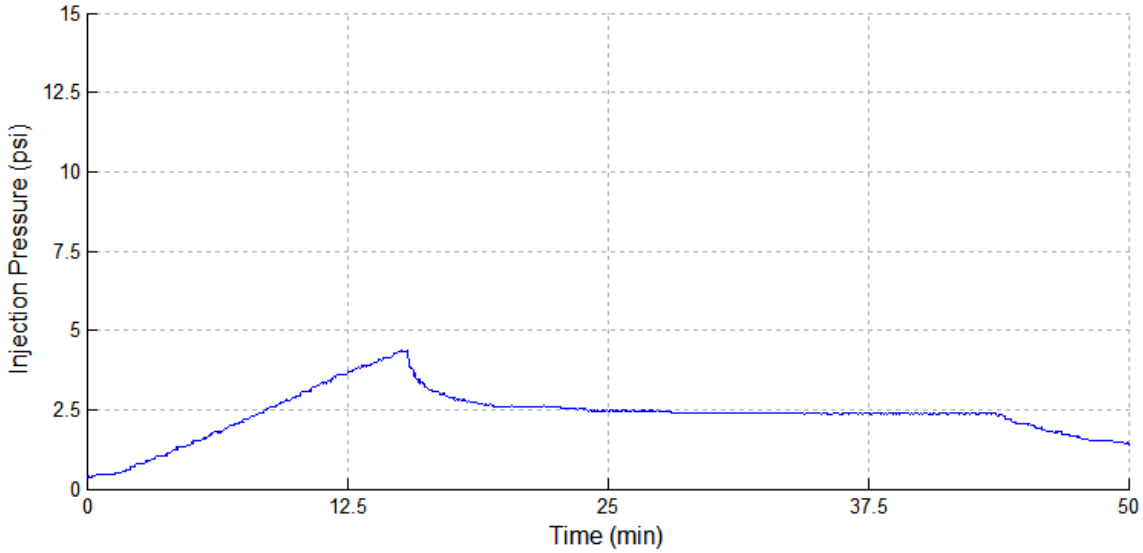

Figure 89: Polymer strength test in Core 6F-27 after 24 hours of shut in time

The flow initiation pressure here was close to 4 psi, corresponding to a pressure gradient of nearly 8 psi/ft. Although it's unclear if this pressure was held back due to the syneresis polymer or the polymer gel in the slot, the flow initiation pressure and aperture would correspond to a gel filling the slot with a yield stress of nearly 29 Pa, more than double the initial yield stress of the polymer dispersion injected.

5.4.4 Core 6FP-28

Instead of injecting hundreds of pore volumes of pH ~2.3 HCl acid solution, core 6FP-28 was injected with 160 fracture volumes of pH = 1 HCl solution. Injecting several stages of pH 2.3 acid took several days, as each stage took roughly 5 hours. By decreasing the acid volume and compensating by increasing the concentration of hydrogen ions by 20 fold, the total experimental time is reduced. The amount of

portlandite consumed is estimated from the cumulative consumption of injected acid, but as previously mentioned the cement reacts with hydrochloric acid differently below a certain pH (around pH 2) and iron rich, insoluble minerals are produced. This obviously means that the portlandite is no longer the only mineral being consumed by the hydrochloric acid (as neither can contribute the necessary iron ions), but the amount of portlandite removed from the system will be estimated using the same methods as before. The acid injection pH and pressure data are shown below in Figure 90.

Core	Aperture	pH of Acid Injected	Residence Time	Volume Injected	Fracture Type
6FP-28	0.288 mm	2.21	8 min	130 FVs	Cement-Plastic Sawed

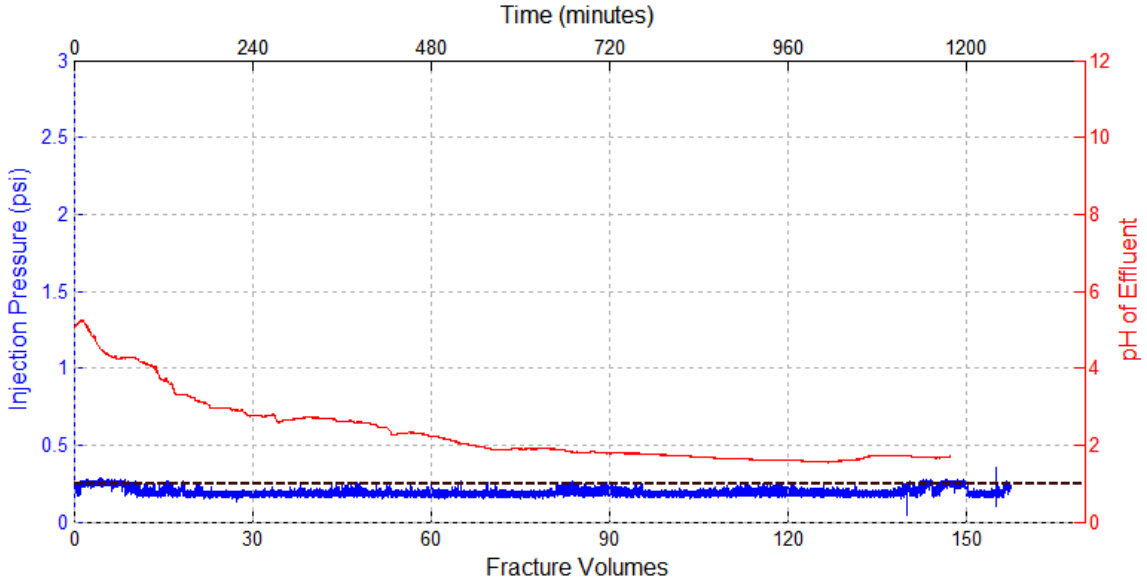

Figure 90: Data recorded during acid injection (pH = 1 HCl solution) into Core 6FP-28; black dashed line indicates pH of injected acid

Again, the pressure drop through the fracture is negligible. The pH of the effluent is initially close to 5, indicating that the water initially in the fracture and the acid had mixed to some extent before reaching the pH probe, similar to the behavior seen in Core 6FP-24. Some of this mixing could occur inside the fracture, but it is likely that

most of the mixing occurs inside the pH measurement cell, downstream from the fracture. The pH measurement cell requires a small, but non-negligible, volume of fluid before the liquid level reaches the pH probe. The volume of this fracture is also quite small, causing less high-pH fluid to be mixed with the low-pH acid, resulting in a lower overall pH. These two experiments used low pH (below 1.5) HCl solutions, so the mixing between the basic water initially present in the fracture and injected acid results in a lower pH than weaker acid pre-flushes. The effluent pH history again asymptotically approaches the injection acid pH, but does so in fewer fracture volumes than cores injected with less concentrated acid solutions, such as Core 6FP-27. Photographs during this acid injection are shown in Figure 91.

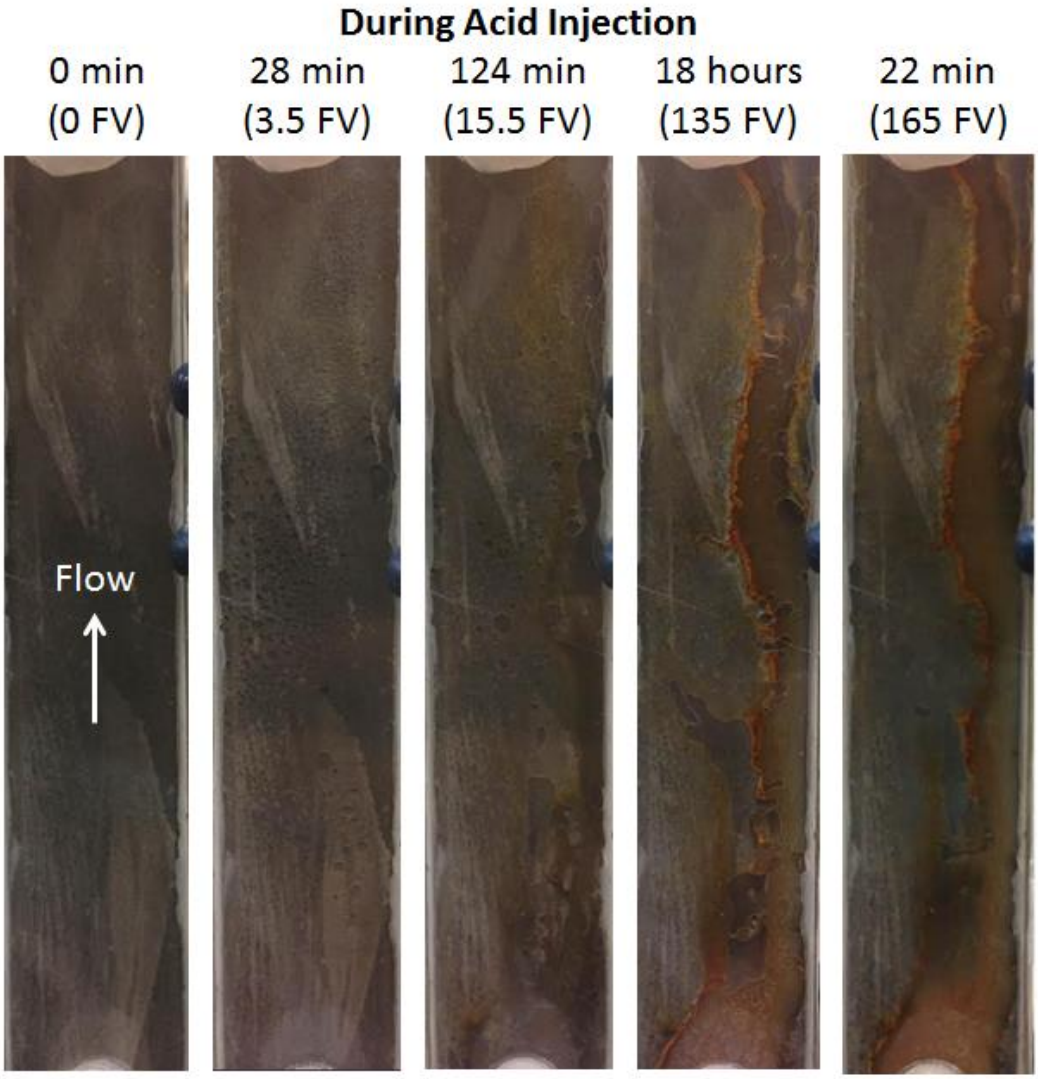

Figure 91: Photographs of Core 6FP-28 during acid injection (pH 1 hydrochloric acid).

Bubbles began to form in the slot immediately as acid contacted the cement. Batch experiments had shown that hydrochloric acid below a certain pH (around pH 1.1) will effervesce when in contact with cement, but above this pH no bubbles are formed. This effervescence is thought to be the source of some of the noise and non-monotonic behavior seen in Figure 90. As the bubbles accumulate on the cement surface, they coalesce to form larger bubbles and eventually will become large enough to flow upwards and out of the core's outlet. These bubbles potentially move past the pH probe

near the outlet, causing a brief period of inaccurate readings, or can preferentially occupy the outflow lines, causing the injection acid to remain in the core longer than the set residence time, leading to larger pH values temporarily. By two hours of acid injection, the cement face in the right half of the core is discolored brown, and after 18 hours there is a brown channel on the right side of the core and the left side of the core is generally the original color of the cement. Between these two regions is a concentrated streak of brown/orange, rust-colored mineral.

Using the effluent pH history, original acid pH, and flow rate data, the total portlandite dissolved is estimated to be around 0.411 grams, the largest amount of the acid pre-flush experiments. It is also the lowest pH of hydrochloric acid injected into a core. As the injection pH decreases, the amount of effervescence increases and more bubbles are expelled.

After acid injection, deionized water was injected into the core to measure the hydraulic aperture again. The hydraulic aperture of Core 6FP-28 increased after acid injection, as shown below in Table 18. This is the opposite effect observed in Core 6FP-27, but the mechanism for the aperture increase is intuitive: the acid dissolves minerals in the flow channel and transports them out of the core, thereby enlarging the flow channel. The parameters that affect whether the hydraulic aperture will be increased or decreased after acid injection, however, is not well known and is still under investigation.

Flow Rate (mL/min)	Pressure Drop Before Acid Injection	Pressure Drop After Acid Injection
200	3.69	2.41
160	2.90	1.88
100	1.80	1.14
20	0.33	0.20
0	0.00	0.00
Hydraulic Aperture (mm)	0.211	0.246

Table 18: Injection pressures at various rates of water injection and estimated hydraulic aperture of Core 6FP-28 before and after HCl acid injection

Immediately after the second hydraulic aperture test, Core 6FP-28 was injected with 50 fracture volumes of 3 wt% Carbopol 934 with 0 wt% NaCl. The pressure drop and effluent pH during the polymer injection is shown below in Figure 92.

Core	Aperture	Polymer Injected	Residence Time	Volume Injected	Fracture Type
6FP-28	0.220 mm	3 wt% Carbopol 934 0 wt% NaCl	1 min	52 FVs	Cement-Plastic Sawed

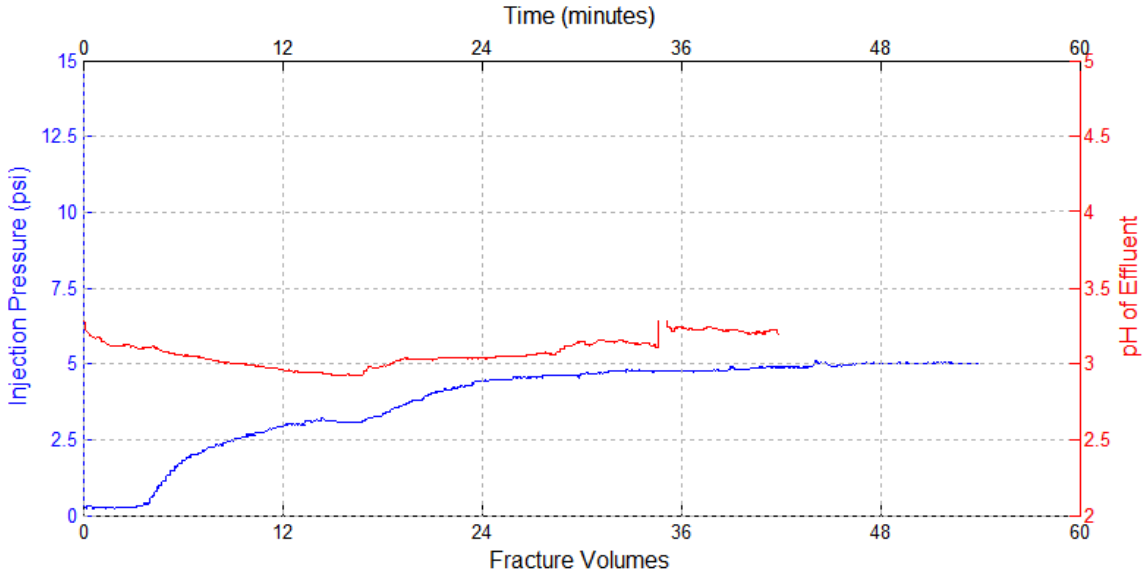

Figure 92: Data recorded during polymer injection (3 wt% Carbopol 934, 0 wt% NaCl, and DI water) into Core 6FP-28 following injection of pH 1.0 HCl solution.

In general, slower injection rates lead to longer pressure equilibrium times, as higher pressures allow fluid to move into the pressure lines faster than lower pressures.

The slow pressure buildup is thereby easily accounted for. However, around 14 fracture volumes the pressure drop has plateaued, but then starts to increase again. The apparent viscosity at the 14 FVs is around 230 cP, then increases to 380 cP at 48 FVs. These are similar to the apparent viscosities seen in Core 6FP-24. However, compared to 6FP-24, the aperture of Core 6FP-28 is larger and the flow rate is slower, both of which would result in an increase in apparent viscosity due to the shear thinning nature of the polymer dispersion.

The pH of the effluent at this time stops decreasing and begins to increase, similar to the pH behavior of Core 6FP-24, shown in Figure 78. The pH probe was cleaned at the 35 fracture volume mark, to ensure accurate pH measurements, but continues to record a pH around 3.25, indicating that the pH record is accurate. The pH and pressure trends rising together does make sense, however, as the increase in pH will increase the viscosity (consistency index and yield stress) of the polymer dispersion, driving up the pressure drop since the injection rate is constant. Photographs taken during polymer injection are shown below in Figure 93.

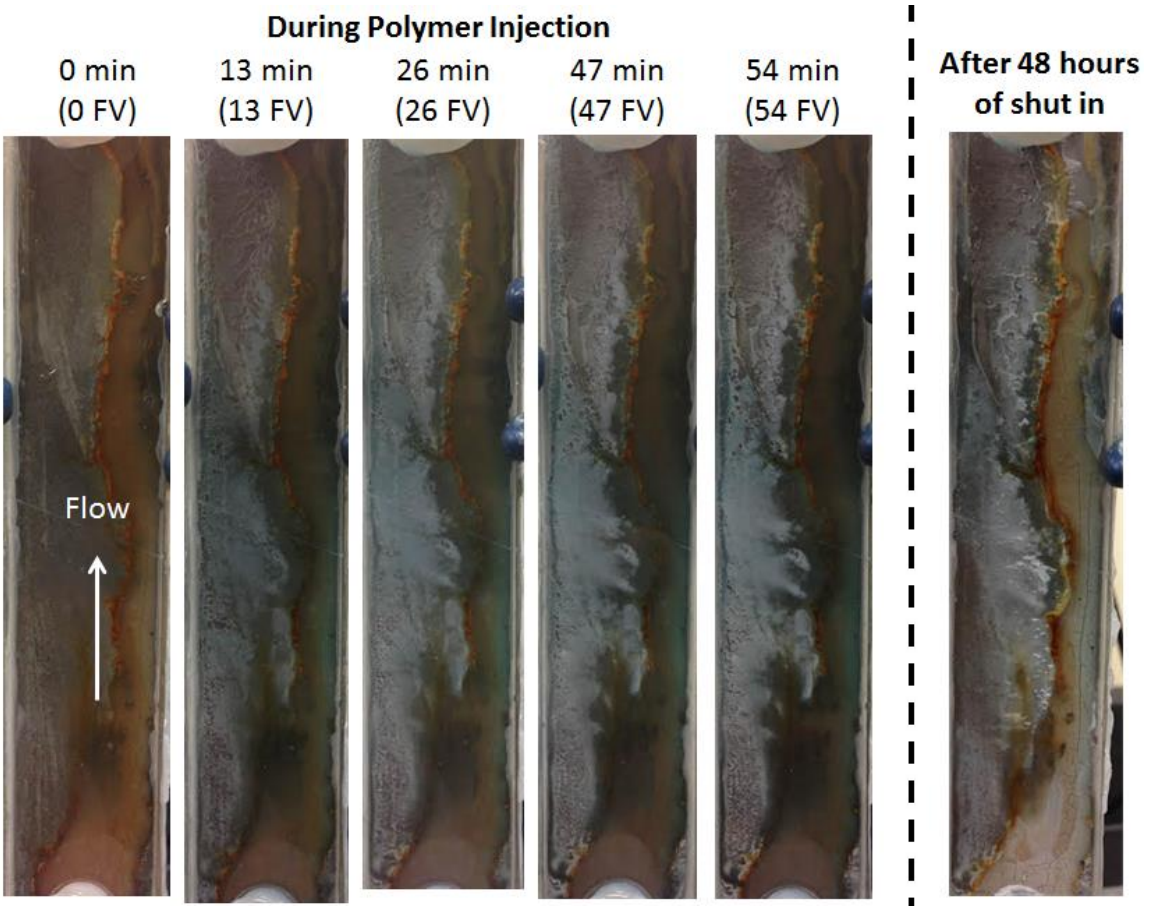

Figure 93: Photographs of Core 6FP-28 during polymer injection (3 wt% Carbopol 934, 0 wt% NaCl, deionized water) after pre-flush of pH 1.0 HCl solution.

The region of the cement face that had the most contact with the hydrochloric acid solution (the right side in the pictures) showed almost no syneresis effects during polymer injection, and only minor syneresis after 24 hours of shut in. The left side of the fracture, which had less acid contact, accumulated a significant amount of syneresed polymer on the cement face. While most polymer flow occurred in the right channel, bubbles (from the prepared polymer dispersion) and syneresed polymer particles were seen moving upwards along the whole width of the core, indicating that the flow wasn't entirely restricted to one channel. These bubbles and particles were too small to be captured in a photograph.

After the 48 hours of shut in following polymer injection, Core 6FP-28 was connected to the long term pressure manifold at around 2.5 psi/ft and has held pressure for 40 days and continues to hold pressure.

5.5 Discussion and Conclusions of Acid Pre-flush Experiments

The results of the four acid pre-flush and subsequent polymer injection experiments are shown in Table 19. Each of these cores were injected with 52 fracture volumes of 3 wt% Carbopol 934 and 0 wt% NaCl after the acid pre-flush at a rate of 1 fracture volume per minute.

Core	Aperture Before Acid (mm)	Aperture After Acid (mm)	pH of Acid Injected	Portlandite Consumed (g)	Flow Initiation Pressure Gradient	Hold Back 2.5 (psi/ft)	Effective Yield Stress (Pa)
6FP-24	0.157	0.168	1.18	0.229	n/a[1]	4 months	>5
6FP-26	0.270	0.314	2.21	0.004	2.6 psi/ft	n/a	9
6FP-27	0.288	0.229	2.28	0.254	8 psi/ft	n/a	21
6FP-28	0.211	0.246	1.00	0.411	n/a	1 month	>7

Table 19: Results of HCl acid pre-flush and subsequent polymer injection experiments, with various fracture and acid solution parameters. [1] Cores were either tested for the flow initiation pressure or the length of 2.5 psi/ft hold back – but never both. The flow initiation pressure was not tested for 6FP-24 or 6FP-28; the hold back time was not tested for Core 6FP-26 or 6FP-27.

It should be noted that, though there is a precedent for aperture reduction after acid injection, from Huerta (2013), this behavior is only seen in Core 6FP-27. Huerta et al correlates the aperture reduction with "slow flow rate and low acid concentration," which seems to agree with the observations in all four acid injection experiments. The fact that Core 6FP-26 undergoes aperture enlargement, despite being injected with similar acid solution as Core 6FP-27, could be ascribed to the lower amount of acid injected, and therefore lower amount of portlandite dissolved. This also agrees with Huerta et al's

observation that the aperture does not decrease until a certain injection time or amount of acid threshold is crossed.

The ability for the polymer gel to withhold pressure increased relative to cores without a pre-flush in every experiment, except for Core 6FP-26. This core was subjected to a polymer strength test and failed when the pressure gradient reached 2.6 psi/ft, close to the pressure gradient used in the long-term pressure tests. Therefore it is uncertain whether the core would have held back the 2.5 psi/ft pressure gradient during the long-term exposure to constant pressure. Of these four experiments, Core 6FP-27 was injected with considerably less acid than the others, and by comparing Core 6FP-26 and Core 6FP-27 it can be concluded that the amount of acid injected is a significant factor in the polymer gel's performance after placement. During polymer injection, it is seen from 6FP-27 in Figure 88 that the acid pre-flush serves to reduce, but not eliminate, the amount of syneresis flow channel constriction. Without an acid pre-flush, the effluent pH generally decreases monotonically, but with a low pH (~1) acid pre-flush is used the effluent pH decreases then begins to increase about 15 FVs into polymer injection, as in Figure 92.

5.5.1 Effect of Acid Pre-flush on Syneresis

Photographs taken after polymer injection in Core 6FP-27 and Core 6FP-28 show that the amount of white, syneresed polymer present after shut in is only partially reduced compared to experiments where an acid pre-flush was not utilized, such as 6FP-11. Nevertheless, polymer gel filled fractures with an acid pre-flush were able to hold back more pressure and for longer than gel in fractures that had not been pre-flushed with acid. For example, Core 6FP-4 and Core 6FP-27 both had significant regions of the fracture filled with syneresed polymer after 18 to 24 hours of shut in, as shown below in Figure

94. The extent of syneresis in these cores can be seen best near injection inlet, yet Core 6FP-27 held back a pressure gradient of 8 psi/ft, while Core 6FP-4 immediately failed to prevent flow at a 2.5 psi/ft gradient. The extent of syneresis in the top parts of 6FP-27 is less severe than in Core 6FP-4, and this region is thought to be integral to the core's performance.

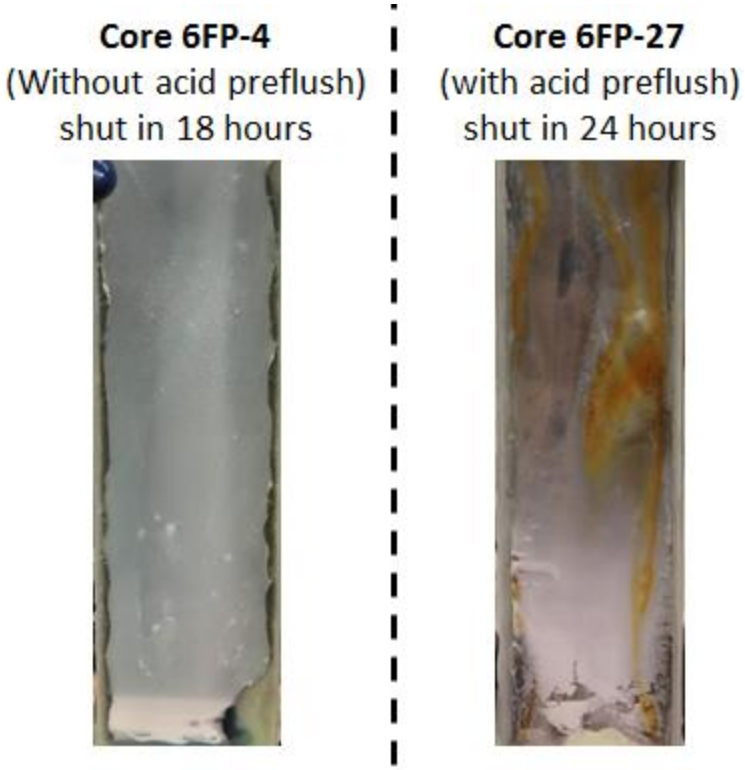

Figure 94: Comparison of bottom half of Core 6FP-4 (without acid pre-flush) and Core 6FP-27 (with acid pre-flush) after 18 to 24 hours of shut in. Both cores injected with 3 wt% Carbopol 934 with 0 wt% NaCl.

As predicted, the use of a HCl acid pre-flush serves to protect the subsequent polymer dispersion injected into the fracture from syneresis and allows polymer gel to block fractures from fluid flow. The effect of HCl is attributed to the reduction of calcium content at the cement surface as HCl reacts with portlandite. Though syneresis

is not entirely prevented, the partial prevention does still yield valuable improvements in polymer performance.

5.5.2 Effluent pH Rebound

During polymer injection after acid pre-flush into Core 6FP-24 and Core 6FP-28, the pH of the effluent decreased with time, but began to increase around 15 FVs injected. The pressure drop and effluent pH curves for both cores are shown again in Figure 95. This effect, which will be referred to as effluent "pH rebound," is only seen in these two cores that were pre-flushed with HCl acid solution at a pH 1.18 and 1.00. The effluent pH histories during polymer injection in Core 6FP-26 and Core 6FP-27, which were pre-flushed with HCl acid at pH 2.21 and 2.28, respectively, were monotonically decreasing.

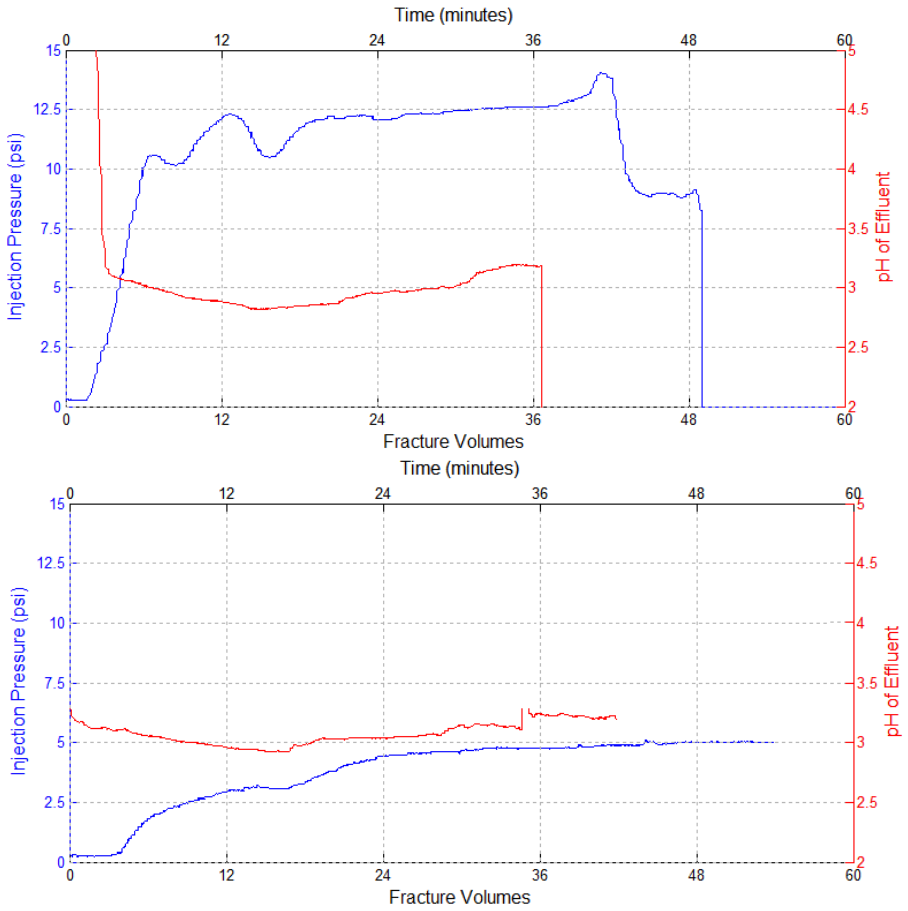

Figure 95: Pressure drop and effluent pH history of Core 6FP-24 (top) and Core 6FP-28 (bottom) during polymer injection (3 wt% Carbopol 934 and 0 wt% NaCl) after acid pre-flush. The effluent "pH rebound" effect around 14 FVs of injection.

This behavior is speculated to be due to the low pH of the injected HCl acid pre-flush prior to polymer injection and related to the red-orange iron-rich precipitate that formed on the cement fracture face during acid injection. This iron-rich precipitate acts as a kind of barrier between the quickly reacting portlandite in the cement and the polymer dispersion filled fracture. As polymer dispersion is injected into the fracture, it is possible that the polymer begins to react with the iron-rich precipitate or begins to strip off the precipitate via drag. During this period, the effluent pH slowly decreases as the reaction rates slow.

As the iron-rich precipitate is removed, it begins to expose the portlandite-rich cement surface. This portlandite reacts quickly with the polymer dispersion and the effluent pH increases as more of the cement surface is exposed. It is unclear as to how the polyacrylic acid is able to react or strip away this iron-rich layer and is currently being investigated.

Chapter 6 Conclusions and Future Work

6.1 Conclusions

The objective of this thesis research was to determine the ease of placement of pH-sensitive polymer dispersions into a cement fracture and the extent of subsequent flow blockage by the polymer gel formed. The initial viscosity of the polymer dispersion can be tailored by varying the concentration of salt, typically NaCl, allowing the polymer to be easily injected into small fractures. Polymer dispersions were injected into various cement-cement fractured cores and proved able to resist fluid flow after a shut-in period. However, the pressure drop during injection in these cores was nonmonotonic and irregular, making injection pressure difficult to predict and diagnose.

To better understand the behavior of the polymer dispersion inside the cement fractures, one half of cement cores was replaced by a clear plastic plate. It was determined from the experimental data and visual inspection of the cores that polymer syneresis – the expulsion of fluids from the polymer gel matrix – was a major factor in the pressure changes and temporary fluid blockages observed in polymer injection experiments. It was determined that the primary cause of the syneresis was calcium cations in released from the cement into solution. This syneresis effect was seen to be detrimental to the stability and strength of the gel inside the cement fracture, but also aided in the blockage of fluid flow in some cases.

A procedure for preventing or decreasing the detrimental effects of syneresis was developed involving injection of hydrochloric acid prior to polymer injection in order to remove calcium from the cement surface. This reduction in cement calcium content was seen to moderately reduce syneresis inside the fracture, while still allowing the polymer dispersion to neutralize and gel. The pressure gradients induced by supercritical CO_2 plumes in GCS formations are thought to be between 0.1 and 1 psi/ft. It has been shown

here that polymer dispersion placed in a cement fracture with an acid pre-flush is capable of holding back fluid at gradients as high as 8 psi/ft, and reduces the flow rate of subsequent fluid leakage for cases when the brine pushes through the polymer gel..

In the context of well integrity in CO_2 storage formations, these polymer gels could be a promising alternative to a typical cement squeeze job in wells that exhibit microfrcatures or microannuli around the casing.

6.2 FUTURE WORK

Improvements are likely needed upon the polymer formulation for application in leaky GCS wells and research is currently underway to improve the polymer's performance and reliability. One main concern is the effect of cations, such as sodium from formation brine or calcium from cement dissolution, on the yield stress of the polymer gel via syneresis and partial binding of polymer chains. While the acid pre-flush described here has been shown to reduce these effects, it is also possible for the acid pre-flush to create additional problems, such as damaging casing or creating additional leakage pathways in the cement or surrounding rock. The use of nano-clay particles, in the form of laponite, is being investigated as a way to cross link the polymer chains and prevent subsequent cation exposure from binding to these chains, destroying the viscosity and yield stress of the gel.

Experiments were conducted in epoxy core holders as a way to test multiple cores simultaneously. These epoxy core holders thus excluded the possibility of using representative reservoir pressures and temperatures found in GCS formations. Future work will use steel Hassler core holders to determine the effects of high temperature and pressure on the injectivity of the polymer dispersion and subsequent displacement performance.

Appendix A Cement Fracture Core and Experiment Preparation

Epoxy core holders can be a cheap and efficient way to perform multiple core flood experiments, but are subject to much lower pressure limits than a steel Hassler core holder. In typical porous media, the pressure limit of these cores is around 100 psi. In a cement fractured core, this pressure limit is reduced to around 50 psi. This is because pressure build up in the fracture pushes the two cement halves apart from each other relative to the size of the core, creating large stresses on the plastic and epoxy. For example, a 6" by 1" cement fracture at 50 psi will result in a force of 300 pounds pushing the core apart.

The following process is used to create the epoxy core holder with a cement-cement fractured core.

1. Materials required (shown in Figure 96): two cement halves fractured during the Brazilian test[1]; one polycarbonate tube, 1.5" wide and 9" long; two core endcaps with NPT female fittings (diagram shown in Figure 97). Also need quick-epoxy (Devcon 5 Minute Epoxy Gel) and 24 hour set epoxy (Versamid 125).

[1] See Chapter 4.2.1 for the prodcedure to prepare the fractured core.

Figure 96: Materials required for epoxy core holder. Polycarbonate tube, fractured cement core, and core endcaps.

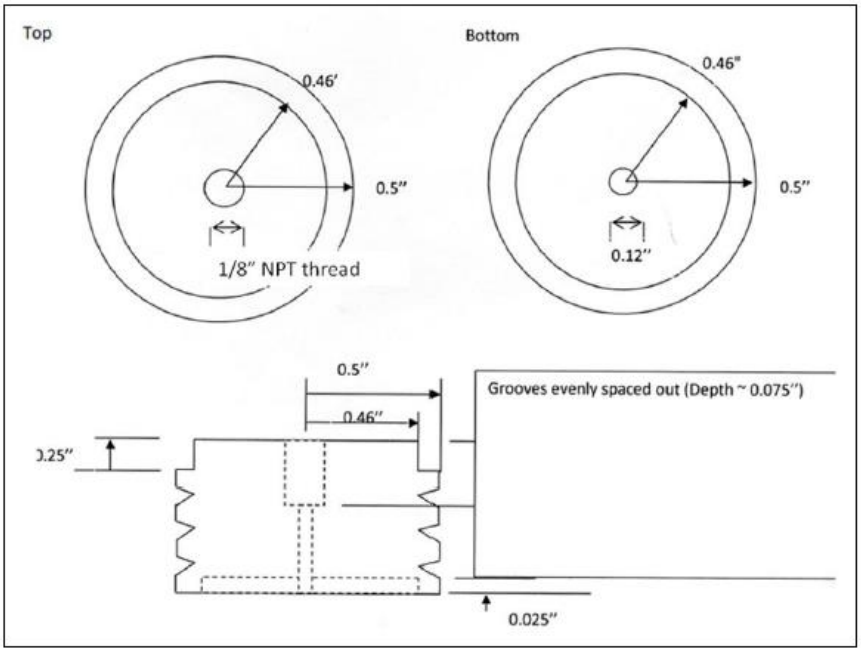

Figure 97: Diagram of core endcaps for epoxy core holders. One is placed at both top and bottom of each core to be inserted into polycarbonate tube and epoxied into place.

2. The two cement halves must be quick-epoxied along the edge of the fracture to prevent the 24-hour epoxy from flowing into the fracture, which would preclude subsequent use for flow experiments. The core endcaps are then quick-epoxied to the cement core and the inlet/outlet holes of the endcaps are taped shut. The end product should be a cement core with endcaps that is entirely sealed from the outside. The sealed cement fracture is shown in Figure 98.

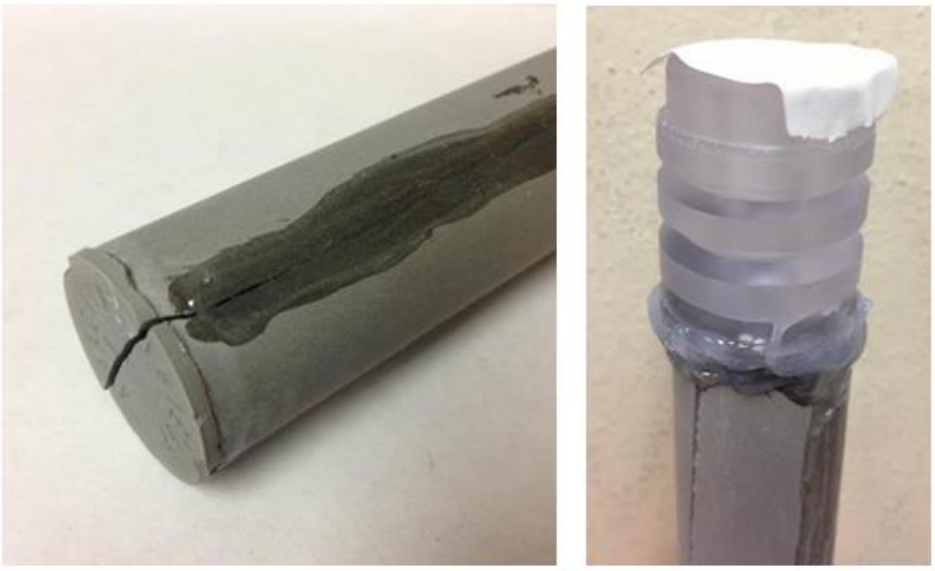

Figure 98: Quick-epoxy gel used to seal outside of cement fracture and endcaps.

3. The polycarbonate tube bottom is sealed by using a rubber stopped covered with wax paper. Wax paper allows the rubber stopper to be easily removed after epoxy set and is easily cut away afterwards. This is shown in Figure 99.

Figure 99: Wax paper and rubber stopped used to seal bottom of polycarbonate tube.

4. The cement core is placed into the polycarbonate tube and rests on the rubber stopped at the bottom. 24-hour epoxy is then prepared and poured into the open top of the tube. Figure 100 shows the core before epoxy is poured in and during epoxy setting. The epoxy is very viscous and takes some time to reach the bottom of the cement core, then takes 24 hours to reach full strength. It is recommended to wait up to 48 hours until putting core on vacuum to ensure proper epoxy setting.

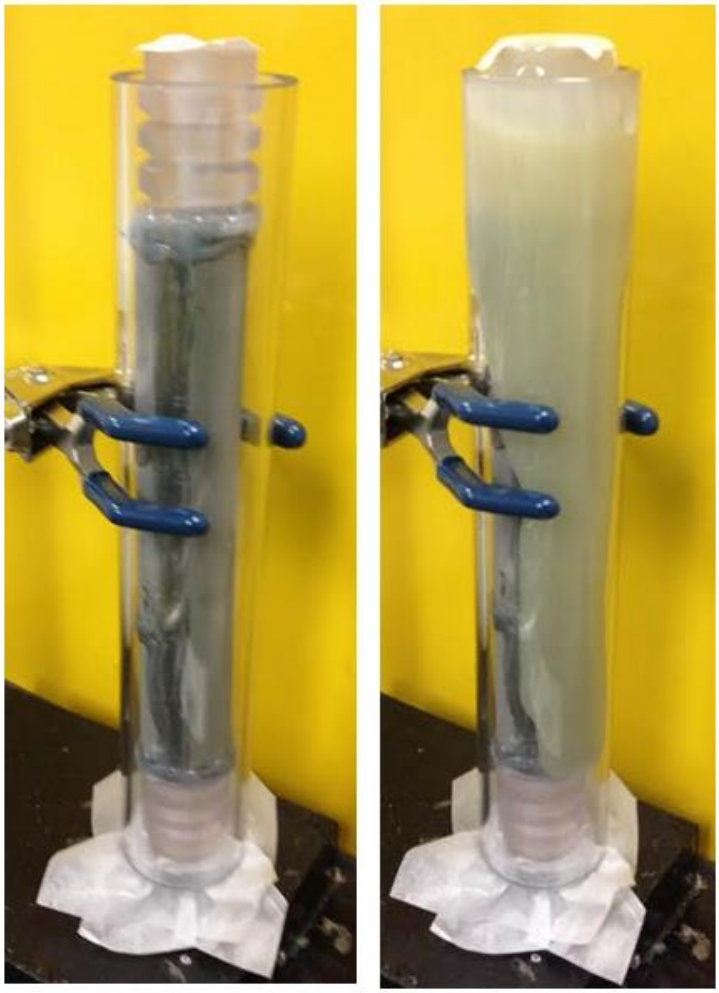

Figure 100: Cement fractured core placed into polycarbonate tube (left) and 24 hour epoxy poured into the space between the core and tube (right).

5. After epoxy has cured, tape and wax paper are removed from the top and bottom of the core. A male NPT-to-Swagelok tube fitting adapter is then placed into the NPT hole at each endcap and a ball valve and tubing set is connected to the fitting, as seen in Figure 101. The core is then ready to be vacuumed and saturated with water in preparation for polymer injection experiments.

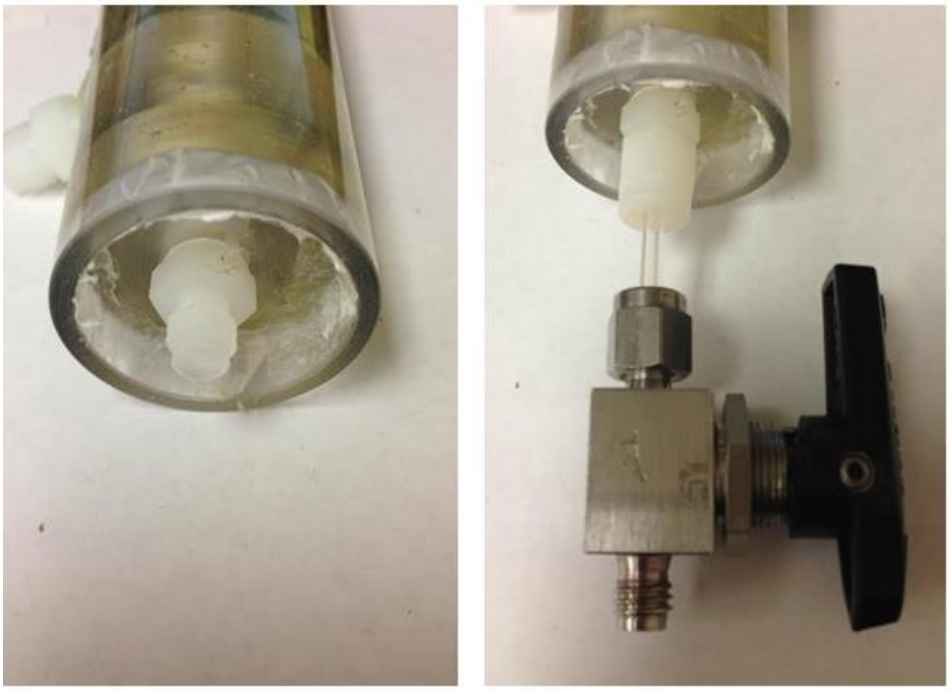

Figure 101: Plastic NPT fitting placed in core endcap and connected to ball valve.

Appendix B Pressure Measurements with Yield Stress Fluid

Obtaining accurate pressure data during polymer injection was more difficult than initially expected. The pressure drop across a core in an epoxy core holder is traditionally measured with the pressure lines connected to the inlet and outlet fluid lines, outside of the core end cap. A diagram of the setup is shown in Figure 102 below. Porous media cores are generally injected with Newtonian fluids, which have no yield stress, or at least fluids with low viscosities and yield stresses. Therefore the pressure drop between the inlet of the epoxy core holder and the core itself is negligible.

Injecting polymer dispersion into cement fractures is quite different. The polymer dispersion has a large yield stress and consistency index, and become larger as the polymer reacts with the cement surface. This results in pressure losses in the space between the pressure lines and the cement core itself, increasing the observed pressure drop across the core. To counter this problem, pressure taps were installed at the top and bottom of the core by drilling holes into the epoxy core holder. The new setup is shown alongside the previous setup, also in Figure 102. The new pressure taps allow for accurate pressure measurements without inlet/outlet endcap effects.

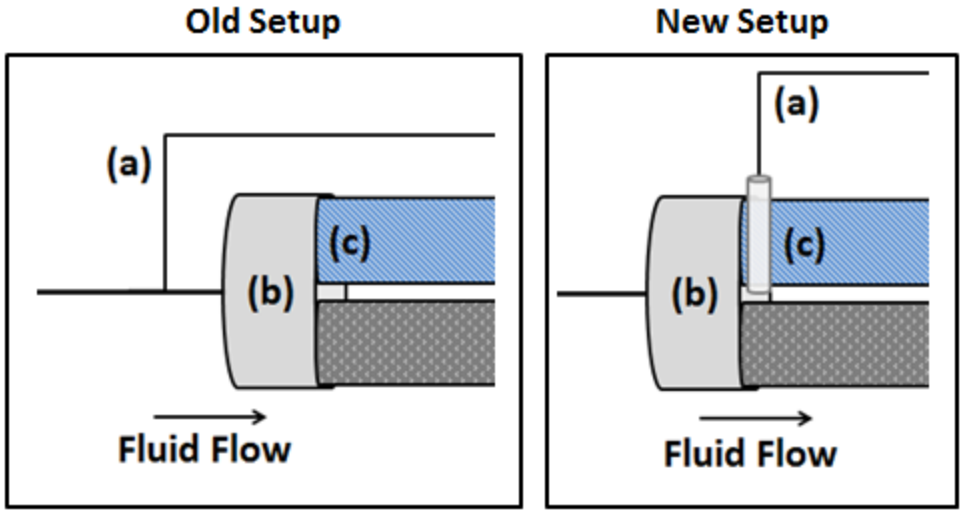

Figure 102: Diagram of typical epoxy core holder pressure measurement setup. High pressure line (a), core inlet endcap (b), and plastic plate and cement fracture (c). Old setup is traditionally used for core floods with low viscosity, Newtonian fluids; new setup was designed for high viscosity yield stress fluids.

These pressure lines, however, can still record inaccurate pressures due to the yield stress of the polymer that goes into the pressure lines. As the pressure in the core increases, small amounts of polymer dispersion will flow into the pressure lines, due to the compression of air in the lines or the expansion of the nylon tubes themselves. For the pressure at the transducer to increase, additional fluid must flow into the line and exert more force on the transducer. The pressure lines are about 6 feet long in order to go between the core and the pressure transducer. At high pressures (10+ psi) several inches of these lines can be filled with polymer dispersion (near the core inlet) or polymer gel (near the core outlet).

When these lines are filled with polymer gel, the gel's yield stress can create a pressure block between the transducer and the core, preventing the gel from moving further into the pressure line and transmitting the actual pressure. This effect is intensified at high pressures and with small diameter pressure lines. As discussed in

Chapter 3, the flow initiation pressure (FIP) of a Herschel-Bulkley fluid in a tube is given as

$$\Delta \mathrm{P} = 2\frac{\tau_w \Delta \mathrm{L}}{R}$$

where ΔL is the length of the polymer in the tube, R is the radius of the tube, τ_w is the yield stress at the wall, and ΔP is the FIP. As the radius of the pressure line decreases, the FIP will increase. Additionally, the length of polymer gel in the pressure line increases along with pressure, as more polymer is forced into the pressure line.

To put this in perspective, if a length of 6 inches of a 1/8 inch OD plastic tube is filled with a polymer gel with a yield stress of 100 Pa, it will take roughly 5 psi to move the polymer gel forward. If the pressure at the core is greater than 5 psi above the core exit pressure (which is 1 atm for all experiments in this work), then more gel will be pushed into the pressure line, increasing the length of gel in the tube and the FIP as a result. This process moves forward until the core pressure can no longer move the polymer gel. In practice, this means that the pressure transducer will see a pressure that is 5 psi lower than the actual pressure. A schematic of this behavior is shown below in Figure 103 with hypothetical pressure values.

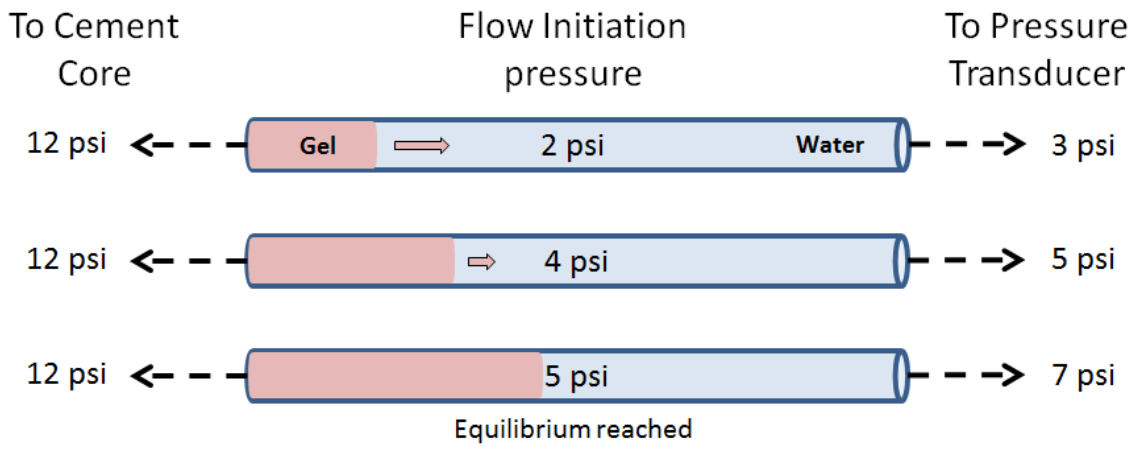

Figure 103: Effect of flow initiation pressure on pressure transducer measurements. The tubing connects the pressure transducer and the cement core.

The maximum yield stress of a neutralized 3 wt% Carbopol 934 is over 300 Pa, which would give a 15 psi FIP in this tube, skewing the pressure three times as much. The FIP will have similar effects on both the high (upstream) and low (downstream) pressure lines, and the pressure transducer will measure the difference in pressure between the two lines. However, the fact that the effect is seen in both lines does not totally offset the problem, because the outlet polymer gel will have a higher yield stress than the inlet polymer dispersion.

This was a key problem seen during polymer injection and had to be corrected. Of the variables controlling FIP, the length of polymer in the pressure line and the radius of the pressure line could easily be changed. The largest tubing size that could be accommodated with the cores was a ¼" plastic line. This larger line has a 2.5 times larger radius, but more importantly the area increased by a factor of six, meaning that the same volume of polymer gel in the line will occupy one sixth of the length as before. Only the first 6 inches or so of each pressure line was replaced by the large diameter tubing, keeping the volume relatively constant. In effect, the larger tubing cuts the FIP down by a factor of 15. During experiments, polymer is generally observed within the

first one to two inches of the tubing, yielding a FIP that is less than 1 psi for a 100 Pa yield stress fluid. Between the reduced FIP and the partially offsetting effect from both high and low pressure lines, the error becomes relatively negligible. Also, in case the problem persists, the pressure lines can be firmly shaken or agitated to encourage polymer slug movement.

Another potential issue with small pressure lines is the increased time needed for the pressure in the pressure lines to equilibrate. Because polymer dispersion will resist flow in small tubes more than large tubes, the measured pressure drop will appear to take more time to reach steady state. An example of this behavior in a hypothetical, nonreactive slot is shown in Figure 104.

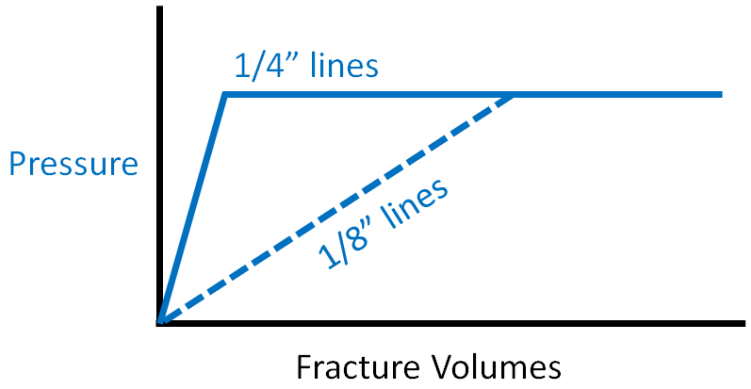

Figure 104: Example of measured pressure build up in fracture using 1/4" and 1/8" pressure lines during polymer injection. Smaller tubing causes polymer dispersion to move slowly in pressure line, causing pressure to appear to build slowly.

Similar problems may arise due to syneresed polymer in the fluid. As the polymer dispersion comes in contact with the cement's calcium and hydroxide, syneresis polymer is formed and is often deposited on the cement face, but a portion of the syneresis polymer breaks free from the surface and moves with the fluid flow. Figure 105 shows a sample collected during polymer injection that consists of a water phase and pieces of syneresis polymer. This type of effluent is generally seen during the first few

fractures volumes of polymer injection when the flow rates are low and residence time is high (16+ min). Under these conditions, the pieces of syneresis polymer are also found in the low pressure lines. If the pieces are large enough, the pressure line could become temporarily plugged and report pressures that are lower than the actual core pressure. A blockage in the low pressure line will cause the pressure drop to appear higher than it truly is; a blockage in the high pressure line would cause it to appear lower. With enough pressure, the blockage can be cleared and hydraulic connection between core and transducer restored, but this will show up in the pressure drop data as a sudden jump up or down, depending on which line is blocked.

Figure 105: Small pieces of syneresis polymer in free water from polymer dispersion in a glass vial (bubbles at top)

It should be noted that the pH of the syneresis polymer in water shown in Figure 105 is 11.35, which is close to the pH of water initially in cement fractures. The pH of the fluid makes it hard to distinguish from the water that initially saturated the fracture, but the pieces of syneresis polymer can be seen in the outlet lines.

Appendix C Bubble Flow Phenomenon in Yield Stress Fluid

Though the mechanism causing this phenomenon is not known, these observations are consistent with and can be explained by the fact that the polymer dispersion has a yield stress influencing the rheology. Because the viscosity of the bubble is negligible compared to the polymer dispersion, the polymer around the bubble has a pressure gradient driving it forward while the bubble simply has one pressure. This creates a local pressure difference at the tip of the bubble (towards the direction of flow), which exerts a shear stress on the polymer dispersion at the tip. A diagram of a large bubble is shown in Figure 106

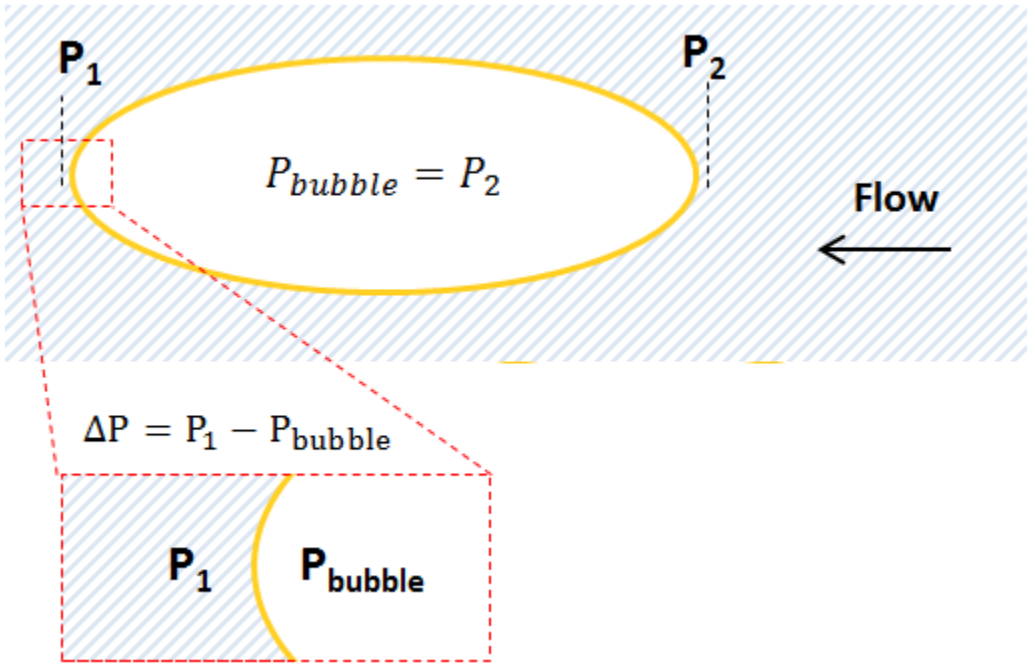

Figure 106: Diagram of large bubble in polymer dispersion during flow through a plastic-plastic plate slot. The low viscosity of the bubble results in a single bubble pressure that will be higher than the pressure at the tip of the bubble.

As the size of the bubble increases, the local pressure difference at the tip of the bubble increases, thereby increasing the local shear stress until the bubble becomes large

enough that the shear stress exceeds the polymer's yield stress at the tip. The increased pressure at the bubble tip is then able to move the polymer and propels the bubble forward relative to the polymer dispersion, resulting in an increased bubble velocity. A diagram of a large and small bubbles is shown in Figure 107.

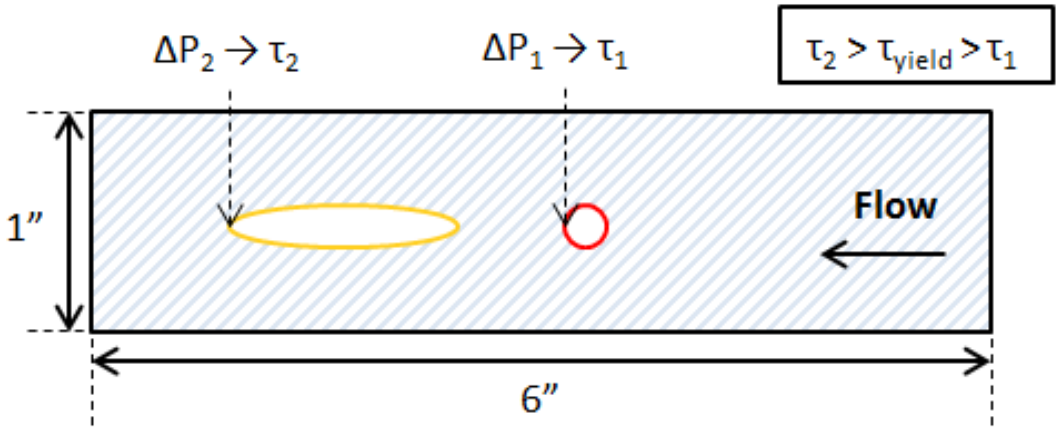

Figure 107: Diagram of large and small bubbles in polymer dispersion during flow through a plastic-plastic plate slot. View is through the plastic plate and polymer flow is from right to left. Large bubble is outlined in yellow and small bubble is outlined in red.

The shear stress caused by the large bubble is large enough to overcome the polymer's yield stress and thus increase its velocity, while the red bubble's shear stress is below the yield stress and will therefore have the same velocity as the polymer dispersion. Bubbles were generally not intentionally used to inject polymer dispersion into cement fractures, nor were they expected to influence the results of the polymer gel's ability to hold back pressure, but these observations allowed for better understanding of the dynamics of a yield stress fluid in slot flow.

References

API, 2011. Specification for Cements and Materials for Well Cementing.

Barry, B.W. and Meyer, M.C., 1978. The Rheological Properties of Carbopol Gels I. Continuous Shear and Creep Properties of Carbopol Gels. International Journal of Pharmaceutics, 2 (1779) 1-25.

Beddoe, R.E., Dorner, H.W., 2005. Modelling acid attack on concrete: Part I. The essential mechanisms. Cem. Concr. Res. 35, 2333–2339.

Bourgoyne, A.T. Jr., Chenevert, M.E., Millheim, K.K., Young, F.S., Jr., 1986. Applied Drilling Engineering, SPE Textbook Series. Society of Petroleum Engineers.

Bruant, R.G., Guswa, A.J. Celia, M.A., Peters, C.A., 2002. Peer Reviewed: Safe Storage of CO2 in Deep Saline Aquifers. Environmental Science & Technology. 36, 240A-245A.

Burton, M., Bryant, S., 2009. Eliminating Buoyant Migration of Sequestered CO2. SPE Reserv. Eval. Eng. 12.

EPA (Environmental Protection Agency), 2012. Inventory of U.S. Greenhouse Gas Emissions and Sinks: 1990-2010, U.S. Environmental Protection Agency, Office of Atmospheric Programs, EPA 430-R-12-001.

Featherstone, J.L. and Powell, D.R., 1981. Stabilization of Highly Saline Geothermal Brines. Journal of Petroleum Technology, April 1981, p. 727-734

Goodwin, K.J. 1984. Principles of Squeeze Cementing. Permian Basin Oil & Gas Recovery Conf., SPE 12603.

Grachev, M.A., Annenkov, V.V., Likhoshway, Y.V., 2008. "Silicon nanotechnologies of pigmented heterokonts". BioEssays: News and Reviews in Molecular, Cellular and Developmental Biology 30 (4): 328–37. doi:10.1002/bies.20731. ISSN 1521-1878. PMID 18348175. Retrieved 2009-02-03.

Hepple, R. and Benson, S., 2002. Implications of surface seepage on the effectiveness of geologic storage of carbon dioxide as a climate change mitigation strategy. Lawrence Berkley National Laboratory, LBNL-51267.

Hesson, B.H., 2013. California department of conservation's division of oil, gas, and geothermal resources: orphan well program. SPE 165340.

Huerta, N.J. Time dependent leakage of CO2 saturated water along a cement fracture. PhD dissertation, University of Texas at Austin, Austin, Texas (December 2013)

IPCC (Intergovernmental Panel on Climate Change), 2001. Third Assessment Report – Climate Change 2001, the third assessment report of the intergovernmental panel on climate change. IPCC/WMO/UNEP.

IPCC, 2013. Working Group I Contribution to the IPCC Fifth Assessment Report Climate Change 2013: The Physical Science Basis.

Kaldi, J. G., Gibson-Poole, C.M., and Payenberg, T.H.D, 2009. Geologic Input to Selection and Evaluation of CO2 Geosequestration Sites, in M. Grobe, J. C. Pashin, R. L.

Kelessidis, V.C., Maglione, R., Tsamantaki, C., Aspirtakis, Y., 2006. "Optimal determination of rheological parameters for Herschel-Bulkley drilling fluids and impact on pressure drop, velocity profiles and penetration rates during drilling" Journal of Petroleum Science and Engineering 52, p. 203-224, 2006.

Kutchko, B.G., Strazisar, B.R., Huerta, N., Lowry, G.V., Dzombak, D.A., Thaulow, N., 2009. CO2 Reaction with Hydrated Class H Well Cement under Geologic Sequestration Conditions: Effects of Flyash Admixtures. Environ. Sci. Technol. 43, 3947–3952.

Nicot, J.P., 2009. A survey of oil and gas wells in the Texas Gulf Coast, USA, and implications for geological sequestration of CO2. Environ. Sci. Technology 39, 602-611.

Nordbotten, J.M., Celia, M.A., and Bachu, S., 2004. Analytical solutions for leakage rates through abandoned wells. Water Resource Research, 40 (4), W04204.

Noveon, 2002. Neutralizing Carbopol® and Pemulen® Polymers in Aqueous and Hydroalcoholic Systems. Technical Data Sheet TDS-237, Jan. 2002 Edition

Oldenburg, C.M., Bryant, S.L., and Nicot, J.P., 2009. Certification framework based on effective trapping for geologic carbon sequestration. Inj. J. of Greenhouse Gas Control 3, 444-457, 2009, LBNL-1549E.

Orr, F.M., 2004. Storage of Carbon Dioxide in Geologic Formations. Journal of Petroleum Technology, 56(9): 90-97.

Soter, K., 2003 Removal of sustained casing pressure utilizing a workover rig. Louisiana Sate University.

Szymczak, P., Ladd, A.J.C., 2009. Wormhole formation in dissolving fractures. J. Geophys. Res. Solid Earth 114, 1–22.

Toor, I.A. 1983. Problems in Squeeze Cementing. Middle East Oil Tech. Conf. SPE 11499.

TRRC, 2013. Rule 13: "Casing, Cementing, Drilling, Well Control, and Completion Requirements."

Watson, T.L., Bachu, S., 2008. Identification of wells with high CO2-leakage potential in mature oil fields developed for CO2-enhanced oil recovery. SPE/DOE Improved Oil Recovery Symposium, Tulsa, OK, USA. 19-23 April 2008.